THE UNIVERSITY OF HULL

SOLID PARTICLES AT FLUID INTERFACES: EMULSIONS, LIQUID MARBLES, DRY OIL POWDERS AND OIL FOAMS

being a Thesis submitted for the Degree of Doctor of Philosophy
in the University of Hull

by

Andrew Terhemen Tyowua
B.Sc. (Hons) Chemistry (BSU, Nigeria)

November, 2014

Acknowledgments

I am very grateful to the Tertiary Education Trust Fund of Nigeria for a Ph.D. scholarship award, the University of Hull, UK for a studentship and Shiseido, Japan for partial financial assistance. My deepest appreciation goes to my academic supervisor Professor B.P. Binks for his excellent supervision and moral support. I thank Mr Shaun Johnston who worked with me during his M.Chem. project to obtain some data and Mr Tony Sinclair for scanning electron microscopy. My gratitude also goes to the members of the Surfactant and Colloid Group of the University of Hull, my colleagues and members of the Chemistry Department, Benue State University (BSU), Nigeria, the Vice-Chancellor of BSU, Professor Charity Angya and the Dean of Faculty of Science, BSU, Professor Msugh Kembe for their support, friendship and encouragement.

I owe a debt of gratitude to all my friends especially Professor F.E. Okieimen, Dr. S.G. Yiase, Rev. Fr. Moses Orti, Professor R.A. Wuana, Professor S.T. Ubwa, Dr. L. Leke, Pharm. Ntan Kunama, Dr. Sunday Elaigwu, Dr. Moses Iorungwa, Miss Secivir Tarzaan, Messrs Titus Iangba, Ahola Orgeh, Patrick Igboon, Kwaghkaa Hange, Charles Uba, Bernard Chia Surnen, Jande Tersoo, Gberindyer Pius, Koko Benedict, Emmanuel Ubuo, Akuma Stephen, Msugh Targema, Reuben Tyohemba, Francis Tsav and Alfred Aliemen for their numerous support during this Ph.D. programme. I truly feel that with you I have no excuse for failure. I am also in debt to my fiancée, Pharm. Maryam Pius who I love, for her love, kindness, patience and encouragement.

I gratefully acknowledge my family for their support and encouragement throughout this period. I am especially thankful to my father Mr Christopher Tyowua Ibier, my mother Mrs Icher Tyowua and my younger sister Miss Mngunengen Tyowua for their love and unconditional support. Lastly, I am thankful to my ‘in-laws’: Messrs Luka Adamu, Anthony Dauda, John Pius and Peter Pius for their trust and patience.

To late Mrs C.O. Ogebe (my college chemistry teacher), late Mr Msughter Ukume (my friend), late Engr. Moses Ioramo (my cousin) and late Mr John Dzuamo (my friend).

> *‘Great spirits have always encountered violent opposition from mediocre minds. The mediocre mind is incapable of understanding the man who refuses to bow blindly to conventional prejudices and chooses instead to express his opinions courageously and honestly.’* Albert Einstein (1940)

> *‘I am grateful to all those people who said no. It is because of them I did it myself.’* Wayne W. Dyer (1989)

Publications

The work presented in this thesis has given rise to the following publications:

Patent

1. B.P. Binks, T. Sekine and **A.T. Tyowua**, Whipped oily composition and a method of manufacturing the same, JP2013-149719, 2013.

Journal Papers

2. B.P. Binks, S.K. Johnston, T. Sekine and **A.T. Tyowua**, Particles at oil-air surfaces: powdered oil and oil foam, *submitted to Colloids Surf. A.*
3. B.P. Binks, T. Sekine and **A.T. Tyowua**, Dry oil powders and oil foams stabilised by fluorinated platelet clay particles, *Soft Matter*, 2014, **10**, 578−589.
4. B.P. Binks, L. Isa and **A.T. Tyowua**, Direct measurement of contact angles of silica particles in relation to double inversion of Pickering emulsions, *Langmuir*, 2013, **29**, 4923−4927 (not included in the thesis).
5. B.P. Binks and **A.T. Tyowua**, Influence of the degree of fluorination on the behaviour of silica particles at air-oil surfaces, *Soft Matter*, 2013, **9**, 834−845.

Oral Presentations

6. B.P. Binks and **A.T. Tyowua**, Behaviour of fluorinated platelet clay particles at oil-air interfaces: dry oil powders and oil foams, *Postgraduate Research Colloquium, The University of Hull, UK* (2014).
7. B.P. Binks and **A.T. Tyowua**, Silica particles in air-oil systems: dispersions, foams and liquid marbles, *International Soft Matter Conference, Rome* (2013).
8. B.P. Binks, A. Rocher and **A.T. Tyowua**, Silica particles at air-water, oil-water and air-oil surfaces, *Frontiers of Silica Research, Sweden* (2013).

Poster Presentations

9. B.P. Binks and **A.T. Tyowua**, Behaviour of fluorosilica particles at air-oil surfaces, *Science Showcase, Hull, UK* (2013).
10. B.P. Binks and **A.T. Tyowua**, Oil foams and oil liquid marbles stabilised by fluorinated silica particles, *Postgraduate Research Colloquium, The University of Hull, UK* (2013).
11. B.P. Binks and **A.T. Tyowua**, Fluorosilica particles at air-oil surfaces, *26th Conference of the European Colloid and Interface Society, Sweden* (2012).

Abstract

The behaviour of different particle types at oil-water, oil-oil and liquid (and/or oil)-air interfaces in terms of the type of materials they stabilise has been studied. For the oil-water interfaces, oil-in-water o/w Pickering emulsions (composed of tricaprylin or Miglyol 812N and water) were stabilised using rod- and cube-shaped $CaCO_3$ particles. For the oil-oil interfaces, oil-in-oil o/o and oil-in-oil-in-oil o/o/o Pickering emulsions, comprising solely of sunflower/olive/rapeseed oil and PDMS 20−100 cS, were prepared using fluorinated and hydrocarbon-coated fumed silica, fluorinated ZnO, fluorinated clay (sericite and bentonite), polytetrafluoroethylene PTFE, Bentone 34, rod-shaped $CaCO_3$ and Calofort SV particles as the stabilising agents. Finally, for the oil-air interfaces, oil liquid marbles, dry oil powders and oil foams were prepared using the fluorinated particles mentioned above as stabilisers. The following summary can be made about these particle-stabilised materials:

The rod- and cube-shaped $CaCO_3$ particle-stabilised o/w emulsions were white, basic (pH = 8 to 9) and were composed of μm-size polydisperse and flocculated tricaprylin and Miglyol 812N droplets. The stability of the emulsions, containing equal volume fraction of oil and water, to creaming and coalescence increased with increasing concentration of the rod-shaped $CaCO_3$ particles. Those stabilised by 3−5 wt. % of the particles remained completely stable to creaming for over 3 years, but released a relatively small fraction of the oils. No such stable emulsions were obtained regardless of the particle concentrations when the volume fraction of oil ϕ_o in the emulsions was reduced to 0.2. When ϕ_o in the emulsions was varied from 0.95 to 0.05 at a constant particle concentration (4 wt. %), ‘oily liquids’ form when $\phi_o = 0.95{-}0.8$, relatively stable o/w emulsions form when $\phi_o = 0.7{-}0.5$ and unstable o/w emulsions form when $\phi_o < 0.5$. Using the relatively stable o/w emulsions ($\phi_o = 0.5$, 4 wt. % of the $CaCO_3$ particles), it was observed that addition of electrolyte and pH adjustment induce coalescence and creaming or sedimentation in the emulsions. The stability of these emulsions was also affected by the method of emulsion preparation and particle shape.

The o/o and o/o/o emulsions were white, polydisperse and unflocculated with the average droplet size ranging from a few mm to μm. The type of emulsions obtained depends on the particle type and % SiOH for the fumed silica particles. Some of the emulsions were kinetically stable for over a month. The kinetic stability of the emulsions increased with increasing particle concentration. At relatively high particle concentrations (≥ 1 wt. %), some of the o/o emulsions (equal volumes of oil) remained stable to creaming/sedimentation and

coalescence for over a month. No stable o/o emulsions were obtained when the volume fraction of oil in the emulsions (composed of sunflower oil and PDMS 50 cS) was varied from 0.05 to 0.9 at constant particle concentration (1 wt. %). However, a catastrophic phase inversion was observed as expected. Transitional phase inversion was observed in some cases. The inversion occurred if the viscosity of the PDMS oils in a vegetable oil is varied in the presence of 75% SiOH fluorinated fumed silica particles or the % surface SiOH on the hydrocarbon-coated fumed silica particles in a vegetable oil-PDMS oil combination is varied from 100−14% SiOH. For the hydrocarbon-coated fumed silica particles, multiple emulsions were observed near the point (23 and 20% SiOH) of inversion in some cases. The multiple emulsions occurred before or after inversion. The vegetable oil-PDMS oil-glass three-phase contact angle θ_{oo} values were measured and were seen to correlate with the type of emulsions stabilised by the 100% SiOH and 14% SiOH fumed silica particles.

Many of the liquid marbles stabilised by the fluorinated fumed silica particles remained stable for more than 90 min whilst some of the oil foams remained kinetically stable for up to a year. The formation of these materials was seen to depend on the surface tension γ_{la} of the oils, the degree of particle fluorination or apparent surface energy γ_{sa} of the particles and energy input. An oil dispersion of particles forms in liquids of relatively low γ_{la} with particles of low fluorine content where the apparent advancing particle-liquid-air contact angle $\theta_{la} <$ 20°. Particle-stabilised oil foams were obtained in oils of relatively high tension (> 32 mN m^{-1}) and particles of moderate fluorine content. The oils of lower tension (*e.g.* 27 mN m^{-1}) and particles of high fluorine content also formed foams. For foams, the apparent advancing θ_{la} was between 82−145°. In many of the oil-particle systems forming foams by vigorous agitation, oil liquid marbles were also stabilised with particles of highest fluorine content encapsulating oils of lower γ_{la}.

Unlike the fluorinated fumed silica and fluorinated bentonite clay particles, the fluorinated sericite and fluorinated ZnO particles were able to stabilise dry oil powders in addition to oil liquid marbles and oil foams. Upon vigorous agitation, oil dispersions were obtained in oils of relatively low tension (< 26 mN m^{-1}) and particles of relatively high apparent γ_{sa}. For liquids of higher tension and particles of moderately high apparent γ_{sa} where the apparent advancing θ_{la} is between 73 −130°, foams were obtained. For many of the oils having tension > 27 mN m^{-1} and particles for which apparent advancing $\theta_{la} >$ 65°, oil liquid marbles and dry oil powders were obtained. The dry oil powders did not leak oil for over 2 years. The dry oil powders inverted to ultra-stable oil foams above a critical oil : particle ratio COPR.

List of Symbols and Abbreviations

$A_{ow/la}$	Surface area of a bare swollen droplet/bubble
$\acute{\alpha}$	Shear rate
$c(x)$	Aqueous (oil) phase solubility of oil (water) molecules within a droplet
$c(\infty)$	Aqueous (oil) phase solubility of oil (water) molecules from a planar interface
c_i	Electrolyte concentration
C_a	Capillary number
D_c	Diameter of a cylindrical fluid drop
ρ	Density of a liquid
$\Delta\rho$	Density difference
e	Elementary charge
η	Viscosity of a liquid medium
$\acute{\eta}$	Viscosity of emulsion continuous phase
$\acute{\eta}_{eff}$	Viscosity of emulsion
ε	Dielectric constant of a medium
ε_o	Permittivity of free space
f	Correction factor required to account for the additional volume of the liquid lifted during the detachment of the du Noüy ring from an interface
$f(\kappa_D a)$	Henry’s function
f_w	Fraction of water released in an o/w emulsion
f_o	Fraction of oil released in an o/w emulsion
$f_{\mathrm{PDMS\ oil}}$	Fraction of PDMS oil released from a vegetable oil-PDMS oil emulsion
f_{vo}	Fraction of vegetable oil released from a vegetable oil-PDMS oil emulsion
f_{suno}	Fraction of sunflower oil released from a sunflower oil-PDMS oil emulsion
f_{oo}	Fraction of olive oil released from an olive oil-PDMS oil emulsion
f_{ro}	Fraction of rapeseed oil released from a rapeseed oil-PDMS oil emulsion
F	Maximum force required to detach a du Noüy ring from a fluid interface
g	Gravitational constant
ΔG	Particle detachment energy
ΔG_{sphere}	Minimum particle detachment energy for a spherical small solid particle
ΔG_{rod}	Minimum particle detachment energy for a rod-shaped small solid particle with hemispherical ends
ΔG_{disk}	Minimum particle detachment energy for a rounded disk-shaped/cube-shaped small solid particle

$\Delta_f G$	Free energy of formation of particle-stabilised emulsions and foams
$\Delta_d G$	Free energy of forming a particle-coated droplet/bubble
$\Delta G'$	Free energy of adsorption of a particle to the droplet/bubble surface
ΔG_m	Free energy of adsorption of a spherical particle at liquid-air interface
γ_{eff}	Effective surface tension of a liquid marble
γ_{ie}	Internal phase-external phase interfacial tension
γ_{si}	Solid particle-internal phase interfacial tension
γ_{se}	Solid particle-external phase interfacial tension
γ_{ow}	Oil-water interfacial tension
γ_{so}	Solid particle-oil interfacial tension
γ_{sw}	Solid particle-water interfacial tension
γ_{sa}	Solid particle-air interfacial tension/apparent solid surface energy
γ_{sl}	Solid particle-liquid interfacial tension
$\gamma_{la(\mathrm{exp})}$	Measured (uncorrected) values of surface tension
γ_{la}	Liquid-air interfacial tension/liquid surface tension
$\gamma_{\mathrm{o_1 o_2}}$	Vegetable oil ($\mathrm{o_1}$)-PDMS oil ($\mathrm{o_2}$) interfacial tension
$\gamma_{\mathrm{so_1}}$	Fumed silica particle-vegetable oil interfacial tension
$\gamma_{\mathrm{so_2}}$	Fumed silica particle-PDMS oil interfacial tension
$\gamma_{\mathrm{o_1}}(\gamma_{\mathrm{o_2}})$	Surface tension of vegetable oil (PDMS oil)
$\gamma^{p}_{\mathrm{o_1}}(\gamma^{p}_{\mathrm{o_2}})$	Polar component of the surface tension of vegetable oil (PDMS oil)
$\gamma^{d}_{\mathrm{o_1}}(\gamma^{d}_{\mathrm{o_2}})$	Dispersive component of the surface tension of the vegetable oil (PDMS oil)
h	Film thickness/separation
h_{eq}	Equilibrium film thickness
$h_{critical}$	Critical distance between two particle-stabilised films
k	Boltzmann constant
κ^{-1}	Capillary length of a liquid
κ_D^{-1}	Debye length
l	Radius of flat spot contact zone for liquid marbles
l'	Average length of cube-shaped $CaCO_3$ particles
L	Average length (including hemispherical ends) of rod-shaped $CaCO_3$ particles
L'	Average length (excluding hemispherical ends) of rod-shaped $CaCO_3$ particles
L_c	Length of a cylindrical fluid drop (excluding its hemispherical ends)
n_d	Number of droplets (bubbles) in emulsion (foam)
n_p	Number of particles coating a droplet/bubble

N	Rotational speed (revolutions per min) of a spinning drop tensiometer
N_A	Avogadro's constant
ω	Rotational speed (radians per second) of a spinning drop tensiometer
p	Perimeter of the three-phase contact line during surface tension measurement using the du Noüy ring method
p_c	Capillary pressure of the curved menisci around a surfactant-stabilised film
P_c	Capillary pressure arising from the deformation of an oil-water or liquid-air interface around adsorbed particles
$P_c^{critical}$	Critical capillary pressure which reduces h to $h_{critical}$
P_c^{max}	Maximum capillary pressure that the film withstands before rupturing
ΔP	Laplace pressure
ϕ	Volume fraction of a liquid phase in an emulsion
ϕ_o	Volume fraction of oil in an emulsion
ϕ_c	Slope angle at contact line
ϕ_{suno}	Volume fraction of sunflower oil in a sunflower oil-PDMS oil emulsion
$\phi_{\mathrm{o/o}}$	Volume fraction of a simple o/o emulsion in an o/o/o emulsion
$\Pi(h)$	Disjoining pressure
$\Pi_{vdw}(h)$	van der Waals disjoining pressure
$\Pi_{elec}(h)$	Electrostatic disjoining pressure
Π^{max}	Maximum disjoining pressure
$\Pi_{cap}(h)$	Disjoining pressure associated with the capillary stabilisation of fluid films stabilised by spherical solid particles
r	Radius of a spherical small solid particle
r_r	Radius of a platinum or platinum-iridium alloy wire of a du Noüy ring
r_{rod}	Average radius of rod-shaped $CaCO_3$ particles
R	Gas constant
R'	Radius of a sphere
R_r	Radius of a du Noüy ring
R_c	Radius of a cylindrical fluid drop
$\Delta_a S$	Entropy change due to the de-mixing of particles
τ	Line tension
T	Absolute temperature
$\theta_A(\theta'_A)$	Apparent contact angle of liquid marbles (corresponding bare liquids)
θ_d	Contact angle between the liquid meniscus and the surface of the du Noüy ring

θ_o	Solid particle-vegetable/PDMS oil-air contact angle
θ_{oo}	Solid particle-vegetable oil-PDMS oil contact angle
θ_{ow}	Solid particle-oil-water contact angle
θ_{wa}	Solid particle-water-air contact angle
θ_{oa}	Solid particle-oil-air contact angle
θ_{la}	Solid particle-liquid-air contact angle/apparent contact angle
θ'_{la}	Equilibrium solid particle-liquid-air contact angle associated with liquid marbles
V	Volume of rod- or cube-shaped $CaCO_3$ particles
V_{marble}	Estimated volume of a liquid marble
V_{m}	Molar volume of oil or water
x	Radius of a liquid droplet
x'	Radius of a spherical gas bubble
ζ	Zeta potential
z_i	Valence of counter-ion
BET	Brunauer-Emmett-Teller
BSE	Backscattered electrons
CL	Cathodoluminescence
COPR	Critical oil : particle ratio
IEP	Isoelectric point of proteins
HLB	Hydrophile-lipophile balance
LDV	Laser Doppler velocimetry
OTFE	Oligomeric tetrafluoroethylene
PTFE	Polytetrafluoroethylene
DCDMS	Dichlorodimethylsilane
DLVO	Derjaguin-Landau-Verwey-Overbeek
PVDF	Poly(vinylidene) fluoride
PEEK	Poly(ether ether ketone)
PEI	Poly(ether imide)
PDMS	Polydimethylsiloxane
PMMA	Polymethylmethacralate
R	Alkyl group
SE	Secondary electrons
SEM	Scanning electron microscope

CONTENTS

Chapter 4-Oil-Oil Pickering Emulsions 126

Chapter 5-Influence of the Degree of Fluorination on the Behaviour of Fumed Silica Particles at Oil-Air Surfaces 183

Chapter 1

Introduction

1.1 The Colloidal State and Soft Matter

The atoms and molecules of classical chemistry are extremely small and have molar masses (measurable by freezing point depression), which are < 1000 g mol^{-1}. Macroscopic particles fall into the realm of classical physics and have been studied extensively by classical mechanics. The colloidal state resides between these two extremes. A colloidal system is obtained when small solid particles, liquid droplets or bubbles of one phase are dispersed in a second phase. Either or both phases may be in gas, liquid, solid or supercritical phase states. The particles of colloidal systems are small ($\approx 1-1000$ nm in diameter or length) and hence have high surface area-to-volume ratio, which accounts for some of their unique physical properties. For example, their solutions may have undetectable freezing point depressions and their dispersions (even if very dilute) have the tendency to sediment out very slowly. Whereas particles of classical chemistry may have one or a few electrical charges, colloidal particles may bear several thousands of charges and the charges can significantly affect the action of neighbouring species.[1]

Soft matter is a class of condensed matter comprising of a variety of physical states that are susceptible to small external influences. They have large response functions (*i.e.* a small external influence has a big effect). They have complex microscopic structure, composition and internal dynamics. They include liquid crystals, liquid marbles, dry water (oil) powders, colloidal systems, polymers, granular materials and a number of biological materials like membranes and proteins.[2,3] Colloidal systems have been divided into emulsions, foams, suspensions, gels and aerosols.[4,5] Emulsions, foams, liquid marbles and dry oil powders are the focal point of this work.

1.2 Emulsions, Foams and Liquid marbles

1.2.1 Emulsions and Foams

Emulsions are thermodynamically unstable heterogeneous mixtures of two immiscible liquids (*e.g.* water and oil) in which one of the liquids is dispersed as droplets of microscopic or colloidal size (typically > 1 μm) in the bulk of the other liquid in the presence of emulsifiers, which enhance their kinetic stability.[5,6] The dispersed phase may also be referred to as discontinuous, inner or internal phase, whilst the continuous phase is also known as the outer or external phase.[7] Simple emulsions are often classified as oil-in-water (o/w, *e.g.* condensed milk) and water-in-oil (w/o, *e.g.* oil based cosmetic creams) emulsions depending on which phase forms the dispersed phase. Water-in-water (w/w) emulsions in which water droplets are dispersed in water[8] and oil-in-oil (o/o) emulsions where oil droplets are dispersed in oil[9] are rare types of simple emulsions. Complex emulsion systems like oil-in-water-in-oil (o/w/o) emulsions where an o/w emulsion is in turn dispersed in an oil, water-in-oil-in-water (w/o/w) emulsions where a w/o emulsion is in turn dispersed in water and oil-in-oil-in-oil emulsions (o/o/o) where an o/o emulsion is in turn dispersed in an oil are also known.[10]

Foams are liquid-air systems in which gas bubbles are dispersed in a liquid in the presence of stabilisers (foaming agents). Generally, pure water foams are considered as highly “concentrated emulsions” of air and water (denoted as a/w).[10,11] There are many similarities and differences between stable emulsions and foams. A summary of the differences and similarities between these systems is as follows:

- *Dispersed and continuous phase:* The dispersed phase for an emulsion is usually liquid droplets whilst that for a foam is normally gas bubbles, but the continuous phase for both systems is a liquid.[12,13]
- *Size of dispersed phase:* Gas bubbles in surfactant-stabilised foams are bigger than oil or water droplets in many surfactant-stabilised emulsions. The solubility of small gas bubbles (< 0.1 μm) in foams is higher than that of small oil or water droplets (< 0.1 μm) in emulsions. As a result, the degree of Ostwald ripening (see later) in foams is higher than that in emulsions and hence the difference in the size of dispersed phase.[5]
- *Structure of dispersed phase:* Gas bubbles in foams are generally polyhedral especially if they are stabilised by surfactants. However, oil droplets (o/w) and water droplets (w/o) in emulsions are spherical but concentrated emulsions form polyhedral structures.[14]
- *Instability mechanism:* Foam instability results from thin film drainage (creaming), coalescence and disproportionation (Ostwald ripening or bubble coarsening)[5] and that for emulsion occurs through creaming (o/w), sedimentation (w/o), coalescence, flocculation and Ostwald ripening[6] (see later).
- *Effect of diffusion:* Gas diffusion in foams and that of liquid droplets (< 0.1 μm) in emulsions leads to Ostwald ripening.[15]

- *Stabilisers:* Emulsions and foams are kinetically stabilised by surfactants or nanoparticles or a mixture of both (see later).

1.2.2 Liquid marbles

Aussillous and Quéré[16-19] have shown, more than a decade ago, that hydrophobic powders can spread over water and create a surface film. Their pioneering work has intrigued and formed the basis of liquid marble research. Liquid marbles are liquid-in-air materials (*cf.* foams). They are non-stick millimetre size droplets obtained by encapsulating liquid droplets in micro- or nanoparticles of low surface energy, which have low affinity for the surfaces of the liquid droplets themselves.[16-28] Liquid marbles demonstrate very low friction when rolling on solid substrates. Typical examples of liquid marbles abound in nature. The waste disposal protocol of galling aphids ends up in the formation of liquid marbles. Phloem-feeders excrete large volumes of honey-dew waste in which young or immobile insects can become stuck or asphyxiated. As honeydew is defecated, it is covered with a powdery wax secreted from the anus by the aphid, thus creating a wax-covered sphere which the soldier aphids then roll or kick out of a hole.[29] The principle being used here is a simple one of encapsulating a liquid entirely in a hydrophobic powder. Liquid marble formation also occurs after rain as "summer ice,"[16] after wild-fire creates hydrophobic soil[30,31] and in wet granulation of a highly hydrophobic fine powder.[32] Liquid marbles are separated from a solid or liquid support by air pockets. They are also non-wetting and exhibit a large apparent contact angle θ_A (> 115°, measured into the liquid) on a substrate. The shape of liquid marbles is dictated by the interplay of liquid surface tension γ_{la} and gravity. Whilst surface tension forces dominate in small liquid marbles and are quasi-spherical in shape with a small flat spot where they rest on a solid substrate, large ones are flattened by gravity forces and have a puddle shape.[25] The θ_A comes from the extent of this flat spot contact zone whose radius l depends on the volume of the encapsulated liquid. For water liquid marbles, the size of the flat spot follows the rule[16]

$$l/\kappa^{-1} = (2/3)^{0.5}\left(R'/\kappa^{-1}\right)^{n} \tag{1.1}$$

where R' is the radius of a sphere of equivalent volume, $n = 3/2$ (for large marbles, *i.e.* > 100 μL) or $n = 2$ (for small marbles, *i.e.* < 100 μL), κ^{-1} is the capillary length given by $(\gamma_{la}/\rho g)^{0.5}$ with ρ and g being the density of the liquid and the gravitational constant respectively. For quasi-spherical liquid marbles, $R' << \kappa^{-1}$, but for puddle-shaped liquid marbles $R' >> \kappa^{-1}$.[19] For example the κ^{-1} of water at 25 °C is 2.7 mm and small water liquid marbles (< 100 μL and $R' <$ 2.9 mm) stabilised by poly(2-(diethylamino)ethyl methacrylate) modified polystyrene latex particles are quasi-spherical.[33] However, large ones (> 100 μL and $R' >$ 2.9 mm) adopt a puddle shape.[33] The effective surface tension γ_{eff} of a liquid marble may be smaller or larger than the γ_{la} of the encapsulated liquid depending on the types of interactions (*e.g.* capillary and electrostatic) between the solid particles encapsulating the liquid marble.[25,34] The floating of liquid marbles on the surface of liquids like water has also been reported.[35] Liquid marbles move down easily on an inclined solid substrate with little or no resistance and the deformation of fast moving liquid marbles has also been reported.[16] As the speed of motion increases, centrifugal forces become larger than centripetal forces and the shape of a liquid marble changes from quasi-spherical or puddle to peanut or doughnut shape. Diamagnetically levitated droplets yield similar shapes.[16,18-20] Water liquid marbles stabilised with spherical fumed silica nanoparticles undergo various shape transformations upon freezing which are dependent on the hydrophobicity of the particles, but the original shape of the marbles is recovered once re-melted.[36] For liquid marbles stabilised by the most hydrophobic particles (14% surface residual SiOH), a vertically prolonged morphology with a pointed protrusion on the top is formed on freezing. For those stabilised with the less hydrophobic particles (50−61% surface residual SiOH), a lateral expanded flying saucer-shaped morphology is formed.[36] The different responses to freezing result from the different heterogeneous nucleation sites owning to the different positions of the particles at the water-air interface.[36] Liquid marbles can be viewed as the opposite of foams; however some similarities and differences exist. The differences and similarities between foams and liquid marbles are:

- *Continuous phase:* The continuous phase for a foam is usually a liquid,[37] whilst that for a liquid marble is air.[16]
- *Size of dispersed phase:* The size of a liquid marble is far-far greater than that of a gas bubble in many foams. For example, a 10 μL liquid marble is about 2 × 10^4 times bigger than a gas bubble having a volume-diameter of 100 μm.
- *Instability mechanism:* The processes leading to kinetic instability in foams are film drainage (creaming), coalescence and disproportionation (Ostwald ripening or bubble coarsening).[5] For liquid marbles, instability is mainly due to evaporation of the encapsulated liquid droplet[38] (see later). The higher the vapour pressure of a liquid, the higher the rate of diffusion controlled evaporation and the lower the stability of the liquid to evaporation and vice versa.[39]

- *Shape of dispersed phase:* The structure of gas bubbles in foams may be spherical or polyhedral,[40] but that of liquid marbles is usually quasi-spherical or puddle-like (when at rest)[41] and peanut, disk, doughnut or wheel-shaped (when in motion).[16,18]

1.2.3 Applications of Emulsions, Foams and Liquid Marbles

Important applications of emulsions and foams are ubiquitous. Liquid and solid foams are encountered extensively in the food and beverage industries (*e.g.* cake and beer), cosmetic and personal care industries (*e.g.* body creams, soap and shampoo), textile industries, oil recovery and mineral processing.[42] Emulsions are the end products of many food, cosmetic, agrochemical, petroleum and pharmaceutical industries.[1,10]

Applications of liquid marbles are related to their non-stick properties. The use of liquid marbles for bearing, as micro-pumps and other microfluidic applications have been proposed.[19,43] The use of liquid marbles for gas sensing[44], water storage[45] and remote sensing of water pollution[35] has been demonstrated. Pickering emulsions (millimetre-size) have been prepared from liquid marbles.[46] Water and oil liquid marbles are elements of dry water[47] and dry oil powders,[48] respectively, which are promising candidates in the pharmaceutical and cosmetic industries. Detailed applications of liquid marbles can be found in the reviews of Bormashenko[49] and McHale and Newton.[20]

These numerous applications of emulsions, foams and liquid marbles have made the study of these systems very important and interesting especially in terms of stability.

1.3 The Stability of Emulsions, Foams and Liquid Marbles

1.3.1 Stability of Emulsions

A number of processes are responsible for the breakdown of emulsions and foams (as mentioned earlier in sec. 1.2.1). Emulsion instability occurs through creaming (or sedimentation), flocculation, coalescence, Ostwald ripening and phase inversion (Figure 1.1) which may take place simultaneously or consecutively depending on the conditions.[6,50] ***Creaming*** (typical of o/w emulsions) is the upward movement of oil droplets under gravity or in a centrifuge to form a concentrated layer at the top of the emulsion without any change in the droplet size distribution. This process begins with the development of a concentration gradient in the vertical direction and it is followed by the appearance of a distinct boundary between an upper cream layer and a lower depleted emulsion layer.[6] ***Sedimentation***, which occurs in w/o emulsions is analogous to creaming and involves the downward movement of water droplets under gravitational or centrifugal force.[6]

Figure 1.1. Schematic representation of the processes responsible for the breakdown of a kinetically stable emulsion: (a) kinetically stable emulsion, (b) creaming, (c) sedimentation, (d) flocculation, (e) coalescence, (f) Ostwald ripening and (g) phase inversion. The green circles represent emulsion droplets and the white background is the continuous phase.

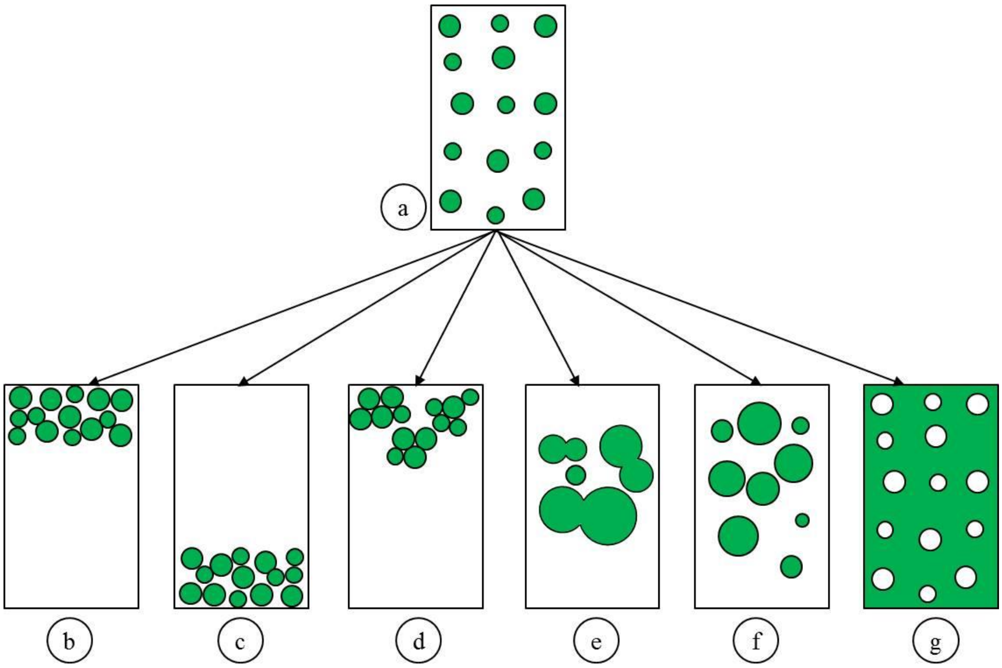

Flocculation is enhanced by polydispersity of the emulsion. It refers to the aggregation of emulsion droplets without rupture of the stabilising thin film layer. In surfactant-stabilised emulsions, it occurs when the interaction free energy between the droplets is slightly negative (*i.e.* secondary minimum) at certain separation.[6] Unlike creaming and sedimentation which are reversible, flocculation may be reversible or irreversible depending on the strength of the inter-droplet forces. Flocculation enhances creaming (or sedimentation) in dilute emulsions. This is so because flocs rise (or sediment) faster than individual droplets due to their large effective radius except in concentrated emulsions where the formation of a gel-like network structure can have a stabilising effect. ***Coalescence*** is an irreversible process whereby two or more emulsion droplets fuse together to form a single large droplet. Here the interaction free energy between the droplets is significantly negative (*i.e.* primary minimum) at certain separation such that thin film rupture is the only likely possibility.[6] ***Ostwald ripening*** (also known as isothermal distillation or molecular diffusion) is the process whereby large droplets grow at the expense of smaller ones. It is caused by diffusion driven mass transport of dispersed phase molecules from one droplet to another through the continuous phase due to the solubility differences of the bigger and smaller droplets.[6] This is because the solubility of an approximately spherical substance increases with decreasing size, according to equation 1.2.[51] The symbol $c(x)$ represents the aqueous phase solubility (mol m^{-3}) of oil or water present within a droplet of radius x, $c(\infty)$ represents the solubility in a system with only a planar interface, γ_{ow} represents the oil-water interfacial tension, R is the gas constant (J mol^{-1} K^{-1}), T is the absolute temperature (K) and V_m represents the molar volume (m^3 mol^{-1}) of the oil (for o/w) or water (for w/o). As such, materials contained within the smaller droplets tend to dissolve and diffuse through the continuous phase re-condensing onto the larger ones. This provides the driving force for the growth of the emulsion droplets. This leads to an overall increase in the size of the emulsion droplets and a corresponding decrease in the interfacial area.[6] ***Phase inversion*** refers to the changing of one emulsion system (say o/w) to another system (say w/o). Phase inversion is a fundamental step in the manufacture of a number of important food products like butter and margarine, but it is undesirable in other products because it alters the product's appearance, texture, stability and taste. Phase inversion is favoured by a change in the composition or environmental conditions of an emulsion like emulsion dispersed phase volume fraction, emulsifier type, solvent conditions, temperature or mechanical agitation. The physicochemical basis of phase inversion is believed to be extremely complex, involving aspects of flocculation, coalescence and emulsion formation.[6]

$$c(x) = c(\infty)\exp\left(\frac{2\gamma_{ow}V_m}{xRT}\right) \tag{1.2}$$

1.3.2 Stability of Liquid Foams

As mentioned previously, certain physical processes are responsible for foam destabilisation. These processes include drainage (or creaming), coalescence (or film rupture) and disproportionation (Ostwald ripening or bubble coarsening) and are illustrated in Figure 1.2. ***Foam drainage*** refers to the physical separation of the gaseous and liquid phases of the foam under gravity. In draining foams, light gas bubbles move upwards forming a denser foam layer on the top, whilst the heavier liquid phase is concentrated at the bottom. Bubbles accumulated on the top usually rearrange and deform to form highly packed foams with polyhedral cells. The microstructure of such a foam is characterised by thin films (or lamellas) between the faces of the touching cells and the so called Plateau borders at the intersection of three neighbouring thin films. ***Coalescence*** occurs when the thin films formed after drainage are not stable enough to keep the touching cells apart, resulting in the merging together of neighbouring bubbles. ***Ostwald ripening*** or ***disproportionation*** is the growth of big gas bubbles at the expense of small ones and it is driven by the difference in the Laplace pressure in the gas bubbles. For a spherical gas bubble of radius x' and liquid-air interfacial tension γ_{la}, the Laplace pressure ΔP is given by $2\gamma_{la}/x'$ (*cf.* equation 1.2), showing that ΔP varies inversely as x'. This causes diffusion of gas molecules from smaller bubbles to larger ones, through the continuous phase, over time.[15,52-56]

Figure 1.2. Schematic representation of the processes responsible for the breakdown of a kinetically stable foam: (a) kinetically stable foam, (b) drainage, (c) coalescence and (d) Ostwald ripening. The green circles represent air bubbles and the white background is the continuous (liquid) phase.

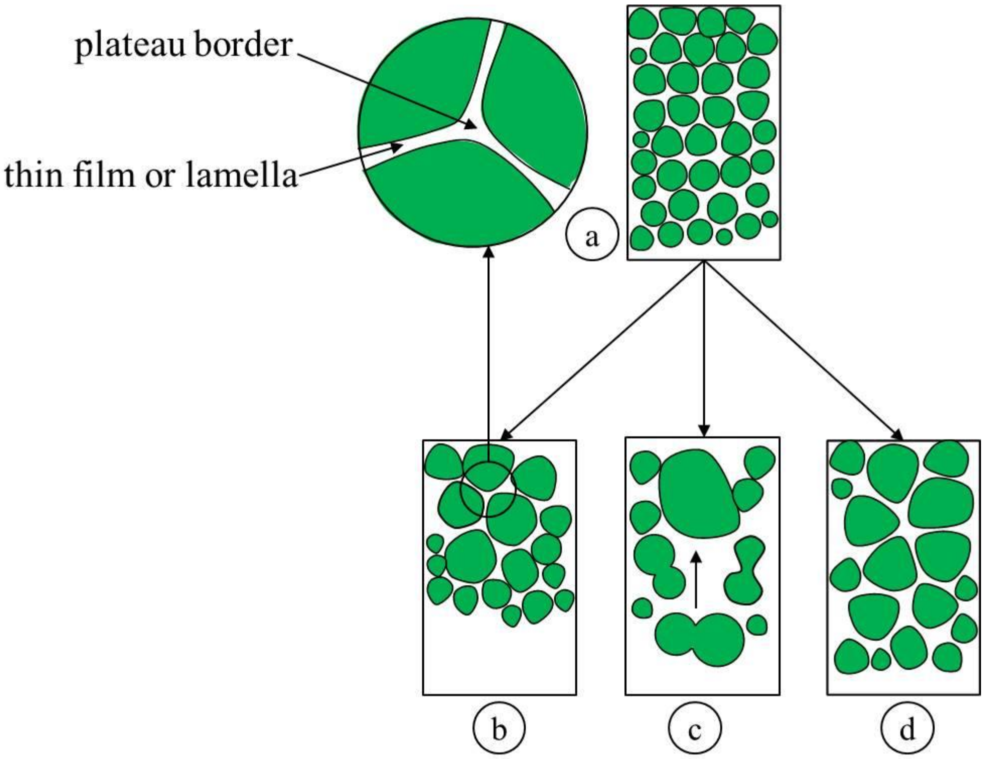

1.3.3 Stability of Liquid Marbles

The stability of liquid marbles to evaporation at a given temperature depends on the vapour pressure of the encapsulated liquid at that temperature and the degree of particle coating. The rate of evaporation is relatively fast for relatively high vapour pressure (or highly volatile) liquids compared with relatively low vapour pressure (less volatile) ones.[39] The particle coating on a liquid marble reduces the rate of evaporation of the encapsulated liquid: the higher the degree of particle coating, the lower the rate of evaporation of the encapsulated liquid and vice versa. Liquid marbles buckle and crumple eventually as the encapsulated liquid evaporates because the particles encapsulating the liquid droplet are progressively forced together[38,57,58] as shown in Figure 1.3. Hollow spherical shells are sometimes left after complete evaporation of the encapsulated liquid.[32,59]

Figure 1.3. Photo of (a) top and (b) side view of a water liquid marble (5 µL) stabilised by polytetrafluoroethylene (PTFE) particles during evaporation at 21−25 °C and relative humidity of 54%, showing the eventual buckling and crumpling of the liquid marble as the encapsulated water evaporates. Taken from ref. 57.

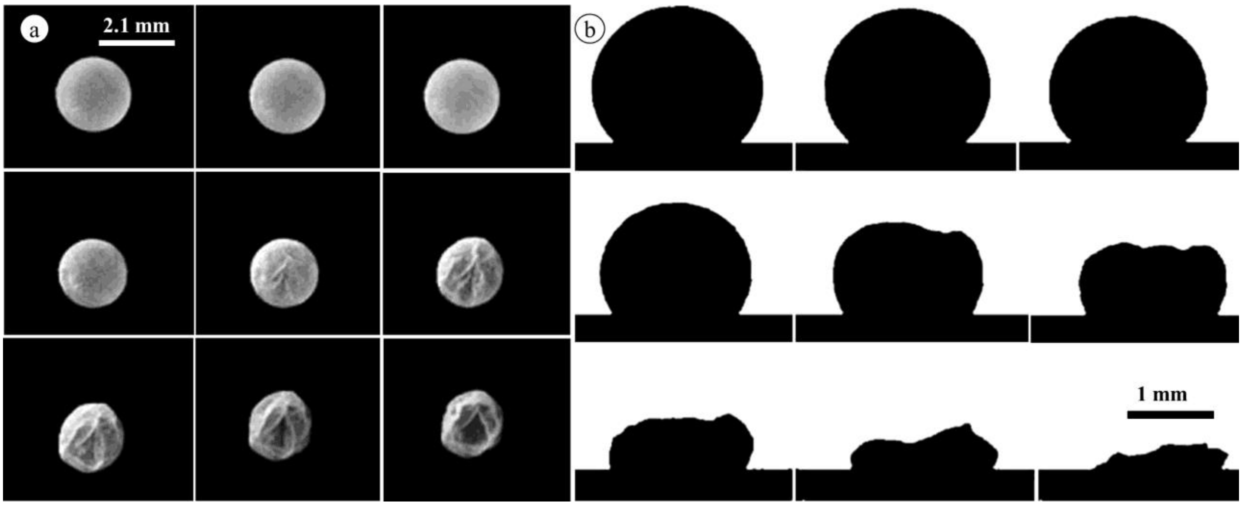

1.4 Stabilisation of Emulsions, Foams and Liquid Marbles

1.4.1 Stabilisation of Emulsions and Foams

Emulsions and foams are usually kinetically stabilised using substances known as stabilisers which include surfactants (surface-active molecules),[60-68] globular proteins,[69-74] polymers,[75-77] solid nanoparticles[13,50,52,78-81] and nanoparticle-surfactant mixtures leading to phase inversion in some cases.[82-84] The aim of this section is to look at particle-stabilised emulsions and foams under two themes: conditions necessary for stabilisation and the mechanism of stabilisation which will be compared with surfactants and the other stabilisers where possible.

1.4.1.1 Particle-Stabilised Emulsions and Liquid Foams: Conditions Necessary for Stabilisation

The fact that finely divided solid particles can act as stabilisers in emulsions has been known since the beginning of the last century. Ramsden[85] reported the formation of a membrane of solid particles enveloping both air bubbles in water and oil droplets in water, giving rise sometimes to ‘persistently deformed sharply angular and grotesque shapes of the emulsified globules’. Four years later, Pickering,[86] citing the work of Ramsden, noted that particles which are wetted more by water than by oil act as emulsifiers for o/w emulsions by residing at the oil-water interface. Particle-stabilised emulsions are often also called Pickering emulsions, but it is not clear why these emulsions are named after Pickering as he was not the first to report them. Finkle *et al.*[87] studied the relationship between the type of solid particle, the nature of the liquid and emulsion type (o/w or w/o). They reported that in an emulsion containing solid particles, one of the liquids will probably wet the solid particles more than the other liquid, with the poorly wetting liquid becoming the dispersed phase. This means that water-wet particles (*i.e.* hydrophilic) like silica would stabilise o/w emulsions whilst particles not wetted by water (*i.e.* hydrophobic), but wetted by oil like carbon black should stabilise w/o emulsions. This is analogous to Bancroft’s rule for surfactant-stabilised emulsions[88] as verified by Binks and Lumsdon[89] using partially hydrophobic silica nanoparticles with toluene-water emulsions at different pH. These ideas have been supported by the experiments of Schulman and Leja[90] using $BaSO_4$ crystals and surfactant, measuring the relevant three-phase contact angles θ_{ow} and determining the emulsion type and stability. The link between emulsion type (for equal volumes of water and oil) and the θ_{ow} at the oil-water interface for different solids and a range of oil has also been reported by Aveyard *et al.*[80] Generally, θ_{ow} is measured through the aqueous phase. Refs. 80 and 90 reported that hydrophilic (hydrophobic) spherical solid particles in which θ_{ow} is $< 90°$ ($> 90°$), o/w (w/o) emulsions are stabilised. However, if the particles are too hydrophilic (low θ_{ow}, *ca.* 0°) or too hydrophobic (high θ_{ow}, *ca.* 180°) they tend to remain dispersed in either the aqueous or oil phase, respectively, and no emulsion is stabilised. Binks[91] has suggested that the wettability of particles, quantified by θ_{ow}, is akin to the hydrophile-lipophile balance (HLB) proposed by Griffin[92,93] to account for the type of emulsions stabilised by surfactants. According to Griffin, surfactants with relatively small HLB number (3−6) should stabilise w/o emulsions whilst those with relatively large HLB number (8−40) should stabilise o/w emulsions. Important differences and similarities between surfactant molecules and spherical nanoparticles have been covered in the reviews of Binks[91] and Aveyard *et al.*[80] Even though much is known about particle-stabilised aqueous emulsions, very little is known about particle-stabilised non-aqueous emulsions. The reasons for this are not clear. The few papers existing on the subject have reported that hydrophobic particles are the ideal particles for stabilising these emulsions.[94-97]

Recently, the use of colloidal particles (solely[52,98] or in combination with amphiphiles[78,84]) to stabilise liquid-air materials like foams has gained significant attention. This is partly due to success with emulsions and partly due to the fact that solid particles alone have been known to stabilise different types of foams in certain natural processes. For example, foams are stabilised by colloidal particles such as bacteria, soil, insoluble precipitates of hydrolysed cations such as iron hydroxides and viruses in waste water.[11] Similar to oil-water systems, particle wettability, quantified by the contact angle the particles make with the liquid (water w or oil o)-air (a) θ_{wa} or θ_{oa}, dictates the type of end material which could be a foam or liquid marble. Spherical hydrophilic (oleophilic) particles exhibiting $\theta_{wa}(\theta_{oa}) < 90°$ prefer to stabilise aqueous (oil) foams.[99-101] However, the spherical hydrophobic and oleophobic particles exhibiting θ_{wa} (θ_{oa}) > 90° preferentially stabilise water and oil liquid marbles,[39,101] respectively. Again, none of these materials are stabilised when the particles are too hydrophilic (oleophilic) or too hydrophobic (oleophobic). In the last instances, particles of high hydrophobicity or oleophobicity might temporary adsorb at the water-air or oil-air interface to temporary stabilise foams which collapse rapidly to release the gas in the air bubbles which appears as 'climbing films.'[102,103]

A good number of solid particles (only or in combination with other amphiphiles) have been used separately as stabilisers of simple or complex emulsions and foams. In the case of emulsions some of these particles include iron oxide, aluminium oxide, partially hydrophobised silica,[104] calcium carbonate,[105] clay[106] and carbon black.[107] For aqueous foams, the particles commonly used are partially hydrophobised silica,[52] polymeric particles like PTFE, poly(vinylidene) fluoride PVDF, poly(ether ether ketone) PEEK, poly(ether imide) PEI,[98] aluminium oxide plus short chain amphiphiles,[79] laponite clay plus surfactants[108,109] and calcium carbonate plus anionic surfactants.[84] The particles commonly used in stabilising oil foams are oligomeric tetrafluoroethylene OTFE,[101,110] partially fluorinated silica[39] and fluorinated clay particles.[48] Apart from particle wettability, the effectiveness of solid particles in stabilising emulsions and foams also depends on particle size, particle surface energy, particle shape, particle concentration, particle-particle interactions[91] and other factors like line tension,[111] as discussed below. For successful stabilisation, the particles need to be smaller than the droplets so that they can be properly located around the droplets. Tavacoli *et al.*[112] have shown that emulsion droplets stabilised by solid particles become unstable beyond a size threshold set by gravity. The size of the particle does not correlate to the size of the droplets formed in the stable emulsions.

Generally the overall stability is inversely proportional to particle size, with the smaller particles giving a higher packing efficiency and so producing a more homogenous layer. Some studies have shown that stable emulsions can only be obtained if the particles are weakly flocculated,[106,113,114] but particle flocculation has been avoided in other studies by adsorption of suitable amphiphilic molecules (surfactants) on the particles.[115] The adsorption of amphiphiles on particle surfaces changes their wettability and in some cases induces emulsion phase inversion.[105] The adsorption of the particles at oil-water and liquid-air interfaces occurs by self-assembly and is spontaneous if the interfacial tension between the internal *i* and external *e* phases γ_{ie} exceeds the difference between the solid *s*-internal phase interfacial tension γ_{si} and the solid-external phase interfacial tension γ_{se}, *i.e.* $\gamma_{ie} > |\gamma_{si} - \gamma_{se}|$.[116] With reference to Figure 1.4, the balance between these interfacial tensions, ignoring effects of line tension τ, is given by Young equation for a spherical solid particle (*s*) at planar oil (*o*)-water (*w*) and liquid (*l*)-air (*a*) interfaces by equation 1.3. The τ is the excess free energy per unit length of the three-phase contact line.

Figure 1.4. Schematic representation of a spherical solid particle at an oil-water interface (left) and a liquid-air interface (right) showing the various interfacial tensions and the contact angle (< 90°) measured into the more polar phase.

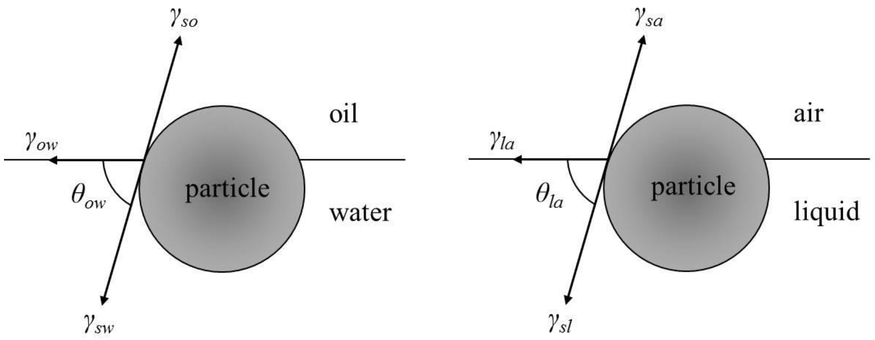

$$\gamma_{ow}\cos\theta_{ow} = \gamma_{so} - \gamma_{sw}; \text{ oil-water interface} \quad (1.3a)$$

and

$$\gamma_{la}\cos\theta_{la} = \gamma_{sa} - \gamma_{sl}; \text{ liquid-air interface} \quad (1.3b)$$

Kinetically stable emulsions and foams have been obtained with particles of different shapes *viz* spherical,[50,117] disk-shaped,[106] cube-shaped,[118] peanut-shaped,[118] ellipsoidal[119] and platelet[120] particles for emulsions and spherical,[40,52] rod-shaped[77] and platelet[48] particles for foams. Comparison of the effectiveness of these particles in stabilising these systems is not straightforward as the chemical composition, size and method of preparation of the particles are different. However, using hydrophilic hematite particles of different aspect ratios (*i.e.* 1−6, where 1 corresponds to spherical particles), it has been shown[119] that relatively small amount of the high aspect ratio (> 4.6) particles is required to stabilise decane-in-water emulsions compared with the low aspect ratio ones. This shows that anisotropic particles are better stabilisers of emulsions compared with isotropic ones, but further investigation is needed. Irrespective of particle shape, the kinetic stability of emulsions and foams increases with increasing particle concentration.[50] In emulsions, the average droplet size decreases as particle concentration increases and eventually becomes independent of particle concentration. This is because the droplet size of the emulsions in the first and second regimes is controlled by droplet coalescence and droplet breakage, respectively.[121] Generally during emulsification, work is done by the applied shear stresses against the fluid interfacial tension (γ') to elongate and rupture larger droplets into smaller ones.[6] In order to deform a single droplet of radius x, the viscous shear stress of the continuous phase ($\acute{\eta}\acute{\alpha}$) must overcome the Laplace pressure (γ'/x), where $\acute{\eta}$ is the continuous phase viscosity and $\acute{\alpha}$ is the shear rate. For rupturing to occur, the capillary number C_a ($= \acute{\eta}\acute{\alpha}x/\gamma'$) must exceed a critical value of the order of unity. In certain cases seen experimentally, however, a droplet is stretched under shear into an enlongated liquid thread that undergoes a capillary instability and breaks into a chain of droplets.[6] The critical capillary number is greater than unity and the elongated droplets look like liquid cylinders whose radius becomes the radius of the droplets. In a real emulsion of many interacting droplets, $\acute{\eta}$ is replaced by an elevated effective viscosity ($\acute{\eta}_{eff}$) which takes into account the volume fraction (ϕ) of the inner phase. Thus, the viscosity of the emulsion and not just that of the continuous phase alone determines the shear stress governing the rupturing and hence the droplet radius x.[6] Experiments have shown that particles adsorbed at fluid interfaces interact through van der Waals, electrostatic and capillary forces, which are either attractive or repulsive and hence affect the packing of the particles.[11,122-124] Stability is enhanced if the forces enhance the degree of particle coating on the fluid interfaces and vice versa.[125] Lastly, theoretical studies have shown that τ has a significant influence on the free energy of particle-stabilised emulsions. Typical values of τ are of the order of $\geq \pm 10^{-11}$N.[126] It has been shown that values of τ of $\pm 10^{-6}$ N have drastic effects on the thermodynamic stability of particle-stabilised emulsions at least for particles of radii 10−20 nm.[80]

1.4.1.2 Particle-Stabilised Emulsions and Liquid Foams: Mechanism of Stabilisation of Emulsions and Liquid Foams by Small Solid Particles

The overall stability of emulsions and foams is determined by the stability of the thin liquid films between the neighbouring droplets/bubbles. In systems stabilised by ionic surfactants, film stability is described reasonably by accounting for the van der Waals attractive forces which tend to push the droplets/bubbles against each other and the electrostatic interactions which tend to push the droplets/bubbles away from each other (Derjaguin-Landau-Verwey-Overbeek DLVO theory).[127,128] For non-ionic surfactants and flexible polymer chains, film stability is accounted for by considering the steric repulsion between the film surfaces which originates from the overlapping of the hydrophilic heads (or chains) of the surfactant (polymer) in the interior. In the case of charged flexible polymers, both electrostatic and steric interactions are operative.[121,129-132] The formation of emulsions in the presence of globular proteins, at high electrolyte concentration and/or around the isoelectric point (IEP) of the protein, has been described by considering the globular protein molecule as small nanoparticles. Just like in the case of ionic surfactants, the stability of o/w emulsions stabilised by the protein molecules at low electrolyte concentrations and pH away from the IEP can be successfully explained by considering the electrostatic and van der Waals interactions.[131] Both electrostatic and steric interactions can be explained in terms of excess osmotic pressure of water in the thin film. This excess pressure is created by the concentration gradient of counter-ions (for ionic surfactants) or hydrophilic segments (for non-ionic surfactants and polymers) between the middle of the film and the bulk continuous phase.[120] The osmotic pressure tends to "suck in" water from the bulk phase, thus creating an effective repulsion between the film surfaces and tends to stabilise emulsions and foams. This implies that for such a film to be in mechanical equilibrium, the repulsive surface forces in the film need to be counterbalanced by surface forces pushing the film surfaces against each other. Theoretical analysis shows that the condition for mechanical equilibrium in the film may be given by $\Pi(h) = p_c$.[121,127] $\Pi(h)$ is the disjoining pressure, p_c is the capillary pressure of the curved menisci around the film which tends to squeeze the liquid from the film and h is the film thickness/separation. The disjoing pressure is excess force per unit area due to the overlapping of the surface layers of approaching droplets or gas bubbles. The molecular theory of surface forces gives expressions for the $\Pi(h)$ corresponding to different types of molecular interactions like van der Waals, electrostatic, steric and oscillatory interactions. According to the DLVO theory, the overall $\Pi(h)$ for emulsions and foams stabilised by ionic surfactant contains contributions from the van der Waals $\Pi_{vdw}(h)$ and electrostatic

$\Pi_{elec}(h)$ disjoining pressures. When the disjoining pressure isotherm, $\Pi(h)$ *versus* h curve, is entirely negative (positive), the thin film between the droplets/bubbles is unstable (stable) and ruptures (does not rupture) causing the two droplets to coalesce. However, if the isotherm has a maximum Π^{max}, the thin liquid film may be stable if the maximum is above the p_c of the droplets/bubbles (Figure 1.5).[127,128]

Figure 1.5. Sketch of the disjoing pressure $\Pi(h)$ *versus* film thickness h (solid curve). The two main contributions to $\Pi(h)$ are the repulsive electrostatic disjoing pressure $\Pi_{elec}(h)$ and the attractive van der Waals disjoining pressure $\Pi_{vdW}(h)$ forces, both given by broken curves. The h_{eq} is the equilibrium film thickness.The green circles represent liquid droplets (in emulsions) or gas bubbles (in foams) and are considered to be coated with the necessary surfactant (*e.g.* cationic as shown in the inset).

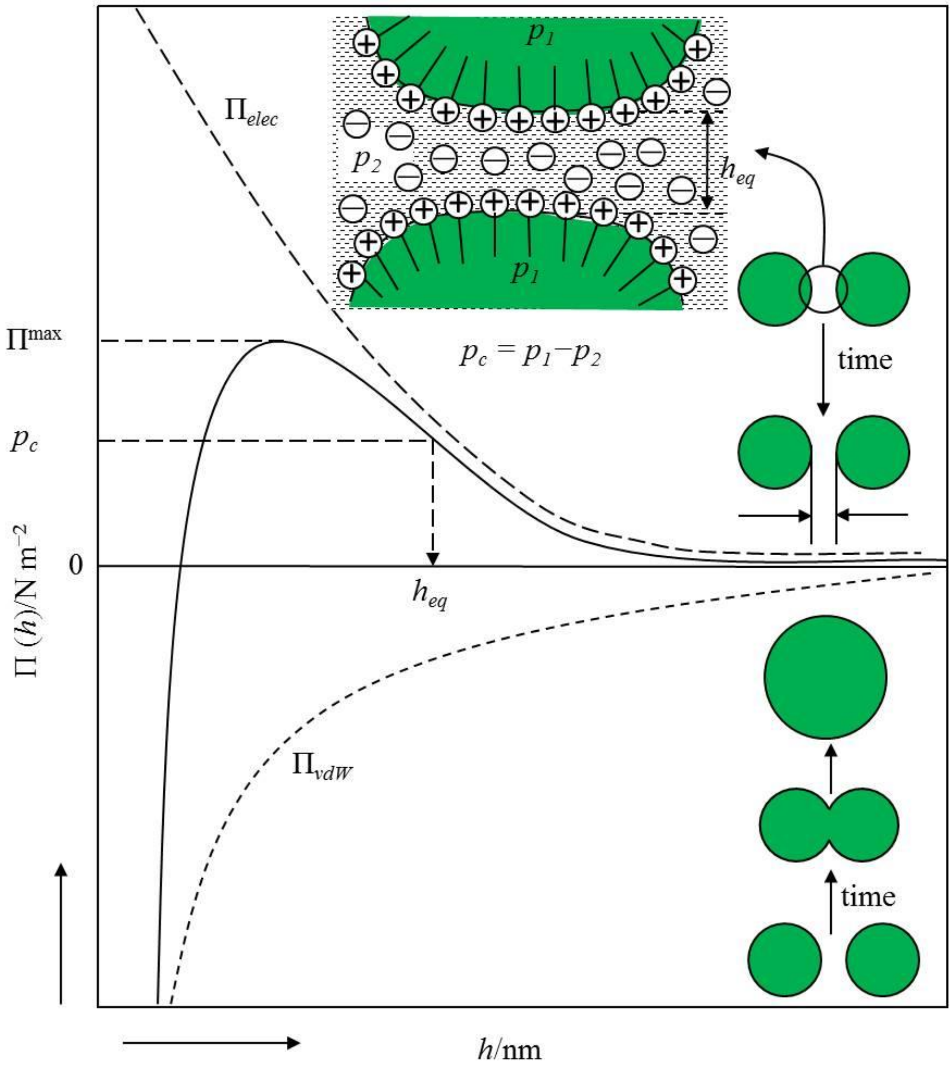

Colloidal particles stabilise emulsions and foams by adsorbing at the oil-water or liquid-air interface to form a monolayer or multilayer around the dispersed droplets/bubbles. This 'armours' the droplets/bubbles and prevents coalescence. The formation of a three-dimensional network of particles in the continuous phase around the droplets due to particle-particle interactions offers additional stabilisation. The three-dimensional network of particles enhances the viscosity of the continuous phase reducing the rate and extent of creaming or sedimentation.[80,133] Particle-stabilised emulsions and foams are more kinetically stable compared with the surfactant-stabilised ones.[80,91,134,135] This outstanding stability has been linked to the strength with which the particles are held at an oil-water or liquid-air interface. This strength is quantified by the particle detachment energy ΔG[136]. The ΔG represents the minimum amount of energy required to remove a particle from an interface into one of the phases in the absence of τ. For a spherical particle of radius r at a planar oil-water or liquid-air interface, the particle detachment energy ΔG_{sphere} is[50]

$$\Delta G_{sphere} = \begin{cases} \pi r^2 \gamma_{ow} (1 \pm \cos\theta_{ow})^2; \text{ oil-water interface} & (1.4a) \\ \pi r^2 \gamma_{la} (1 \pm \cos\theta_{la})^2; \text{ liquid-air interface} & (1.4b) \end{cases}$$

The sign in the brackets is negative (positive) if the particle can be removed easily into the more polar (less polar) phase. The value of ΔG is usually relatively large compared with the thermal energy kT (where k is the Boltzmann constant and T is the absolute temperature). Because of the large value of ΔG, the capillary pressure (P_c) arising from the deformation of the oil-water or liquid-air interface around the adsorbed particles when liquid is squeezed out of the thin film between liquid droplets/gas bubbles is also large.[137] The large value of P_c is the main reason why particle-stabilised emulsions are stable to coalescence. P_c is discussed in detail later. The variation of ΔG_{sphere} with θ_{ow} and γ_{ow} for a typical particle at an oil-water interface has been described theoretically in different papers.[50,116,138] A plot of ΔG_{sphere} *versus* θ_{ow} for an oil-water interface typical of heptane-water interface in ref. 50 has been reproduced in Figure 1.6 (a) along with ΔG_{sphere} *versus* θ_{wa} for a water-air interface (Figure 1.6 (b)). It can be seen that in both cases ΔG_{sphere}: (i) into water is smaller than that into oil (air) for hydrophilic particles (θ_{ow}, $\theta_{wa} < 90°$) and vice versa for hydrophobic particles (θ_{ow}, $\theta_{wa} > 90°$), (ii) increases from zero with increasing $\theta_{ow}(\theta_{wa})$ reaching a maximum at 90° and then decreases to zero at 180° and (iii) is much greater than the thermal energy kT except for very small and large values of $\theta_{ow}(\theta_{wa})$. The adsorption of particles at these fluid interfaces is considered irreversible due to the large detachment energy compared with surfactant molecules which are usually in dynamic equilibrium. This is another reason why particle-stabilised emulsions and foams are exceptionally stable. Lastly, ΔG_{sphere} for the water-air interface > that for the oil-water interface, as expected from the fluid interfacial tensions.

Figure 1.6. (a) Free energy ΔG_{sphere} of detachment of a spherical particle (r = 10 nm) into water (●) and into oil (○) for an oil-water interface (γ_{ow} = 50 mN m^{-1}) and (b) ΔG_{sphere} of detachment of the same particle into water (◆) and into air (◇) for water-air interface (γ_{wa} = 72 mN m^{-1}) calculated by using equation 1.4 *versus* the three-phase contact angles (θ_{ow} or θ_{wa}). Figure 1.6 (a) has been reproduced from ref. 50.

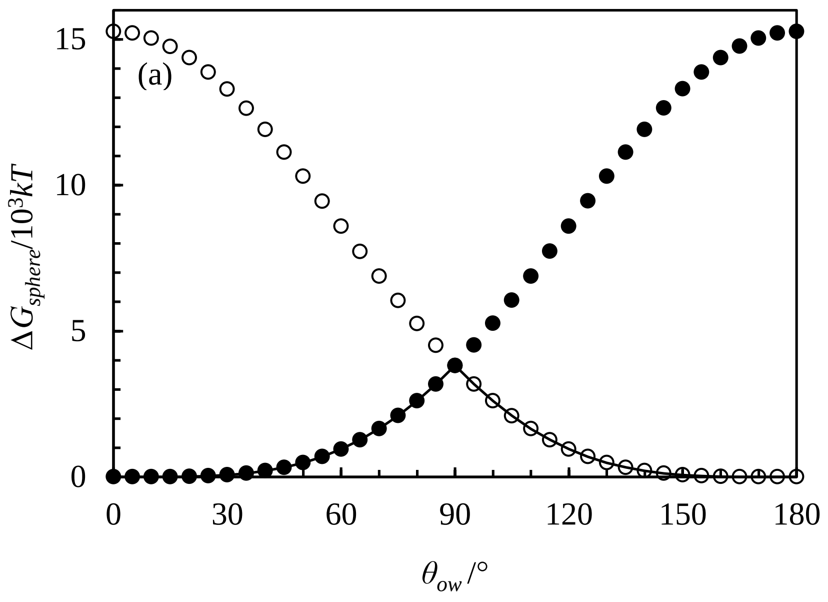

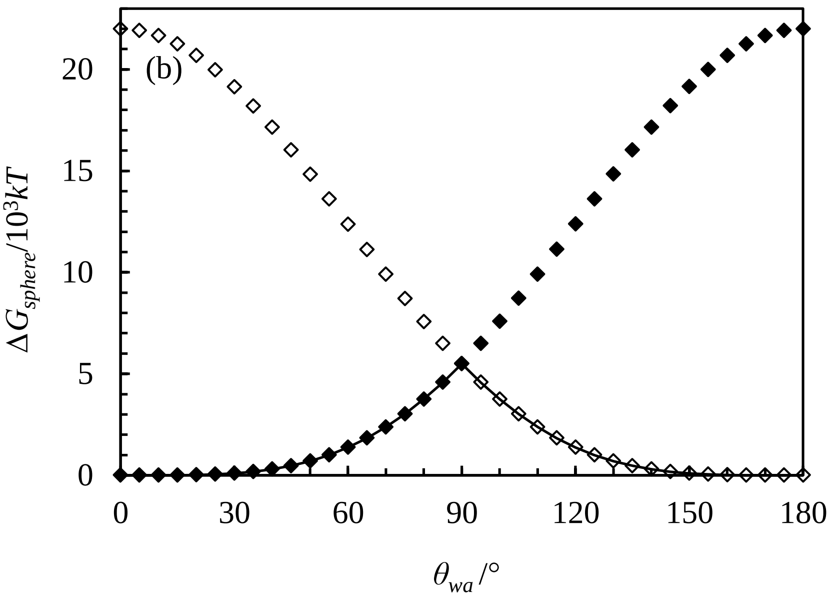

With reference to Figure 1.7, the appropriate minimum particle detachment energy for a rod-shaped particle with hemispherical ends ΔG_{rod} and for a rounded disk-shaped particle ΔG_{disk} at an oil-water, in the absence of τ, is given in equation 1.5 and 1.6,[50] respectively. The corresponding equations for liquid-air interfaces (*e.g.* water-air) can be obtained by replacing γ_{ow} and θ_{ow} with γ_{wa} and θ_{wa}, respectively. Theoretical comparison of these energies shows that the magnitude of particle detachment energy for the same volume of particle follow the order: $\Delta G_{sphere} < \Delta G_{rod} < \Delta G_{disk}$.[50] Theoretically, it has been shown that spherical particles (r = 10 nm) exhibiting θ_{ow} of 8º ($\Delta G_{sphere} \approx 0.4\ kT$) can hardly remain permanently adsorbed at an oil-water interface. Nevertheless, a rounded disk-shaped particle made of the same material and having the same volume ($a/b \approx 2$) and θ_{ow} ($\Delta G_{disk} \approx 10\ kT$) would remain permanently adsorbed at the same interface.[50] This shows that re-shaping spherical particles into rods or disks at constant volume can improve their attachment to fluid interfaces and hence the stability of the end materials. This is in line with recent experimental findings.[118] This might be very advantageous when stabilisation of emulsions and foams by these solid particles is pursued.

Figure 1.7. Cross section of a: (a) rod-shaped colloidal particle with hemispherical ends, (b) rounded disk-shaped colloidal particle along their long semi-axis a and (c) corresponding cross section of the particles along their short semi-axis b at a planar oil-water or water-air interface making contact angle of $\theta_{ow}(\theta_{wa})$ with the interfaces. Taken from ref. 50.

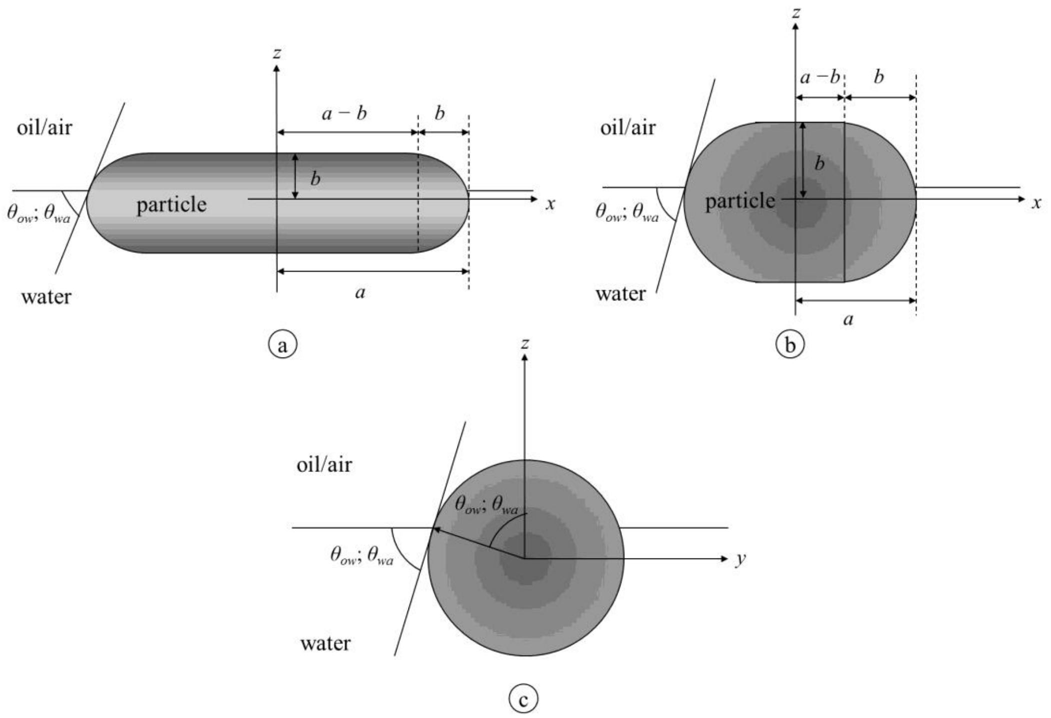

$$\Delta G_{rod} = \begin{cases} \pi\,\gamma_{ow} b^2 \left(1-\cos\theta_{ow}\right)\left[1+\dfrac{4\left(a/b-1\right)\left(\sin\theta_{ow}-\theta_{ow}\cos\theta_{ow}\right)}{\pi\left(1-\cos\theta_{ow}\right)^2}\right]; \\ 0^{\circ} \le \theta_{ow} \le 90^{\circ} \\ \pi\,\gamma_{ow} b^2 \left(1-\cos\theta_{ow}\right)\left[1+\dfrac{4\left(a/b-1\right)\left(\sin\theta_{ow}-\theta_{ow}\cos\theta_{ow}\right)}{\pi\left(1-\cos\theta_{ow}\right)^2}\right] + 4\,\pi\,\gamma_{ow} b^2 \cos\theta_{ow}\left(a/b\right); \\ 90^{\circ} \le \theta_{ow} \le 180^{\circ} \end{cases} \tag{1.5}$$

$$\Delta G_{disk} = \begin{cases} \pi\,\gamma_{ow} b^2 \left(1-\cos\theta_{ow}\right)\left[1+\dfrac{\left(a/b-1\right)^2}{1-\cos\theta_{ow}}+\dfrac{2\left(a/b-1\right)\left(\sin\theta_{ow}-\theta_{ow}\cos\theta_{ow}\right)}{\left(1-\cos\theta_{ow}\right)^2}\right]; \\ 0^{\circ} \le \theta_{ow} \le 90^{\circ} \\ \pi\,\gamma_{ow} b^2 \left(1-\cos\theta_{ow}\right)\left[1+\dfrac{\left(a/b-1\right)^2}{1-\cos\theta_{ow}}+\dfrac{2\left(a/b-1\right)\left(\sin\theta_{ow}-\theta_{ow}\cos\theta_{ow}\right)}{\left(1-\cos\theta_{ow}\right)^2}\right] \\ +\,2\,\pi\,\gamma_{ow} b^2 \cos\theta_{ow}\left[\left(a/b-1\right)^2+\pi\left(a/b-1\right)+2\right]; 90^{\circ} \le \theta_{ow} \le 180^{\circ} \end{cases} \tag{1.6}$$

Theoretical investigation has shown that, the ΔG of a Janus particle (*i.e.* an amphiphilic solid particle, *cf.* surfactants) for fluid interfaces is about 3 times larger than that of the same particle of homogenous wettability and they remain strongly adsorbed for even average contact angles approaching 0 or 180°.[138] This might also be advantageous when stabilisation of emulsions and foams with these particles is pursued. The free energy of particle attachment to fluid interfaces, $\Delta G' = -\Delta G$, is negative for all contact angles except 0 and 180°. This means that the adsorption of solid particles at fluid interfaces is thermodynamically favourable. Although this might not be true in the case of relatively small particles in the presence of positive τ acting to contract the contact line[111]. The free energy of formation of particle-stabilised emulsions and foams $\Delta_f G$ (equation 1.7, for spherical particles)[139] is positive. This means that particle-stabilised emulsions and foams are thermodynamically unstable. However, some Janus particle-stabilised emulsions are thermodynamically stable.[139]

$$\Delta_f G = n_d \Delta_d G = n_d\left[A_{ow(la)}\,\gamma_{ow(la)} + n_p\left(\Delta G' - T\Delta_a S\right)\right] \tag{1.7}$$

The n_d stands for the number of droplets(bubbles) in the emulsion(foam), n_p is the number of particles coating a droplet(bubble), $\Delta_d G$ represents the free energy of forming a particle-coated droplet(bubble), $A_{ow(la)}$ is the surface area of a bare swollen droplet(bubble), $\gamma_{ow(la)}$ denotes the oil-water(liquid-air) interfacial tension, $\Delta G'$ is the free energy of adsorption of a particle to the droplet(bubble) surface, T is the absolute temperature of the system and $\Delta_a S$ is the entropy change due to the de-mixing of particles from the phase in which they were initially dispersed.

Emulsion droplets or foam bubbles may share a particle layer or exist as individual particle-coated droplets or bubbles[121] as shown in Figure 1.8. The P_c represents the 'pressing force' per unit area required to reduce the distance h between two emulsion droplets or foam bubbles coated with spherical solid particles to a critical distance $h_{critical}$. $h_{critical}$ is of the order of 30 nm.[140] At this distance, the film spontaneously thins down and ruptures under the action of attractive van der Waal forces. Suppose that the pressure inside a particle-coated emulsion droplet or foam bubble is P_1 and that in the continuous phase is P_2, $P_c = P_1 - P_2$. Two types of film thinning have been proposed depending on whether the particles form a monolayer or bilayer inside the film as shown Figure 1.8. In the first, typical of films containing particle monolayer, h decreases as P_c increases up to the critical capillary pressure $P_c^{critical}$ which reduces h to $h_{critical}$. $P_c^{critical}$ is the maximum capillary pressure $P_c^{\max}$ that the film withstands before it ruptures. In the second, typical of films containing a bilayer of particles, P_c passes through a maximum $P_c^{\max}$ before the condition $h = h_{critical}$ is reached. After $P_c^{\max}$ is reached, the subsequent film thinning down to $h_{critical}$ is spontaneous as the film is mechanically unstable. $P_c^{\max}$, here also, represents the maximum capillary pressure that the film resists before it ruptures. Stable films (irrespective of the number of particle layers) have high $P_c^{\max}$. This prevents the thinning down of the liquid film between emulsion droplets and foam bubbles. This also makes particle-stabilised emulsions and foams stable against coalescence. Several mathematical forms of $P_c^{\max}$ are available.[137,141-144] The general form is given in equation 1.8.[145] The positive (negative) sign refers to o/w emulsions and liquid foams (w/o emulsions) and p and z are functions of particle arrangement. Numerical values of p and z can be found in ref. 145. Suppose that the disjoining pressure associated with the capillary stabilisation of fluid films stabilised by spherical colloidal particles is $\Pi_{cap}(h)$ for a regular array of particles (monolayer or bilayer), the condition for mechanical equilibrium of the fluid films, at least at the phenomenological level, is $P_c = \Pi_{cap}(h)$.[137]

Figure 1.8. Schematic illustration of the structure of a (a) monolayer and (b) bilayer of spherical solid particles stabilising an emulsion/foam film, (c) the curved shaped of the meniscus around a particle in the monolayer with θ as $\theta_{ow(wa)}$, ϕ_c as the slope angle at contact line and h as the film thickness or distance between two emulsion droplets/foam bubbles and (d) curves showing the dependence of h on P_c for a film stabilised by (i) particle monolayer and (ii) particle bilayer. Taken from ref. 121.

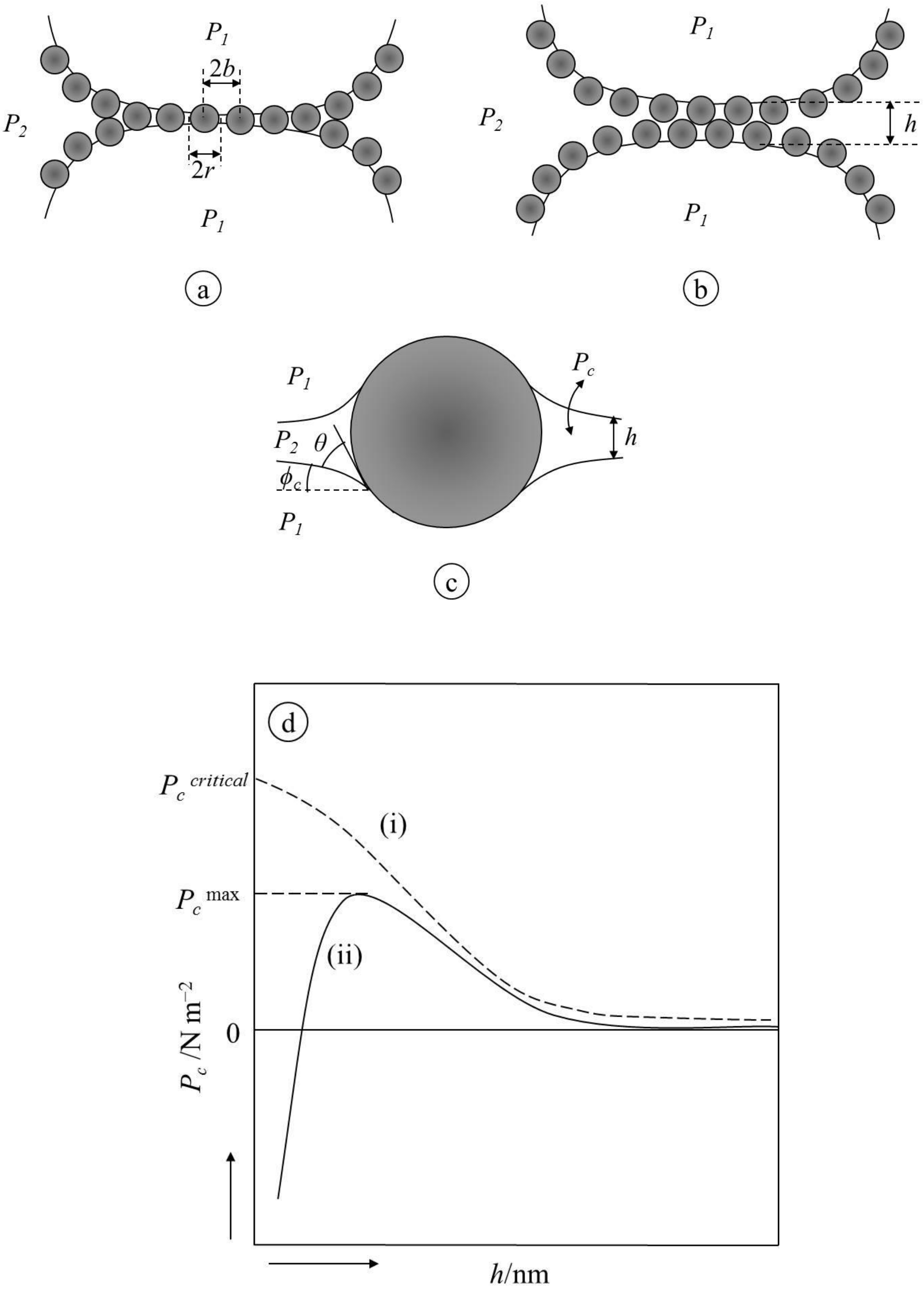

$$P_c^{\max} = \pm \frac{2p\gamma_{ow(wa)}\left(\cos\theta_{ow/wa} \pm z\right)}{r} \tag{1.8}$$

According to equation 1.8, $P_c^{\max}$ is proportional to $1/r$. That is, relatively small particles will give more stable films. $P_c^{\max}$ is affected by particle arrangement *e.g.* interparticle distance in the adsorption layers and that it is proportional to the cosine of the three-phase contact angles. The lower angles correspond to higher $P_c^{\max}$ (*i.e.* to more stable films). In other words, 0° (or 180°) and 90° correspond to stable and unstable films, respectively, which is the exact opposite of the predictions of ΔG. The combined effect of ΔG_{sphere} and $P_c^{\max}$ on films containing single layer and close-packed double layer of particles has been studied.[145] For a single layer of particles, kinetically stable o/w emulsions and foams were predicted at $15° < \theta_{ow(wa)} < 90°$ whilst kinetically stable w/o emulsions were predicted at $90° < \theta_{ow} < 165°$. For a double layer of particles, kinetically stable o/w emulsions and foams were predicted at $15° < \theta_{ow(wa)} < 129°$ whilst kinetically stable w/o emulsions were predicted at $50° < \theta_{ow} < 165°$. In both cases, optimum contact angle of stabilisation lies between 70−86° for o/w emulsions and foams and 94−110° for w/o emulsions. Although measurement of the contact angles small solid particles make with fluid interfaces is difficult, these predictions are in good agreement with experiments.[101,146] Finally, the stability of particle-stabilised emulsions and foams to Ostwald ripening has been explained in terms of the mechanical resistance of the particle-coated surfaces to shrinkage and/or expansion.[147]

1.4.2 Stabilisation of Liquid Marbles

Unlike emulsions and foams which can be kinetically stabilised by surfactants, polymers, proteins and small solid particles or a mixture of surfactant and small solid particles, liquid marbles are stabilised by only low surface energy small solid particles. The examples of these particles are given in Table 1.1. Such particles might be hydrophobic with low affinity for water,[36,148] superhydrophobic with extremely little affinity for water,[149] oleophobic with low affinity for oils,[101] superoleophobic with extremely little affinity for oils,[150] omniphobic with low affinity for both water and oils[39,48] or superomniphobic with very little affinity for water and oils.[151] These particles may be spherical or non-spherical,[48] but are required to exhibit θ_{la} (measured into the liquid) of more than 90°. Because of the relatively low γ_{la} of oils, fluorinated solid particles which have low surface energy γ_{sa} are needed for the formation of oil liquid marbles.[39,48,152] The relatively low γ_{la} of oils compared with the γ_{sa} of common solid particles accounts for the reason why only few oil liquid marbles have been prepared by colloid science researchers. The free energy ΔG_m due to the adsorption of a spherical particle, with radius r, at a liquid-air interface (ignoring effects of τ) to form a liquid marble is

$$\Delta G_m = -\pi r^2 \gamma_{la} \left(1 + \cos\theta'_{la}\right)^2 \quad (1.9)$$

where θ'_{la} is the equilibrium liquid-air contact angle. The value of ΔG_m is negative (*cf.* equation 1.4) and indicates that the adsorption of particles of low γ_{sa} on the liquid-air interface to form a liquid marble is thermodynamically favourable.

Table 1.1. Brief summary of some particles that have been used in the preparation of liquid marbles. The number in brackets after a liquid represents its surface tension (mN m^{-1}) at 25 °C.

Liquid	Solid particle	Diameter/μm	θ_{la}/°	Ref.
Water (71.8)	Hydrophobised lycopodium	−	−	16
	Sporopollenin capsules	25	−	153
	Hydrophobised Cu	9−320	157	148
	Polymethylmethacralate PMMA	42	120	148
	PTFE	5−6	97−102	57
	Graphite	2−30	155.4	58
	Hydrophobic silica of residual SiOH 61−14%	0.02−0.03	73−126	36
	Hydrophobised spherical glass beads	42−165	110	154
	Janus particles composed of silica and α-Fe_2O_3	≈ 0.395	72 & 100	155

Table 1.1 (continued).

Liquid	Solid particle	Diameter/µm	θ_{la}/°	Ref.
Water,dimethyl sulfoxide DMSO (43.5), toluene (28.4), hexadecane (26.3), ethanol (22.1) and octane (21.6)	Fluorinated decyl polyhedral oligomeric silsesquioxane POSS/ Fe_2O_3 composite	< 70	143−171	156
Water, diiodomethane (58), DMSO, dimethyl formamide (36.4), 1,4-dioxane (33.7), toluene, ethanol and methanol (22.5)	Poly[2-(perfluorooctyl) ethylacylate] PFA-C_8	1.4 ± 0.3	−	28
Water and oils (26−63)	Fluorinated silica	0.02−0.03	28−149	39
Water and oils (20−37)	Fluorinated platelet clay particles	−	39−148	48

1.5 Presentation of Thesis

The aim of this work is to investigate the behaviour of different particle types at fluid interfaces in terms of the kind of materials they stabilise. The fluid interfaces that have been investigated are oil-water, oil-oil and liquid (or oil)-air interfaces. The study shows that for the oil-water interfaces, edible o/w Pickering emulsions were stabilised by rod- and cube-shaped $CaCO_3$ particles. For the oil-oil interfaces, o/o and o/o/o Pickering emulsions were stabilised by fluorinated and hydrocarbon-coated fumed silica, fluorinated ZnO, fluorinated sericite and bentonite clay, PTFE, Bentone 34 and Calofort SV particles. Lastly, for the oil-air interfaces, oil liquid marbles, dry oil powders and oil foams were stabilised by using the fluorinated fumed silica, fluorinated sericite and bentonite clay or fluorinated ZnO particles.

For the purpose of convenience and flow, the work has been divided into seven chapters. The foregoing chapter gives a broad view on the pioneering work on solid particles at fluid interfaces. The principles and relevant data on the subject are highlighted. Chapter 2 describes the materials and experimental protocol used in the study. Some results are also included in this chapter partly for clarity and partly to avoid repetition. Chapter 3 contains results of the rod- and cube-shaped $CaCO_3$ particle-stabilised edible o/w emulsions. The effects of pH and added electrolyte on the stability of the emulsions are reported. In addition, the stability of the rod-shaped $CaCO_3$ particle-stabilised emulsions is compared with that stabilised by the cube-shaped ones. In chapter 4, stabilisation of o/o and o/o/o Pickering emulsions using the particles listed previously is described. An attempt is made to correlate the type of emulsions obtained with the three-phase contact angles. The influence of the degree of fluorination on the behaviour of silica particles at oil-air interfaces is reported in chapter 5. The focus of the report is on the type of materials obtained as the surface chemistry of the particles changes from hydrophilic to hydrophobic and then to omniphobic. This work leads to chapter 6 where the stabilisation of dry oil powders and oil foams by fluorinated solid particles of varying degrees of fluorination and hence omniphobicity is reported. The results of the study are discussed in terms of the apparent surface energy of the particles and the apparent contact angle the particles make with the oils. Finally, a brief summary of conclusions and suggestions for future work are given in chapter 7.

1.6 References

1. L.L. Schramm, *Emulsions, Foams and Suspensions: Fundamentals and Applications*, Wiley, Weinheim, 2005.
2. I. Hamley, *Introduction to Soft Matter*, Wiley, Chichester, 2000.
3. R.A.L. Jones, *Soft Condensed Matter*, Oxford University Press, Oxford, 2002.
4. K.S. Birdi, ed., *Handbook of Surface and Colloid Chemistry* CRC Press, New York, 2009.
5. E. Dickinson, ed., *An Introduction to Food Colloids*, Oxford University Press, Oxford, 1999.
6. B.P. Binks, ed., *Modern Aspect of Emulsion Science,* Royal Society of Chemistry, Cambridge, 1998.
7. S. Magdassi and E. Touitou, *Novel Cosmetic Delivery Systems*, Marcel Dekker, New York, 1999.
8. K.A. Simon, P. Sejwal, R.B. Gerecht and Y.-Y. Luk, *Langmuir*, 2006, **23**, 1453−1458.
9. M. Kobašlija and D.T. McQuade, *Macromolecules*, 2006, **39**, 6371−6375.
10. A. Aserin, ed., *Multiple Emulsions Technology and Applications*, John Wiley and Sons, New York, 2008.
11. T.N. Hunter, R.J. Pugh, G.V. Franks and G.J. Jameson, *Adv. Colloid Interface Sci.*, 2008, **137**, 57−81.
12. T. Cosgrove, ed., *Colloid Science: Principles, Methods and Applications*, Blackwell Publishing, Oxford, 2005.
13. E. Dickinson, *Curr. Opin. Colloid Interface Sci.*, 2010, **15**, 40−49.
14. R.J. Pugh, *Adv. Colloid Interface Sci.*, 2005, **114−115**, 239−251.
15. R.M. Pashley and M. E. Karaman, *Applied Colloid and Surface Chemistry*, John Wiley and Sons Ltd., Sussex, 2008.
16. P. Aussillous and D. Quéré, *Nature*, 2001, **411**, 924−927.
17. D. Quéré and P. Aussillous, *Chem. Eng. Technol.*, 2002, **25**, 925−928.
18. P. Aussillous and D. Quéré, *J. Fluid Mech.*, 2004, **512**, 133−151.
19. P. Aussillous and D. Quéré, *Proc. R. Soc. Chem. Lond. A*, 2006, **462**, 973−999.
20. G. McHale and M.I. Newton, *Soft Matter*, 2011, **7**, 5473−5481.
21. J.R. Dorvee, A.M. Derfus, S.N. Bhatia and M.J. Sailor, *Nat. Mater.*, 2004, **3**, 973−999.
22. N. Eshtiaghi, J.S. Liu, W. Shen and K.P. Hapgood, *Powder Technol.*, 2009, **196**, 126−132.
23. H.T. Nguyen, K.P. Hapgood and W. Shen, *Chem. Eng. J.*, 2010, **201**, 396−405.
24. E. Bormashenko, Y. Bormashenko and A. Musin, *J. Colloid Interface Sci.*, 2009, **333**, 419−421.
25. E. Bormashenko, R. Progreb, G. Whyman and A. Musin, *Colloids Surf. A*, 2009, **351**, 78−82.
26. D. Vella, P. Aussillous and L. Mahadevan, *Europhys. Lett.*, 2004, **68**, 212−218.
27. R.A. Venkateswara, M. M. Kulkarni and S. Bhagat, *J. Sci.*, 2005, **285**, 413−418.
28. D. Matsukuma, H. Watanabe, H. Yamaguchi and A. Takahara, *Langmuir*, 2011, **27**, 1269−1274.
29. N. Pike, D. Richard, R. Foster and L. Mahadevan, *Proc. R. Soc. Lond. B*, 2002, **269**, 1211−1215.
30. G. McHale, N.J. Shirtcliffe, M.I. Newton, F.B. Pyatt and S.H. Doerr, *Appl. Phys. Lett*, 2007, **90**, 054110.
31. G. McHale, N.J. Shirtcliffe, M.I. Newton and F.B. Pyatt, *Hydrol. Processes*, 2007, **21**, 2229−2238.
32. K.P. Hapgood and B. Khanmohammadi, *Powder Technol.*, 2009, **189**, 253−262.

33. S. Fujii, M. Suzaki, S.P. Armes, D. Dupin, S. Hamasaki, K. Aono and Y. Nakamura, *Langmuir*, 2011, **27**, 8067−8074.
34. T. Arbatan and W. Shen, *Langmuir*, 2011, **27**, 12923−12929.
35. E. Bormashenko and A. Musin, *Appl. Surf. Sci.*, 2009, **255**, 6429−6431.
36. D. Zang, K. Lin, W. Wang, Y. Gu, Y. Zhang, X. Geng and B.P. Binks, *Soft Matter*, 2014.
37. H.-J. Butt, K. Graf and M. Kappl, *Physics and Chemistry of Interfaces*, Wiley-VCH & Co. KCoA, Weinheim, 2003.
38. M. Dandan and H.Y. Erbil, *Langmuir*, 2009, **25**, 8362−8367.
39. B.P. Binks and A.T. Tyowua, *Soft Matter*, 2013, **9**, 834−845.
40. A. Stocco, F. Garcia-Moreno, I. Manke, J. Banhart and D. Langevin, *Soft Matter*, 2011, **7**, 631−637.
41. E. Bormashenko, R. Pogreb, G. Whyman, A. Musin, Y. Bormashenko and Z. Barkay, *Langmuir*, 2009, **25**, 1893−1896.
42. R.K. Prud'homme and S.A. Khan, *Foams-Theory, Measurements and Applications*, Marcel Dekker, New York, 1996.
43. E. Bormashenko, R. Pogreb, Y. Bormashenko, A. Musin and T. Stein, *Langmuir*, 2008, **24**, 12119−12122.
44. J. Tain, T. Arbatan, X. Li and W. Shen, *Chem. Commun.*, 2010, **46**, 4734−4736.
45. J. Tain, T. Arbatan, X. Li and W. Shen, *Chem. Eng. J.*, 2010, **165**, 347−353.
46. E. Bormashenko, P. Roman and A. Musin, *J. Sci.*, 2011, **366**, 196−199.
47. B.P. Binks and R. Murakami, *Nat. Mater.*, 2006, **5**, 865−869.
48. B.P. Binks, T. Sekine and A. T. Tyowua, *Soft Matter*, 2014.
49. E. Bormashenko, *Curr. Opin. Colloid Interface Sci.*, 2011, **16**, 266−271.
50. B.P. Binks and T.S. Horozov, eds., *Colloidal Particles at Liquid Interfaces*, Cambridge University Press, Cambridge, 2006.
51. W. Thomson (Lord Kelvin), *Proc. R. Soc.*, 1871, **7**, 63.
52. A. Stocco, E. Rio, B.P. Binks and D. Langevin, *Soft Matter*, 2011, **7**, 1260-1267.
53. D. Myers, *Surfaces, Interfaces and Colloids: Principles and Applications*, VCH Publishers, Weinheim, 1991.
54. F. Krauss Juillerat, U. T. Gonzenbach, A. R. Studart and L. J. Gauckler, *Mater. Lett.*, 2010, **64**, 1468−1470.
55. S. Hilgenfeldt, S.A. Koehler and H. A. Stone, *Phys. Rev. Lett.*, 2001, **86**, 4704−4707.
56. D. Exarowa and P.M. Kruglyakov, Elsevier, Amsterdan, 1998.
57. A. Tosun and H. Y. Erbil, *Appl. Surf. Sci.*, 2009, **256**, 1278−1283.
58. M.D. Doganci, B.U. Sesli, H. Y. Erbil, B.P. Binks and I.E. Salama, *Colloids Surf. A*, 2011, **384**, 417−426.
59. N. Eshtiaghi, J.S. Liu and K.P. Hapgood, *Powder Technol.*, 2010, **197**, 184−195.
60. J. Angarska, C. Stubenrauch and E. Manev, *Colloids Surf. A*, 2007, **309**, 189−197.
61. R. Farajzadeh, R. Krastev and P.L.J. Zitha, *Colloids Surf. A*, 2008, **324**, 35−40.
62. N. Garti and A. Aserin, *Adv. Colloid Interface Sci.*, 1996, **65**, 37−69.
63. G. Gotchev, T. Kolarov, K. Khristov and D. Exerowa, *Adv. Colloid Interface Sci.*, 2011, **168**, 79−84.
64. K. Khristov, H. Petkova, L. Alexandrova, M. Nedyalkov, D. Platikanov, D. Exerowa and J. Beetge, *Adv. Colloid Interface Sci.*, 2011, **168**, 105−113.
65. J.-C. Baret, F. Kleinschmidt, A. El Harrak and A. D. Griffiths, *Langmuir*, 2009, **25**, 6088−6093.
66. J. Weiss, N. Herrmann and D.J. McClements, *Langmuir*, 1999, **15**, 6652−6657.
67. K. Ahmad, C.C. Ho, W.K. Fong and D. Toji, *J. Colloid Interface Sci.*, 1996, **181**, 595−604.

68. K. Pays, J. Giermanska-Kahn, B. Pouligny, J. Bibette and F. Leal-Calderon, *Langmuir*, 2001, **17**, 7758−7769.
69. S. Damodaran, *J. Food Sci.*, 2005, **70**, R54−R66.
70. S. Tcholakova, N.D. Denkov, D. Sidzhakova, I.B. Ivanov and B. Campbell, *Langmuir*, 2005, **21**, 4842−4855.
71. E. Dickinson, *J. Food Eng.*, 1994, **22**, 59−74.
72. S. Tcholakova, N.D. Denkov, I.B. Ivanov and B. Campbell, *Langmuir*, 2002, **18**, 8960−8971.
73. S. Tcholakova, D.N. Denkov, B.I. Ivanov and B. Campbell, *Adv. Colloid Interface Sci.*, 2006, **123−126**, 259−293.
74. S.C. Mehta and P. Somasundaran, *Langmuir*, 2008, **24**, 4558-4563.
75. S.T.A. Regismond, F.M. Winnik and E.D. Goddard, *Colloids Surf. A*, 1998, **141**, 165−171.
76. Z.-L. Chen, Y.-L. Yan and X.-B. Huang, *Colloids Surf. A*, 2008, **331**, 239−244.
77. R.G. Alargova, D.S. Warhadpande, V.N. Paunov and O.D. Velev, *Langmuir,* 2004, **20**, 10371−10374.
78. U.T. Gonzenbach, A.R. Studart, E. Tervoort and L.J. Gauckler, *Langmuir*, 2006, **22**, 10983−10988.
79. U.T. Gonzenbach, A.R. Studart, E. Tervoort and L.J. Gauckler, *Angew. Chemie Int. Ed.*, 2006, **45**, 3526−3530.
80. R. Aveyard, B.P. Binks and J.H. Clint, *Adv. Colloid Interface Sci.*, 2003, **100–102**, 503−546.
81. A.R. Studart, H.C. Shum and D.A. Weitz, *J. Phys. Chem. B*, 2009, **113**, 3914−3919.
82. B.P. Binks, A.J. Johnson and J.A. Rodrigues, *Soft Matter*, 2010, **6**, 126−135.
83. B.P. Binks and J.A. Rodrigues, *Angew. Chem. Int. Ed.*, 2007, **46**, 5389−5392.
84. Z.G. Cui, Y.Z. Cui, C.F. Cui, Z. Chen and B.P. Binks, *Langmuir*, 2010, **26**, 12567−12574.
85. W. Ramsden, *Proc. Roy. Soc.*, 1903, **72**, 156−164.
86. S.U. Pickering, *J. Chem. Soc.*, 1907, **91**, 2001−2021.
87. P. Finkle, H.D. Draper and J.H. Hildebrand, *J. Am. Chem. Soc.*, 1923, **45**, 2780−2788.
88. W.D. Bancroft, *J. Phys. Chem.*, 1912, **17**, 501−519.
89. B.P. Binks and S.O. Lumsdon, *Phys. Chem. Chem. Phys.*, 2000, **2**, 2959−2967.
90. J.H. Schulman and J. Leja, *Trans. Farad. Soc.*, 1954, **50**, 598−605.
91. B.P. Binks, *Curr. Opin. Colloid Interface Sci.*, 2002, **7**, 21−41.
92. W.C. Griffin, *J. Soc. Cosmet. Chem.*, 1949, **1**, 311−319.
93. W.C. Griffin, *J. Soc. Cosmet. Chem.*, 1954, **5**, 259−265.
94. R.D. Vartanian, *Stable mineral oil-silicone oil compositions*, US Pat., 3 445 385, 1969, American Cyanamide Company.
95. Y. Nonomura, K. Fukuda, S. Komura and K. Tsujii, *Langmuir*, 2003, **19**, 10152−10156.
96. Y. Nonomura, T. Sugawara, A. Kashimoto, K. Fukuda, H. Hotta and K. Tsujii, *Langmuir*, 2002, **18**, 10163−10167.
97. T.K. Jones and M. Nair, *Oil-in-oil dispersions stabilised by solid particles and methods of making the same*, US Pat., 8 323 392 B2, 2012, Eastman Kodak Company.
98. J.C.H. Wong, E. Tervoort, S. Busato, U.T. Gonzenbach, A.R. Studart, P. Ermanni and L.J. Gauckler, *J. Mater. Chem.*, 2009, **19**, 5129−5133.
99. A.R. Studart, U.T. Gonzenbach, E. Tervoort and L.J. Gauckler, *J. Am. Ceram. Soc.*, 2006, **89**, 1771−1789.
100. A.R. Studart, U.T. Gonzenbach, I. Akartuna, E. Tervoort and L.J. Gauckler, *J. Mater. Chem.*, 2007, **17**, 3283−3289.
101. B.P. Binks, A. Rocher and M. Kirkland, *Soft Matter*, 2011, **7**, 1800−1808.

102. B.P. Binks, J.H. Clint, P.D.I. Fletcher, T.J.G. Lees and P. Taylor, *Chem. Commun.*, 2006, 3531−3533.
103. P.D.I. Fletcher and B.L. Holt, *Langmuir*, 2011, **27**, 12869−12876.
104. I. Akartuna, A.R. Studart, E. Tervoort and L.J. Gauckler, *Adv. Mater.*, 2008, **20**, 4714−4718.
105. Z.G. Cui, C.F. Cui, Y. Zhu and B.P. Binks, *Langmuir*, 2011, **28**, 314−320.
106. N.P. Ashby and B.P. Binks, *Phys. Chem. Chem. Phys*, 2000, **2**, 5640−5646.
107. W.C. Moore, *J. Am. Chem. Soc.*, 1919, **41**, 940−946.
108. S. Zhang, Q. Lan, Q. Liu, J. Xu and D. Sun, *Colloids Surf. A*, 2008, **317**, 406−413.
109. S. Zhang, D. Sun, X. Dong, C. Li and J. Xu, *Colloids Surf. A*, 2008, **324**, 1−8.
110. R. Murakami and A. Bismarck, *Adv. Funct. Mater.*, 2010, **20**, 732−737.
111. R. Aveyard and J.H. Clint, *J. Chem. Soc., Faraday Trans.*, 1996, **92**, 85−89.
112. J.W. Tavacoli, G. Katgert, E.G. Kim, M.E. Cates and P.S. Clegg, *Phys. Rev. Lett.*, 2012, **108**, 268306.
113. B.P. Binks and S.O. Lumsdon, *Phys. Chem. Chem. Phys.*, 1999, **1**, 3007−3016.
114. B.R. Midmore, *Colloids Surf. A*, 1998, **132**, 257−265.
115. D.E. Tambe and M.M. Sharma, *J. Colloid Interface Sci.*, 1993, **157**, 244−253.
116. P.A. Kralchevsky and K. Nagayama, *Adv. Colloid Interface Sci.*, 2000, **85**, 145−192.
117. B.P. Binks and S.O. Lumsdon, *Langmuir*, 2000, **16**, 8622−8631.
118. J.W.J. de Folter, E.M. Hutter, S.I.R. Castillo, K.E. Klop, A.P. Philipse and W.K. Kegel, *Langmuir*, 2014, **30**, 955−964.
119. B. Madivala, S. Vandebril, J. Fransaer and J. Vermant, *Soft Matter*, 2009, **5**, 1717−1727.
120. Y. Nonomura and N. Kobayashi, *J. Colloid Interface Sci.*, 2009, **330**, 463-466.
121. S. Tcholakova, N.D. Denkov and A. Lips, *Phys. Chem. Chem. Phys.*, 2008, **10**, 1608−1627.
122. M. Oettel and S. Dietrich, *Langmuir*, 2008, **24**, 1425−1441.
123. F. Bresme and M. Oettel, *J. Phys. Condens. Matter*, 2007, **19**, 413101.
124. B.J. Park, J.P. Pantina, E.M. Furst, M. Oettel, S. Reynaert and J. Vermant, *Langmuir*, 2008, **24**, 1686−1694.
125. S. Simovic and C.A. Prestidge, *Langmuir*, 2004, **20**, 8357−8365.
126. Y. Gu, *Colloids Surf. A*, 2001, **181**, 215−224.
127. B.V. Derjaguin, *Theory of Stability of Colloids and Thin Liquid Films*, Plenum Press, New York, 1989.
128. B.V. Derjaguin, N.V. Churaev and V.M. Muller, *Surface Forces*, Plenum Press, New York, 1987.
129. J.N. Israelachvili, *Intermolecular and Surface Forces*, Academic Press, New York, 1992.
130. V. Bergeron, Å. Waltermo and P.M. Claesson, *Langmuir*, 1996, **12**, 1336−1342.
131. N.D. Denkov, S. Tcholakova and I.B. Ivanov, Globular proteins as emulsions stabilisers-similarities and differences with surfactants and solid particles, Lyon, 2000.
132. C. Stubenrauch and R.v. Klitzing, *J. Phys.: Condens. Matter*, 2003, **15**, R1197−R1231.
133. B.P. Binks and S.O. Lumsdon, *Langmuir*, 2000, **16**, 2539−2547.
134. H.A. Wege, S. Kim, V.N. Paunov, Q. Zhong and O.D. Velev, *Langmuir*, 2008, **24**, 9245−9253.
135. Z. Du, M.P. Bilbao-Montoya, B.P. Binks, E. Dickinson, R. Ettelaie and B.S. Murray, *Langmuir*, 2003, **19**, 3106−3108.
136. S. Levine, B.D. Bowen and S.J. Partridge, *Colloids Surf.*, 1989, **38**, 345−364.
137. N.D. Denkov, I.B. Ivanov, P.A. Kralchevsky and D.T. Wasan, *J. Colloid Interface Sci.*, 1992, **150**, 589−593.
138. B.P. Binks and P.D.I. Fletcher, *Langmuir*, 2001, **17**, 4708-4710.
139. R. Aveyard, *Soft Matter*, 2012, **8**, 5233−5240.

140. I.B. Ivanov, B. Radoev, E. Manev and A. Scheludko, *Trans. Faraday Soc.*, 1970, **66**, 1262−1273.
141. M. Visschers, J. Laven and R. van der Linde, *Prog. Org. Coat.*, 1997, **31**, 311−323.
142. G. Kaptay, *Colloids Surf. A*, 2003, **230**, 67−80.
143. P. M. Kruglyakov and A. V. Nushtayeva, *Adv. Colloid Interface Sci.*, 2004, **108–109**, 151-158.
144. P.M. Kruglyakov, A.V. Nushtayeva and N.G. Vilkova, *J. Colloid Interface Sci.*, 2004, **276**, 465−474.
145. G. Kaptay, *Colloids Surf. A*, 2006, **282–283**, 387−401.
146. B.P. Binks, L. Isa and A.T. Tyowua, *Langmuir*, 2013, **29**, 4923−4927.
147. S.I. Kam and W.R. Rossen, *J. Colloid Interface Sci.*, 1999, **213**, 329−339.
148. P. McEleney, G.M. Walker, I.A. Larmour and S.E.J. Bell, *Chem. Eng. J.*, 2009, **147**, 373−382.
149. G.M. Walker, P. McEleney, A.H. Al-Muhtaseb and S.E.J. Bell, *Chem. Eng. J.*, 2013, **228**, 984−992.
150. J. Yang, Z.-Z. Zhang, X.-H. Men and X.-H. Xu, *J. Dispersion Sci. Technol.*, 2011, **32**, 485−489.
151. H. Kim, K. Noh, C. Choi, J. Khamwannah, D. Villwock and S. Jin, *Langmuir*, 2011, **27**, 10191−10196.
152. B.P. Binks and A. Rocher, *Phys. Chem. Chem. Phys.*, 2010, **12**, 9169-9171.
153. B.P. Binks, A.N. Boa, M.A. Kibble, G. Mackenzie and A. Rocher, *Soft Matter*, 2011, **7**, 4017−4024.
154. C.P. Whitby, X. Bian and R. Sedev, *Soft Matter*, 2012, **8**, 11336−11342.
155. S.-H. Kim, S. Lee and S.-M. Yang, *Angew. Chem. Int. Ed.*, 2010, **49**, 2535−2538.
156. Y. Xue, H. Wang, Y. Zhao, L. Dai, L. Feng, X. Wang and T. Lin, *Adv. Mater.*, 2010, **22**, 4814−4818.

Chapter 2

Experimental

2.1 Materials

2.1.1 Oil-Water Interfaces: Tricaprylin- and Miglyol 812N-Water Interfaces

2.1.1.1 Solid Particles

Hydrophilic $CaCO_3$ (rod- and cube-shaped) particles were used for the tricaprylin- and Miglyol 812N-water interfaces. Strictly speaking, the shape of these particles is only near to rods and cubes. The $CaCO_3$ particles were from Maruo Calcium Company Japan. According to the manufacturer, the rod-shaped $CaCO_3$ particles also known as Whiscal A possess the following properties: average fibre length 20−30 μm, average width 0.5−1 μm, surface area 7 m^2 g^{-1}, Mohs hardness 3.5−4, pH 8.3−10.3 (10 wt. % water suspension), transition temperature to CaO 900 °C and moisture content 0.3 %. The cube-shaped ones (Cube-Type A) have sides of average length 4−7 μm. In addition, the density of the particles lies between 2.6 and 2.8 g cm^{-3}. The contact angle (41°) of a water drop on compressed particle disk of the rod-shaped $CaCO_3$ particles has been reported by Zhou *et al.*[1] where they were used in the presence of oleic acid to stabilise aqueous foams. The particles were used at their unadjusted (≈ 9) or adjusted pH, or in the absence or presence of salt. In the former, 0.5 M aqueous solution of NaOH (97% pure) or 3 M aqueous solution of HCl (≈ 36% pure) both from Fisher Scientific were used to adjust the pH. In the latter, different concentrations (1−1000 mM) of NaCl (> 99.5% pure, BDH Chemicals) were used. The rod-shaped $CaCO_3$ particles were prepared by addition of aqueous $Ca(OH)_2$ solution to an aqueous bath (at a constant temperature of > 60 °C) containing CO_2 gas or to which CO_2 is being blown into. The rod-shaped $CaCO_3$ particles were then collected as precipitates.[2] In the case of the cube-shaped $CaCO_3$ particles, drops of an aqueous calcium salt solution were added to an aqueous carbonate solution or vice versa, with one of the solutions containing a buffering agent and mixed together. The resulting $CaCO_3$ suspension or the diluted suspension was allowed to stand or agitated (≥ 1 hour) and the cube-shaped $CaCO_3$ particles were obtained as precipitates.[3]

2.1.1.2 Oil and Water

Tricaprylin (purity above 99%, Aldrich) and Miglyol 812N from Sasol were used as oils. The former is a C_8-triglyceride whilst the latter is a mixture of C_8–C_{10} triglycerides. The oils were passed twice through basic alumina to remove polar impurities before use. Water was passed through an Elga Prima reverse osmosis unit and then a Milli-Q reagent water system. The treated water (referred henceforth as Milli-Q water) has a surface tension of 71.8 mN m^{-1}, pH of 6.9 and a resistivity of 18 MΩ cm at 25 °C.

2.1.2 Oil-Oil Interfaces

2.1.2.1 Solid Particles

Six broad particle types (Table 2.1) were used. They include dichlorodimethylsilane DCDMS, $Si(CH_3)_2Cl_2$, coated and fluorinated fumed silica particles both from Wacker Chemie, Burghausen. The silica particles have varying percentages of residual surface SiOH group. Fluorinated clay (sericite and bentonite) and fluorinated ZnO particles both from Diato Kasei Kogyo Company Ltd. Japan, Calofort SV from Specialty Minerals, UK and $CaCO_3$ particles were also used. The other particles are PTFE (E and E Ltd., UK) and Bentone 34 (Rheox Ltd., UK). The DCDMS-coated and fluorinated fumed silica particles were composed of aggregates of particles of primary diameter 20−30 nm and were obtained by surface chemical modification from hydrophilic fumed silica (100% SiOH). The 100% SiOH silica particles are normally prepared by hydrolysis of volatile $SiCl_4$ in an oxygen-hydrogen flame at 1200 °C. Their surfaces contain 100% SiOH group and they have Brunauer-Emmett-Teller (BET) surface area of 200 m^2 g^{-1}. The properties of silica particles are determined mainly by the percentage of SiOH and SiOSi groups present on their surfaces. During flame hydrolysis, particles of SiO_2 collide and coalesce to give smooth and relatively spherical primary particles whose diameters are between 20−30 nm. These primary particles collide and may fuse together at lower temperatures to form stable aggregates of diameter between 100–500 nm which can be destroyed by sonication. Figure 2.1 (upper) is an example of a scanning electron microscope SEM image of fairly monodisperse silica particles (not one of the fumed silica particles) with 100% surface SiOH groups alongside with sketches showing how these groups are modified. These surface groups can easily be modified by reaction with suitable chemical compounds. For example, the DCDMS-coated and fluorinated fumed silica particles having between 88−14% and 75−50% residual surface SiOH groups, respectively, were obtained by reacting the −OH groups on the surfaces of the 100% SiOH fumed silica particles with varying amounts of DCDMS and the fluorinating agent, respectively. Tridecafluoro-1,1,2,2-tetrahydrooctyltrimethoxysilane, $CF_3(CF_2)_5(CH_2)_2Si(OCH_3)_3$, denoted as TDF-$Si(OCH_3)_3$ was used as the fluorinating agent. To obtain the DCDMS-coated fumed silica particles of varying percentage of residual surface SiOH group, the 100% SiOH fumed silica particles were reacted with DCDMS in the presence of varying molar amounts of water, followed by drying at 300 °C for 1 hour.[4] For fluorination, the 100% SiOH fumed silica particles (100 g) were fluidised in a glass cylinder using a mechanical stirrer. After purging the cylinder with nitrogen for 15 min, 10.5 g (75% SiOH fluorinated fumed silica), 21 g (59% SiOH fluorinated fumed silica) or 27.8 g (50% SiOH fluorinated fumed silica) of TDF-$Si(OCH_3)_3$ was added as an aerosol using a mono-component nozzle with a nitrogen pressure of 10 bar. No excess reagent was obtained, *i.e.* the reaction was complete. The mixture was then stirred for 15 min and placed in a nitrogen-purged oven for 2 hours at 150 ºC. Cooling to room temperature was performed under a blanket of nitrogen. The reaction of alkoxysilanes with inorganic (*e.g.* silica) surfaces (described above) involves four steps as shown in Figure 2.1 (lower).[5] The first involves hydrolysis of labile alkoxy groups ($-OCH_3$) to yield $-OH$ groups, followed by condensation of neighbouring chains to form oligomers comprising of a backbone of Si−O−Si bonds with pendant R (alkyl) and −OH groups on either sides. The −OH groups of these oligomers then hydrogen bond with SiOH groups on the particle surfaces, followed by covalent bond formation (R−Si−O−Si) upon drying. After surface chemical modification, some SiOH groups on the silica surfaces remain. The residual SiOH content is usually determined by titration with aqueous NaOH. The 100% SiOH silica contains about 2 SiOH groups nm^{-2}. Silanisation and fluorination decrease the SiOH content and the number of SiOH groups per gram of particle.[6]

SEM (Figure 2.2) mentioned above is a very useful instrument for studying the surfaces of solid particles because it offers a much higher resolution and depth of focus than optical microscopes. Unlike an optical microscope which uses photons to illuminate a sample, the SEM uses electrons produced by an electron gun *e.g.* tungsten filament, lanthanum hexaboride (LaB_6) thermionic emitter and field emission gun for illumination and the visualisation of sample surfaces. The electron beam generated by the electron gun is accelerated by high voltage (typically between 0.2−20 kV) passing through a system of apertures and electromagnetic lenses to produce a thin beam of electrons which scans (or interacts with) the surface of the particle sample to a depth of approximately 1 μm. The depth varies with the accelerating voltage and sample density. The interaction of the electron beam with the surfaces of the particle (which are composed of atoms) produces various kinds of signals. These signals include secondary electrons (SE) which represent loosely bound electrons that have been knocked off the sample, backscattered electrons (BSE) which are scattered at angles between 0–180° due to the interaction of the electrons with positively charged nucleus, X-rays which are produced by the removal of electron(s) from the inner shell of an atom in the sample, light (cathodoluminescence CL), specimen current and transmitted electrons which are detected by the necessary detectors. The SE are inelastic in nature, have energy of < 50 eV and produce topographic images. The BSE, however, are elastic in nature, have energy of 50 eV (or even up to the primary beam energy) and produce images showing atomic number contrast. The SE and BSE are the most important signals in scanning electron microscopy and are required for generating SEM images which are always monochrome. The BSE are also used along with the X-rays to obtain information about the elemental composition of the sample. The CL is used to obtain information about the optical activity of the sample.[7]

Table 2.1. Particle type, treatment reagent, industrial name and codename of particles used.

Particle	Treatment reagent	Industrial name	Codename
Silica	DCDMS	100% SiOH silica	HDK N20 (unmodified)
		88% SiOH silica	SLM 4330002/68-18
		78% SiOH silica	SLM 4330002/68-15
		70% SiOH silica	SLM 4330002/68-12
		61% SiOH silica	SLM 433002-MM 038/2a-d
		51% SiOH silica	SLM 4330002/68-10
		42% SiOH silica	SLM 4330002/68-20
		33% SiOH silica	SLM 433002-MM 10212
		25% SiOH silica	SLM 433002/1211
		23% SiOH silica	SLM 433002/113-1
		20% SiOH silica	HDK H18
		14% SiOH silica	SLM 433002/MM 004_ 1c-f
	TDF-$Si(OCH_3)_3$	75% SiOH silica	SLM 433002-MM 04g/2
		59% SiOH silica	SLM 433002-MM 04g/1
		50% SiOH silica	SLM 433002MM 04g/4
Sericite	Perfluoroalkyl phosphate	PF-0 (Raw sericite)	–
		PF-5 Eight Pearl 300S-Al	F-51576
		PF-8 Eight Pearl 300S-Al	S-0108012G
		PF-10 Eight Pearl 300S-Al	S-1010072G
		PF-10 Eight Pearl 300S-Al[a]	S-0207162G
		PF-10 FSE-Al	S-0110181G
		PF-12 Eight Pearl 300S-Al	S-0108013G
ZnO		PFX-10 ZnO (TP)	S-0111061S
Bentonite		PFX-10 Kunipia F	S-0103292Y
	–	Bentone 34	E8015
$CaCO_3$	–	Whiscal A	–
	Stearate	Calofort SV	–
Polymer	$(CF_2{-}CF_2)_n$	Zonyl MP1400 (PTFE)	–

Figure 2.1. (upper) SEM image of fairly monodisperse hydrophilic silica particles having 100% surface SiOH groups along with sketches showing how the surface SiOH groups become modified upon silanisation and fluorination. (lower) reaction of alkoxysilane with surfaces of hydrophilic silica particles:[5] (a) hydrolysis, (b) condensation, (c) hydrogen bonding and (d) covalent bond formation.

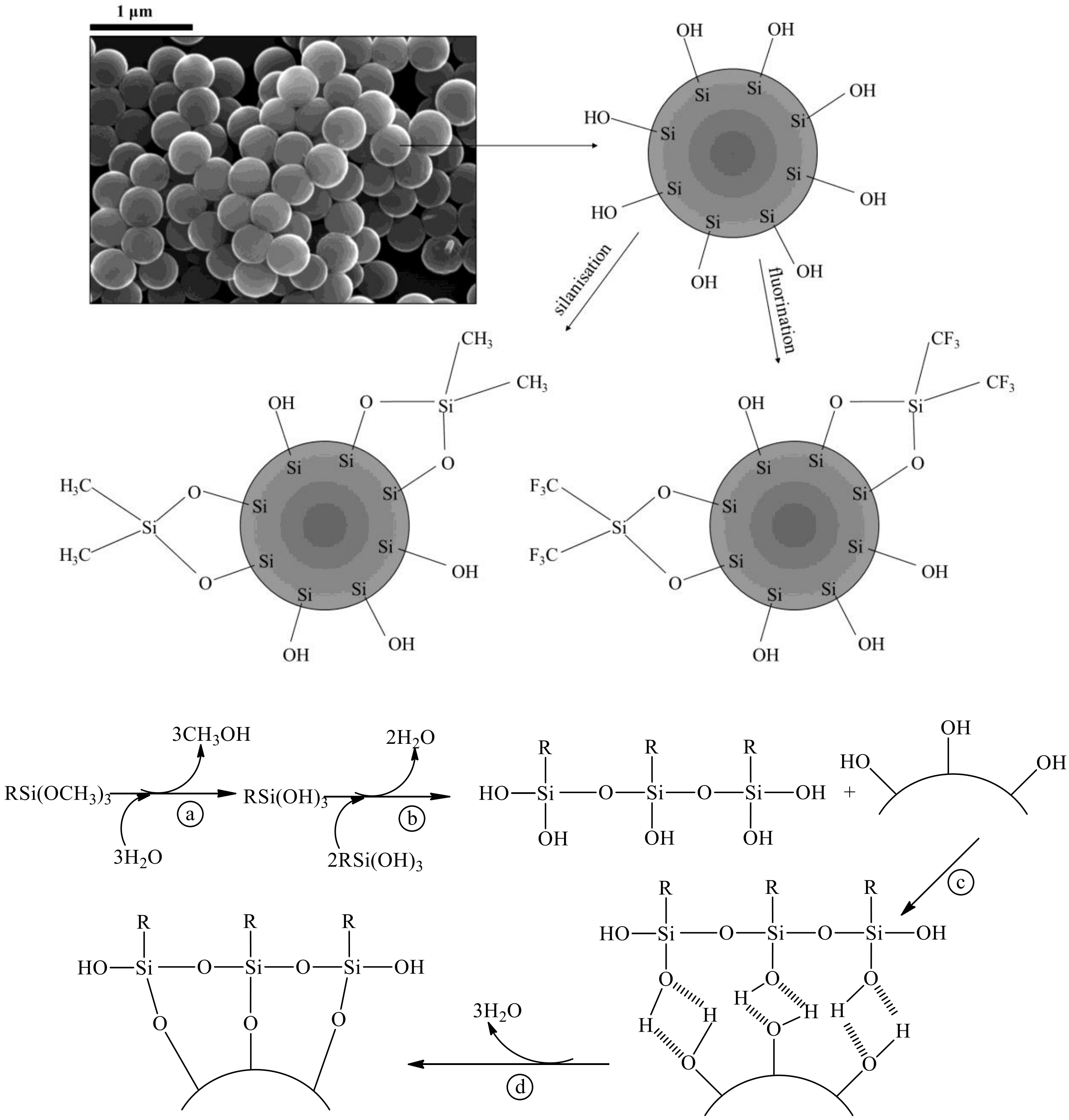

Figure 2.2. Schematic representation of an SEM; taken from *www.zeiss.co.uk/microscope/en.*

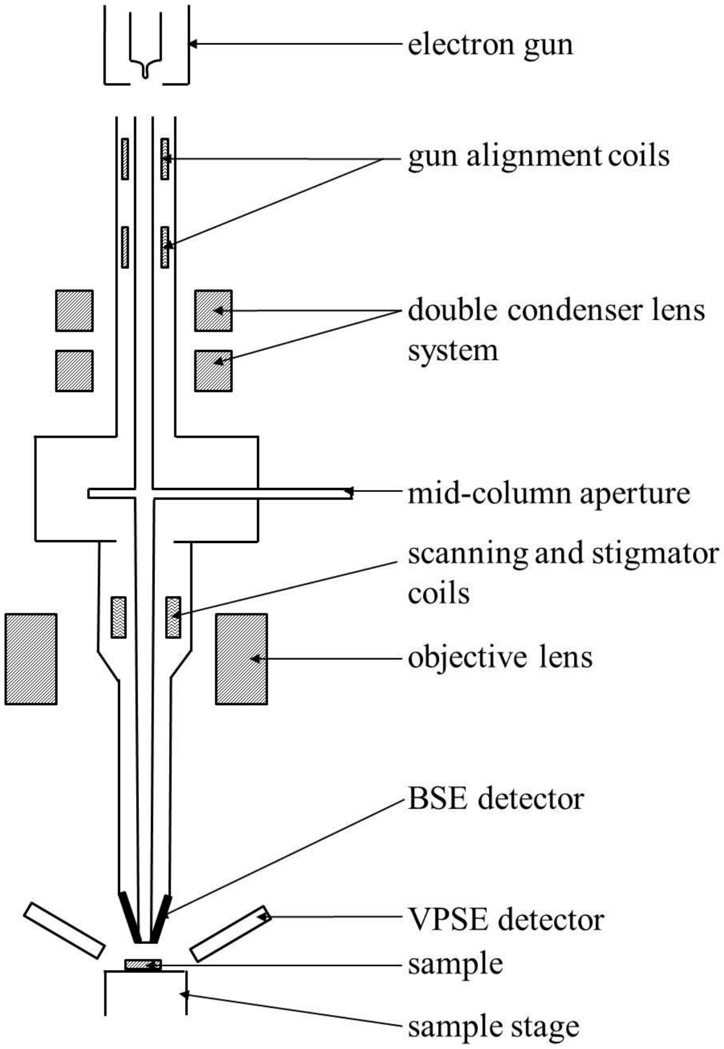

Whilst the fumed silica particles were fluorinated with TDF-Si$(OCH_3)_3$, the clay and the ZnO particles were fluorinated with perfluoroalkyl phosphate. These particles are common in cosmetics enabling the preparation of a long lasting make-up resilient to perspiration and sebum thus promoting a more natural and healthy appearance. The platelet sericite particles (PF-5, 8, 10 and 12 Eight Pearl 300S-Al) were obtained by treating raw omniphilic sericite particles (PF-0 Eight Pearl 300S-Al) with varying amounts of C_9–C_{15} perfluoroalkyl phosphate diethanolamine salt. This resulted to varying degrees of omniphobicity, with the PF-12 Eight Pearl 300S-Al particles being the most omniphobic. The perfluoroalkyl phosphate diethanolamine salt $[F_3C(CF_2)_n(CH_2)_2O]_mPOO[(ONH_2(CH_2CH_2OH)_2]_2$, where n = 6–18 and $2 > m > 1$, is the precursor of the perfluoroalkyl phosphate as shown in Figure 2.3. However, only a given amount of the perfluoroalkyl phosphate salt was used to prepare the fluorinated bentonite clay (PFX-10 Kunipia F), fluorinated sericite (PF-10 FSE-Al and PF-10 Eight Pearl 300S-Al^a) and fluorinated

ZnO (PFX-10 ZnO (TP)) particles from their omniphilic precursors. Prior to fluorination, the particles were mixed with sodium aluminate and sulphuric acid leading to the formation of small crystals (≈ 200 nm) of $Al(OH)_3$ on their surfaces rendering them positively charged and enabling an easy and uniform reaction with the anionic phosphate reactant. The presence of $Al(OH)_3$ crystals on the particles surfaces also make them textured (see later). The difference between the PF-10 Eight Pearl 300S-Al and PF-10 Eight Pearl 300S-Al^a is that the former contains 4 wt. % of $Al(OH)_3$ (just like the PF-5, 8 and 12 Eight Pearl 300S-Al ones) whilst the latter contains 5 wt. % of $Al(OH)_3$. Sericite is a white, monoclinic, powdered mica mineral composed mainly of SiO_2 (≈ 54%), Al_2O_3 (≈ 31%) and K_2O (≈ 7%). The particles are plate-like of average size around 5 μm. They are characterised by a three-layered unit cell consisting of a SiO_2 tetrahedron, an Al_2O_3 octahedron and a SiO_2 tetrahedron held together by potassium ionic bonds.[8] During chemical modification of the particles, the intermediate perfluoroalkyl phosphoric acid bonds to the particle surface through the formation of metal salts and/or hydrogen bonds depending on the alkalinity of the particles and imbue omniphobic properties to the particle surfaces. Bentonite (a montmorillonitic clay) is characterised by one Al octahedral sheet placed between two Si tetrahedral sheets. The isomorphous substitution of Al^{3+} for Si^{4+} in the tetrahedral layer and Mg^{2+} for Al^{3+} in the octahedral layer results in a net negative surface charge on the clay. This charge imbalance is offset by exchangeable cations (typically Na^+ and Ca^{2+}) at the clay surface. The layered structure of bentonite allows its expansion when wet. Na^+ and Ca^{2+} are strongly hydrated in the presence of water, resulting in a hydrophilic environment at the clay surface.[9]

Calofort SV is obtained by coating precipitated $CaCO_3$ particles with stearate. It is composed of agglomerates whose primary particles have an average size of 0.07 μm and surface area of $17-25$ m^2 g^{-1}. It is used in rigid and plasticised polyvinylchloride formulations to improve impact strength, surface gloss and whiteness. Calofort SV is hydrophobic and has been used previously[10] to prepare stable waterless emulsions. Hydrophobic Bentone 34 (a rheological additive) is the organic (hydrocarbon) derivative of bentonite clay.

Figure 2.3. Scheme for the conversion of omniphilic sericite particles to omniphobic particles using perfluoroalcohol phosphate.

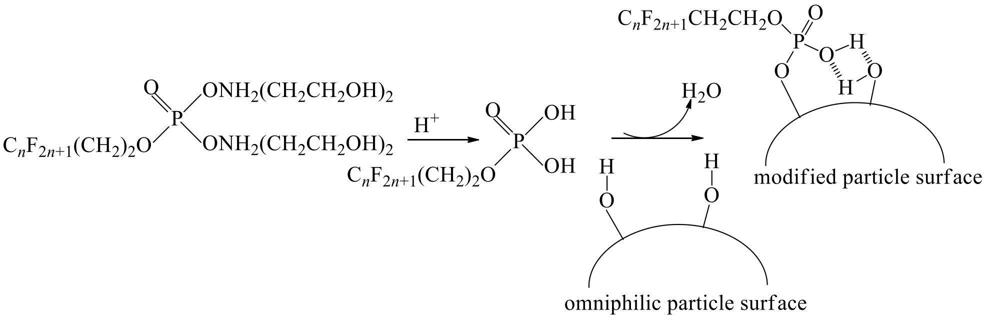

2.1.2.2 *Oils*

The oils used are given in Table 2.2. They include sunflower oil (Tesco), castor oil (Sigma-Aldrich), olive oil (Sigma), rapeseed oil from *Brassica rapa* (Fluka), mineral oil (Sigma-Aldrich) and silicone oils (polydimethylsiloxane PDMS)-20, 50 and 100 cS-from Dow Corning. Sunflower, olive, mineral and rapeseed oils were passed twice through a column containing basic alumina to remove polar impurities before use. The rest of the oils were used as received.

Table 2.2. The density ρ (at 25 °C) of vegetable, mineral and PDMS oils used.

Oil	ρ/± 0.01 g cm^{-3}
Sunflower oil	0.92
Castor oil	0.96
Olive oil	0.91
Rapeseed oil	0.92
Mineral oil	0.92
PDMS 20 cS	0.95
PDMS 50 cS	0.96
PDMS 100 cS	0.97

2.1.3 Liquid (and/or Oil)-Air Interfaces

2.1.3.1 *Solid Particles*

Four broad types of solid particles, namely fluorinated fumed silica, fluorinated platelet clay (sericite and bentonite) and fluorinated ZnO particles (described in sec. 2.1.2.1) were used. The behaviour of the fluorinated fumed silica particles was compared with the 100% SiOH and

14% SiOH fumed silica particles and that of the fluorinated clay particles was compared with the omniphilic PF-0 Eight Pearl 300S-Al particles.

2.1.3.2 Oils and Other Liquids

Many of the oils used with the fumed silica particles were different from those that were used with the fluorinated clay and fluorinated ZnO particles. Many of the oils used with the fluorinated clay particles were of cosmetic importance as the work was intended for cosmetic applications. The chemical structure, source, density ρ and γ_{la} of all the oils and liquids in the former case are given in Table 2.3. The liquids range from non-polar alkanes to polar oils like tricaprylin and geraniol to very polar liquids like glycerol and water. α-Bromonaphthalene and diiodomethane are liquids of high cohesive energy density in which molecules interact only through dispersion forces. All the oils were used as received except tricaprylin and Miglyol 812N which were passed through basic alumina twice before use. Ethanol and acetone, 99% pure, were from Aldrich. The cosmetic oils (silicone, mineral, vegetable, ester and UV-absorbing oils) were supplied by Shiseido Japan and were used as received. The name, chemical structure and ρ of these oils are given in Table 2.4. For comparison, *n*-alkanes (C_5–C_{16}) were also used. Such alkanes include pentane (Aldrich, *ca*. 98%), hexane (Fisher Scientific, *ca*. 95%), heptane (Sigma-Aldrich, *ca*. 99%), octane (Sigma-Aldrich, > 98%), decane (Avocado, *ca*. 99%), dodecane (Sigma, ≥ 99%), tetradecane (Aldrich, *ca*. > 99%) and general purpose grade hexadecane from Fisher Scientific. In parallel experiments, α-Bromonaphthalene, diiodomethane, ethylene glycol, formamide, glycerol, *n*-hexadecane and water were used as probe liquids to estimate the surface energies of the particles from contact angle data. Air used in both cases was that present in the laboratory ($N_2 \approx 78\%$, $O_2 \approx 21\%$, $Ar \approx 0.9\%$ and $CO_2 \approx 0.04\%$). It is worth mentioning that the term ‘oil’ is loosely used in this work to refer to liquids other than water. Strictly speaking, oils are non-polar liquids possessing low (< 5) dielectric constant.

Table 2.3. Name, chemical structure, source, purity, density ρ and surface tension γ_{la} (both at 20 °C) of all the liquids used. The ρ and γ_{la} of water (at 20 °C) are ≈ 1.00 g cm^{-3} and 72.8 mN m^{-1}, respectively. The ρ and γ_{la} values are quoted to ± 0.01 g cm^{-3} and ± 0.1 mN m^{-1}, respectively.

Liquid	Structure	Supplier	Purity/%	ρ/g cm^{-3}	γ_{la}/mN m^{-1}
Perfluorohexane	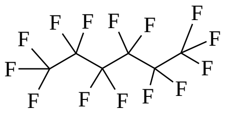	Aldrich	99	1.71	11.9
PDMS 50 cS	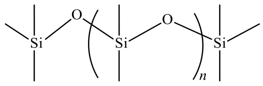	Dow Corning	100	0.96	21.4
Cyclohexane	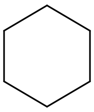	Aldrich	> 99	0.78	25.5
n-Hexadecane		Aldrich	> 99	0.77	27.5
Toluene	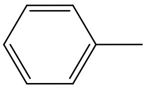	Fisher	99	0.87	28.4
Benzene	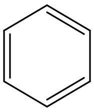	Fison	> 99	0.88	28.9
(*R*)-(+)-Limonene	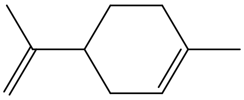	Aldrich	98	0.84	29.0
Isopropyl myristate	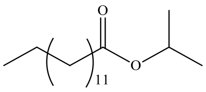	Aldrich	> 98	0.85	29.4
Tricaprylin	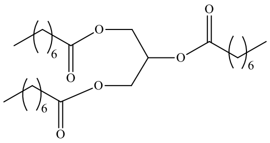	Aldrich	> 99	0.95	29.5
Miglyol 812N	C_8–C_{10} triglycerides	Sasol	–	1.01	30.3

Table 2.3 (continued).

Liquid	Structure	Supplier	Purity/%	ρ/g cm^{-3}	γ_{la}/mN m^{-1}
Squalane	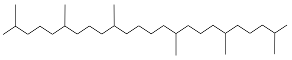	Aldrich	99	0.81	31.1
Geraniol	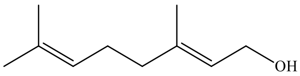	SAFC	> 97	0.88	31.6
α-Hexylcinnam-aldehyde	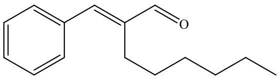	SAFC	> 95	0.95	35.3
Sunflower oil	Mixture of long chain triglycerides, mainly C_{18}	Co-op	> 99	0.92	33.9
Eugenol	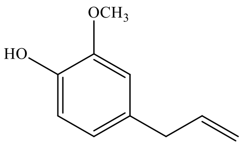	Aldrich	> 99	1.07	36.4
Benzyl acetate	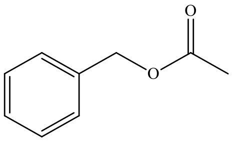	SAFC	> 99	1.05	38.0
Tricresyl phosphate	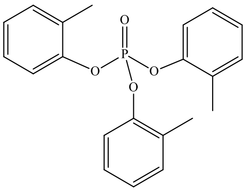	Aldrich	> 98	0.85	29.4
α-Bromonaphtha-lene	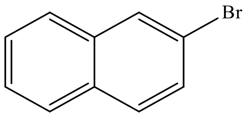	Aldrich	97	1.48	44.6
Ethylene glycol	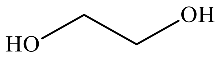	Aldrich	> 99	1.11	47.7
Diiodomethane	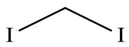	Aldrich	> 99	3.33	50.8
Formamide	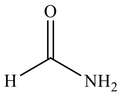	Aldrich	> 99	1.13	58.2
Glycerol	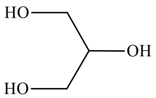	Aldrich	99	1.26	63.4

Table 2.4. Name, chemical structure, density ρ and surface tension γ_{la} (both at 25 °C) of the cosmetic oils used. The ρ and γ_{la} values are quoted to ± 0.01 g cm^{-3} and ± 0.1 mN m^{-1}, respectively.

Oil	Structure	ρ/g cm^{-3}	γ_{la}/mN m^{-1}
Cyclomethicone	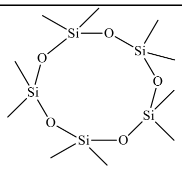	0.96	20.2
PDMS 6 cS (n = 5−10)	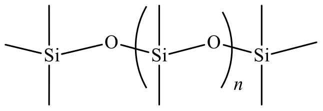	0.92	20.6
PDMS 20 cS	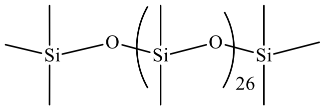	0.95	20.8
Isocetane	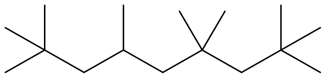	0.79	26.7
Phenyl silicone	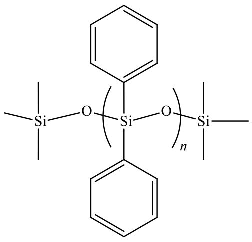	0.99	27.6
Tripropylene glycol trimethylacetate	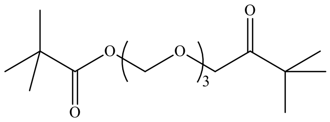	0.95	29.3
Squalane	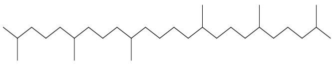	0.81	30.7
Glyceryl tri(2-ethyl-hexanoate)	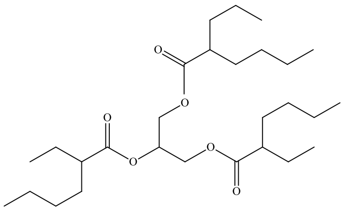	0.95	30.8
Pentaerythritol tetra-(2-ethylhexanoate)	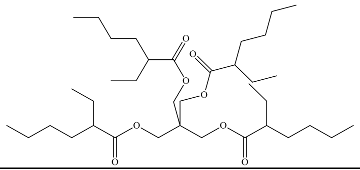	0.96	32.1

Table 2.4 (continued).

Oil	Structure	ρ/g cm^{-3}	γ_{la}/mN m^{-1}
Liquid paraffin	Mixture of heavy alkanes	0.86	32.3
Cetyl 2-ethylhexanoate	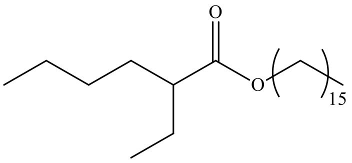	0.86	32.6
Macadamia nuts oil	Mixture of triglyceride of oleic, palmitoleic, linoleic and linolenic acids	0.87	35.1
Jojoba oil	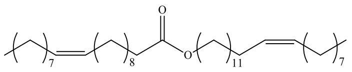	0.87	35.2
2-Ethylhexyl-4-methoxycinnamate	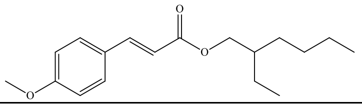	1.00	36.8

2.2 Methods

2.2.1 Oil-Water Interfaces: Tricaprylin- and Miglyol 812N-Water Emulsions Stabilised by Anisotropic $CaCO_3$ Particles

2.2.1.1 Characterisation of $CaCO_3$ Particles

2.2.1.1.1 Scanning Electron Microscopy of Particles

$CaCO_3$ particles were viewed as received and from a dried sample of their suspension. The dry samples were applied to a carbon sticky disk. After excess sample was removed with compressed air, particles that stuck to the disk were coated with a thermally evaporated carbon film (≈ 5 nm thick) using an Edwards High Vacuum Coating Unit. Micrographs were taken with the Zeiss EVO 60 SEM at a beam voltage of 20 kV and probe current of 70 pA. Both the rod- and cube-shaped $CaCO_3$ particle suspensions (0.34 wt. %) were prepared by dispersing 1 g of the particles in 15 cm^3 of water using a Branson ultrasonic digital sonifier 450 operating at 20% amplitude for 2 min (inclusive of 2 s operation and 2 s rest periods). During sonication, it was necessary to cool the mixture in an ice bath to prevent it from warming up. The required volume (0.5 cm^3) of each mixture was diluted with 9 cm^3 of Milli-Q water to obtain suspensions having concentration ≈ 0.34 wt. %. About 15 μL of the diluted suspension was pipetted onto the SEM cover slip and studied similarly using the SEM, after drying at ambient conditions. Micrographs (Figure 2.4) were obtained directly into a computer using hardware and software designed in-house and edited using Photoshop 7 software. The average length L and radius r_{rod} of the rod-shaped particles, measured from Figure 2.4 by averaging the L and r_{rod} of 30 particles, are approximately 13 μm and 0.4 μm respectively. In contrast, L = 20−30 μm and r_{rod} = 0.25−0.5 μm according to the manufacturer. The average length l' of the cubed-shaped particles, also measured from Figure 2.4 by averaging l' of 30 particles, is approximately 3 μm compared with 4−7 μm given by the manufacturer. Because of the polydisperse nature of the rod- and cube-shaped $CaCO_3$ particles, the standard deviation of the 30 separate measurements is ≈ 4 μm. Based on these measurements, the volume V of the rod- and cubed-shaped $CaCO_3$ particles (calculated using equation 2.1) is approximately 6.4 μm^3 and 27 μm^3, respectively. For calculating V, the rod-shaped particles were liken to cylinders having hemispherical ends with their average length (excluding the hemispherical ends) as L' = 12.2 μm. Clearly, the volume of the cube-shaped $CaCO_3$ particles is about four times that of the rod-shaped ones.

Figure 2.4. SEM micrographs of rod-shaped (upper) and cube-shaped (lower) hydrophilic $CaCO_3$ particles viewed as received (left) and from a dried sample (15 μL) of an aqueous suspension (0.34 wt. %) of the particles (right).

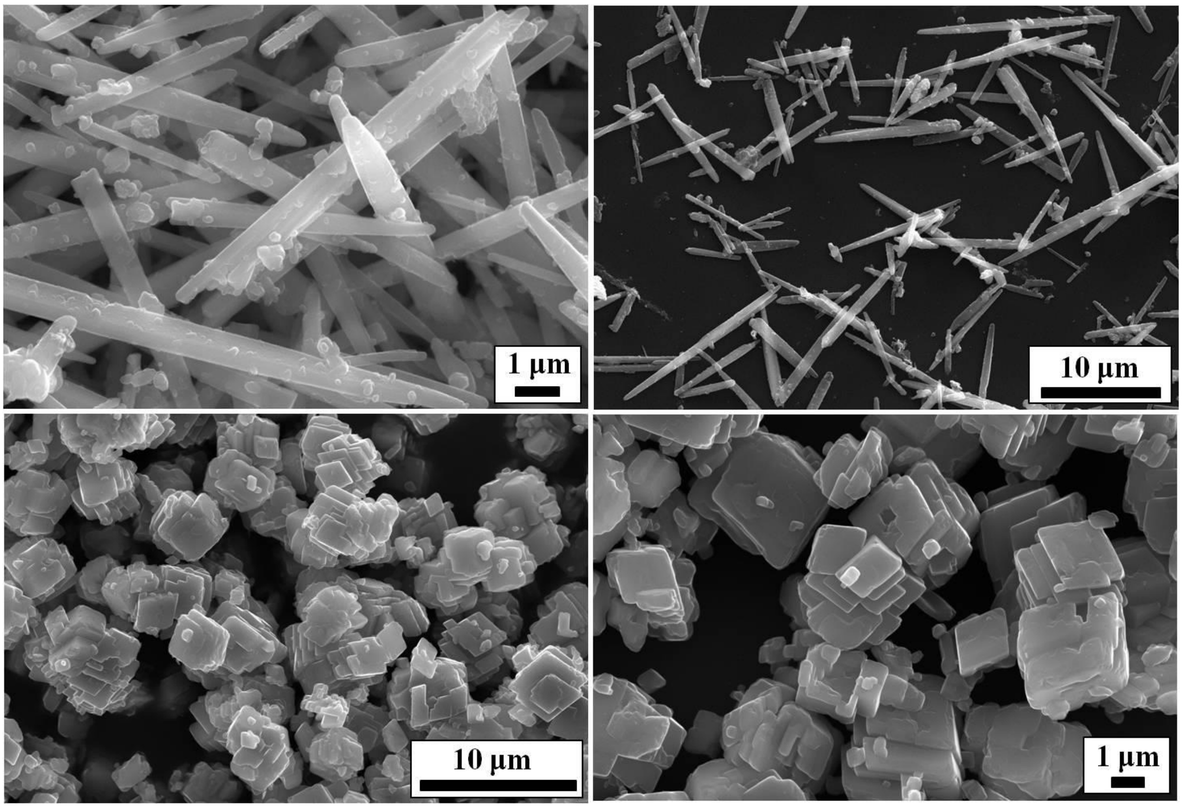

$$V = \begin{cases} \pi\, r_{\mathrm{rod}}^2 L' + \dfrac{4}{3}\pi\, r_{\mathrm{rod}}^3 & \text{rod-shaped} \\ l^3 & \text{cube-shaped} \end{cases} \tag{2.1}$$

2.2.1.2 Zeta Potential of Particles

The zeta potential ζ of both the rod- and cube-shaped $CaCO_3$ particles was determined separately, firstly, in aqueous suspensions (0.125 wt. %) of different pH values and secondly in NaCl solutions of different concentrations. In the first instance, the required mass (0.125 g) of particles was dispersed in 10 cm^3 of Milli-Q water using a Branson ultrasonic probe with a head of diameter 0.6 cm operating at 20% amplitude for 2 min (inclusive of 2 s operation and 2 s rest periods) with constant cooling in an ice bath. The suspension was then made up to 100 cm^3 using Milli-Q water. The pH of 2.5 cm^3 of the suspension was adjusted from 8.8 (rod-shaped particles) or 9.2 (cube-shaped) to other values (between *ca.*10–13) using 0.5 M NaOH solution. For the effect of salt concentration, 2.5 cm^3 of NaCl solution of varying concentrations (0–1000 mM) containing 0.125 wt. % of $CaCO_3$ particles was used. The required mass (about 3 mg) of particles was dispersed in the various NaCl solutions using a Branson ultrasonic probe at the same conditions mentioned previously. The stability of these suspensions to sedimentation was assessed by noting the time it took all the particles to settle at the bottom of the vessel. Due to the relatively large size and low surface charge (see later) of the $CaCO_3$ particles, the particles of all the dispersions settled at the bottom of the vessels about 1 hour after preparation. After 24 hours, the suspensions were re-dispersed by hand shaking and their ζ was measured by using a Malvern Zetasizer Nano series. It was not possible to measure ζ for dispersions containing above 0.1 M.

The Malvern Zetasizer Nano series measures the electrophoretic mobility U of the particles in the suspension and converts it to ζ by using the Henry equation which is given by equation 2.2. The ε_o is the permittivity of free space, ε is the dielectric constant of the medium, η stands for viscosity of the medium and $f(\kappa_D a)$ is the Henry's function which is approximately equal to 1.5 (for moderate electrolyte concentration) or 1 (for relatively high electrolyte concentration). For $f(\kappa_D a) \approx 1.5$, the Henry's equation translates to the Smoluchowski model. The U is obtained by performing an electrophoresis experiment on the sample and measuring the velocity of the particles using laser Doppler velocimetry (LDV) described schematically in Figure 2.5. In LDV, a beam of light from the laser is split into the incident and reference beams. The reference beam is modulated to create the Doppler effect. The laser beam passes through the sample cell where it is scattered by the particles at an angle of 13°. During electrophoresis, the particles in the suspension move through the sample cell (to the necessary electrode) in response to an applied electric field as they possess electric charges. This causes the intensity of light detected to fluctuate with a frequency proportional to the speed of the particles. This information is detected and sent to the digital signal processor and then to the computer where the Zetasizer software produces a frequency spectrum from which the U and hence the ζ is calculated. The role of the attenuator and compensation optics in Figure 2.5 is to regulate the amount of light passing through the sample cell and correct for the thickness of the sample cell wall and the dispersant refraction, respectively.

$$U = \frac{2\zeta\varepsilon\varepsilon_o f(\kappa_D a)}{3\eta} \tag{2.2}$$

Figure 2.5. Schematic illustration of the working principle of Malvern Zetasizer Nano series (taken from Malvern Zetasizer Nano series manual): (a) laser, (b) incident beam, (c) beam splitter, (d) reference beam, (e) attenuator, (f) sample cell, (g) scattered beam, (h) compensation optics, (i) combining optics, (j) detector, (k) digital signal processor and (l) computer.

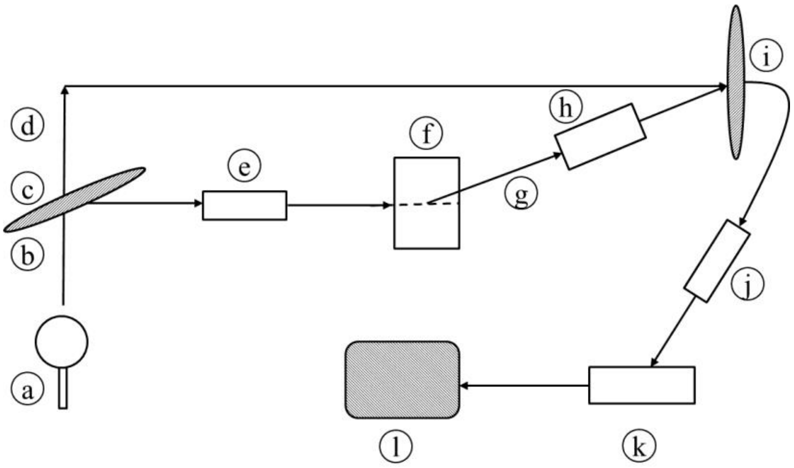

2.2.1.2.1 Preparation and Characterisation of Tricaprylin- and Miglyol 812N-Water Emulsions

Emulsions (containing varying volume fraction of oil ϕ_o) were prepared using the powdered particle and particle dispersion methods. The emulsions were prepared in screw cap glass vials of inner diameter 2.4 cm and height 7.2 cm, using an IKA T25 digital Ultra-Turrax homogeniser with an operating head of inner diameter 1.3 cm at 13000 rpm for 3 min at ambient conditions. Mathematically, ϕ_o is volume(cm^3) of oil in an emulsion divided by the sum of the volume(cm^3) of oil and water in the emulsion. The powdered particle method involves measuring the required volume of water into a glass vial, followed by addition of the required amount of the particles and then the required volume of oil and finally homogenisation. In the particle dispersion method, the required amount of particle is dispersed in the required volume of water using a Branson ultrasonic probe at 20% amplitude for 2 min (inclusive of 2 s operation and rest periods with constant cooling in an ice-bath) before the required volume of oil is added and homogenised. Using the first method, batch emulsions containing equal volumes (7 cm^3) of water and oil or 11.2 cm^3 of water and 2.8 cm^3 of oil (*i.e.* $\phi_o = 0.5$ or 0.2) were prepared in the presence of different concentrations (0.1−5 wt. %) of the rod-shaped $CaCO_3$ particles. In addition, emulsions containing varying ϕ_o (0.05−0.95) were prepared at a fixed particle concentration (4 wt. %). All the particle concentrations used throughout this work are with respect to the total volume (14 cm^3) of oil and water in the emulsions. The control emulsions were prepared in the absence of the particles. For the second method, emulsions containing equal volumes (7 cm^3) of water and oil were prepared in the presence of 4 wt. % of the rod- and cube-shaped $CaCO_3$ particles.

Immediately after homogenisation, the continuous phase of the emulsions was inferred from the drop test and conductivity measurements using a Jenway 4510 conductivity meter with Pt/Pt black electrodes. The pH of the emulsions was measured using a Fisherbrand Hydrus 400 pH meter immediately after preparation. For optical microscopy, a drop of an emulsion was diluted with 8 drops of Milli-Q water. A drop of the diluted emulsion was then viewed on a dimple glass slide (Fisher Scientific) using the Olympus BX-51 optical microscope fitted with a DP50 digital camera. The camera was connected to a computer having Image-Pro Plus 6.0 software (Media Cybernetics). Cryo-SEM was also carried out on the 2 wt. % of the rod-shaped and 4 wt. % of the cube-shaped $CaCO_3$ particle-stabilised tricaprylin emulsions prepared by the powdered particle method. An emulsion sample was pipetted onto an aluminium cryo stub, to a thickness of 3−4 mm, and plunged into liquid nitrogen slush (−210 °C). The frozen sample was transferred to a cryo system (Quorum Technologies PP3010T) cold stage (−140 °C) and the temperature was raised to −70 °C and kept constant for about 10 min. Because the pressure in the chamber is quite low (10^{-6} to 10^{-5} mbar), some of the frozen water in the continuous phase of the emulsions sublime and condense on the anticontaminator surface (−170 °C) leaving part of some of the emulsion droplets exposed. The droplets surfaces were then sputter-coated with platinum and transferred to the SEM cold stage and examined at −140 °C at a beam voltage of 15 kV and probe current of between 20 and 30 pA.

The stability of the emulsions to creaming and coalescence was assessed by noting the fraction of water f_w and the fraction of oil f_o released in 4 months, respectively. $f_w(f_o)$ equals the volume of water(oil) released divided by the initial volume of water(oil) in the emulsion. Photos of the glass vials containing the emulsions and other photos shown throughout the thesis were taken with a Canon PowerShot SX220 HS camera. The size distribution of the emulsions was determined by light diffraction using a Malvern Mastersizer 2000 instrument. Determination of emulsion droplet size distribution by light diffraction and other techniques requires dilution of the emulsion to low dispersed phase volume fractions. In surfactant-containing systems, the diluting phase needs to be of the same composition as the continuous phase of the emulsion to prevent desorption of surfactant molecules from the surfaces of the emulsion droplets.[11] In order to obtain a protocol for diluting the emulsions in this study, the effect of the rod-shaped $CaCO_3$ particle concentration (2×10^{-3} to 4×10^{-3} wt. %) in the diluting phase on the droplet size of the emulsion was studied on the 2 wt. % of rod-shaped $CaCO_3$ particle-stabilised emulsions (prepared by the powdered particle method). The droplet size of the emulsions remained unchanged when diluted with only water or with the $CaCO_3$ particle dispersion (see Appendix 1) and thus only water was used to dilute the emulsions for sizing. The emulsions (10 to 12 drops) were dispersed in about 150 cm^3 of water in the sample presentation unit by stirring at 1500 rpm and used for droplet size distribution measurement.

Laser diffraction measures the emulsion droplet size distributions by measuring the angular variation in the intensity of light scattered as a laser beam passes through the diluted emulsion sample in the presentation chamber. Large emulsion droplets scatter light at small angles relative to the laser beam, but small emulsion droplets scatter light at large angles (Figure 2.6). The angular scattering intensity data is then analysed to calculate the size of the emulsion droplets responsible for creating the scattering pattern using the Mie theory of light scattering. The Mie theory requires the optical properties of the emulsion droplets and the continuous phase. The size of the emulsion droplets is reported as a volume equivalent sphere diameter.

Figure 2.6. Schematic illustration of the working principle of Malvern Mastersizer 2000 (taken from Malvern Mastersizer 2000 manual): (a) source of laser beam, (b) first optical system, (c) focused laser beam, (d) emulsion sample, (e) diffracted light, (f) second optical system, (g) focused diffracted light, (h) light angle detector and (i) computer.

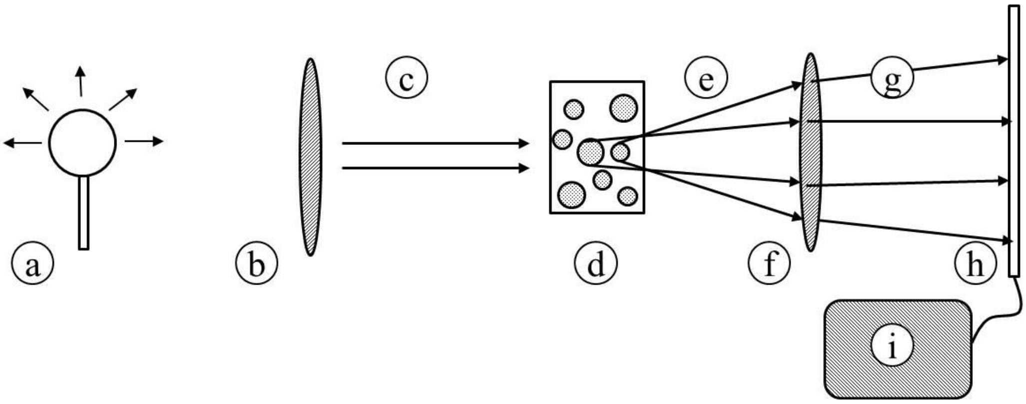

2.2.1.2.2 *Effect of Salt Concentration on the Stability of the Emulsions*

The effect of salt concentration on the stability of the emulsions was studied in the range of 1–1000 mM NaCl. Batch emulsions containing equal volumes (7 cm^3) of water and oil were prepared by the powdered particle method in the presence of 4 wt. % of $CaCO_3$ particles in screw cap glass vials. The required mass of $CaCO_3$ particles was placed in aqueous NaCl solutions of different concentrations, followed by addition of the required volume of oil and then homogenised using the IKA T25 digital Ultra-Turrax homogeniser at 13000 rpm for 3 min. The stability of the emulsions to creaming and coalescence was assessed by noting the f_w and the f_o released in a month, respectively. Where the emulsion droplets are small enough to be viewed under a microscope, *e.g.* below 0.05 M NaCl (emulsions containing rod-shaped $CaCO_3$ particles) or 0.5 M NaCl (emulsions containing cube-shaped $CaCO_3$ particles), one drop of the emulsion was diluted with 8 drops of an aqueous solution containing the same [NaCl] as the emulsion. The diluted emulsion was then viewed on a dimpled glass slide using the Olympus BX-51 optical microscope fitted with a digital camera. In the case of Miglyol 812N emulsions stabilised by cube-shaped $CaCO_3$ particles, it was not necessary to dilute a sample of the emulsion before viewing because of the relatively small number of oil droplets they contain. The optical micrographs obtained were used to determine the droplet size of the tricaprylin emulsions by averaging the diameter of at least 100 droplets. Miglyol 812N emulsions have droplets of irregular shape and it was not possible to determine their average diameter.

2.2.1.2.3 Effect of pH on the Stability of the Emulsions

The effect of pH on the stability of the emulsions was investigated in the pH range of 4–12 at ambient conditions. Batch emulsions containing equal volumes (7 cm^3) of water and oil were prepared by the powdered particle method in the presence of 4 wt. % of $CaCO_3$ particles in screw cap glass vials using the IKA T25 digital Ultra-Turrax homogeniser at 13000 rpm for 3 min. Immediately after preparation, the pH of the emulsions was adjusted from around 8 for rod-shaped $CaCO_3$ stabilised emulsions or 9 for cubed-shaped $CaCO_3$ stabilised emulsions to the desired pH. pH adjustment was done by using drops of a 3 M aqueous solution of HCl or a 0.5 M aqueous solution of NaOH. Again, the stability of the emulsions to creaming and coalescence was assessed by noting the f_w and the f_o released after a month respectively. At higher pH values (> 8) where the emulsion droplets are small enough to be viewed under a microscope, one drop of the emulsion was diluted with 8 drops of water at the same pH as the emulsions and viewed on a dimpled glass slide using the Olympus BX-51 optical microscope. Again, Miglyol 812N emulsions stabilised by the cube-shaped $CaCO_3$ particles were not diluted before viewing because of the relatively small number of emulsion droplets they contain. Similarly, the optical micrographs obtained were used to determine the size of the emulsions by averaging the diameter of at least 100 droplets.

2.2.2 Oil-Oil and Liquid (and/or Oil)-Air Interfaces

2.2.2.1 Characterisation of Fluorinated Fumed Silica Particles

2.2.2.1.1 Elemental Content and Scanning Electron Microscopy

The elemental content (C, H, N and F) of the fluorinated fumed silica particles was carried out by Medac Ltd., UK. C, H and N were determined by quantitative dynamic flash combustion analysis using the Thermo Scientific FlashEA 1112 CHNS-O Analyser. F was determined by ion chromatography using a Metrohm 761 Compact Ion Chromatography after Schöniger flask combustion. Dynamic flash combustion analysis is performed as follows. The sample is held in a tin capsule placed inside an autosampler drum and purged with continuous flow of helium and dropped at pre-set intervals into a vertical quartz tube maintained at 900 ºC. Once the sample is dropped in the furnace, the helium stream is temporarily enriched with pure oxygen which promotes a violent reaction (flash combustion) once the sample and the tin capsule melt. Quantitative combustion is then achieved by passing the mixture of combustion gases over copper to remove excess oxygen and to reduce the nitrogen oxides to elemental nitrogen. The resulting mixture is then directed to a chromatographic column where the individual components are separated and eluted as nitrogen, carbon dioxide and water. These are then detected by a thermal conductivity detector (TCD) coupled to an automatic EAGER300 workstation which gives output signal proportional to the concentration of the individual components of the mixture. For Schöniger combustion, the required amount of the desired sample is combusted in the presence of oxygen in a platinum basket on an ashless filter paper placed in a Schöniger combustion flask. The platinum basket and combustion flask are usually cleaned with 0.5 N of NaOH and 50 v/v. % of H_2O_2 solutions prior to combustion. After combustion, the Schöniger flask is shaken on a mechanical shaker for 30 min to allow absorption of gaseous combustion products followed by addition of deionised water. The flask stopper and platinum basket are then washed with deionised water into the flask. The solution (100 cm^3) for ion chromatography is then prepared from the content of the Schöniger flask. The instrument is calibrated by running a standard solution and the chromatogram obtained is used to identify and calculate the concentration of the F^- in the sample when analysed. As shown in Table 2.5, the fluorinated fumed silica particles contain < 0.1 wt. % of nitrogen but the carbon and fluorine content increases as the degree of fluorination increases. The hydrogen content of the particles is also not constant, but it is independent of the degree of fluorination.

Table 2.5. Carbon, hydrogen, nitrogen and fluorine content (wt. %) of the various fluorinated fumed silica particles.

Particles	Nitrogen	Carbon	Hydrogen	Fluorine
75% SiOH fluorinated silica	< 0.10	1.78	1.34	5.42
59% SiOH fluorinated silica	< 0.10	3.52	1.21	9.91
50% SiOH fluorinated silica	< 0.10	5.13	1.45	10.86

SEM was used to image the dry 100% SiOH, 14% SiOH and fluorinated fumed silica particles. The procedure described in sec. 2.2.1.1.1 was used to obtain the SEM images of the particles. As shown in Figure 2.7, all the particles consist of partially fused and aggregated primary particles and there appears to be no change in their structure following silanisation or fluorination.

Figure 2.7. SEM images of (a) 100% SiOH, (b) 14% SiOH, (c) 75% SiOH fluorinated, (d) 59% SiOH fluorinated and (d) 50% SiOH fluorinated fumed silica powders at two magnification.

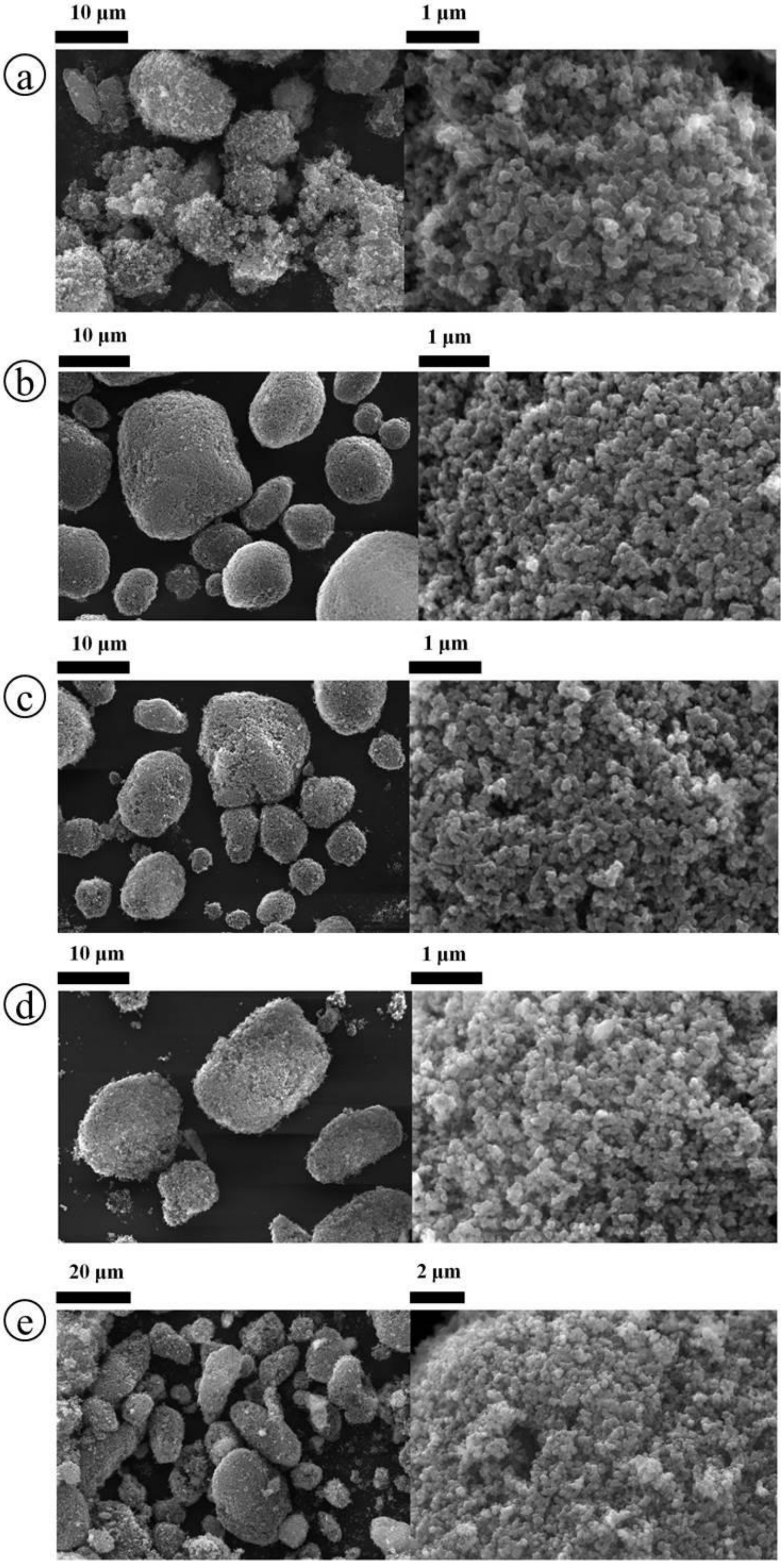

2.2.2.1.1.1 Measurement of Fumed Silica Particle-Liquid-Air Contact Angles

Since it is difficult to measure the θ_{la} small solid particles make with liquid surfaces, glass slides spin coated with a layer of the particles was used to gain an idea of these angles using the sessile drop method. Because the measured values of θ_{la} are not the true angles the particles make with the liquid surfaces, they are considered as apparent contact angles. Firstly, separate ethanol dispersions containing 1.5−8 wt. % of 14% SiOH silica particles were used to spin coat separate hydrophilic glass slides (3.6 cm × 2.5 cm). The dispersions were obtained by dispersing the required mass of the particles in ethanol (5 g) in a screw cap glass vial (inner diameter 1.8 cm and height 7.2 cm) using the Branson ultrasonic digital sonifier 450. Sonication was at 30% amplitude for 2 min (inclusive of 4 s operation and 2 s rest periods) with constant cooling in an ice bath. These dispersions (750 μL) were used to spin coat the hydrophilic glass slides (Fisher Scientific) using a Cookson Electronics P6700 spin coater at 800 rpm for 40 s (inclusive of 5 s acceleration and 5 s deceleration periods) and dried at ambient conditions for 24 hours in petri dishes. The apparent advancing θ_{la} made by sessile water and *n*-hexadecane drops (0.1 cm^3) with the spin coated glass slides was measured with a Krüss DSA Mk 10 instrument. The results of 4 separate measurements were averaged. As shown in Figure 2.8, the apparent θ_{la} for water droplets initially increases with increasing [14% SiOH fumed silica] in the ethanol dispersion and became constant at concentrations above 5 wt. % where the glass slides are presumably sufficiently coated by the silica particles. The apparent θ_{la} for *n*-hexadecane was constant irrespective of the particle concentration. Based on the foregoing, dispersions of the rest of the silica particles were prepared similarly using different solvents with the particle concentration varying between 4 to 9 wt. % as shown in Table 2.6. This was dependent on the viscosity of the dispersion and the nature of the particle coating obtained from it upon spin coating. In summary, the particle concentrations and solvents used for the rest of the particles were 9 wt. % of 100% SiOH fumed silica particles in ethanol-water (1:3) mixture, 8 wt. % in ethanol for 75% SiOH, 5 wt. % in acetone for 59% SiOH and 4 wt. % in cyclohexane for 50% SiOH fluorinated fumed silica particles. The apparent advancing and receding θ_{la} of a sessile liquid droplet in air on these surfaces were measured. The required volume (0.1 cm^3) of a liquid for apparent advancing θ_{la} was placed on the particle-coated glass slides using a glass syringe having a needle of inner diameter 0.1 mm. To obtain the apparent receeding θ_{la}, 0.05 cm^3 of liquid was withdrawn from the 0.1 cm^3 droplet used previously for apparent advancing θ_{la}. The average of 4 separate measurements is reported (see chapter 5; Table 5.2). The apparent advancing θ_{la} of the seven probe liquids was used to calculate the apparent γ_{sa} of the particles (see sec. 2.2.2.3). For comparison, the apparent θ_{la}(advancing) the probe liquids make with the surfaces of a PTFE substrate was also measured (similarly) and used for the calculation of its apparent surface energy as shown in sec. 2.2.2.3.

Figure 2.8. Apparent advancing contact angle θ_{la} (± 2°) of sessile water (●) and *n*-hexadecane (○) droplets (0.1 cm^3) on hydrophilic glass slides coated with 14% SiOH fumed silica particles *versus* [14% SiOH fumed silica particles] in ethanol dispersions used to spin coat the glass slides. The apparent advancing θ_{la} of both water and *n*-hexadecane on a hydrophilic glass slide is < 5° and it is consistent with previous findings.[12]

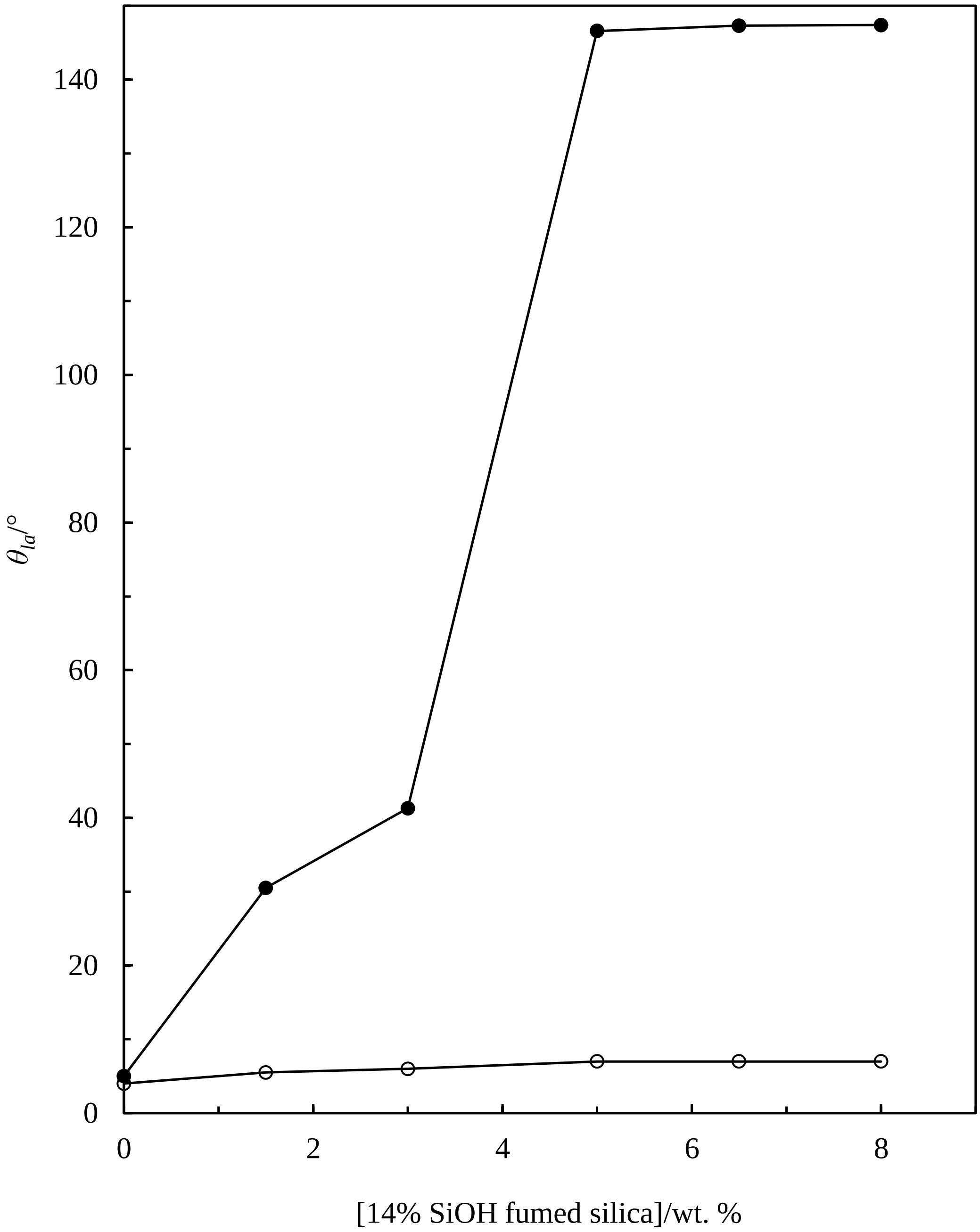

Table 2.6. Particle type, particle concentration, solvent and nature of spin coated glass slide surfaces. ✗: surface is not good for measurement of apparent θ_{la} either due to crack of particle layer or insufficient particle coating, ✓: surface is good for measurement of apparent θ_{la} as a result of good particle coating and lack of substantial cracks.

Fumed silica particles	[Particle]/wt. %	Solvent	Result
14% SiOH silica	1.5	Ethanol	✗
	3	Ethanol	✗
	5	Ethanol	✓
	6.5	Ethanol	✓
	8	Ethanol	✓
75% SiOH fluorinated silica	5	Ethanol	✗
	5	*n*-Hexane	✗
	5	Toluene	✗
	5	Perfluorohexane	✗
	5	Acetone	✗
	8	Ethanol	✓
59% SiOH fluorinated silica	5	Ethanol	✗
	5	*n*-Hexane	✗
	5	Toluene	✗
	5	Perfluorohexane	✗
	5	Acetone	✓
50% SiOH fluorinated silica	4	Cyclohexane	✓
100% SiOH silica	9	Ethanol-water (1:3)	✓

2.2.2.2 Characterisation of Fluorinated Clay and Fluorinated ZnO Particles

2.2.2.2.1 General Morphology and Elemental Analysis

SEM was used to characterise the particles in terms of morphology and elemental content. SEM images were obtained from the powdered particles whilst their elemental information was gathered from compressed disks composed of the particles (see particle disk formation procedure later). To obtain an evenly distributed monolayer of dry particles for SEM study, a sample mount (carbon sticky disk) containing a self-adhesive was pressed into a powdered bed of the particles. Loosely held particles were removed with compressed air. The sample mount was afterwards thermally coated with a thin layer (*ca*. 15 nm) of carbon using an Edwards High Vacuum Coating Unit and examined with the Zeiss EVO 60 SEM at a beam current of 40 μA and probe current of 101 pA. Micrographs were obtained directly into a computer using hardware and software designed in-house and edited using Photoshop 7 software. Thereafter, using similar conditions, the particle disks were stuck to the SEM sample mount and probed for elemental content. Their energy dispersive X-ray (EDX) elemental maps were also stored and processed, similarly.

The SEM images of the sericite particles are shown in Figure 2.9. As can be seen, the PF-0 Eight Pearl 300S-Al particles are made up of agglomerated, relatively smooth platelet particles (primary particle size *ca*. 2 μm and several nm thick) compared to the treated ones which are discrete and textured due to the presence of crystals of $Al(OH)_3$ used to augment the fluorination reaction. Elemental analysis shows that the particles contain C, O, F, Na, Mg, Al, Si, P, S, Cl, K, Ti and Fe (Figure 2.10 and Appendix 2), just like many other sericite particles.[37] Carbon, fluorine and phosphorus are present in varying amounts depending on the degree of fluorination (Table 2.7). Hydrogen was not detected because SEM does not detect elements below carbon in the periodic table.

Figure 2.9. SEM images of powdered sericite particles: PF-(a) 0, (b) 5, (c) 8, (d) 10 and (c) 12 Eight Pearl 300S-Al. Scale bar = 2 μm.

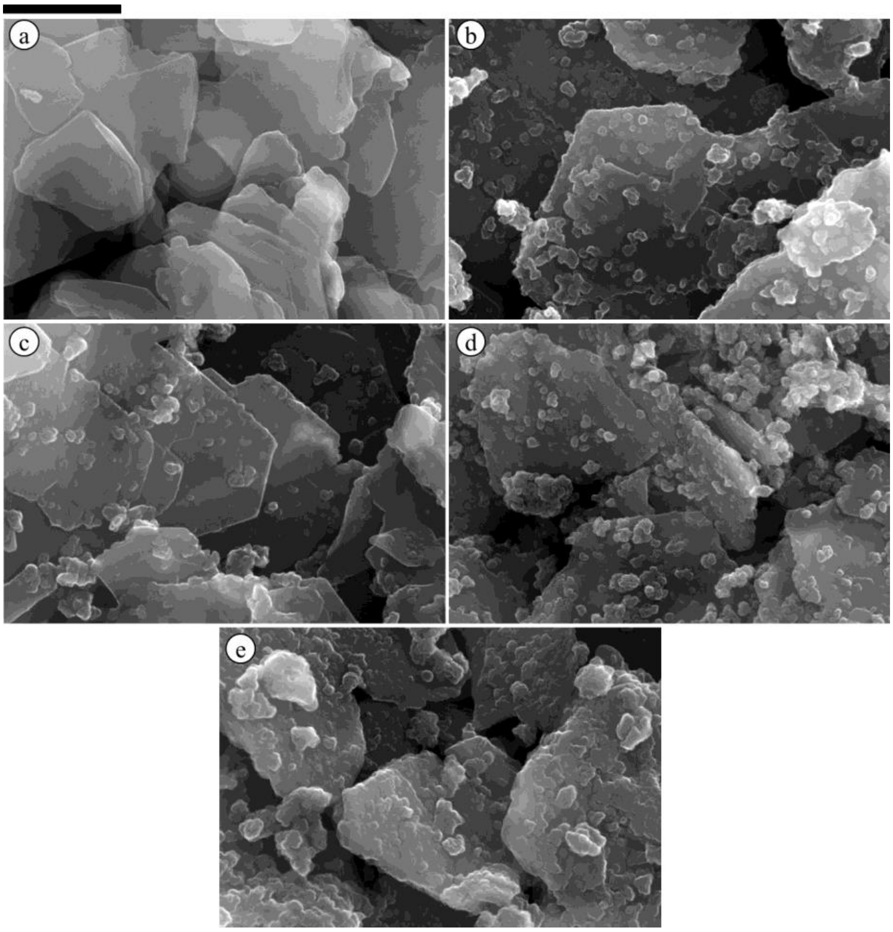

Figure 2.10. EDX maps of PF-(a) 0, (b) 5, (c) 10 and (d) 12 Eight Pearl 300S-Al sericite particles.

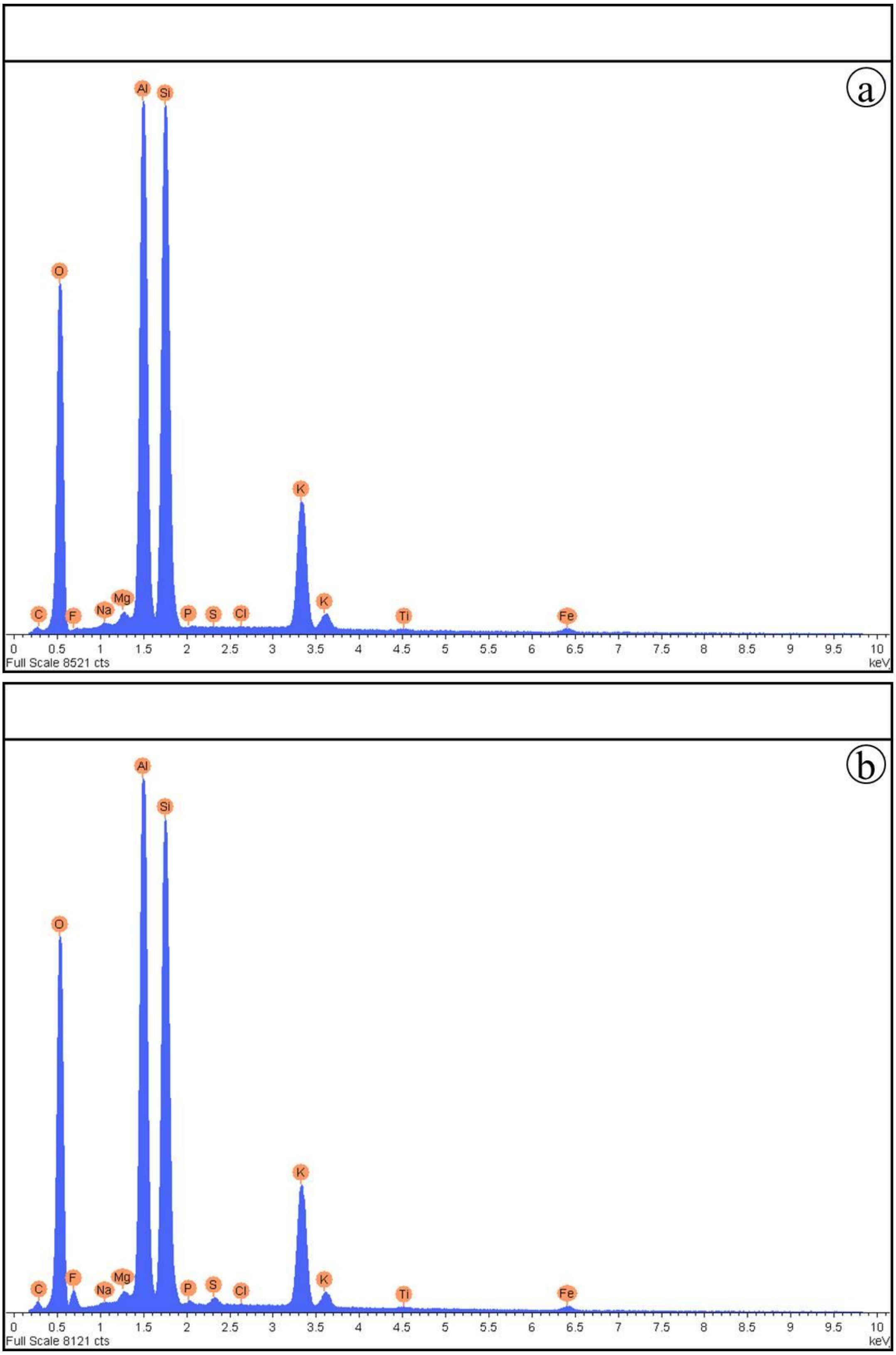

Figure 2.10 (continued).

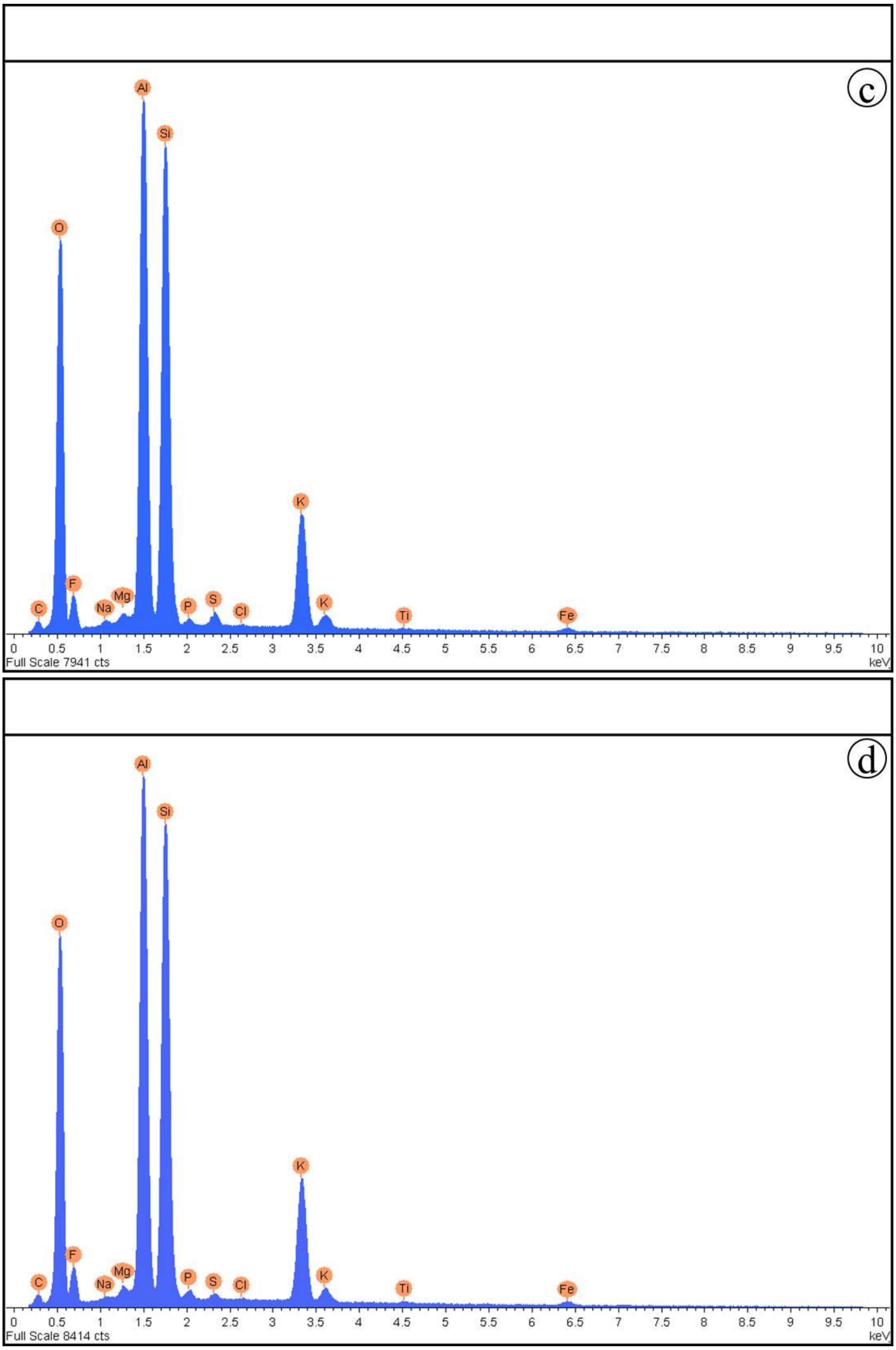

Table 2.7. Elemental composition (wt. %) of the Eight Pearl 300S-Al sericite particles used.

Particle	wt. %												
	C	O	F	Na	Mg	Al	Si	P	S	Cl	K	Ti	Fe
PF-0	1.15	50.45	0	0.15	0.32	17.37	22.15	0	0	0	7.67	0.14	0.60
PF-5	3.13	48.29	4.55	0.09	0.25	16.61	19.17	0.20	0.35	0	6.67	0.10	0.59
PF-8	3.64	46.14	7.53	0.11	0.30	16.08	18.42	0.26	0.29	0.05	6.49	0.12	0.58
PF-10	4.24	46.41	8.22	0.22	0.21	15.71	17.71	0.34	0.53	0.07	5.76	0.09	0.50
PF-12	4.76	45.13	8.85	0.12	0.28	15.59	17.76	0.43	0.27	0.05	6.09	0.15	0.54

The SEM images of the PFX-10 Kunipia F, PF-10 Eight pearl 300S-Al^{a}, PF-10 FSE-Al and PFX-10 ZnO (TP) particles are shown in Figure 2.11. The PFX-10 Kunipia F, PF-10 Eight pearl 300S-Al^{a} and PF-10 FSE-Al particles are also composed of textured discrete platelet primary particles whilst the PFX-10 ZnO (TP) particles are made up of textured relatively spherical particle agglomerates (size > 3 μm). The individual particles of the PFX-10 Kunipia F are > 400 μm in size and several nm thick. These particles are several times larger than those of the PF-10 Eight Pearl 300S-Al^{a} and PF-10 FSE-Al particles which are only *ca*. 6 μm long and a few nm thick. The Elemental composition of the particles is shown qualitatively and quantitatively in Figure 2.12 and Table 2.8 respectively. Al, Si and O are predominant in PFX-10 Kunipia F, PF-10 Eight Pearl 300S-Al^{a} and PF-10 FSE-Al particles whilst Zn and O are predominant in the PFX-10 ZnO (TP) particles as expected. Note that hydrogen is not detected just like in the previous particles. The SEM images of the Bentone 34, Calofort SV and Zonyl MP1400 particles are given in Figure 2.13. The Bentone 34 and Zonyl MP1400 particles are composed of shapeless agglomerates of size between 5−30 μm and 0.7−10 μm, respectively. The Calofort SV particles are made up of a network of spherical particles having primary particle diameter ≈ 91 nm.

Figure 2.11. SEM images of powdered (a) PFX-10 Kunipia F, (b) PFX-10 ZnO (TP), (c) PF-10 Eight Pearl 300S-Al^{a} and (d) PF-10 FSE-Al particles.

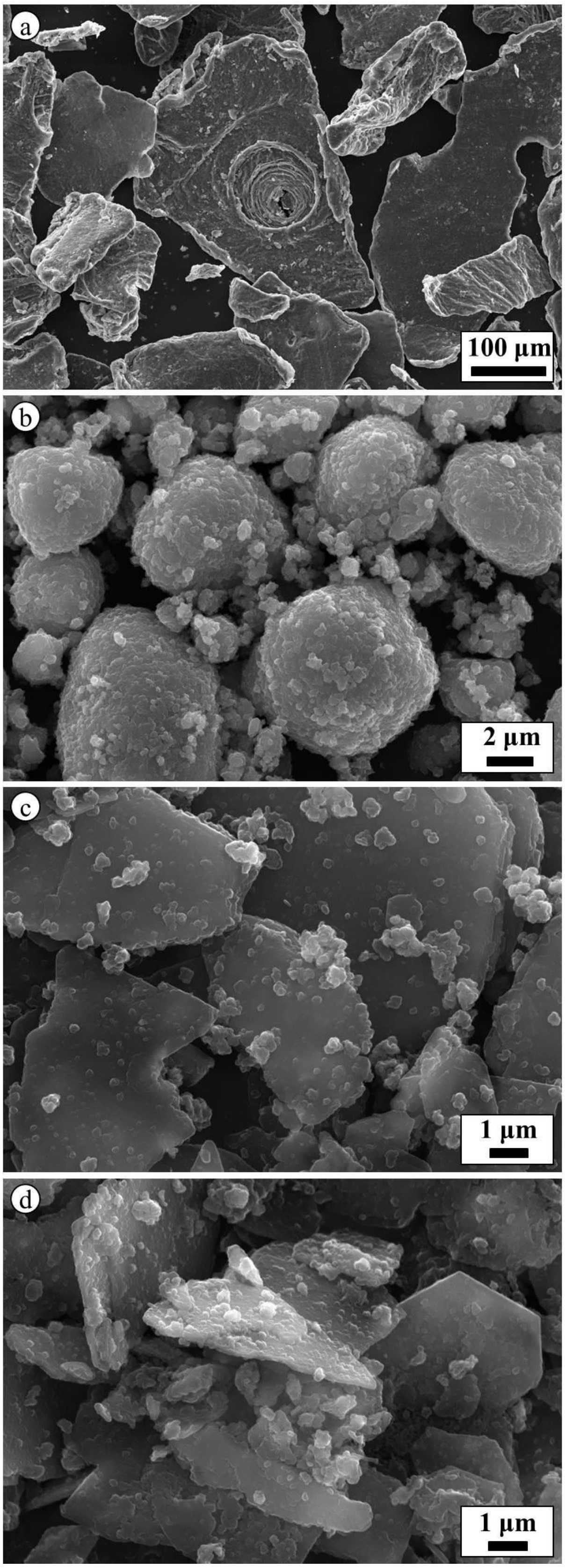

Figure 2.12. EDX maps of (a) PFX-10 Kunipia F, (b) PFX-10 ZnO (TP), (c) PF-10 Eight Pearl 300S-Al^a and (d) PF-10 FSE-Al particles.

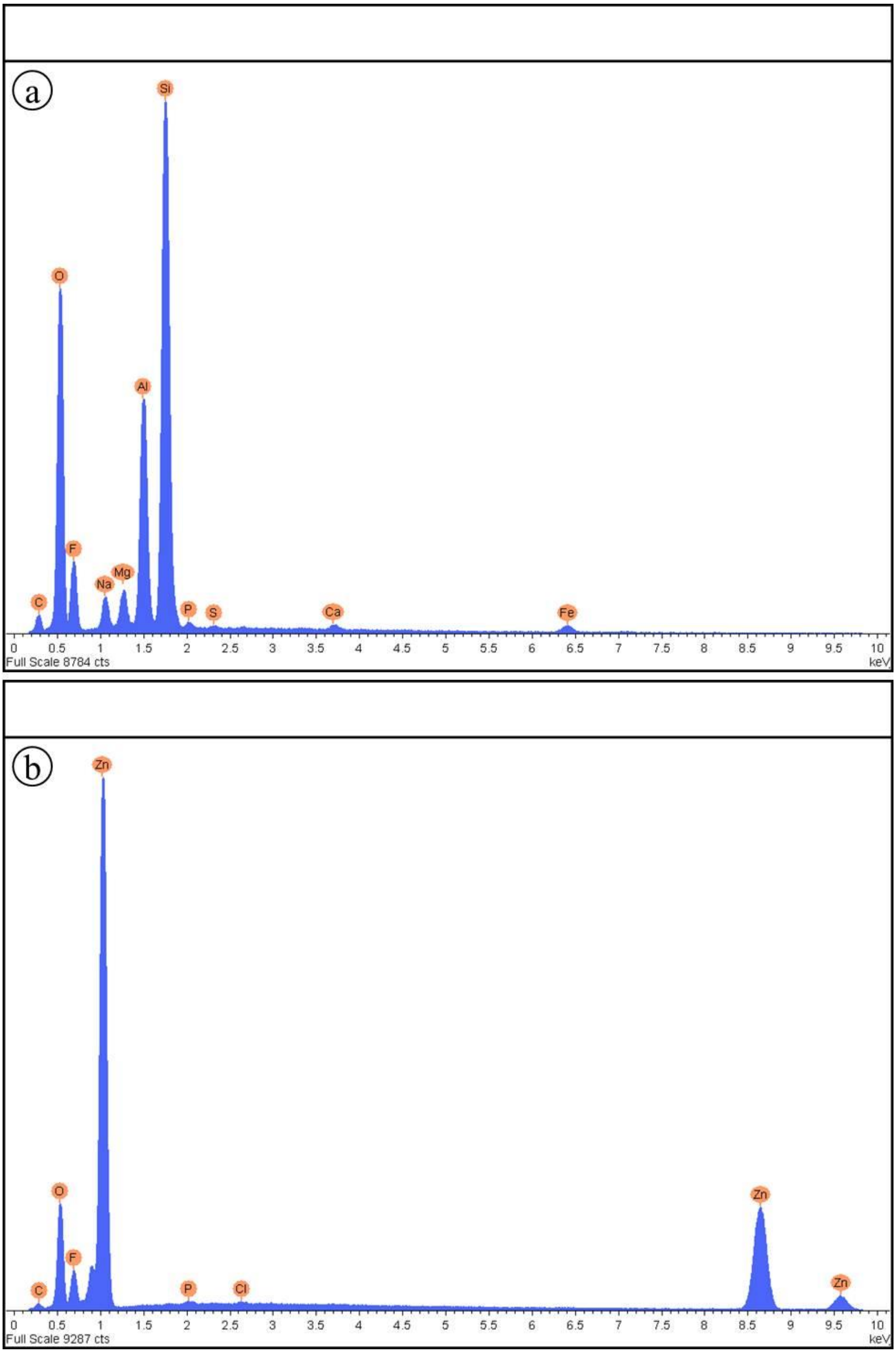

Figure 2.12 (continued).

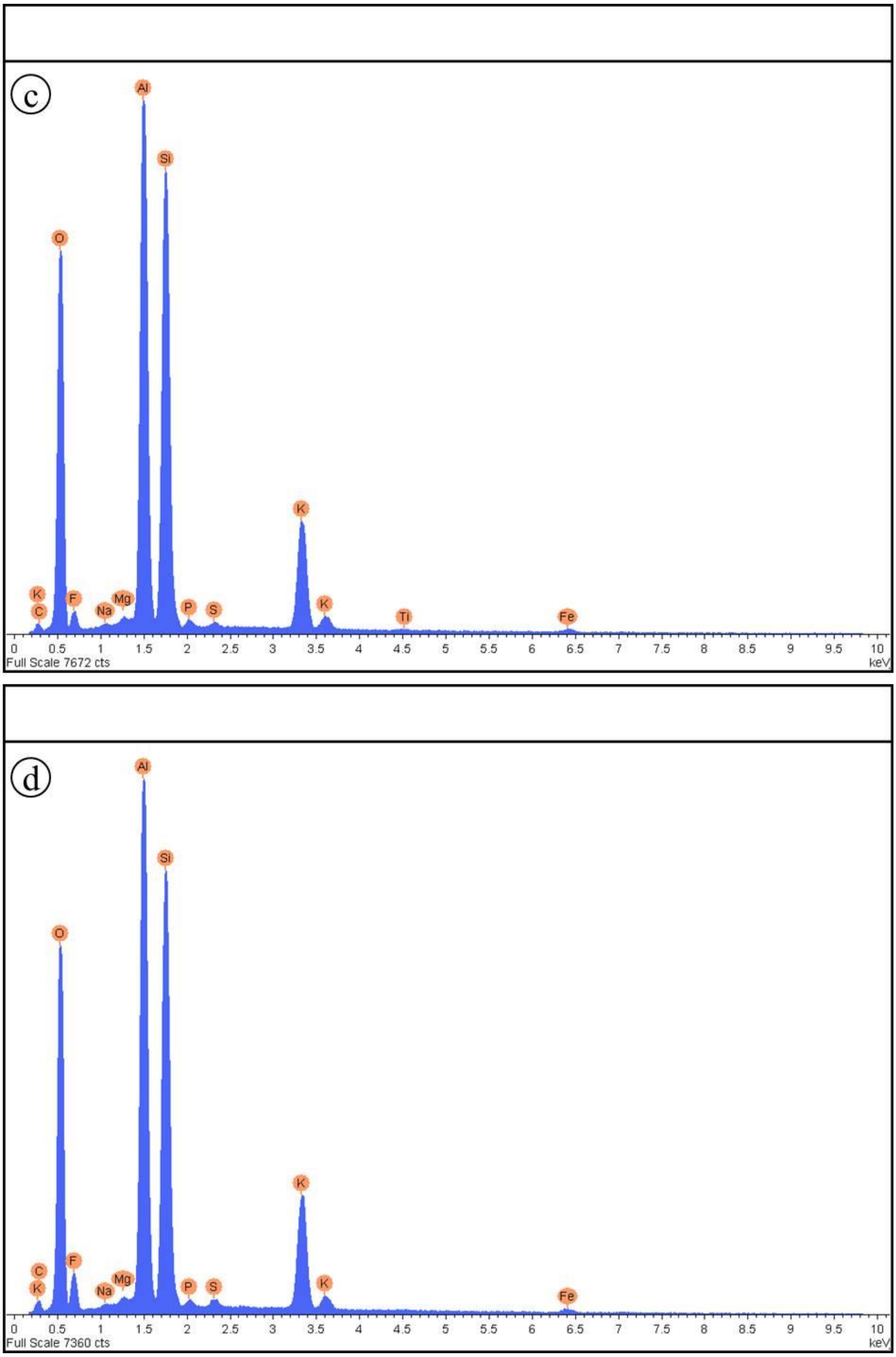

Table 2.8. Elemental composition (wt. %) of the particles shown in Figure 2.11.

	Particle			
wt. %	PFX-10 Kunipia F	PFX-10 ZnO (TP)	PF-10 Eight Pearl 300S-Al[a]	PF-10 FSE-Al
C	7.08	3.87	0.00	2.56
O	40.50	20.25	49.69	45.72
F	17.09	8.56	5.23	9.79
Na	1.97	0.00	0.16	0.16
Mg	1.52	0.00	0.16	0.15
Al	8.42	0.00	17.70	16.87
Si	21.59	0.00	19.37	17.34
P	0.31	0.34	0.42	0.35
S	0.14	0.00	0.24	0.39
K	0.00	0.00	6.40	6.20
Ca	0.28	0.00	0.00	0.00
Ti	0.06	0.00	0.10	0.00
Fe	1.04	0.00	0.54	0.47
Cl	0.00	0.21	0.00	0.00
Zn	0.00	66.78	0.00	0.00

Figure 2.13. SEM images of (a) Bentone 34, (b) Calofort SV and (c) Zonyl MP1400 particles.

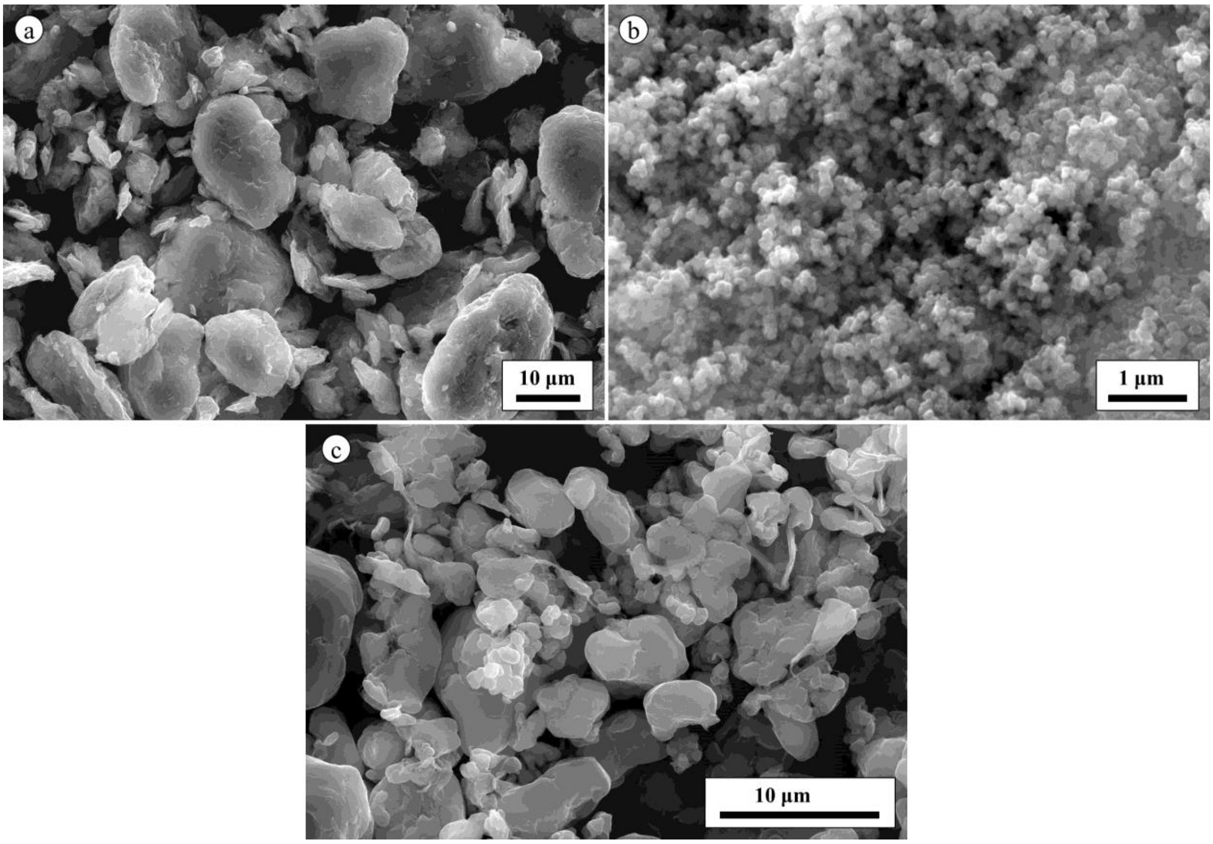

2.2.2.2.2 Measurement of Fluorinated Clay and Fluorinated ZnO Particle-Liquid-Air Contact Angles

Since it is difficult to measure θ_{la} small solid particles make with liquid surfaces, especially if they are irregular and polydisperse, relatively smooth disks (diameter 13 mm and thickness ≈ 1 mm) of the particles were used to gain an idea of θ_{la}. Because the measured values of θ_{la} are not the true angles the particles make with the liquid surfaces, they are considered as apparent contact angles. The disks were obtained by compressing *ca*. 400 or 500 mg of dry particles in a 13 mm diameter steel die with a hydraulic press (Research & Industrial Instrument Co., UK) under a pressure of approximately 9.0×10^8 N m^{-2}. Prior to making the disks, the compression pressure was varied between *ca*. 1.1×10^8 and 9.0×10^8 N m^{-2} on the PF-12 Eight Pearl 300S-Al fluorinated sericite particles (400 mg) so as to decide which compression pressure to use. Generally, the apparent advancing θ_{la} of water (146 ± 2°) and *n*-hexadecane (116 ± 2°) in air measured on the compressed particle disks were fairly consistent throughout the compression pressures used. It is acknowledged that these particle disks may have pores through which the liquids may enter into them, but this was observed to be insignificant as the liquids tend to spread on the disks for relatively low (≤ 5°) contact angles. For all the liquids, except the probe liquids where only advancing contact angle is necessary, both the apparent advancing θ_{la} (0.1 cm^3 of liquid) and receding θ_{la} (0.05 cm^3 of liquid) were measured. Values of apparent θ_{la} were measured with the Krüss DSA Mk 10 instrument using the sessile drop technique by obtaining a profile of a liquid droplet on the particle disks directly into a computer. The required volume (0.1 cm^3) of a liquid for apparent advancing θ_{la} was placed on the disks using a glass syringe having a needle of inner diameter 0.1 mm. To obtain the apparent receeding θ_{la}, 0.05 cm^3 of liquid was withdrawn from the 0.1 cm^3 droplet used previously for apparent advancing θ_{la}. For both the apparent advancing and receeding θ_{la}, an average of 4 separate measurements is reported. The apparent advancing θ_{la} of the seven probe liquids was used to calculate the apparent surface energy of the particles (see sec. 2.2.2.3).

2.2.2.3 Calculation of Surface Energy of Solid Particles

The apparent advancing θ_{la} of the probe liquids on glass slides spin coated with the 100% SiOH, 14% SiOH and fluorinated fumed silica particles are given in Table 2.9. Those on compressed particle disks of the fluorinated clay and fluorinated ZnO particles are given in Tables 2.10 and 2.11. These angles were used to calculate the surface energy γ_{sa} of the solid particles. Because the calculated γ_{sa} is not the true surface energy of the particles, it is regarded as the apparent surface energy of the particles. Several theoretical models, *e.g.* the Owens-Wendt-Rabel-Kaelble,[13] the van Oss[14] and the Wu[15] models, are available for calculating γ_{sa} from contact angle data of at least two polar probe liquids. These models are based on the fact that the γ_{sa} and γ_{la} are decomposable into their polar γ^p and dispersive γ^d components which are additive (equation 2.3).[13,16] The polar component is due to dipolar interactions whilst the dispersive component comes from van der Waals forces between the molecules of the material.[17] The merits and demerits of these models are not obvious. In this work, the method developed by Clint and Wicks,[18] which requires θ_{la} of seven probe liquids (polar and apolar), is used. This method has the advantage of giving a more realistic value of γ_{sa} as both polar and apolar probe liquids are used. The method is also based on the additive nature of γ^p and γ^d. The interfacial tension γ_{AB} between two phases A and B is then expressed in terms of the two components for each phase as given by equation 2.4. The $\gamma_A(\gamma_B)$ is the surface tension of phase $A(B)$ and $\gamma^d{}_{A(B)}$ and $\gamma^p{}_{A(B)}$ represent the dispersive and polar components of the surface tension of the phases, respectively. The Young equation[19] developed for perfectly smooth and chemically homogeneous surfaces, relates θ_{la} of a liquid droplet on a substrate to γ_{la}, γ_{sa} and γ_{sl} as given in equation 1.3. This equation combines with equation 2.5 to give equation 2.6.

$$\gamma = \gamma^d + \gamma^p \tag{2.3}$$

$$\gamma_{AB} = \gamma_A + \gamma_B - 2\left(\sqrt{\gamma_A^d \gamma_B^d} + \sqrt{\gamma_A^p \gamma_B^p}\right) \tag{2.4}$$

$$\gamma_{sl} = \gamma_{la} + \gamma_{sa} - 2\left(\sqrt{\gamma_{sa}^d \gamma_{la}^d} + \sqrt{\gamma_{sa}^p \gamma_{la}^p}\right) \tag{2.5}$$

$$0.5\gamma_{la}(1+\cos\theta_{la}) = \sqrt{\gamma_{sa}^d \gamma_{la}^d} + \sqrt{\gamma_{sa}^p \gamma_{la}^p} \tag{2.6}$$

Equation 2.6 contains two unknowns, $\gamma_{sa}{}^d$ and $\gamma_{sa}{}^p$, the components of the solid surface energy as the other terms exist in the literature for the probe liquids. Finding the unknowns requires θ_{la} from at least two liquids of different polarity so that simultaneous versions of equation 2.6 can be solved. Following the procedure in ref. 18, seven probe liquids (water, glycerol, formamide, ethylene glycol, diiodomethane, α-bromonaphthalene and n-hexadecane) were used to perform least-squares calculation to determine the best combination of γ_{sa}^{d} and γ_{sa}^{p} that fits all the liquids simultaneously. This approach is exemplified in Figure 2.14 for some selected particles. The 3-D surface energy charts are plots of the goodness of fit (= inverse of square of variances) to θ_{la} set against a matrix of possible values of γ_{sa}^{d} and γ_{sa}^{p}. The best fit to all θ_{la} is read from the coordinates of the peak and the values are given in Table 2.12. The γ_{sa}^{p} and γ_{sa}^{d} values for the 100% SiOH fumed silica particles are similar to those reported for a clean crown glass surface (34 and 42 mN m^{-1}).[18] The γ_{sa} of the relatively smooth PTFE substrate is consistent with literature values (18.5 mN m^{-1}),[20] indicating that this approach is not unreasonable. It can be seen that the apparent γ_{sa} of the 100% SiOH fumed silica particles decreases with either hydrophobisation with DCDMS or by fluorination. The calculation shows that for both the fumed silica and clay particles, increasing the degree of fluorination reduces γ_{sa}^{p} to zero and ultimately reduces γ_{sa}^{d} to very low values too. It looks like this calculation is underestimating the surface energy of the particles as it shows that particles like the 14% SiOH silica containing polar groups have γ_{sa}^{p} of 0 mN m^{-1}. However, it clearly shows that the apparent γ_{sa} of the particles decreases as the degree of surface modification increases. For the fumed silica particles, it should be noted that the roughness imparted by the particle coating on the glass slides in addition to fluorination can affect the values of the apparent γ_{sa} measured.

For the DCDMS-coated fumed silica particles having residual surface SiOH group of 88−14%, the apparent γ_{sa} (Table 2.13) was estimated by summing the $\gamma_{sa}^{\ p}$ and $\gamma_{sa}^{\ d}$ components of γ_{sa} calculated by using equations 2.7 and 2.8,[12] respectively. Generally, the γ_{sa} of the fumed silica particles dwindles as the percentage of residual surface SiOH group decreases with increasing degree of hydrophobisation with DCDMS as expected. The γ_{sa} value of the 100% SiOH fumed silica particles calculated using these equations is in good agreement with those measured experimentally (Table 2.12).

$$\gamma_{sa}^{\ p} = 0.200(\%\,\mathrm{SiOH}) + 22.0 \tag{2.7}$$

$$\gamma_{sa}^{\ d} = 0.331(\%\,\mathrm{SiOH}) + 0.92 \tag{2.8}$$

Table 2.9. The surface tension γ_{la} of probe liquids and the corresponding dispersive γ_{la}^{d} and polar γ_{la}^{p} components (at 25 °C), taken from ref. 18, as well as apparent advancing θ_{la} (± 2°) of the probe liquids measured on glass slides composed of the particles and a PTFE substrate in air.

	Tensions/mN m^{-1}					Fluorinated silica			
Liquid	γ_{la}	γ_{la}^{d}	γ_{la}^{p}	100% SiOH	14% SiOH	75% SiOH	59% SiOH	50% SiOH	PFTE
Water	72.8	21.8	51.0	15	147	130	148	149	119
Glycerol	64.0	34.0	30.0	22	141	47	144	140	102
Formamide	58.0	39.0	19.0	14	109	17	140	145	85
Ethylene glycol	48.0	29.0	19.0	15	126	17	142	143	76
Diiodomethane	50.8	50.8	0.0	16	120	113	134	144	101
α-Bromonaphthalene	44.4	44.4	0.0	12	37	16	141	140	87
n-Hexadecane	27.8	27.8	0.0	8	7	9	16	28	35

Table 2.10. Apparent advancing θ_{la} of the probe liquids measured on compressed disks of the Eight Pearl 300S-Al sericite particles in air.

	θ_{la}/± 2°				
Liquid	PF-0	PF-5	PF-8	PF-10	PF-12
Water	27	140	148	138	148
Glycerol	18	128	145	131	146
Formamide	7	135	130	145	139
Ethylene glycol	20	119	135	136	138
Diiodomethane	29	128	131	128	130
α-Bromonaphthalene	17	111	118	134	123
n-Hexadecane	5	90	98	105	118

Table 2.11. Apparent advancing θ_{la} of the probe liquids measured on compressed disks of particles in air. The reported error does not apply to the measurement marked with (^{b}).

	θ_{la}/± 2°			
Liquid	PFX-10 Kunipia F	PFX-10 ZnO (TP)	PF-10 Eight Pearl 300 S-Al^{a}	PF-10 FSE-Al
Water	0^{b}	127	130	139
Glycerol	94	136	145	148
Formamide	88	113	106	133
Ethylene glycol	70	94	114	112
Diiodomethane	88	106	94	123
α-Bromonaphthalene	76	83	104	111
n-Hexadecane	67	77	93	95

Figure 2.14. 3-D surface energy plot for (a) 100% SiOH, (b) 50% SiOH fluorinated fumed silica, (c) PF-0 Eight Pearl 300S-Al, (d) PF-10 Eight Pearl 300S-Al, (e) PFX-10 Kunipia F and (f) PFX-10 ZnO (TP) particles. The ordinate represents the goodness of fit to apparent advancing θ_{la} and is plotted against a matrix of possible values of $\gamma_{sa}{}^{d}$ and $\gamma_{sa}{}^{p}$.

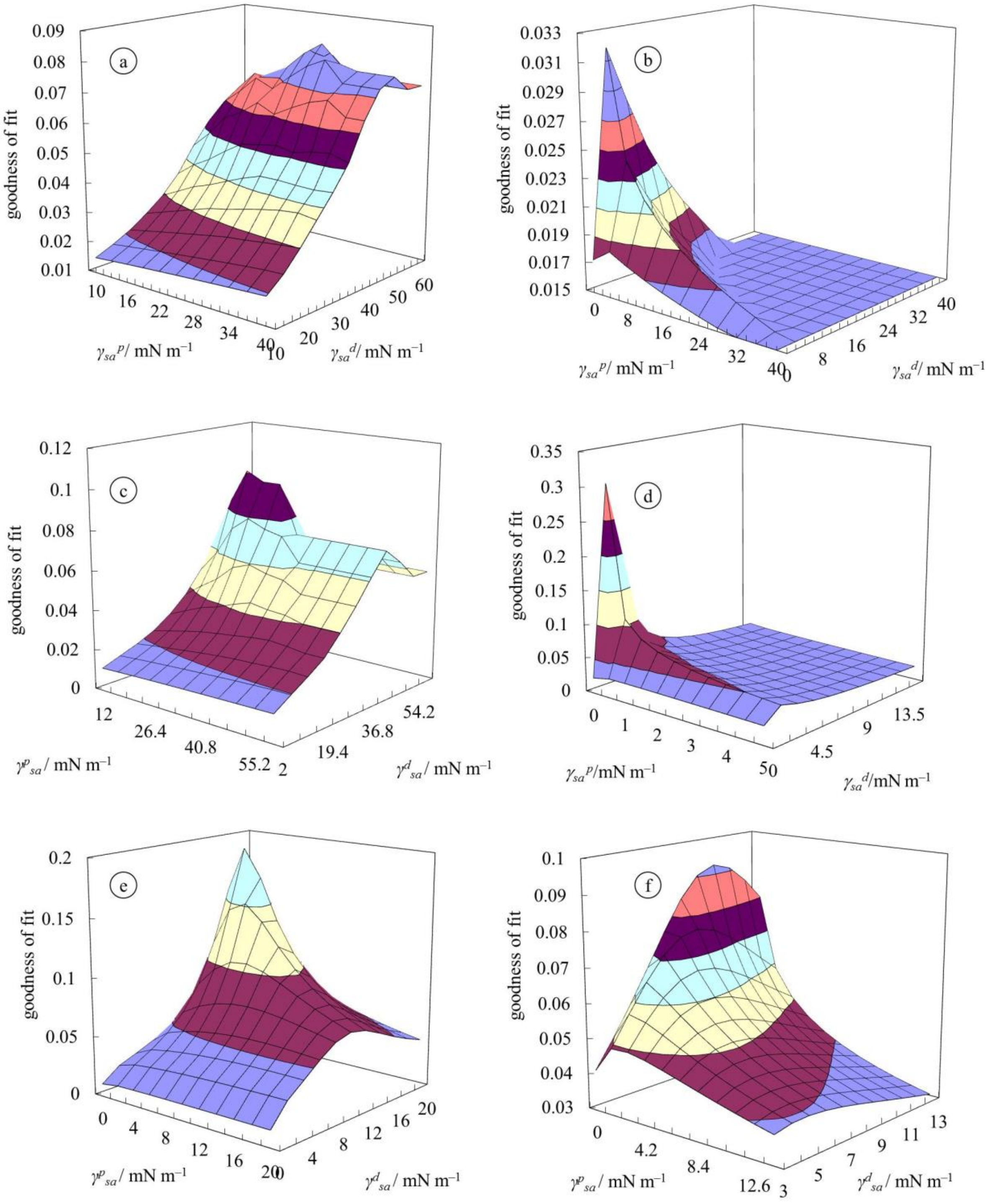

Table 2.12. The apparent surface energy γ_{sa} (calculated from apparent advancing θ_{la} of the probe liquids on spin-coated glass slides or compressed particle disks) of solid particles and PTFE substrate along with their dispersive γ_{sa}^{d} and polar γ_{sa}^{p} components (at 25 °C), all values are ± 0.3 mN m^{-1} except those marked with (^{b}).

Particles	γ_{sa}/mN m^{-1}	γ_{sa}^{d}/mN m^{-1}	γ_{sa}^{p}/mN m^{-1}
Hydrophilic 100% SiOH silica	79.0	49.0	30.0
Hydrophobic 14% SiOH silica	22.0	22.0	0.0[b]
75% SiOH fluorinated silica	35.0	27.0	8.0
59% SiOH fluorinated silia	5.0	5.0	0.0 [b]
50% SiOH fluorinated silica	3.0	3.0	0.0 [b]
PF-0 Eight Pearl 300S-Al	64.2	42.6	21.6
PF-5 Eight Pearl 300S-Al	4.0	4.0	0.0 [b]
PF-8 Eight Pearl 300S-Al	3.0	3.0	0.0 [b]
PF-10 Eight Pearl 300S-Al	2.0	2.0	0.0 [b]
PF-12 Eight Pearl 300S-Al	1.5	1.5	0.0 [b]
PFX-10 Kunipia F	18.0	14.0	4.0
PFX-10 ZnO (TP)	10.0	10.0	0.0 [b]
PF-10 Eight Pearl 300S-Al[a]	6.5	6.5	0.0 [b]
PF-10 FSE-Al	3.9	3.9	0.0 [b]
PTFE substrate	19.5	19.5	0.0 [b]

Table 2.13. The apparent surface energy γ_{sa} of DCDMS-coated fumed silica particles obtained by summing their polar γ_{sa}^{p} and dispersive γ_{sa}^{d} components estimated by using equations 2.7 and 2.8, respectively.

Silica Particles	γ_{sa}/mN m^{-1}	γ_{sa}^{d}/mN m^{-1}	γ_{sa}^{p}/mN m^{-1}
100% SiOH	76.0	42.0	34.0
88% SiOH	69.7	39.6	30.1
78% SiOH	64.3	37.6	26.7
70% SiOH	60.1	36.0	24.1
61% SiOH	55.3	34.2	21.1
51% SiOH	50.0	32.2	17.8
42% SiOH	45.2	30.4	14.8
33% SiOH	40.4	28.6	11.8
25% SiOH	36.2	27.0	9.2
23% SiOH	35.1	26.6	8.5
20% SiOH	33.5	26.0	7.5
14% SiOH	30.4	24.8	5.6

2.2.2.4 Characterisation of Oils and Other Liquids

2.2.2.4.1 Density Measurement

The ρ of the oils was measured with an Anton Paar DMA 35N digital densiometer at 20 or 25 ºC and 3 separate measurements were averaged. The cleaning of the instrument, necessary for accurate measurement, consisted of washing with copious amounts of ethanol and water. The instrument has a filling tube (inner diameter 0.2 cm and length 18 cm) through which the liquid goes into it when the pressure applied at the pump lever is released. Filling the measuring cell with the liquid ($\approx$ 2 cm^3) consisted of pressing down the pump lever as far as possible, submerging the filling tube in the sample and slowly releasing the pump lever.

2.2.2.4.2 Surface Tension Measurement

Measurement of γ_{la} (at 20 or 25 ºC) was with a Krüss K12 digital tensiometer using the du Noüy ring method. The results of 3 separate measurements were also averaged. The cleaning procedure involved rinsing the vessels with 0.5 M alcoholic KOH solution and then with Milli-Q water. The ring was heated to glowing in a blue Bunsen flame prior to all measurements. With the du Noüy ring method, γ_{la} is related to the maximum force F required to detach the ring from the interface (Figure 2.15).[21,22] The ring is usually made of platinum or platinum-iridium alloy of radius R_r between 2−3 cm. The radius r_r of the wire usually ranges from 1/30 to 1/60 of that of the ring (*i.e.* R_r).[23] The γ_{la} is calculated from equation 2.9.[23] The F is the force acting along the three-phase contact line and it is exactly equal to the weight of the liquid meniscus standing above the plane of the fluid interface. p is the perimeter of the three-phase contact line and it is equal to two times the circumference of the ring (*i.e.* $4\pi R_r$). The θ_d stands for the contact angle between the liquid meniscus and the surface of the ring (*i.e.* surface wettability) and it is required to be zero for accurate measurements. f is given by equations 2.10[24] and 2.11[25] and it is a correction factor required to account for the additional volume of the liquid lifted during the detachment of the ring from the interface and varies between 0.75 and 1.05. Finally, the $\Delta\rho$ and g in these equations are the density difference in the fluids and gravitational constant, respectively. All the other symbols retain their known meaning. Measured values of surface tension $\gamma_{la(\mathrm{exp})}$ above 25 mN m^{-1} were corrected with the Huh and Mason[24] correction factor (equation 2.10) whilst those below 25 mN m^{-1} were corrected with the Zuidema and Waters[25] correction factor (equation 2.11). The latter correction was done automatically by the instrument whilst the former correction was done manually.

Figure 2.15. Schematics of the du Noüy ring showing the properties of the ring and how *F* acts on it during a measurement.

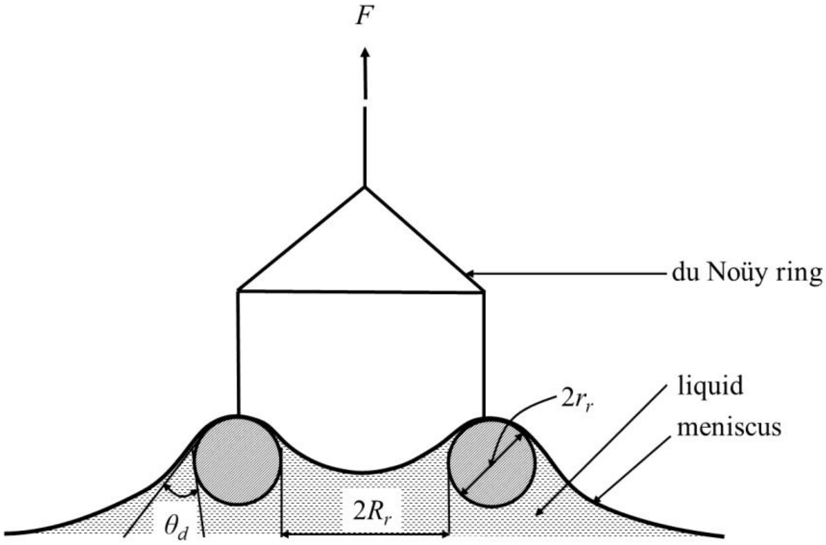

$$\gamma_{la} = \frac{F}{p\cos\theta_d} f = \frac{F}{4\pi R_r} f \tag{2.9}$$

$$f = \frac{\Delta\rho g R_r^2}{4\pi\gamma_{la(\exp)}} \tag{2.10}$$

$$f = 0.725 + \left(\frac{3.63\times10^{-3}\gamma_{la(\exp)}}{\pi^2\Delta\rho R_r^2} - \frac{1.679 r_r}{R_r} + 0.04534 \right)^{0.5} \tag{2.11}$$

2.2.2.4.3 Interfacial Tension Measurement

The vegetable oil (o_1)-PDMS oil (o_2) interfacial tension $\gamma_{o_1o_2}$ was measured using the Krüss spinning drop tensiometer at 25 °C and estimated by using equation 2.12 and Table 2.14.

$$\gamma_{o_1o_2} = \gamma_{o_1} + \gamma_{o_2} - 2\sqrt{\gamma_{o_1}{}^{p}\gamma_{o_2}{}^{p}} - 2\sqrt{\gamma_{o_1}{}^{d}\gamma_{o_2}{}^{d}} \tag{2.12}$$

The symbol $\gamma_{o_1}(\gamma_{o_2})$ is the surface tension of vegetable oil (PDMS oil). $\gamma^p_{o_1}(\gamma^p_{o_2})$ is the polar component of the surface tension of vegetable oil (PDMS oil). Lastly, $\gamma^d_{o_1}(\gamma^d_{o_2})$ is the dispersive component of the surface tension of the vegetable oil (PDMS oil). The spinning drop tensiometer is suitable for measuring fluid interfacial tensions of the order of ≥ 10^{-4} mN m^{-1}.[26] The technique is based on the fact that gravity has little or no effect on the shape of a fluid drop (less dense) suspended in the bulk of another fluid (more dense) contained in a horizontal capillary tube rotating about its horizontal axis where the two fluids remain immiscible. The fluid drop is ellipsoidal at relatively low rotational speed ω, but elongates and becomes cylindrical at relatively high ω where centrifugal forces dominate. Under the latter condition, the radius R_c of the cylindrical fluid drop is detected by the fluid interfacial tension γ' (= $\gamma_{o_1o_2}$ in this work), difference in fluid density $\Delta\rho$ and ω. Based on this, the $\gamma_{o_1o_2}$ can be calculated quite accurately from equation 2.13 provided the ratio of the length L_c of the cylindrical fluid drop to its diameter D_c is ≥ 4.[27] In this work, the spinning drop tensiometer was used to measure the *n*-heptane-water interfacial tension (50.7 ± 0.1 mN m^{-1}: consistent with the literature) prior to measuring $\gamma_{o_1o_2}$. A drop of a vegetable oil (less dense phase) was spun in the bulk of a PDMS oil (denser phase) at very high ω (≈ 8000 rpm) to obtain a cylindrical vegetable oil drop illustrated in Figure 2.16. The D_c and L_c of the vegetable oil drop were measured and used for calculating the $\gamma_{o_1o_2}$ by using equation 2.14 which has been obtained from equation 2.13 (see Appendix 3). The symbols n_T = 1.401 (at 25 °C), n_{o_2}, N and $A \approx 1.572 \times 10^{-8}$ represent the refractive index of the thermosatting oil (which was silicone oil from Avocado Chemicals Ltd. UK), refractive index of the PDMS oils, rotation speed in revolutions per min (*cf.* ω/radians per second) and all sample invariant conversion factors, respectively. The difference in PDMS oil-vegetable oil density ($\Delta\rho$) was obtained by using Table 2.2. The n_{o_2} was measured (at 25 °C) using an Abbe refractometer (Hilger, England) after calibration by measuring the refractive index of Milli-Q water (1.332) at 25 °C. The average of three separate n_{o_2} measurements was 1.400, 1.402 and 1.403 for PDMS 20, 50 and 100 cS, respectively. The measured and calculated values of $\gamma_{o_1o_2}$ are given in Table 2.15 where it can be immediately seen that all the $\gamma_{o_1o_2}$ of the vegetable oil-PDMS oil systems are very low (< 3 mN m^{-1}). There is a good agreement between the measured and calculated values of $\gamma_{o_1o_2}$ for some vegetable oil-PDMS oil systems. Finally, for the olive (rapeseed) oil-

PDMS oil systems, the measured values of $\gamma_{\mathrm{o}_1\mathrm{o}_2}$ increased as the viscosity of the PDMS oil increases.

$$\gamma' = \gamma_{\mathrm{o}_1\mathrm{o}_2} = \frac{\Delta\rho\omega^2 R_c^3}{4}\left(1+\frac{2R_c}{3L_c}\right) \tag{2.13}$$

$$\gamma_{\mathrm{o}_1\mathrm{o}_2} = N^2 D_c^3 A \Delta\rho \left(\frac{n_T}{n_{\mathrm{o}_2}}\right)^3 \left[1+\left(\frac{n_T D_c}{n_{\mathrm{o}_2}}\right) \Big/ 3L_c\right] \tag{2.14}$$

Table 2.14. The surface tension of vegetable and PDMS oils γ_o at 25 °C along with their polar γ^p and dispersive γ^d components. Measured values of γ_o (unmarked) are quoted to ± 0.1 mN m^{-1}. ^{a}Taken (at 20 °C) from ref. 28; ^{b}taken (at 25 °C) from ref. 29.

	Tensions/mN m^{-1}		
Oil	γ_o	γ_o^p	γ_o^d
Sunflower oil	32.2		
	33.3^a	0.4^a	32.9^a
Olive oil	33.1		
	33.0^a	0.1^a	32.9^a
Rapeseed oil	33.8		
PDMS 20 cS	20.8	0.9	19.9
PDMS 50 cS	21.2		
	21.0^b	0.9^b	20.1^b
PDMS 100 cS	21.4	0.9	20. 5

Figure 2.16. Schematic illustration of the spinning drop technique for measuring the vegetable oil-PDMS oil interfacial tension.

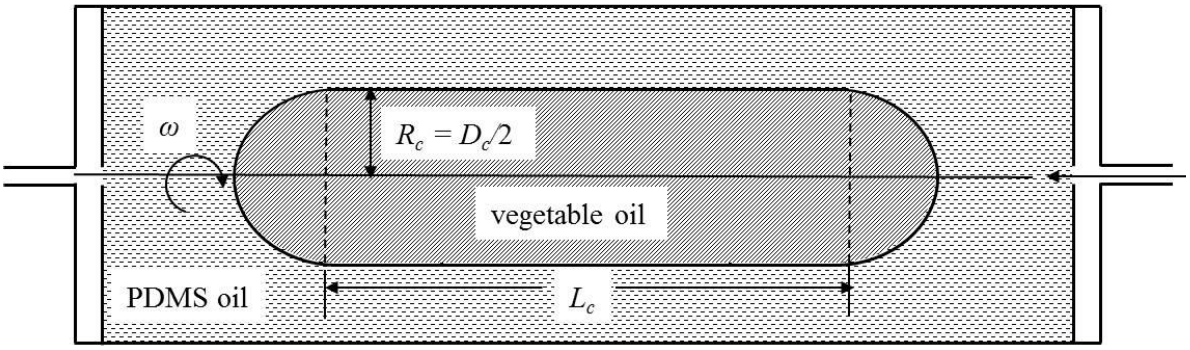

Table 2.15. Measured and calculated vegetable oil-PDMS oil interfacial tension $\gamma_{o_1o_2}$.

	$\gamma_{o_1o_2}$ /mN m^{-1} (at 25 °C)	
Oil-oil system	Measured/ ± 0.2	Calculated from equation 2.12
Sunflower oil-PDMS 20 cS	1.8	1.7
Sunflower oil-PDMS 50 cS	2.7	1.7
Sunflower oil-PDMS 100 cS	1.5	1.6
Olive oil-PDMS 20 cS	1.0	2.0
Olive oil-PDMS 50 cS	2.0	2.0
Olive oil-PDMS 100 cS	2.8	1.9
Rapeseed-PDMS 20 cS	1.0	
Rapeseed-PDMS 50 cS	2.3	
Rapeseed-PDMS 100 cS	2.7	

2.2.2.5 Oil-Oil Interfaces: Oil-Oil Pickering Emulsions

2.2.2.5.1 Measurement of the Extent of Solubility of the Vegetable Oils in the PDMS Oils or Vice Versa

Equal volumes (2.5 cm^3) of a PDMS oil and vegetable oil were placed in a screw-cap glass vial (inner diameter 1.8 cm and height 7.2 cm). The mixture was sheared vigorously (2 min) using an IKA RCT basic magnetic stirrer operating at 1500 rpm at 25 °C and observed how much of the individual oil phases separated out after a day. Apart from castor oil, it was observed that all the vegetable oils were immiscible with the PDMS oils as the original volume of the oils was recovered within a day after shearing. Castor oil was fairly miscible with the PDMS oils. It was estimated that approximately 15, 10 and 30 v/v. % of PDMS 20, 50 and 100 cS, respectively, was soluble in castor oil. Mineral oil was also miscible with the PDMS oils and about 45, 25 and 20 v/v. % of it was soluble in PDMS 20, 50 and 100 cS, respectively. A photograph of glass vials containing these oil-oil mixtures is shown in Figure 2.17.

Figure 2.17. Photo (1 day) after stirring of a mixture of (1) sunflower oil, (2) rapeseed oil, (3) olive oil, (4) castor oil and (5) mineral oil and PDMS (a) 20, (b) 50, (c) 100 cS at 1500 rpm for 2 min using an IKA RCT magnetic stirrer at 25 °C. Apart from the castor oil-PDMS 20 and 50 cS systems, the upper phase is the vegetable oil whilst the lower phase is the PDMS oil. For the castor oil-PDMS 20 and 50 cS, the upper phase is the relatively low density PDMS 20 cS and PDMS 50 cS of similar density with castor oil and the lower phase is the castor oil.

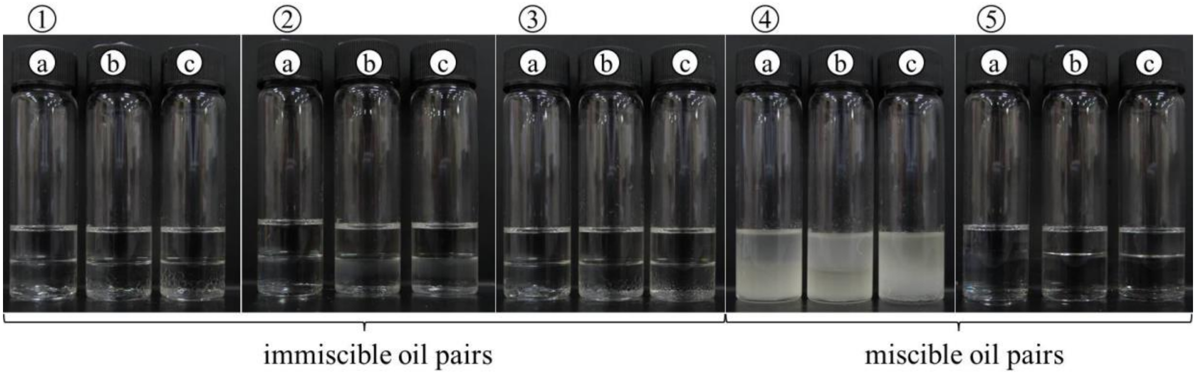

2.2.2.5.2 Preparation of Simple Oil-Oil Pickering Emulsions

2.2.2.5.2.1 Effect of Particle Concentration, Percentage of Surface SiOH Group on Fumed Silica Particles and Method of Preparation on the Stability of the Emulsions

Based on the solubility experiment, attempts were made to prepare emulsions composed of equal volume fraction ϕ of sunflower, olive and rapeseed oils and PDMS 20, 50 and 100 cS in the presence of the 75% SiOH fluorinated fumed silica and PF-5 Eight Pearl 300S-Al sericite particles. The ϕ by definition is the ratio of the volume (cm^3) of vegetable oil in an emulsion to the volume (cm^3) of vegetable oil plus volume (cm^3) of PDMS oil in the emulsion. The particle concentration in the emulsions was 0−2 wt. % relative to the total volume (10 cm^3) of vegetable and PDMS oils in the emulsions. The emulsions were prepared using the powdered particle method in screw cap glass vials (inner diameter 2.4 cm and height 7.2 cm). The required volume (5 cm^3) of a PDMS oil was placed in a screw cap glass vial followed by addition of the required mass of the 75% SiOH fluorinated fumed silica or fluorinated PF-5 Eight Pearl 300S-Al sericite particles. The required volume (5 cm^3) of a vegetable oil was then added. The fluorinated fumed silica particles were spontaneously wetted by the PDMS oils and entered in them, but did not wet the fluorinated PF-5 Eight Pearl 300S-Al sericite particles which remain on their surfaces. For the 75% SiOH fluorinated fumed silica particles, the vegetable oils were added to the PDMS oils after the particles had completely entered in them. The mixture was homogenised using an IKA

T25 digital Ultra-Turrax homogeniser with an operating head of inner diameter 1.3 cm at 12000 rpm for 2 min. Similarly, sunflower oil-PDMS 20 cS emulsions containing equal volumes (5 cm^3) of oils were prepared in the presence of 1 wt. % of 50−59% SiOH fluorinated fumed silica particles, PF-8 to PF-12 fluorinated sericite particles, fluorinated PFX-10 ZnO (TP) particles, fluorinated PFX-10 Kunipia F particles, PTFE and Bentone 34 particles. The particle concentration is relative to the total volume of sunflower oil and PDMS 20 cS in the emulsions.

Sunflower oil-PDMS oil and olive oil-PDMS oil emulsions containing equal volumes (5 cm^3) of the oils were also prepared using the approach described above. The emulsions were prepared in the presence of 1 wt. % of 100−14% SiOH silica particles so as to study the effect of % SiOH on the emulsions. The particle concentration is relative to the total volume of oil in the emulsions. Like in the case of the 75% SiOH fluorinated fumed silica particles, the vegetable oils were added to the PDMS oil-silica particle mixture after the silica particles had completely entered in the PDMS oil.

Because the silica particles were wetted by both the PDMS and vegetable oils, the vegetable oils (5 cm^3) were allowed to completely wet 1 wt. % of 75% SiOH fluorinated silica, 14 and 51% SiOH fumed silica particles. PDMS oil (5 cm^3) was then added to the vegetable oil-silica particle mixtures followed by homogenisation at the conditions stated previously. The particle concentration is with respect to the total volume of vegetable and PDMS oils in the emulsions. It should be noted that in this case the silica particles are initially in the vegetable oil phase and not in the PDMS oil phase.

2.2.2.5.2.2 Effect of Oil Volume Fraction on the Stability of the Emulsions

The effect of oil volume fraction on the stability of the sunflower oil-PDMS 50 cS emulsions was also investigated. Batch emulsions comprising of varying volume fraction of sunflower oil ϕ_{suno} and PDMS 50 cS were prepared by the powdered particle method. The ϕ_{suno} in the emulsions was varied between 0.05 and 0.9. The emulsions were prepared in the presence of 1 wt. % of 75% SiOH fluorinated fumed silica or PF-5 Eight Pearl 300S-Al fluorinated sericite particles. The particle concentration is relative to the total volume (10 cm^3) of vegetable oil and PDMS 50 cS in the emulsions. The required volume of PDMS 50 cS was placed in a screw cap glass vial (inner diameter 2.4 cm and height 7.2 cm) followed by addition of the required mass of the particles and then the required volume of sunflower oil. The fluorinated silica particles were allowed to completely enter the PDMS 50 cS before sunflower oil was added to their systems. Homogenisation was at 12000 rpm for 2 min with the IKA T25 digital Ultra-Turrax homogeniser using an operating head of inner diameter 1.3 cm.

2.2.2.5.2.3 Preparation of Multiple Oil-Oil Pickering Emulsions

The possibility of preparing multiple emulsions using two DCDMS-coated fumed silica particles which prefer to stabilise different o/o (*i.e*. vegetable oil-in-PDMS oil and PDMS oil-in-vegetable oil) emulsions was also investigated at ambient conditions. Multiple emulsions containing varying volume fractions of a simple emulsion $\phi_{o/o}$ were prepared in screw cap glass vials (inner diameter 1.8 cm and height 7.2 cm). The $\phi_{o/o}$ in the emulsions was varied between 0.3−0.7. Firstly, relatively stable sunflower oil-in-PDMS 50 cS and olive oil-in-PDMS 100 cS emulsions stabilised by 1 wt. % of 14% SiOH fumed silica particles (prepared in sec. 2.2.2.5.2.1) were chosen. The required volume (1.5−3 cm^3) of these emulsions were re-emulsified in the required volume (3−1.5 cm^3) of sunflower oil and olive oil dispersions containing 2 wt. % of 51% SiOH fumed silica particles. Secondly, relatively stable PDMS 50 cS-in-sunflower oil and PDMS 100 cS-in-olive oil emulsions stabilised by 1 wt. % of 51% SiOH fumed silica particles (prepared in sec. 2.2.2.5.2.1) were chosen. Similarly, the required volume (1.5−3 cm^3) of these emulsions were re-emulsified in the required volume (3−1.5 cm^3) of sunflower oil and olive oil dispersions containing 2 wt. % of 14% SiOH fumed silica particles. In both cases, the o/o emulsions chosen were prepared by the powdered particle method and they contain equal volumes (5 cm^3) of the oils. Re-emulsification was at 6000 rpm for 1 min (*i.e*. relatively high shear) using the rotor stator homogeniser (described in sec. 2.2.2.5.2.1) or at 500 rpm for 1 min (*i.e*. relatively low shear) using the IKA RCT basic magnetic stirrer. The oil dispersions of the 51 and 14% SiOH fumed silica particles were prepared by allowing the particles (0.2 g) to completely enter the oils (10 cm^3) followed by stirring at 1000 rpm for 1 min at 25 °C using the basic magnetic stirrer.

2.2.2.5.2.4 Characterisation of Simple and Multiple Oil-Oil Pickering Emulsions: Determination of Emulsion Type, Measurement of Emulsion Stability and Optical Microscopy

The drop test was used to infer the continuous phase of both the simple and multiple emulsions. Vegetable oil (PDMS oil) continuous emulsions disperse easily in vegetable oil (PDMS oil), but did not disperse easily in PDMS oil (vegetable oil). The stability of the emulsions to creaming or sedimentation and coalescence was assessed by noting the fraction of PDMS oil $f_{\text{PDMS oil}}$ or vegetable oil f_{vo} and the necessary oil phase, respectively, released in a month. The f_{vo} represents the fraction of sunflower oil (f_{suno}), olive oil (f_{oo}) or rapeseed oil (f_{ro}) released within a given period. Mathematically, the f_{vo} ($f_{\text{PDMS oil}}$) refers to the ratio of the volume (cm^3) of vegetable oil (PDMS oil) released in the emulsions to the initial volume of vegetable oil (PDMS oil) in the emulsions. For optical microscopy, a drop of the silica particle-stabilised emulsions was diluted with 1−5 drops of its continuous phase and viewed on a dimple glass slide (Fisher Scientific). The fluorinated sericite and other particle-stabilised emulsions were viewed undiluted. The emulsions were viewed with the Olympus BX-51 optical microscope. The optical micrographs were used to determine the droplet size of the emulsions by averaging the diameter of 300 emulsion droplets.

2.2.2.5.3 Preparation of Oil-Particle Dispersions

Based on existing literature,[30,31] it was anticipated that the fumed silica particles containing relatively high percentage (≥ 51%) of residual surface SiOH group will not stabilise any oil-oil emulsions. However, it was observed that even the fumed silica particles having 100% surface SiOH group formed stable oil-oil emulsions. As a result, the manner in which the 100 and 14% SiOH fumed silica particles interact with one another once in the PDMS and vegetable oils was investigated. PDMS and vegetable oil dispersions were prepared at 2 wt. % and 5 wt. % of the particles. The required mass of 100 and 14% SiOH silica was placed on the surface of the PDMS and vegetable oils (5 cm^3) in screw cap glass vials (inner diameter 1.8 cm and height 7.2 cm). The glass vials were hand shaken vigorously (10 s) after the particles had completely entered in the oils at rest.

2.2.2.5.4 Solid Particle-Oil-Oil Three-Phase Contact Angles

As mentioned previously, it is difficult to measure the contact angle small solid particles make with fluid interfaces especially if the particles are agglomerated and polydisperse like the fumed silica particles used in this work. Such angles are known to detect the type of end materials the small solid particles stabilise. Three approaches were used to measure the solid particle-vegetable oil-PDMS oil contact angle θ_{oo}. The first utilised compressed disks composed of the particles. For the fumed silica particles, a viscous cyclohexane solution (5.6 wt. %) was prepared by hand shaking (30 s) a mixture of cyclohexane (18 cm^3) and the particles (1 g). The mixture was dried under a vacuum to a constant mass before compressing into disks, but the rest of the particles were used as received. The dried particles (60 mg) were then compressed in a 13 mm diameter steel die with a hydraulic press under a pressure of approximately 1.1×10^8 N m^{-2} into relatively smooth disks (diameter 13 mm and thickness ≈ 0.5 mm). However, the measurement of θ_{oo} was not possible with these disks as they were porous and oils entered in them. Secondly, for the sunflower oil and olive oil/PDMS oil/fumed silica particle systems, θ_{oo} was estimated by using equation 2.15.

$$\cos\theta_{oo} = \frac{\gamma_{\mathrm{so}_1} - \gamma_{\mathrm{so}_2}}{\gamma_{\mathrm{o}_1\mathrm{o}_2}} \qquad (2.15)$$

The symbol γ_{so_1} (γ_{so_2}) represents the fumed silica particle-vegetable oil (fumed silica particle-PDMS oil) interfacial tension and they are given in equations 2.16 and 2.17. γ_{sa}, $\gamma_{sa}{}^{p}$ and $\gamma_{sa}{}^{d}$ represent the surface energy of fumed silica particles, polar and dispersive components of the surface energy of the fumed silica particles (Table 2.13) respectively.

$$\gamma_{\mathrm{so}_1} = \gamma_{sa} + \gamma_{\mathrm{o}_1} - 2\sqrt{\gamma_{sa}{}^{p}\gamma_{\mathrm{o}_1}{}^{p}} - 2\sqrt{\gamma_{sa}{}^{d}\gamma_{\mathrm{o}_1}{}^{d}} \qquad (2.16)$$

$$\gamma_{\mathrm{so}_2} = \gamma_{sa} + \gamma_{\mathrm{o}_2} - 2\sqrt{\gamma_{sa}{}^{p}\gamma_{\mathrm{o}_2}{}^{p}} - 2\sqrt{\gamma_{sa}{}^{d}\gamma_{\mathrm{o}_2}{}^{d}} \qquad (2.17)$$

This approach, however, gave unrealistic values of θ_{oo} presumably as the values of the polar and dispersive components of the surface tension of the oils are not known precisely. As a result, for the sunflower oil/PDMS 20 cS/DCDMS-coated fumed silica particle systems, the θ_{oo} was calculated at varying γ_{o}^{p} (0−1.4 mN m^{-1}) of sunflower oil and fixed γ_{o}^{p} (0.9 mN m^{-1}) of PDMS 20 cS. Similarly, the θ_{oo} was also calculated at varying γ_{o}^{p} (0−1.4 mN m^{-1}) of PDMS 20 cS and fixed γ_{o}^{p} (0.4 mN m^{-1}) of sunflower oil. The aim of these calculations is to investigate the effect of the polar and dispersive components of the surface tension of the oils on the calculated values of θ_{oo}. Lastly, hydrophilic microscope glass slides (Academy Science, UK) having relatively high % of SiO_2 were hydrophobised with DCDMS (purity ≥ 99.5%, Fluka) after cutting them into suitable sizes (2.5 cm × 2.5 cm). The hydrophobised glass slides were used to infer the values of θ_{oo}. The aim is to mimic the surfaces of the 100 and 14% SiOH fumed silica particles and as such, the hydrophilic and the DCDMS-coated glass slides used here are considered as being equivalent to the 100 and 14% SiOH fumed silica particles respectively. The contact angle an oil drop makes with the glass surfaces (in air θ_o or in one of the oils θ_{oo}) was measured using the sessile drop technique by using the Krüss DSA Mk 10 instrument. 10 (5) μL of oil was used for the advancing (receeding) angles. This technique requires analysing the profile of an oil drop obtained on a glass slide. For advancing θ_o, a drop (10 μL) of oil was formed in air on a glass slide using an Eppendorf micropipette. For advancing θ_{oo}, a cubical transparent glass cuvette (inner dimensions 3 cm × 3 cm × 3 cm, OG Hëllma) containing a glass slide was partially filled with a vegetable oil (5.5 cm^3). A PDMS oil drop (10 μL) was then formed on the glass slide using the Eppendorf micropipette. The receding angles were measured after withdrawing 5 μL of the PDMS oil from the initial oil drop used for measuring the advancing ones. The profile of these droplets were obtained separately and analysed and an average of 4 separate contact angle measurements is reported. Similarly, the advancing and receding contact angles of water on the glass slides in air and in the vegetable oils were measured for comparison. The glass slides were hydrophobised by placing them vertically on a Teflon rack in a sealed glass vessel (inner diameter ≈ 8 cm and height 7 cm) containing 500 μL of DCDMS. The glass vessel has two holes on its lid to support the exchange of materials (*e.g.* gas) between it and the environment when they are not sealed. The glass slides were removed after 1 hour and stored in petri dishes and used within 24 hours. About 10 μL of DCDMS remained. Compressed nitrogen gas was passed through the glass vessel prior to addition of DCDMS to drive out most of the air present in it.

2.2.2.6 Liquid (and/or Oil)-Air Interfaces: Liquid Marbles, Dry Oil Powders and Oil Foams

2.2.2.6.1 Oil Liquid Marbles and Oil Foams Stabilised by Fluorinated Fumed Silica Particles

2.2.2.6.1.1 Particle Immersion Test with Agitation

The required volume (3 cm^3) of the desired oil was measured into a screw cap glass vial (inner diameter 1.8 cm and height 7.2 cm). The vial was closed tightly after placing the required amount of particles (50 mg) on the surface of the oil and observing if they entered the oil or not. After about 4 hours, these oil-particle mixtures were hand shaken vigorously for 30 s in a vertical motion. The formation of particle dispersions, oil foams or climbing films was noted. It was confirmed that foams or climbing films do not appear in these liquids in the absence of particles.

2.2.2.6.1.2 Preparation and Characterisation of Oil Foams Stabilised by Fluorinated Fumed Silica Particles

Based on the result of the second part of the immersion test experiment, foams of eugenol, α-hexylcinnamaldehyde, α-bromonaphthalene and benzyl acetate were prepared using four different methods in the presence of varying concentrations (0.1−5 wt. %) of 59% SiOH fluorinated fumed silica particles. The foams were prepared at ambient conditions in screw cap glass vials of inner diameter 2.4 or 1.8 cm and height 7.2 cm using 5 g of the liquids. In the first method, the required mass (5 g) of the desired liquid was placed in separate glass vials. The glass vials were closed tightly after addition of the required mass of particles followed by vigorous hand shaking (30 s) in a vertical motion. In the second method, the particles were first dispersed in the liquid using the Branson ultrasonic sonifier 450 for 1 min at 60% amplitude followed by vigorous hand shaking for 30 s. For the third method, a mixture of the oil and particles (0.5 or 2 wt. %) were aerated in the glass vials using the IKA T25 digital Ultra-Turrax homogeniser with an operating head of inner diameter 0.8 cm at 13000 rpm for 1 min at ambient conditions. For the last method, the latter foams (from the third method) were further hand shaken vigorously for 30 s. Immediately after foaming, the volume of foam was recorded to provide a measure of the foamability and foam stability as a function of time. Photographs of the glass vials containing the foams were taken with the Canon digital camera. For optical microscopy, small foam samples were placed on a dimpled glass slide and observed with the Olympus BX-51 microscope. The mean bubble diameter was obtained by averaging the diameter of 50 individual bubbles on the optical micrographs which were obtained within 2−24 hours of foam preparation.

2.2.2.6.1.3 Preparation and Characterisation of Oil Liquid Marbles Stabilised by Fluorinated Fumed Silica Particles

Liquid marbles (5 or 10 μL) were prepared by rolling the required volume of liquid, from an Eppendorf micropipette, on a bed of fumed silica particles (100 mg) placed on a Teflon substrate (4 cm × 4 cm × 3 mm, Radio Spares UK) positioned at 0.5 cm from the micropipette. This was followed by rolling the liquid drop on the particle bed (to and fro) at an angle of approximately 45º in air at room temperature. The substrate was washed in a warm (40 ºC) detergent solution, rinsed in distilled water at the same temperature and dried prior to the experiment. Some marbles were subsequently transferred to glass slides for photographing. Liquid marbles of 10 μL, stabilised by the 59% SiOH fluorinated fumed silica particles, were allowed to evaporate at room temperature (23 ± 1 ºC) and relatively humidity of 44 ± 5 % after removal of excess particles from the substrate. The profile of the liquid marbles during evaporation was followed using the Krüss DSA Mk 10 instrument (connected to a computer) by taking an image every 5 min.

2.2.2.6.2 Dry Oil Powders and Oil Foams Stabilised by Fluorinated Clay and Fluorinated ZnO Particles

2.2.2.6.2.1 Particle Immersion Test with Agitation

The procedure described in sec. 2.2.2.6.1.1 was followed and the formation of particle dispersions, oil foams or climbing films was noted. It was confirmed that foams or climbing films do not appear in these liquids in the absence of particles prior to the experiment. PDMS 20 cS/PF-10 Eight Pearl 300S-Al and isocetane/PF-10 Eight Pearl 300S-Al are good examples of systems in which only foam was observed. As a result, the effect of dispersing the particles in the liquids before shaking was investigated on them. The PF-10 Eight Pearl 300S-Al particles (50 mg) were dispersed in 3 cm^3 of the liquids using a Branson ultrasonic sonifier for 2 min at 30% amplitude. This was followed by vigorous hand shaking (30 s). The formation of particle dispersion or foam was noted. Using ultrasound, it was necessary to cool the mixture in an ice bath.

2.2.2.6.2.2 Preparation of Oil Liquid Marbles and Dry Oil Powders

The procedure described in sec. 2.2.2.6.1.3 was used to prepare the oil liquid marbles (10 μL). It was anticipated that dry oil powder formation would be possible with all the oil/particle combinations that gave oil liquid marbles. Nonetheless, knowing the amount of particles that must cover a known mass of oil to give it a dry oil powder appearance is fundamental in the preparation of dry oil powders. As such, prior to the experiment, the critical oil : particle ratio (COPR), for the dry oil appearance was determined. The COPR is defined as grams of oil per gram of particles. It was determined by sequential addition of a small amount (≤ 0.25 g) of oil to 0.5 g of particles in screw cap glass vials (inner diameter 1.8 cm, height 7.2 cm), followed by gentle hand shaking (3 min) at an angle of ≈ 45° until the mixture foams. The oil-particle ratio just before foam formation was considered as the COPR. Conscious of the COPR, attempts were made to prepare dry oils from mixtures of all the oils and particles (capable of oil marble formation) using five approaches. The first is described above. With this method, dry oil powder formation was possible for the majority of the oils and particle combinations that gave oil marbles previously. It was confirmed using liquid paraffin and jojoba oil and PF-8 Eight Pearl 300S-Al particles that the sequential addition of oil to the particles serves to increase the size of oil droplets in the dry oil powder. The second approach also involves sequential addition of oil (≤ 0.25 g), but it is followed by vigorous hand shaking (3 min). In the third approach, liquid paraffin or jojoba oil and PF-8 Eight Pearl 300S-Al particles as well as 2-ethylhexyl-4-

methoxycinnamate and PF-12 Eight Pearl 300S-Al particles were used. The type of material formed at 0.2 g of oil below and above the COPR in a non-sequential procedure that lasted for at least 10 min was investigated. The required amount of oil was added at once to the particles (0.5 g) and hand shaken gently for the said time. This approach yielded a dry oil powder below the COPR and oil foam above it for liquid paraffin and jojoba oil, but foam for 2-ethylhexyl-4-methoxycinnamate in both cases. In the fourth, the amount of oil corresponding to the COPR was added at once to 0.5 g of particles in the glass vial followed by gentle hand shaking (5 min). Using squalane, liquid paraffin and glyceryl tri(2-ethylhexanoate), this approach in which a large oil droplet hardly breaks into smaller ones yielded a foam instead of a dry oil powder. For the last method, liquid paraffin, macadamia nuts oil, jojoba oil and 2-ethylhexyl-4-methoxycinnamate and PF-5, 8, 10 and 12 Eight Pearl 300S-Al particles were used. Attempts were made to prepare dry oil powders using the IKA T25 digital Ultra-Turrax homogeniser with an operating head of inner diameter 0.8 cm using a speed of between 4000 and 13000 rpm for 2 min. A known mass of oil (0.2 g below or above COPR) was weighed into a glass vial, followed by addition of particles (0.5 g) and then sheared. In a parallel approach, the particles were placed in the glass vial before oil addition and then sheared. Only oil foams were obtained with both approaches. Thus, dry oil powders were prepared mainly *via* the first method as it gives powders with relatively high oil content for the majority of the oil-particle combinations. Unless stated otherwise, properties of dry oil powders described hereafter are those at the COPR.

2.2.2.6.2.3 Characterisation of Dry Oil Powders and Oil Foams Stabilised by Fluorinated Clay and Fluorinated ZnO Particles

Apart from visual observation, the dispersion test was used to distinguish a dry oil powder from an oil foam. A known mass (*ca*. 400 mg) of the material for a known oil was placed on the surface of the oil (*ca*. 20 cm^3), stirred vigorously and observed whether it dispersed or not. Oil continuous materials (foams) dispersed, but air continuous materials (dry oil powders) did not. Furthermore, small samples of the various materials were placed on a dimple glass slide and viewed with the Olympus BX-51 microscope fitted with a digital camera. Cryo-SEM was also carried out in some cases. Dry oil powder (a small amount of foam) was (placed on an aluminium stub to a thickness of approximately 3−4 mm) sprinkled onto a perforated aluminium stub and plunged into liquid nitrogen slush (–210 ºC). The frozen foam sample was transferred to a cryo system (Quorum Technologies PP3010T) fractured and then sputter coated with platinum and transferred to the SEM cold stage for examination. The dry oil powders were, however, not fractured before being sputter coated with platinum. The coated foams and dry oil powders were examined at –140 ºC at a beam voltage of 15 kV and probe current of between 20–35 pA. An indication of whether the dry oil powders leak or not was obtained by placing them on a Sartorius Stedim filter paper (diameter 70 mm) or a clean Pyrex watch glass (diameter 50 mm) for 1 min. The filter paper and watch glass were observed for degrees of oil staining after removal of the dry oil powders. To investigate the effect of shear on the dry oil powders, 8.5 mg of powder was placed on the back of a hand (surface area *ca*. 13 cm^2) and sheared at room temperature with an index finger. Dry oil powders (0.5 g) of squalane, liquid paraffin and jojoba oil stabilised by PF-8 Eight Pearl 300S-Al particles were hand shaken vigorously (10 s) in a screw cap glass vial to also verify the effect of shear on the powdered materials.

2.3 References

1. J.-W. Kim, D. Lee, H.C. Shum and D.A. Weitz, *Adv. Mater.*, 2008, **20**, 3239−3243.
2. N. Goto, T. Iwashita, I. Motoyama, K. Nomura and Y. Ota, *Process of producing needle-shaped calcium carbonate particles*, US Pat., 4824654, 1989, Yabashi Industries Co., Ltd., Gifu, Japan.
3. E. Noritsugu, H. Hisakazu, M. Norio, O. Kazunori and S. Seiya, *Method for producing calcium carbonate in cubic form,* Japan Pat., WO2001042139 A1, 2001,
4. R.K. Iler, *The Chemistry of Silica*, John Wiley & Sons, New York, 1979.
5. G.L. Witucki, *J. Coat. Technol.*, 1993, **65**, 57−60.
6. B.P. Binks and S.O. Lumsdon, *Langmuir*, 2000, **16**, 8622−8631.
7. G. Lawes, *Scanning Electron Microscopy and X-ray Microanalysis: Analytical Chemistry by Open Learning*, John Wiley and Sons, 1987.
8. Y.-S. Perng, E.I.-C. Wang, C.-C. Lu and L.-S. Kuo, *TAPPI J.*, 2008, **3**, 21−31.
9. Y.-H. Shen, *Chemosphere*, 2001, **44**, 989−995.
10. A.J. Johnson, Ph.D, University of Hull, 2013.
11. B.P. Binks and S.O. Lumsdon, *Langmuir*, 2000, **16**, 2539−2547.
12. B.P. Binks, A.K.F. Dyab and P.D I. Fletcher, *Phys. Chem. Chem. Phys.*, 2007, **9**, 6391−6397.
13. D.K. Owens and R.C. Wendt, *J. Appl. Polym. Sci.*, 1969, **13**, 1741−1747.
14. C.J. Van Oss, M.K. Chaudhury and R.J. Good, *Chem. Rev.*, 1988, **88**, 927−941.
15. S. Wu and K.J. Brzozowski, *J. Colloid Interface Sci.*, 1971, **37**, 686-690.
16. F.M. Fowkes, *J. Phys. Chem.*, 1963, **67**, 2538−2541.
17. C.J. van Oss, *Interfacial Forces in Aqueous Media*, Marcel Dekker, New York, 1994.
18. J.H. Clint and A.C. Wicks, *Int. J. Adhes. Adhes.*, 2001, **21**, 267−273.
19. T. Young, *Philos. Trans. R. Soc. London*, 1805, **95**, 65.
20. C.J. van Oss and R.F. Giese, *Clays Clay Miner.*, 1995, **43**, 474−477.
21. P. Lecomte du Noüy, *J. Gen. Physiol.*, 1919, **1**, 521−524.
22. W.D. Harkins and F.E. Brown, *J. Am. Chem. Soc.*, 1919, **41**, 499−525.
23. R.D. Vold and M.J. Vold, *Colloid and Interface Chemistry*, Addison-Wesley Publishing Co., London, 1983.
24. C. Huh and S.G. Mason, *Colloid Polymer Sci.*, 1975, **253**, 566−580.
25. H. Zuidema and G. Waters, *Ind. Eng. Chem. Anal. Ed.*, 1941, **13**, 312−313.
26. T. Sottmann and R. Strey, *J. Chem. Phys.*, 1997, **106**, 8606−8615.
27. B. Vonnegut, *Rev. Sci. Instr.*, 1942, **13**, 6−9.
28. M.-C. Michalski, S. Desobry, M.-N. Pons and J. Hardy, *J. Amer. Oil Chem. Soc.*, 1998, **75**, 447−454.
29. B.P. Binks and J.H. Clint, *Langmuir*, 2002, **18**, 1270−1273.
30. R.D. Vartanian, *Stable mineral oil-silicone oil compositions*, US Pat., 3 445 385, 1969, American Cyanamide Company.
31. T.K. Jones and M. Nair, *Oil-in-oil dispersions stabilised by solid particles and methods of making the same*, US Pat., 8 323 392 B2, 2012, Eastman Kodak Company.

Chapter 3

Edible Oil-in-Water Pickering Emulsions Stabilised by Anisotropic $CaCO_3$ Particles

3.1 Introduction

Experiments have shown that colloidal particles of suitable wettability can adsorb at oil-water and liquid-air interfaces to stabilise o/w or w/o emulsions (Pickering emulsions) and foams or liquid marbles, respectively. These particles are either isotropic (spherical) or anisotropic (non-spherical). Ellipsoidal, cubic, dumbbell, rod-shaped particles are typical examples of anisotropic particles. Whilst many emulsions have been stabilised with isotropic particles, those stabilised with anisotropic particles are quite few even though theoretical studies[1] have shown that they are more efficient than spherical particles. Some reports on anisotropic particle-stabilised emulsions are summarised below. Fe_3O_4-SiO_2 heterogeneous nanorods were used to stabilise w/o droplets so as to prepare magnetic colloidosomes.[2] The colloidosomes were stable provided the aspect ratio was not more than 4:1. The preparation of stable w/o emulsions through the *in-situ* growth and adsorption of alkyl gallate micro-needles on the surface of water droplets has been reported.[3] In another study, stable o/w and w/o emulsions were obtained by the adsorption of rod and plate-shaped microcrystals of cyclodextrin-oil inclusion complexes on droplet surfaces.[4] Recently, cubes and ellipsoidal particles were used to prepare stable o/w emulsions.[5] However, a detail study of how effective various anisotropic particles which are composed of the same material act as stabilisers of emulsions has not been reported. The aim of this chapter is to compare how effective rod- and cube-shaped $CaCO_3$ particles act as stabilisers of edible o/w emulsions of tricaprylin and Miglyol 812N. The effects of particle concentration, method of emulsion preparation, added electrolyte and pH on the stability of the emulsions were also investigated. Adding electrolyte and/or adjusting the pH of the particle suspension before emulsion preparation potentially enhance particle flocculation by decreasing the electrostatic repulsion between the particles so that mutual attraction between them prevails. The flocculation of particles has a stabilising effect on the emulsions.[6,7] The effect of different electrolytes on the stability of silica-stabilised toluene-in-water emulsions has been studied at various pH values.[8] It was observed that at pH 10 in the presence of $LaCl_3$ (2–5 mM), the emulsions were stable to coalescence and creaming; and that the onset of the increase in stability coincided with the onset of flocculation of the colloidal particles. The increased stability against creaming was linked to the smaller droplet diameter observed at the same salt concentration range. Emulsions containing NaCl, however, were unstable to creaming at all salt concentrations studied (0–5 M) regardless of the pH. Stability to coalescence was best at pH 4 irrespective of NaCl concentration even though the particle suspensions were unflocculated and very stable. These observations are consistent with the effect of electrolytes on particle wettability.[9] Trivalent La^{3+} cations can strongly bind to the negatively charged silica particle surface thus reducing the net charge and making the particles more hydrophobic. This improves the attachment of particles to the droplet surface and thus stabilising the emulsion. Contrary, the binding of monovalent Na^+ ions to the silica surface is weak and as such does not impart hydrophobic properties to the silica particles. It has also been reported that the stability of heptane-in-water emulsions stabilised by hydrophilic precipitated silica particles to coalescence improved in the presence of Ca^{2+} ions.[10] Clearly, the role of electrolytes in emulsions stabilised by hydrophilic particles is to improve particle attachment to the liquid interface by imparting hydrophobicity, increasing the effective particle size by flocculation and diminishing the electrostatic barrier between the fluid interface and the approaching particles.

Certain hydrophobic particles, however, can strongly attach to droplet interfaces without or with small amounts of NaCl in the aqueous phase yielding very stable emulsions.[11] Aqueous suspensions of partially hydrophobised particles flocculate easily at relatively low electrolyte (1:1) concentrations.[12] Therefore, one can speculate that the effect of electrolyte in o/w emulsions stabilised by partially hydrophobic particles might be different to that stabilised by hydrophilic particles. For example, it has been reported that PDMS oil-in-water emulsions stabilised by fumed silica particles are very stable to coalescence irrespective of NaCl concentration, but a strong effect was observed on the creaming stability and was linked to particle interactions in aqueous suspensions.[13] The creaming rate and extent were large at low electrolyte concentrations, but both decreased abruptly at salt concentrations exceeding the critical flocculation concentration of the suspension (*ca.* 1 mM NaCl). The drastic improvement of the stability to creaming is due to the formation of a viscoelastic three-dimensional network of interconnected particles and emulsion droplets.[13]

3.2 Zeta Potential of Particles

Precipitated $CaCO_3$ particles are almost insoluble in water (solubility = 0.014 g dm^{-3} at 25 °C).[14] There is a big debate about the behaviour of $CaCO_3$ particles in water, but Ca^{2+} and

CO_3^{2-} ions have been generally accepted as the potential determining ions.[15] Thus, the hydrolysis of $CaCO_3$ particles can be thought of as:

$$CaCO_{3(s)} \leftrightarrows Ca^{2+}_{(aq)} + CO_3^{2-}{}_{(aq)} \tag{3.1}$$

$$CO_3^{2-}{}_{(aq)} + H^+_{(aq)} \leftrightarrows HCO_3^-{}_{(aq)} + OH^-_{(aq)} \tag{3.2}$$

$$HCO_3^-{}_{(aq)} + H^+_{(aq)} \leftrightarrows H_2CO_{3(aq)} \tag{3.3}$$

$$H_2CO_{3(aq)} \leftrightarrows H_2O_{(l)} + CO_{2(dissolved)} \tag{3.4}$$

$$CO_{2(dissolved)} \leftrightarrows CO_{2(g)} \tag{3.5}$$

and

$$Ca^{2+}_{(aq)} + 2OH^-_{(aq)} \leftrightarrows Ca(OH)_{2(aq)} \tag{3.6}$$

Such that at low pH, reactions 3.2–3.5 proceed to the right (*i.e.* significant amount of CO_3^{2-} is consumed leaving behind significant amount of Ca^{2+}) giving rise to a net positive surface charge. At high pH, reaction 3.2 proceeds to the left (*i.e.* significant amount of CO_3^{2-} is formed) and reaction 3.6 proceeds to the right giving rise to a net negative surface charge.

The zeta potential ζ of the rod- and cube-shaped $CaCO_3$ particles at different pH values and [NaCl] is shown in Figure 3.1. It is seen that the rod-shaped particles have an isoelectric point of around pH = 10.2, whilst that of the cube-shaped ones is around 8.7, just like most $CaCO_3$ particles.[16,17] At unadjusted pH (about 8.8), the rod-shaped particles are positively charged. At pH > 10.2, these particles are negatively charged. The cube-shaped particles are, however, negatively charged at their unmodified pH (9.2), but are positively charged at pH < 8.7. For both particles, the magnitude of the ζ increases with increasing pH just like other hydrophilic particles[18,19] and $CaCO_3$ particles.[20] The charge inversion of the particles with pH is fairly consistent with the above behaviour (reactions 3.1−3.6). Figure 3.1 (b) shows that the ζ of the particles decreases slightly on increasing [NaCl]. This is also consistent with what is seen for other particles.[16] This is because increase in [NaCl] decreases the magnitude of the surface charge and the thickness of the electrical double layer, which is defined by the Debye length (κ_D^{-1}) in equation 3.7.

$$\kappa_D^{-1} = \left(\varepsilon\varepsilon_0 kT \Big/ N_A e^2 \sum_i z_i{}^2 c_i \right)^{0.5} \tag{3.7}$$

The N_A represents the Avogadro's constant, e is the elementary charge, ε is the dielectric constant of the medium, ε_0 is the permittivity of free space, k is the Boltzmann's constant, T is the absolute temperature, z_i is the valence of counter-ion and c_i is the electrolyte concentration. Equation 3.7 actually predicts an inverse relationship between κ_D^{-1} and c_i.

Figure 3.1. Dependence of zeta potential ζ of 0.125 wt. % of rod- (●) and cube-shaped (○) $CaCO_3$ particles in water on (a) pH and (b) [NaCl]. At unadjusted pH (*ca.* 8.8 and 9.2 for rod- and cube-shaped particles respectively), the ζ of rod- and cube-shape $CaCO_3$ particles is 8.5 and –22.3 mV respectively. The error bars represent the standard deviation of 3 separate measurements.

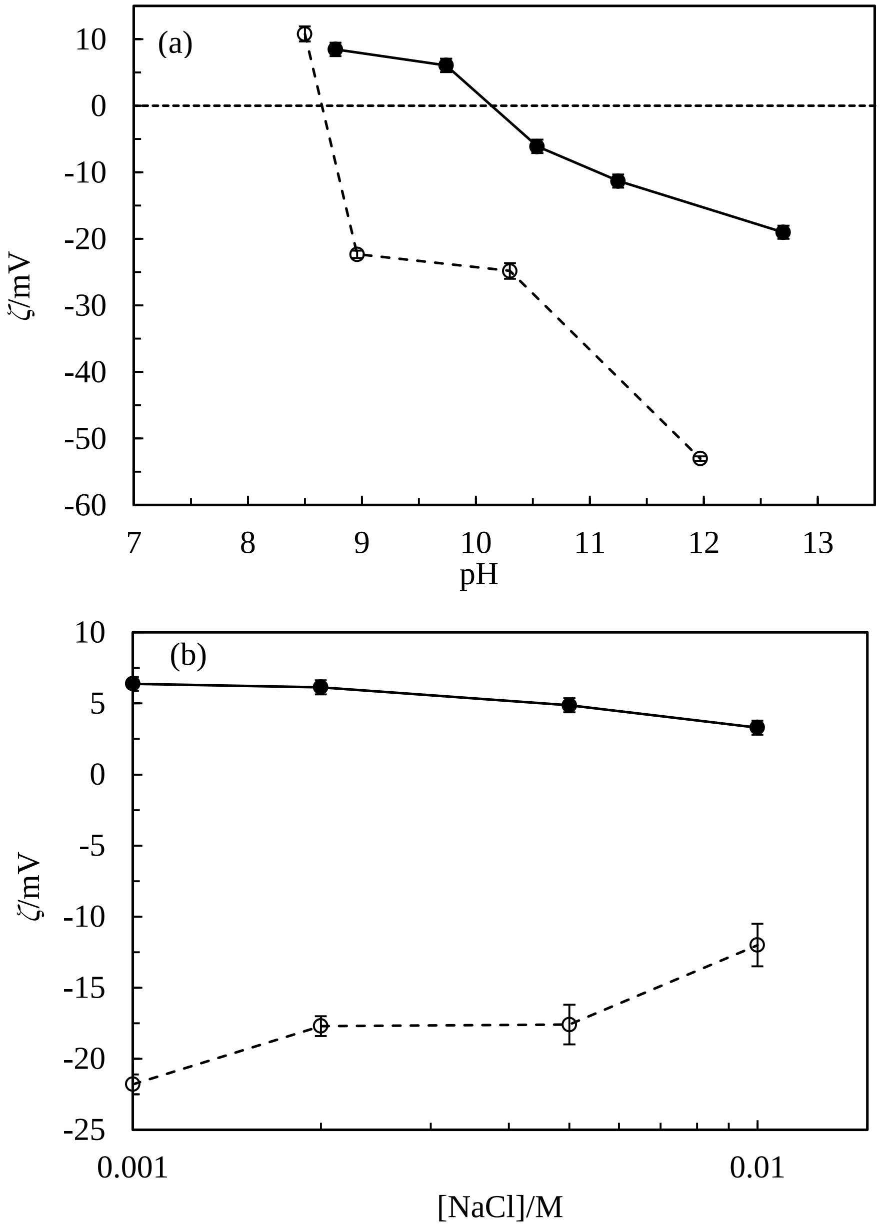

3.3 Effect of Particle Concentration on the Stability of the Emulsions Containing Equal Volume Fraction of Water and Oil

The tricaprylin-water ($pH \leq 8.3$) and Miglyol 812N-water ($pH \leq 8.6$) emulsions stabilised by the rod-shaped hydrophilic $CaCO_3$ particles were of the o/w type because they disperse in water and they have relatively high conductivity values. The formation of o/w emulsions with these particles is consistent with the findings of Finkle *et al.*[21] and Schulman and Leja[22] that water-wet particles would stabilise o/w emulsions whilst oil-wet particles would stabilise w/o emulsions. With reference to Figure 3.2, the conductivity and pH of the emulsions increase with an increase in particle concentration. The emulsions are white (Figure 3.3) and their optical micrographs (Figure 3.4) show that the droplet surfaces are coated by particles. This ‘armours’ the droplets and prevents coalescence. The emulsions also look highly flocculated presumably due to the bridging[23] of the oil droplets by particle layers. As evidence from cryo-SEM images of the 2 wt. % $CaCO_3$ particle-stabilised emulsions (Figure 3.5), the rod-shaped $CaCO_3$ particles adsorb on their long axis to the droplet surfaces forming close-packed particle layers on them. Taking advantage of the partially broken frozen oil droplets, one would see that the particles basically form monolayers on the droplet surfaces. Few areas of particle defects were seen on the droplet surfaces in some cases. It has been reported that rod-shaped nanoparticles are more stable at fluid interfaces when they adsorb on their long axis as a result of high free energy of adsorption.[24] The emulsions are very unstable to creaming and coalescence in the absence of particles, separating completely into clear layers of oil and water within a day compared with those containing particles. Figures 3.6 and 3.7 show the dependence of the emulsions droplet size distribution on particle concentration along with the creaming and coalescence stability of the emulsions respectively. Initially, the average droplet size (d (0.5)) decreases with an increase in particle concentration (< 3 wt. %), but became relatively constant above this concentration. An increase in particle concentration led to a corresponding increase in the stability of the emulsions to creaming and coalescence. As a result, those containing ≥ 3 wt. % of particles were stable to creaming for over 3 years, but released a relatively small fraction of the oils. The decrease in droplet size enhances droplet motion (*i.e.* Brownian motion) which reduces the effect of gravity induced creaming and separation. Generally, the droplets of tricaprylin-in-water emulsions are smaller and more stable to creaming compared with those of the Miglyol 812N-in-water emulsions. Nonetheless, the Miglyol 812N-in-water emulsions are more stable to coalescence compared with the tricaprylin-in-water emulsions.

Figure 3.2. Conductivity (triangles, 3 min after preparation) and pH (circles and crosses, 5 min after preparation) of tricaprylin-in-water and Miglyol 812N-in-water emulsions ($\phi_o = 0.5$) shown in Figure 3.3, prepared using the powdered particle method, as a function of rod-shaped $CaCO_3$ particle concentration.

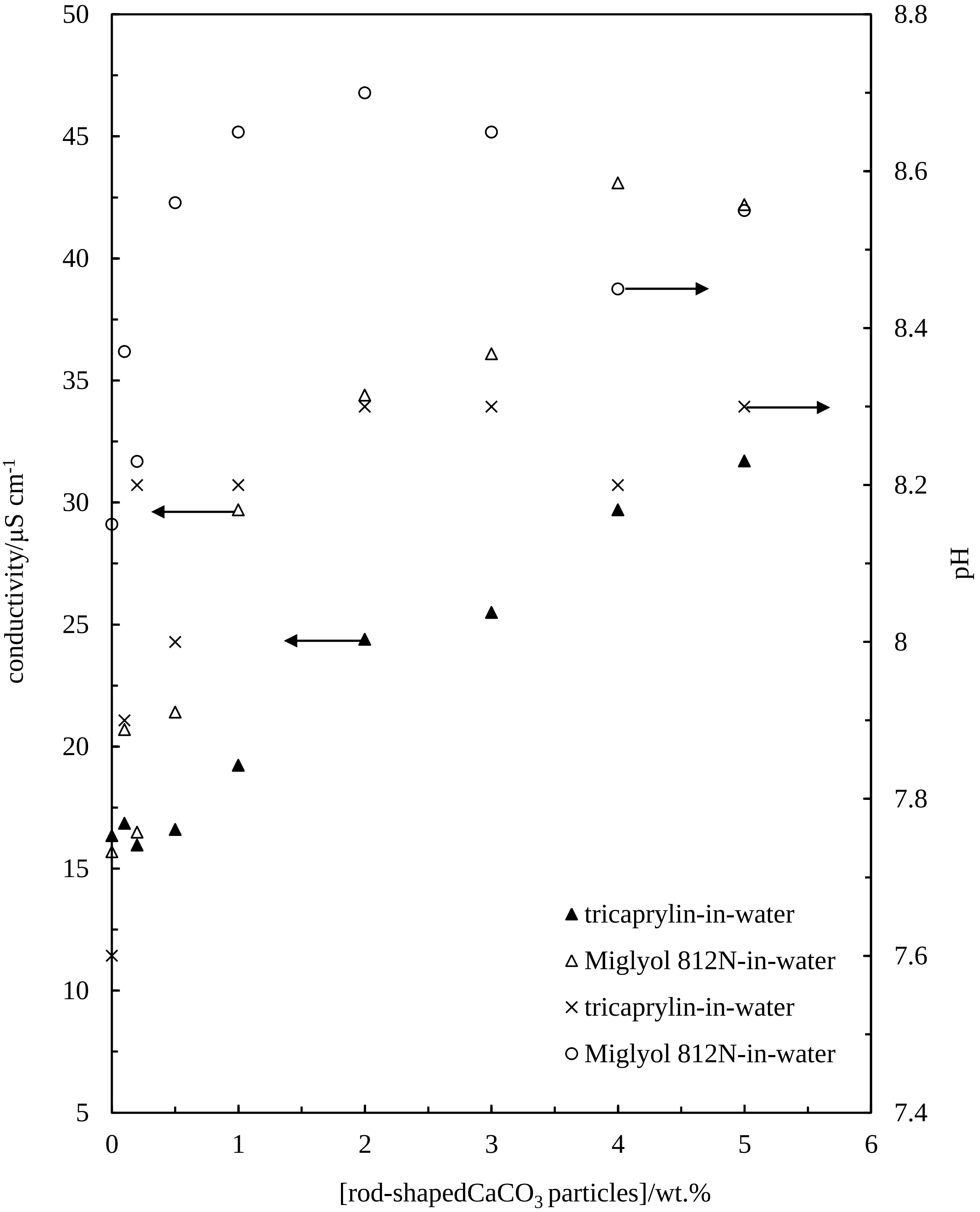

Figure 3.3. Photos (taken 5 months after preparation) of glass vials containing 14 cm^3 of (a) tricaprylin-in-water and (b) Miglyol 812N-in-water emulsions (ϕ_o = 0.5) stabilised by different concentrations (given, wt. %) of rod-shaped $CaCO_3$ particles. The emulsions were prepared by the powdered particle method.

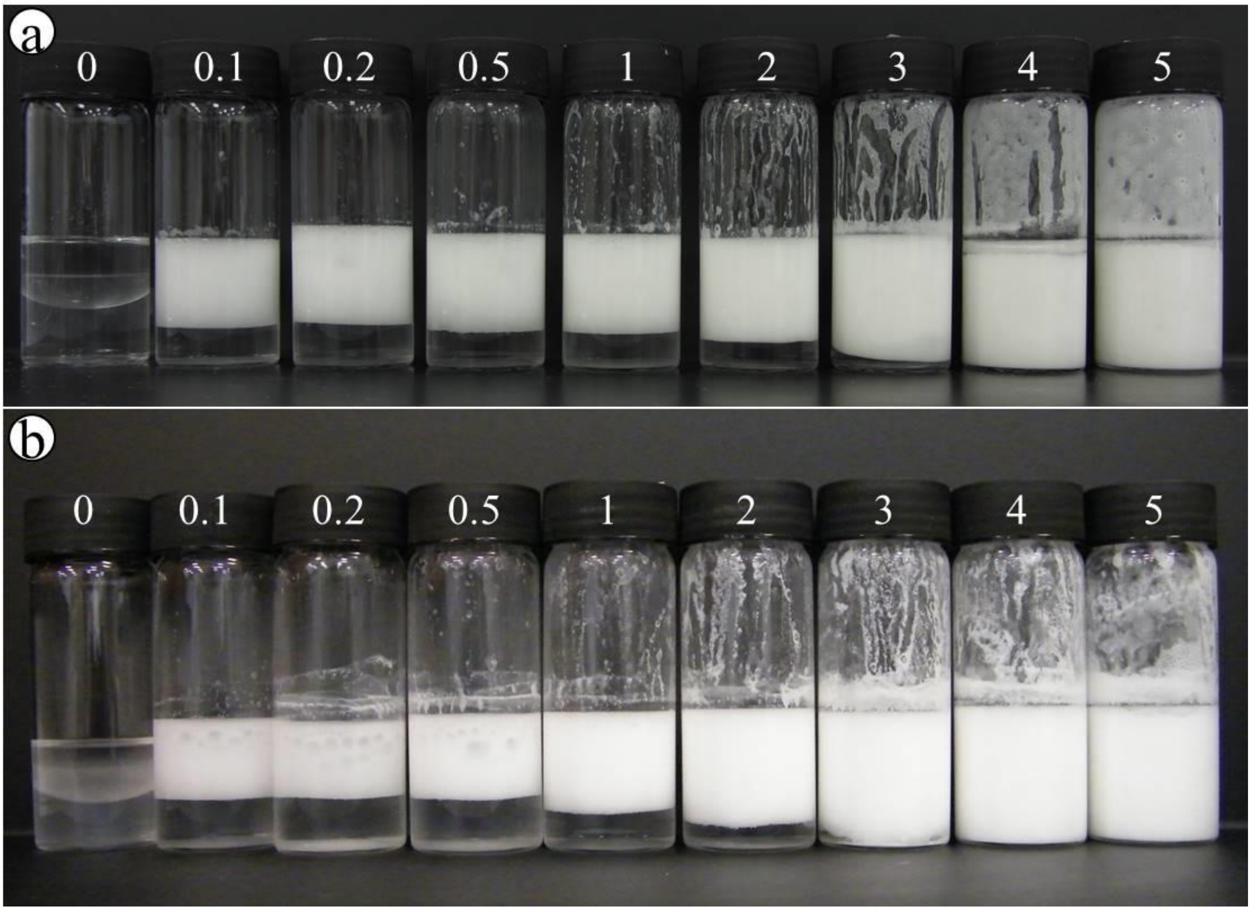

Figure 3.4. Optical micrographs (taken 30 min after preparation) of the (a) tricaprylin-in-water and (b) Miglyol 812N-in-water emulsions, shown in Figure 3.3, at selected particle concentrations (given wt. %).

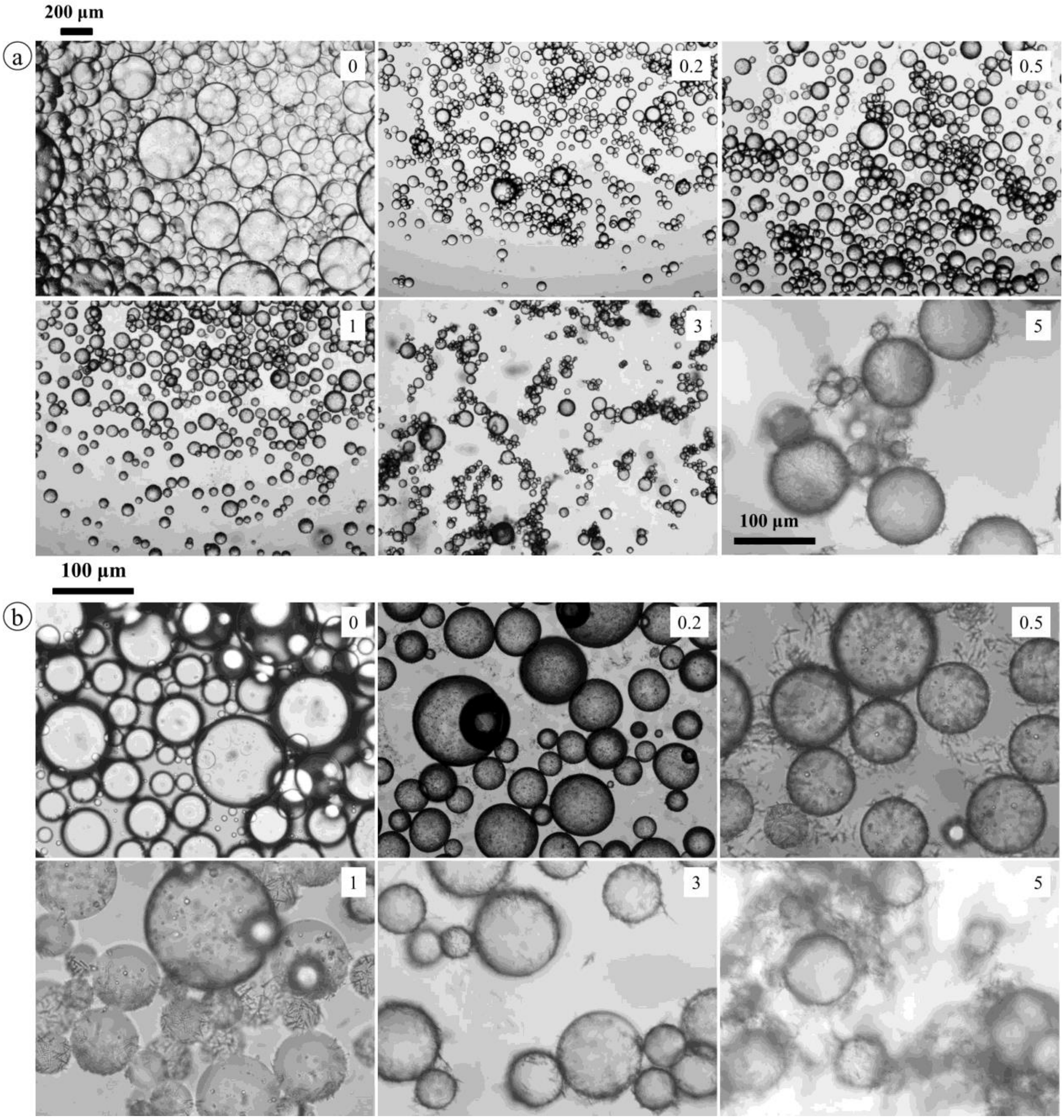

Figure 3.5. Cryo-SEM images (1 week after preparation) of (a) tricaprylin-in-water and (b) Miglyol 812N-in-water emulsions stabilised by 2 wt. % of rod-shaped $CaCO_3$ particles (shown in Figure 3.3) showing the particles on the droplet surfaces. (c) Schematic illustration of the longitudinal dissection of a frozen partially exposed oil droplet showing the rod-shaped $CaCO_3$ particles on the droplet surfaces.

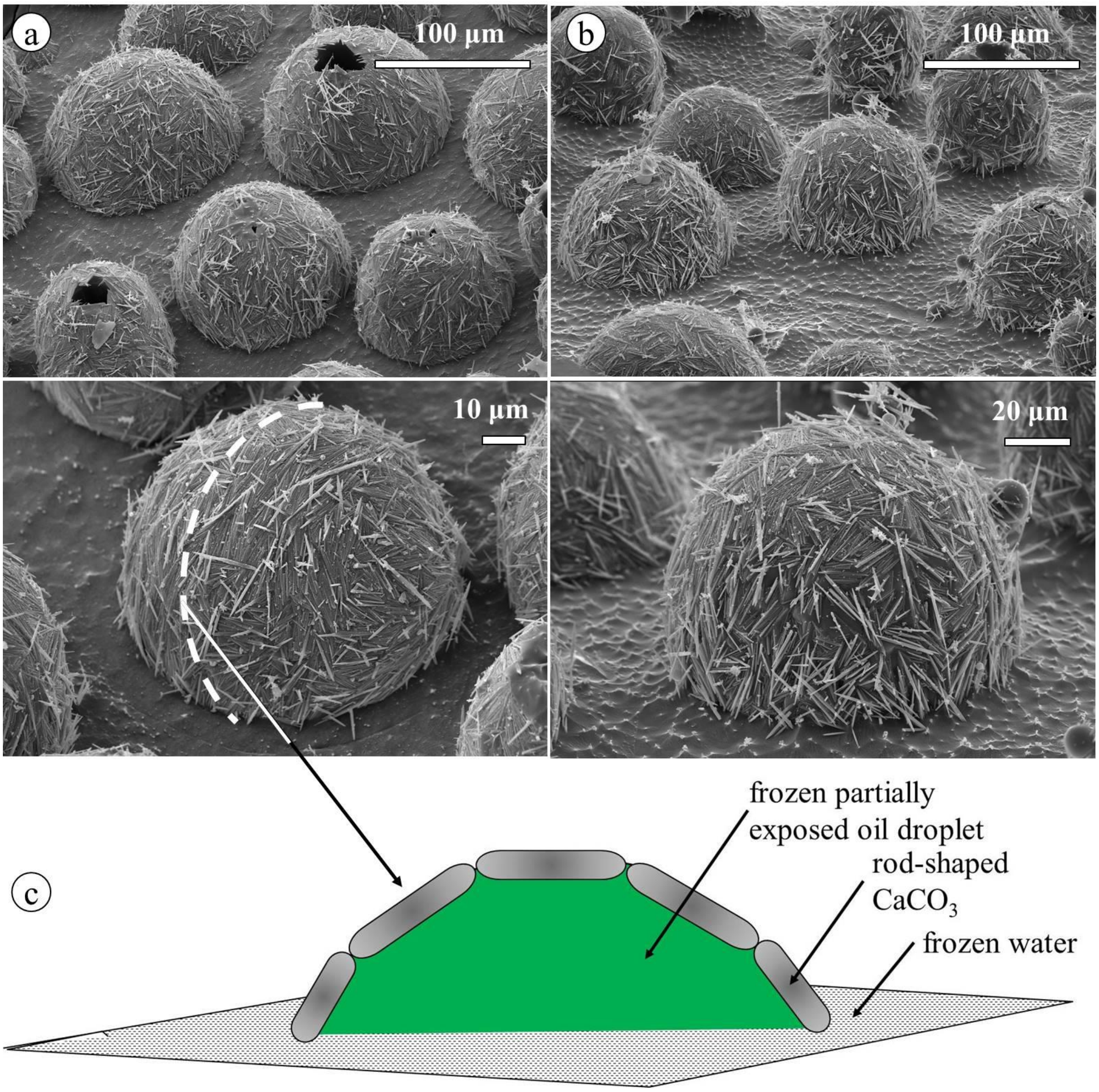

Figure 3.6. Droplet diameter d(0.5) of tricaprylin-in-water (●) and Miglyol 812N-in-water (○) emulsions (ϕ_o = 0.5; 1 hour after preparation) and fraction of water f_w released from the tricaprylin-in-water (◇) and Miglyol 812N-in-water (×) emulsions shown in Figure 3.3 (4 months after preparation) as a function of rod-shaped $CaCO_3$ particle concentration. The error in values of d(0.5) and f_w is ± 2 μm (standard deviation of 3 measurements) and ± 0.05 (propagation error) respectively. The d(0.5) was measured using the Malvern Mastersizer 2000. Data from the mastersizer show that the droplet diameter of the tricaprylin-in-water emulsions ranges from 3−363 μm whilst that of the Miglyol 812N-in-water emulsions ranges from 23−832 μm.

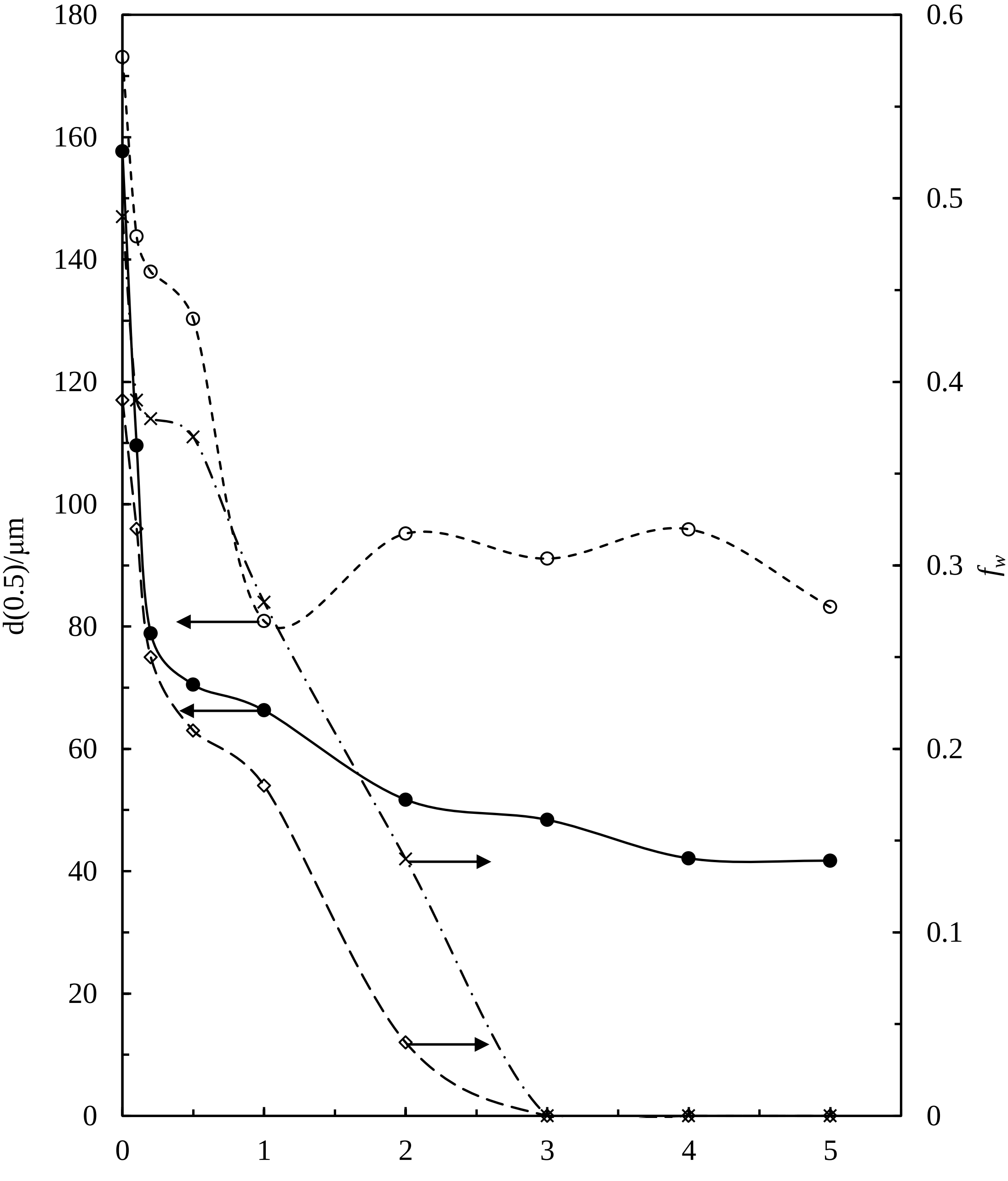

Figure 3.7. Fraction of oil f_o released from tricaprylin-in-water (▲) and Miglyol 812N-in-water (△) emulsions shown in Figure 3.3 (ϕ_o = 0.5) 4 months after preparation and d(0.5) (measured 1 hour after preparation) of the tricaprylin-in-water (●) and Miglyol 812N-in-water (○) emulsions *versus* concentration of rod-shaped $CaCO_3$ particles. The error in values of d(0.5) and f_o is ± 2 μm (standard deviation of 3 measurements) and ± 0.05 (propagation error) respectively.

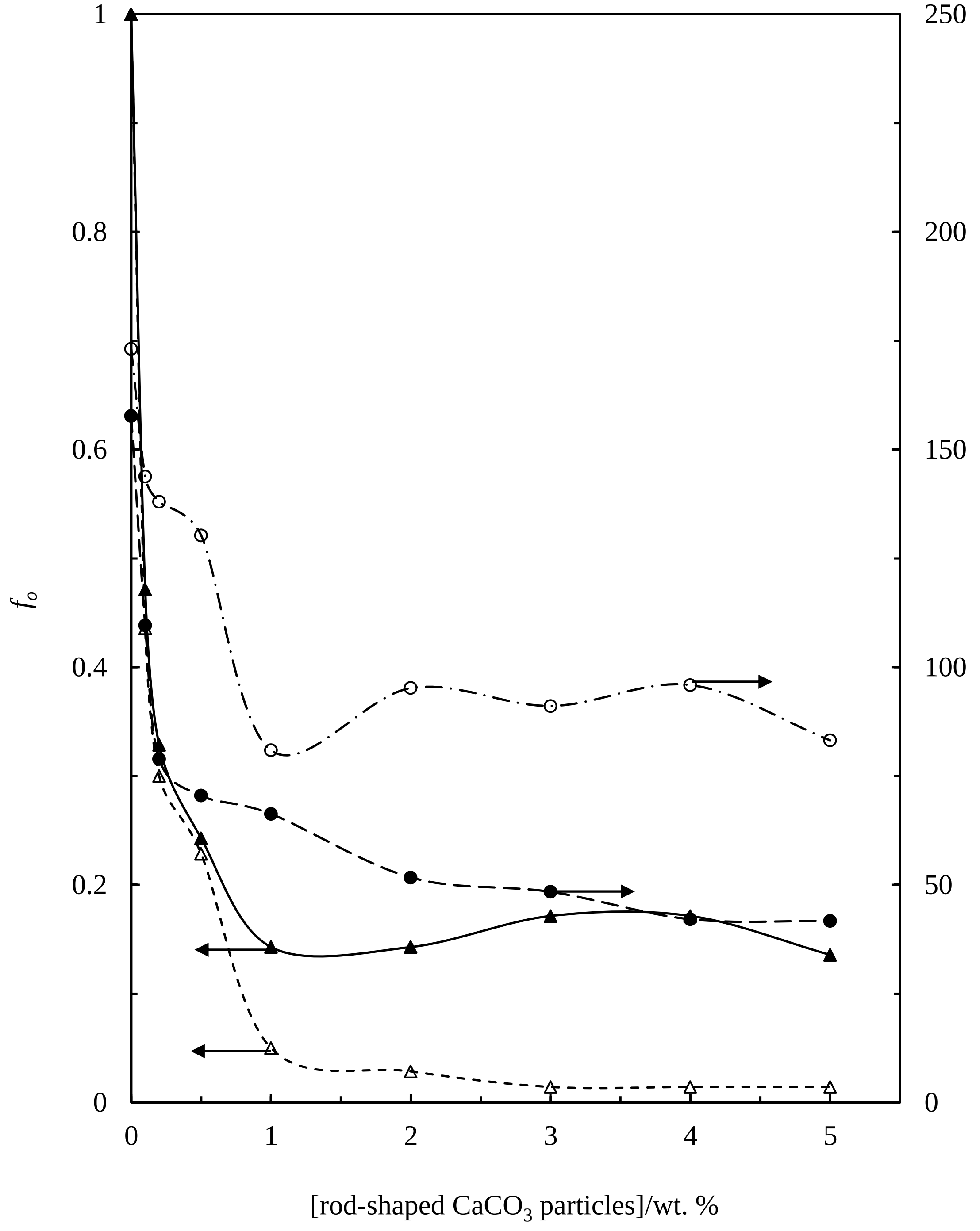

3.4 Effect of Particle Concentration on the Stability of Emulsions Containing Low (0.2) Volume Fraction of Oil

White and flocculated tricaprylin-in-water (pH ≤ 9) and Miglyol 812N-in-water (pH ≤ 8.7) emulsions were also obtained with the ϕ_o = 0.2 systems in the presence of the rod-shaped $CaCO_3$ particles as stabilisers using the powdered particle method at ambient conditions. The emulsion type is evident from the relatively high conductivity values of the emulsions (Figure 3.8) which increase with an increase in particle concentration and the ease with which the emulsions disperse in water. These emulsions were less stable to creaming compared with those of the ϕ_o = 0.5. The emulsions with particle concentrations > 2 wt. % sedimented in the separated water phase (instead of creaming) with a layer of oil (to which unadsorbed particles stuck on) above the water phase as shown by their photos in Figure 3.9. Their microscope images, Figure 3.10, show particle layers on the droplet surfaces. The sedimentation might be due to the difference in densities of the rod-shaped $CaCO_3$ particles, water and oil. The creaming or 'sedimentation' stability of the emulsions increased with an increase in particle concentration, but their droplet size decreased as the particle concentration increases as shown in Figure 3.11. There appears to be an inverse relationship between the droplet size and the creaming stability of the emulsions (*i.e.* the smaller the droplets the higher the creaming stability and vice versa). Again, on the average, the tricaplylin emulsions droplets were smaller than those of Miglyol 812N. At particle concentrations ≤ 1 wt. %, the tricaprylin emulsions were more stable to creaming than the Miglyol 812N emulsions, but the Miglyol 812N emulsions became more stable to creaming than the tricaprylin ones at particle concentrations above 1 wt. % (Figure 3.11). Figure 3.12 shows that the coalescence stability of the emulsions increased with an increase in particle concentration and decrease in droplet size. Finally, the Miglyol 812 N-in-water emulsions are more stable to coalescence than the tricaprylin-in-water emulsions.

Figure 3.8. Conductivity (triangles, 3 min after preparation) and pH (circles and crosses, 5 min after preparation) of tricaprylin-in-water and Miglyol 812N-in-water emulsions ($\phi_o = 0.2$) shown in Figure 3.9, prepared by the powdered particle method, as a function of rod-shaped $CaCO_3$ particle concentration. The inset (separated by the dotted line) is a sketch showing which emulsions creamed or sedimented.

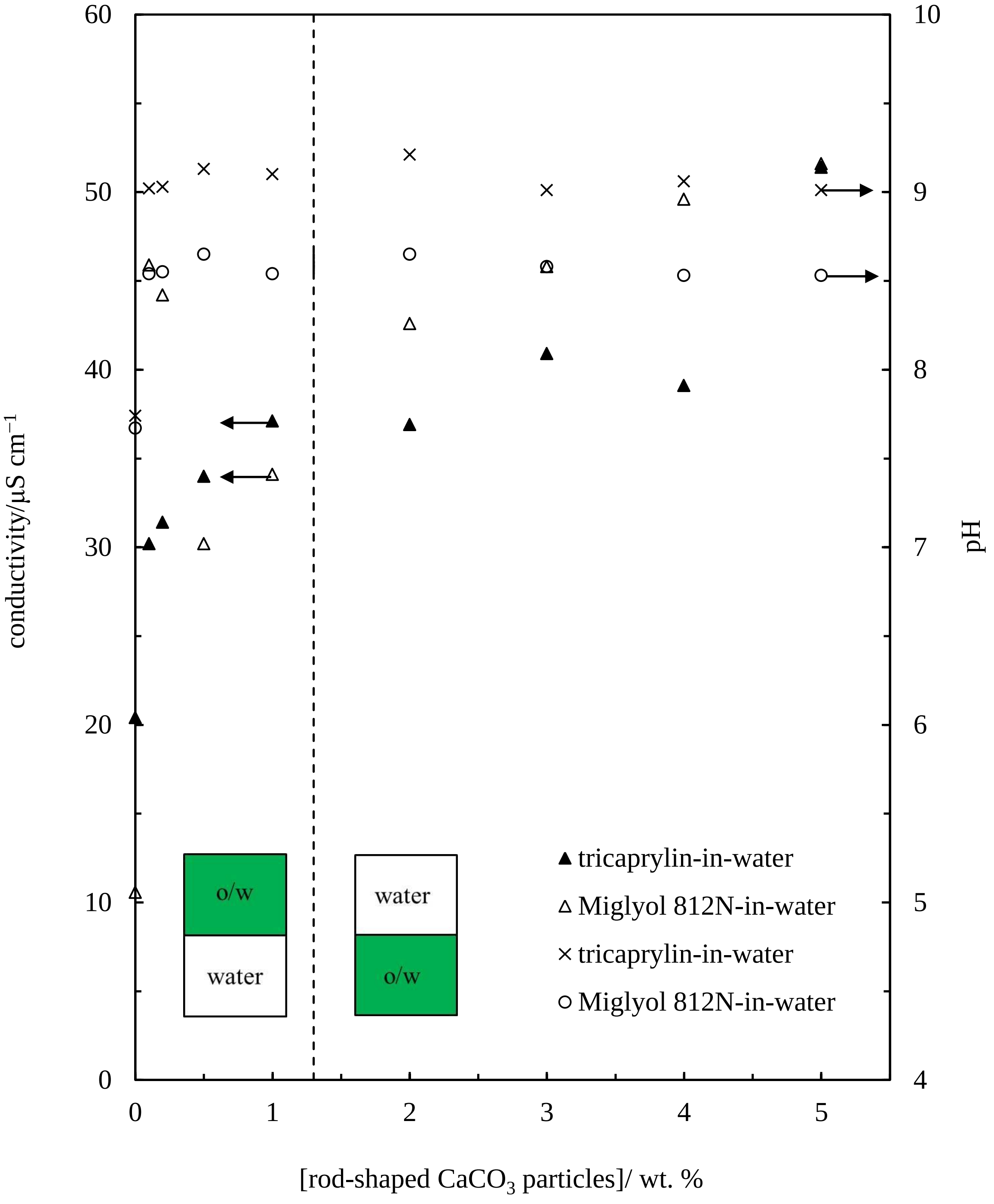

Figure 3.9. Photos (taken 5 months after preparation) of glass vials containing 14 cm^3 of (a) tricaprylin-in-water and (b) Miglyol 812N-in-water emulsions ($\phi_o = 0.2$) stabilised by different concentrations of rod-shaped $CaCO_3$ (given, wt. %). The emulsions were prepared by the powdered particle method.

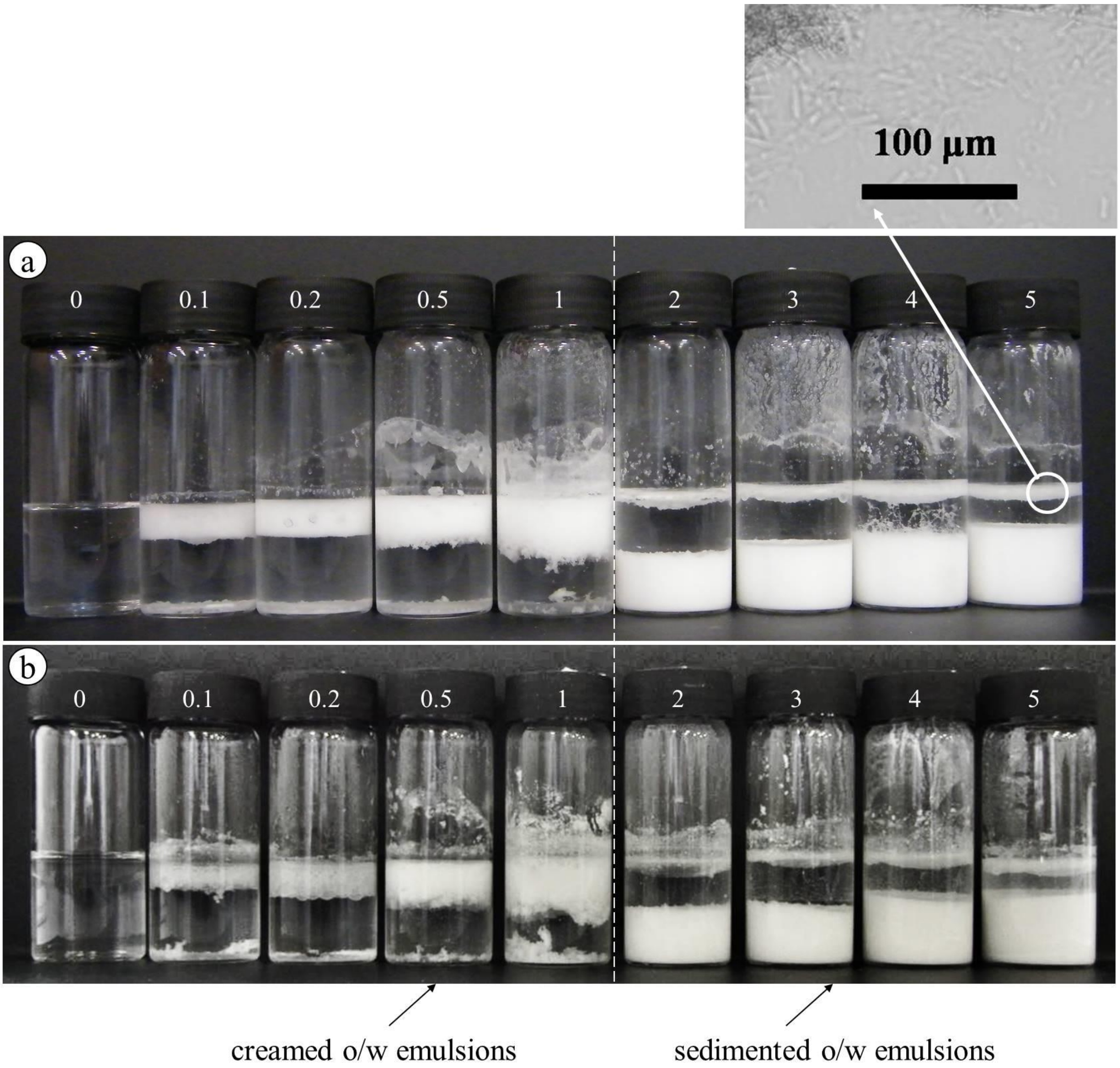

Figure 3.10. Optical micrographs (30 min after preparation) of the (a) tricaprylin-in-water and (b) Miglyol 812N-in-water emulsions shown in Figure 3.9 at selected particle concentrations (given, wt. %).

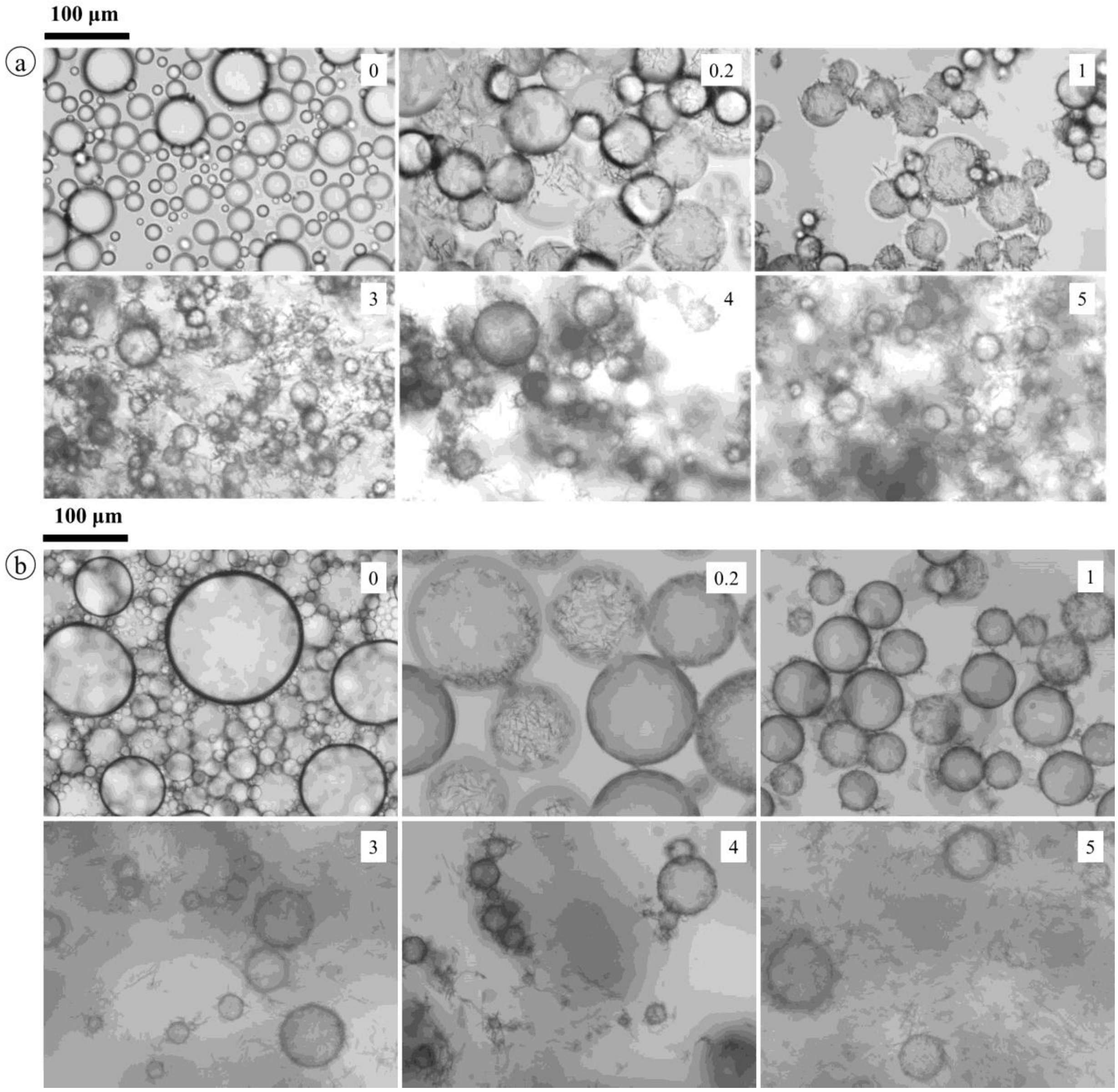

Figure 3.11. Droplet diameter d(0.5) (1 hour after preparation) and fraction of water f_w released from emulsions ϕ_o = 0.2 (4 months after preparation) shown in Figure 3.9 *versus* concentration of rod-shaped $CaCO_3$ particles. Tricaprylin-in-water (●: d(0.5), ▲: f_w) and Miglyol 812N-in-water (○: d(0.5), △: f_w) emulsions. The error in values of d(0.5) and f_o is ± 2 μm (standard deviation of 3 measurements) and ± 0.05 (propagation error) respectively. The creamed and sedimented emulsions are separated by the vertical dotted line. The d(0.5) was measured using the Malvern Mastersizer 2000. Data from the mastersizer show that the droplet diameter of the tricaprylin-in-water emulsions ranges from 10−724 μm whilst that of the Miglyol 812N-in-water emulsions ranges from 12−613 μm.

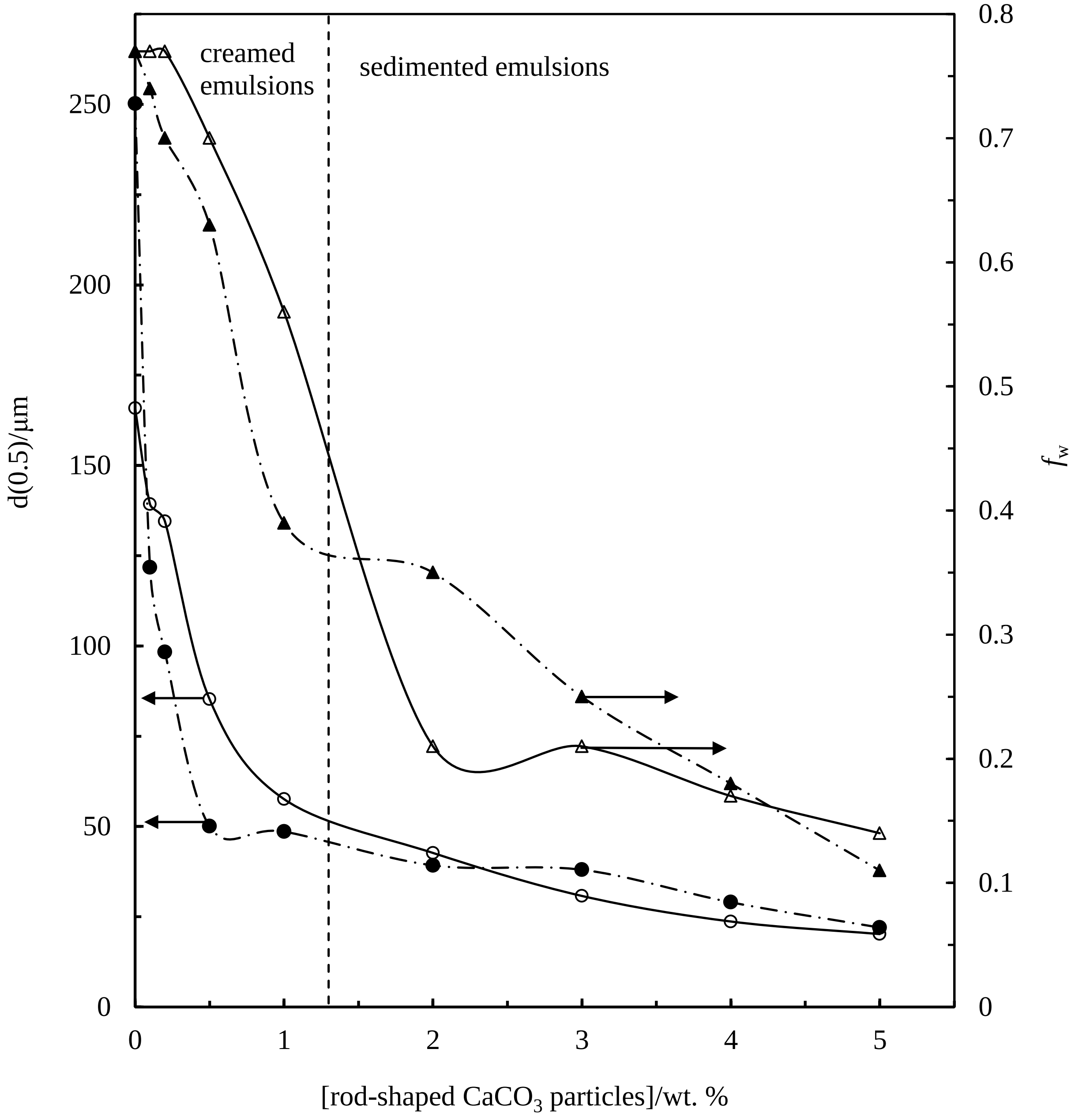

Figure 3.12. Fraction of oil f_o released from tricaprylin-in-water (×) and Miglyol 812N-in-water (+) emulsions shown in Figure 3.9 ($\phi_o = 0.2$), 4 months after preparation, and the corresponding d(0.5) of the tricaprylin-in-water (◆) and Miglyol 812N-in-water (◇) emulsions (1 hour after preparation) *versus* concentration of rod-shaped $CaCO_3$ particles. The error in values of d(0.5) and f_o is ± 2 μm (standard deviation of 3 measurements) and ± 0.05 (propagation error) respectively. The creamed and sedimented emulsions are separated by the vertical dotted line.

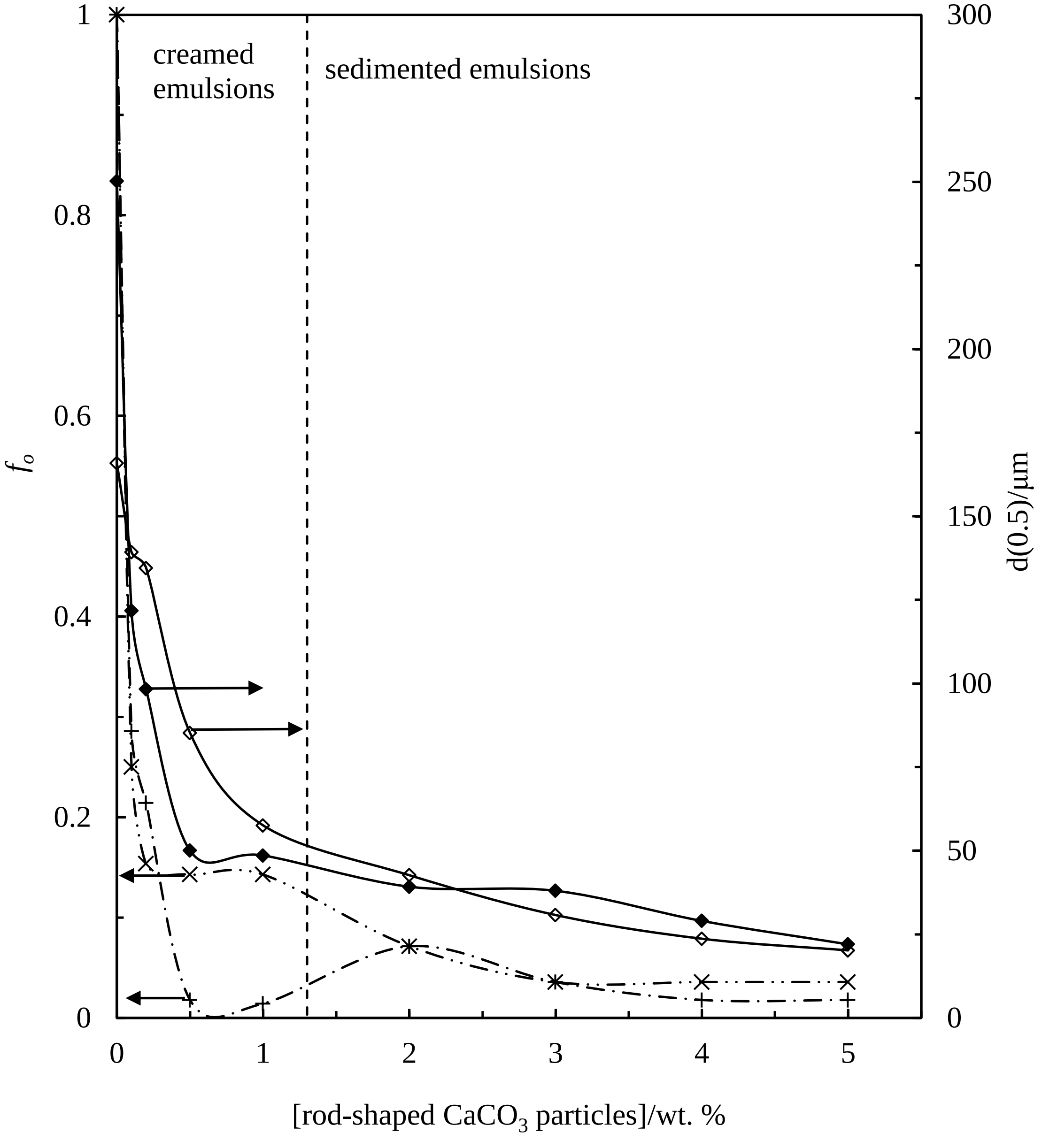

3.5 Effect of Volume Fraction of Oil on the Stability of the Emulsions

The effect of ϕ_o on the stability of the emulsions was studied at a fixed particle concentration (4 wt. %). The particle concentration is relative to the total volume (14 cm^3) of oil and water in the emulsions. The emulsions were prepared by the powdered particle method. A plot of the conductivity and pH of these emulsions *versus* ϕ_o is given in Figure 3.13 and their photos and optical microscope images are shown in Figures 3.14 and 3.15 respectively. 'Oily liquids' (*i.e.* looking just like the oil) with low conductivity values and pH between 7−8 were obtained for systems containing $\phi_o \geq 0.8$. For $\phi_o < 0.8$, o/w emulsions (white and flocculated) were obtained judging from their relatively high conductivity values and their ability to disperse readily in water. The emulsions containing ϕ_o between 0.7−0.5 were stable to creaming for over 3 years, but released relatively small fraction of the oils. Those containing ϕ_o between 0.35−0.05 were unstable and sedimented in the separated water phase (within a day) with a layer of oil (to which unadsorbed particles stuck on) above the water phase. Just like with the other emulsions, the optical micrographs of these o/w emulsions show the presence of particles on the droplet surfaces. Figure 3.16 shows a plot of the f_o and the droplet diameter of the emulsions as a function of ϕ_o. The tricaprylin-in-water and Miglyol 812N-in-water emulsions have comparable droplet size and coalescence stability. The f_o released in the emulsions decreased with decreasing ϕ_o between ϕ_o = 0.7 and 0.5, but increased between ϕ_o = 0.5 and 0.05. Their droplet sizes, however, decreased as ϕ_o decreases. This is unique compared with the other emulsions studied where coalescence stability increases as the droplet size decreases. This can be explained in terms of the emulsion droplet size and size of the rod-shaped $CaCO_3$ particles. As mentioned earlier on,[25,26] the ability of a solid particle to stabilise an emulsion depends on its size among other factors where particles bigger than the emulsion droplets do not effectively stabilise them as opposed to those smaller than the emulsion droplets. As the droplet size of the emulsions is decreasing with decreasing ϕ_o, emulsion droplets either smaller than or comparable to the size of the rod-shaped $CaCO_3$ particles might have been formed at $\phi_o < 0.5$, making it difficult for the particles to adsorb and remain on their surfaces. Consequently, the emulsion droplets will be less stable to coalescence.

Figure 3.13. Conductivity (3 min after preparation) and pH (5 min after preparation) of tricaprylin-in-water (+: conductivity and ▲: pH) and Miglyol 812N-in-water (○: conductivity and △: pH) emulsions stabilised by 4 wt. % of rod-shaped $CaCO_3$ particles shown in Figure 3.14 *versus* volume fraction of oil ϕ_o. The emulsions were prepared using the powdered particle method at ambient conditions. Also shown are regions where 'oily liquids', relatively stable o/w emulsions and sedimented emulsions formed in the batch emulsions.

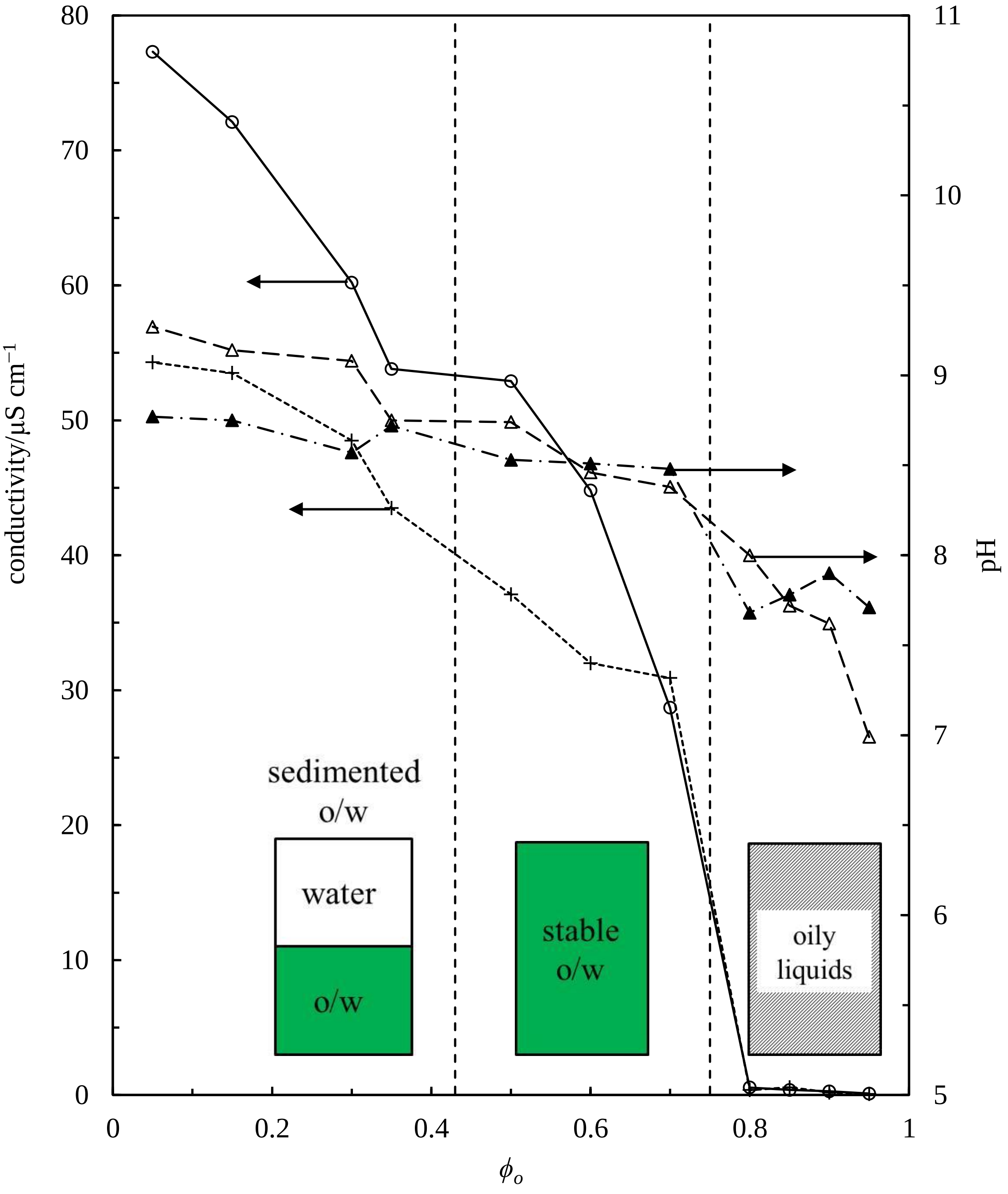

Figure 3.14. Photos (5 months after preparation) of glass vials containing (a) tricaprylin-in-water and (b) Miglyol 812N-in-water emulsions containing different volume fractions of the oils ϕ_o (given) stabilised by 4 wt. % of rod-shaped $CaCO_3$ particles. The emulsions were prepared by the powdered particle method.

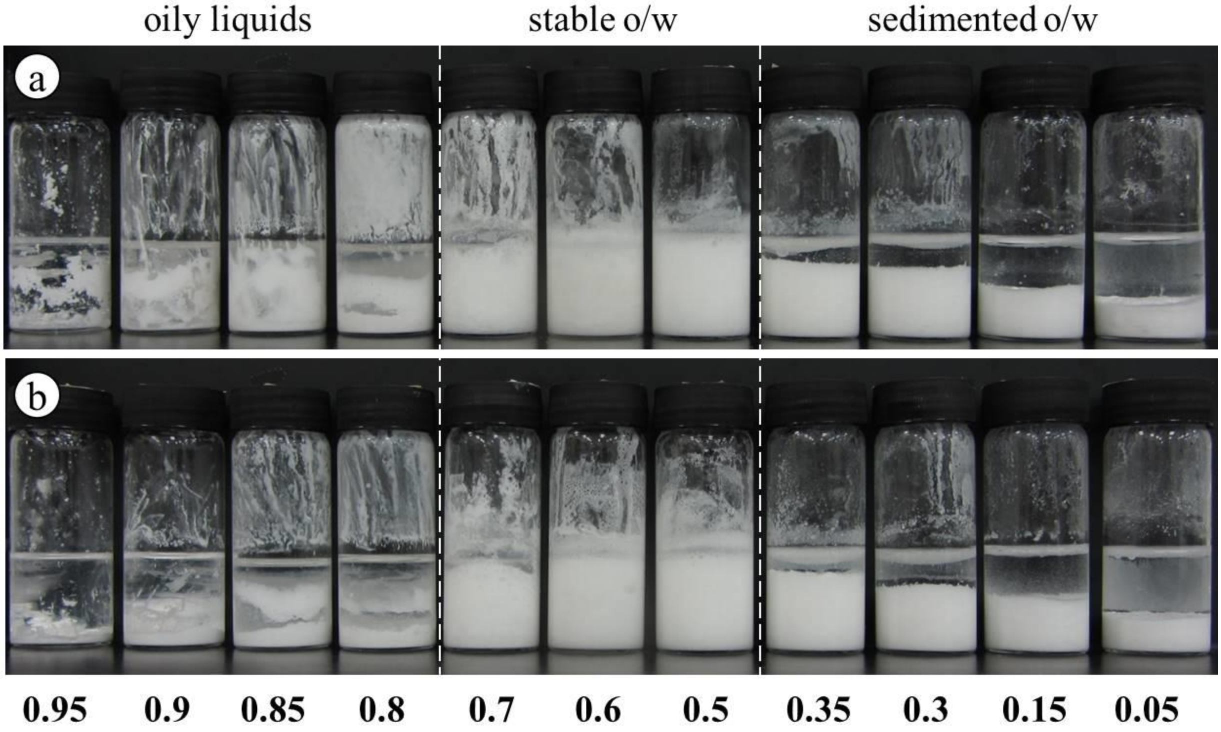

Figure 3.15. Optical micrographs (30 min after preparation) of the (a) tricaprylin-in-water and (b) Miglyol 812N-in-water emulsions, shown in Figure 3.14, at selected ϕ_o (given).

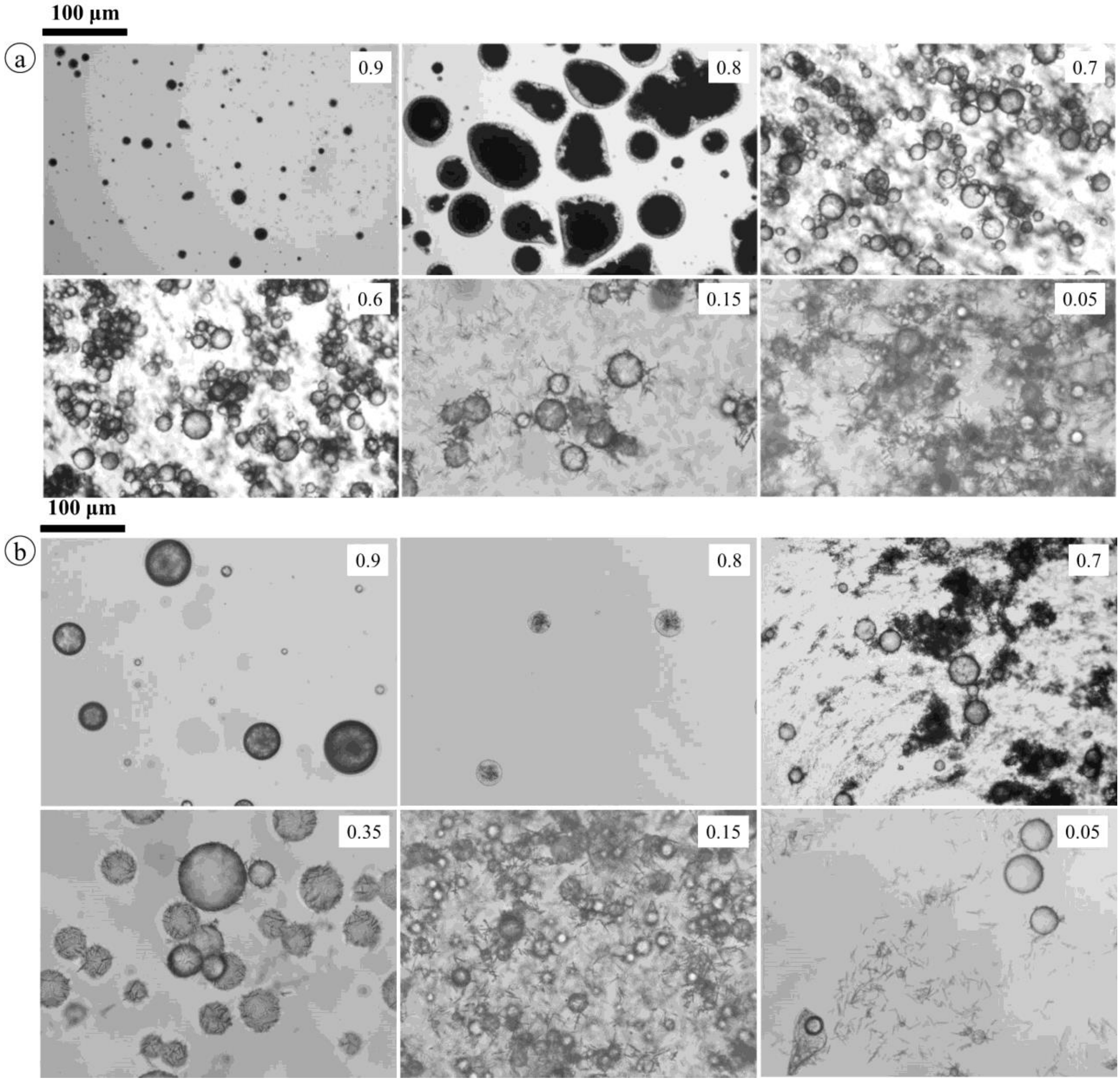

Figure 3.16. Fraction of oil f_o released from tricaprylin-in-water (○) and Miglyol 812N-in-water (+) emulsions (4 months after preparation) containing ϕ_o between 0.05 and 0.7 stabilised by 4 wt. % of rod-shaped $CaCO_3$ particles and their corresponding d(0.5) (1 hour after preparation): tricaprylin-in-water (◆) and Miglyol 812N-in-water (◇) emulsions shown in Figure 3.14. The error in values of d(0.5) and f_o is ± 2 μm (standard deviation of 3 measurements) and ± 0.05 (propagation error) respectively. The d(0.5) was measured using the Malvern Mastersizer 2000. Data from the mastersizer show that the droplet diameter of the tricaprylin-in-water emulsions ranges from 26−724 μm (ϕ_o = 0.3), 13−550 μm (ϕ_o = 0.4−0.7) and 3−479 μm (ϕ_o = 0.85−0.95) whilst that of the Miglyol 812N-in-water emulsions ranges from 40−832 μm (ϕ_o = 0.3), 11−550 μm (ϕ_o = 0.4−0.7) and 3−209 μm (ϕ_o = 0.85−0.95).

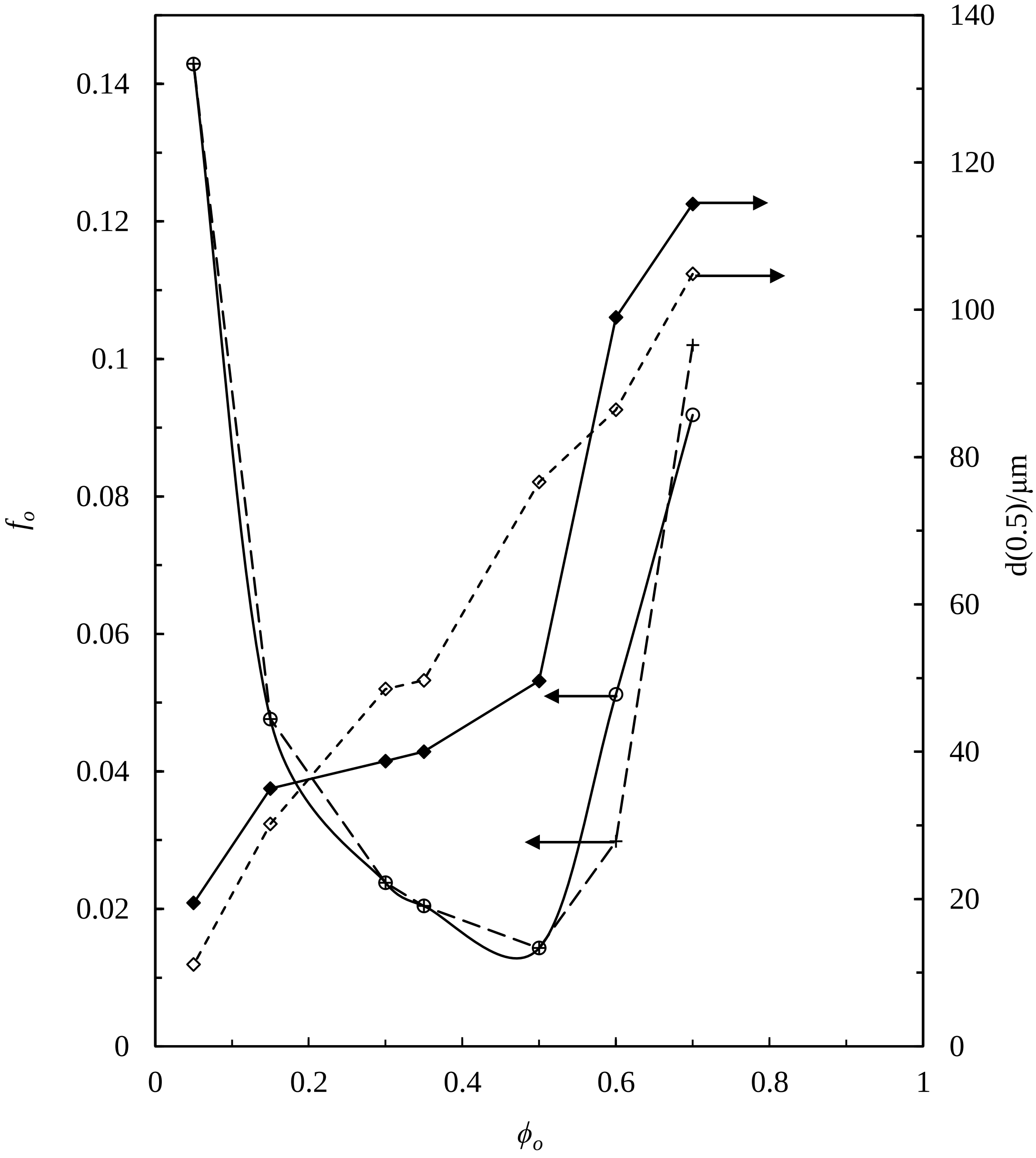

3.6 Effect of Particle Shape and Method of Preparation on the Stability of the Emulsions

The Cube-shaped $CaCO_3$ particles (4 wt. %) were used to prepare tricaprylin-in-water and Miglyol 812N-in-water emulsions (ϕ_o = 0.5) using the powdered particle and the particle dispersion methods. The stability of these emulsions to creaming and coalescence was compared with those (ϕ_o = 0.5) stabilised by the rod-shaped $CaCO_3$ particles (4 wt. %) prepared by the same methods. Photos and optical micrographs of these emulsions are shown, respectively, in Figures 3.17 and 3.18 along with a cryo-SEM image of one of the cube-shaped $CaCO_3$ particle-stabilised emulsions. The cryo-SEM image (Figure 3.18) of the emulsions show that the cube-shaped $CaCO_3$ particles adsorb mainly on their faces to the droplet surfaces forming particle layers on them. Particle monolayers and areas of particle defects are clearly visible on the droplet surfaces. The areas of particle defects seen here are more than those seen on oil droplets coated with the rod-shaped $CaCO_3$ particles (*cf.* Figures 3.5 and 3.18). The droplet size of the rod-shaped $CaCO_3$ particle-stabilised emulsions is similar irrespective of the method of emulsion preparation. The average droplet size of the cube-shaped $CaCO_3$ particle-stabilised emulsions is higher than that of the rod-shaped $CaCO_3$ particle-stabilised ones. Some of the cube-shaped $CaCO_3$ particle-stabilised emulsions droplets are quasi-spherical. The emulsions are polydisperse and flocculated regardless of the type of particles used and method of preparation. After a month, the f_w and f_o released by the cube-shaped $CaCO_3$ particle-stabilised tricaprylin-in-water emulsions prepared by the powdered particle (particle dispersion) method are 0 and 0.014 (0 and 0.06) respectively. For the cube-shaped $CaCO_3$ particle-stabilised Miglyol 812N-in-water emulsions prepared by the powdered particle (particle dispersion) method, the values of f_w and f_o 1 month after preparation are 0.064 and 0.002 (0.1 and 0.04) respectively. In the case of the rod-shaped $CaCO_3$ particle-stabilised tricaprylin-in-water emulsions prepared by the powdered particle (particle dispersion) method, the values of f_w and f_o 1 month after preparation were observed to be 0 and 0.044 (0 and 0.017) respectively. However, for the rod-shaped $CaCO_3$ particle-stabilised Miglyol 812N-in-water emulsions prepared by the powdered particle (particle dispersion) method, these values were 0 and 0.036 (0 and 0.033) respectively. Clearly, the cube-shaped $CaCO_3$ particle-stabilised tricaprylin emulsions prepared by the powdered particle method are more stable to coalescence than those prepared by the particle dispersion method, but the opposite is true for the rod-shaped $CaCO_3$ particle-stabilised emulsions. However, all the emulsions are stable to creaming for over 3 years. Conversely, the cube-shaped $CaCO_3$ particle-stabilised Miglyol 812N-in-water emulsions prepared *via* the powdered particle method are more stable to creaming and coalescence compared with those prepared by the particle dispersion method. Nevertheless, the stability of those stabilised by the rod-shaped particles is similar. For the powdered particle method, the cube-shaped $CaCO_3$ particles give more stable emulsions than those stabilised by the rod-shaped $CaCO_3$ particles. Regarding the particle dispersion method, the cube-shaped $CaCO_3$ particle-stabilised Miglyol 812N-in-water emulsion is more stable than the rod-shaped $CaCO_3$ particle-stabilised one, but the opposite is true for the tricaprylin-in-water emulsions. The reason for the difference in the stability of the rod- and cube-shaped $CaCO_3$ particle-stabilised emulsions is not clear, but might be due to the orientation of the particles on the droplet surfaces due to their shape or the size of the particles themselves.

Figure 3.17. (upper) Photo (1 month after preparation) of (a) tricaprylin-in-water and (b) Miglyol 812N-in-water emulsions ($\phi_o = 0.5$) prepared by the powdered particle method (left) and particle dispersion method (right). (lower) Optical micrographs (2 weeks after preparation) of the corresponding emulsions: (a) tricaprylin-in-water and (b) Miglyol 812N-in-water emulsions prepared by the powdered particle method (left) and particle dispersion method (right). The emulsions were stabilised by 4 wt. % of rod-shaped $CaCO_3$ particles. Scale bar = 100 μm.

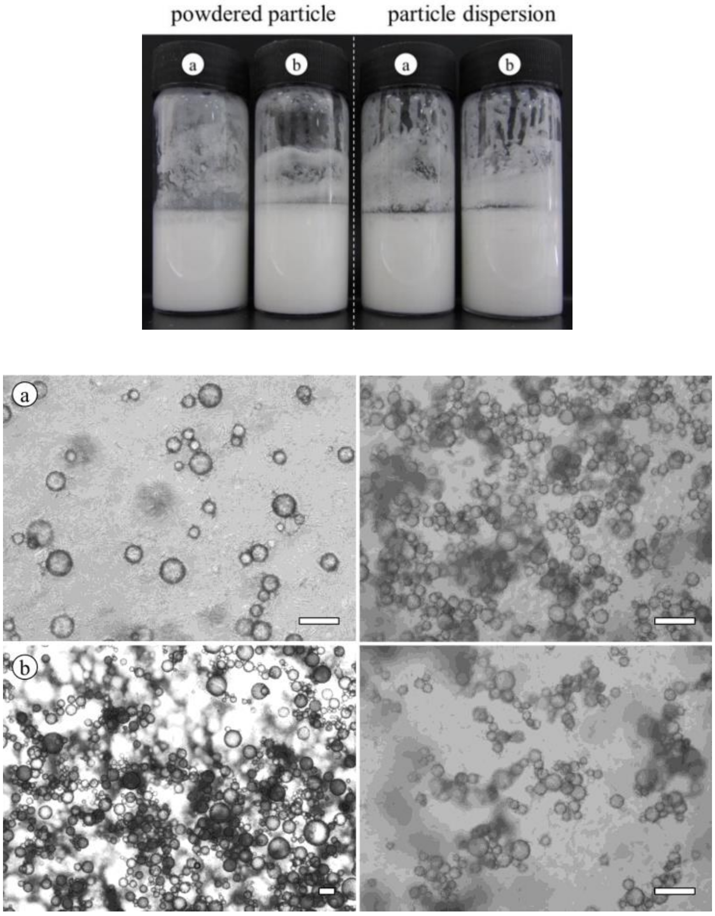

Figure 3.18. (upper) Photo (1 month after preparation) of (a) tricaprylin-in-water and (b) Miglyol 812N-in-water emulsions (ϕ_o = 0.5) prepared by the powdered particle method (left) and particle dispersion method (right). (lower) Optical micrographs (2 weeks after preparation) of the corresponding emulsions: (a) trycaprylin-in-water and (b) Miglyol 812N-in-water emulsions prepared by the powdered particle method (left) and particle dispersion method (right). The emulsions are stabilised by 4 wt. % of cube-shaped $CaCO_3$ particles and (c) is the cryo-SEM image of the Miglyol 812N-in-water emulsion (prepared by the powdered particle method). (d) Schematic illustration of the longitudinal dissection of a frozen partially exposed oil droplet showing the cube-shaped $CaCO_3$ particles on the droplet surfaces.

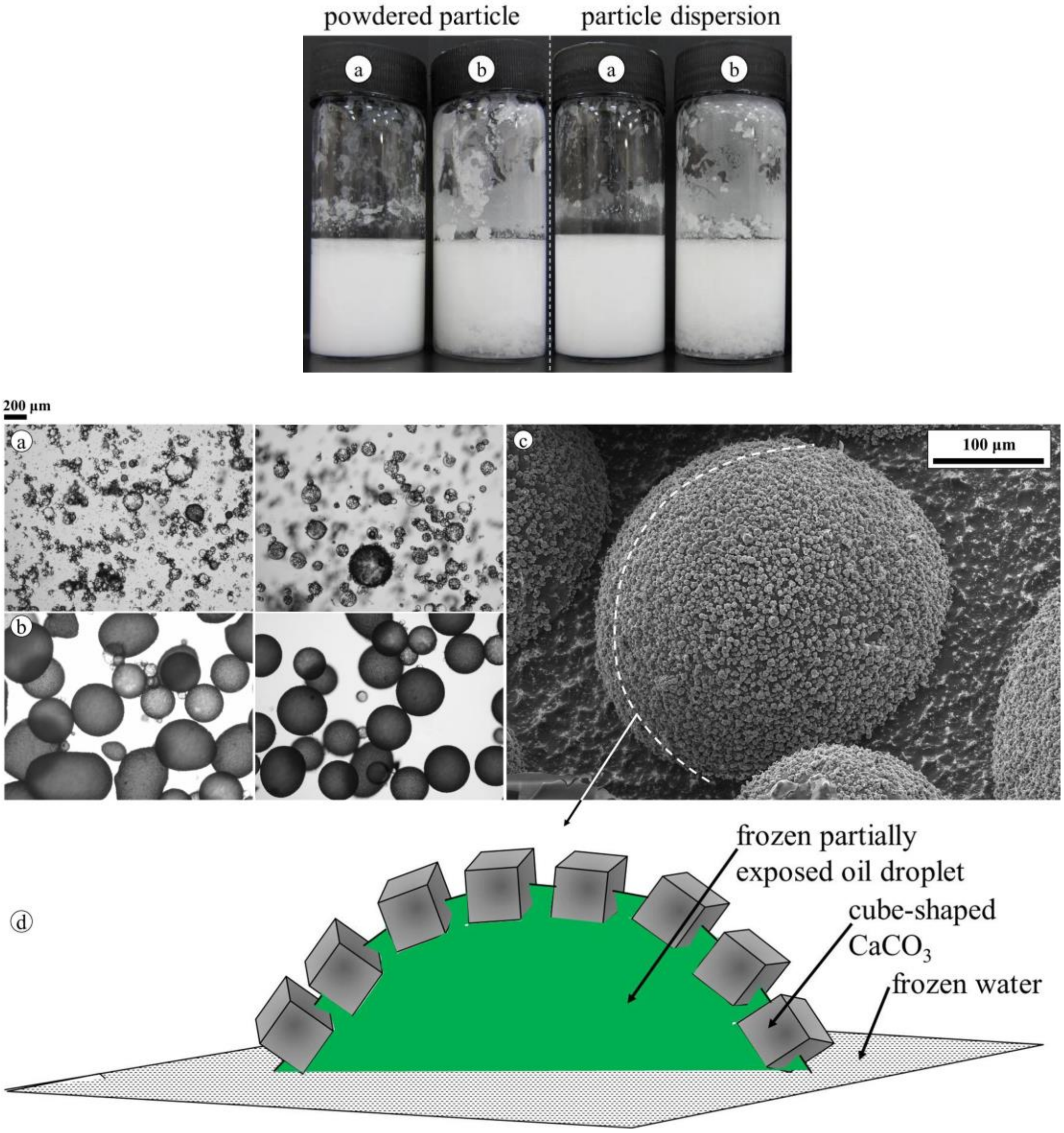

3.7 Effect of Salt on the Stability of the Emulsions

Photos of the rod- and cube-shaped $CaCO_3$ particle-stabilised emulsions (1 month after preparation) are shown in Figure 3.19 and their optical micrographs (viewed 2 weeks after preparation) are shown in Figures 3.20 and 3.21. The emulsions (ϕ_o = 0.5) were prepared by the powdered particle method using 4 wt. % of the particles. The particle concentration is relative to the total volume (14 cm^3) of oil and water in the emulsions. Generally, the rod-shaped particle-stabilised emulsions are white, polydisperse, flocculated and stable to creaming irrespective of [NaCl]. Those containing [NaCl] > 0.05 M were more susceptible to flocculation. The cube-shaped particle-stabilised emulsions were also white, polydisperse and flocculated, but unstable to creaming except the tricaprylin emulsions containing [NaCl] $\leq$ 2 mM in which creaming was not observed. Above 2 mM NaCl, emulsions of tricaprylin show signs of both creaming and sedimentation, which increases as [NaCl] increases. The creamed and sedimented emulsions droplets are separated by a layer of water. Miglyol 812N emulsions stabilised by the cube-shaped particles are less flocculated (except between 10–50 mM NaCl) compared with the other emulsions and the degree of creaming in them increases as [NaCl] increases. The droplets of these emulsions have different shapes and sizes, except those containing 10–50 mM of NaCl which have spherical droplets. Non-spherical emulsions droplets have been reported previously.[27-31] Non-spherical emulsions droplets may result from the fusion of two or more partially particle-coated droplets whose surfaces are fluid until the final droplet surfaces become fully coated with the particles which may jam. The jamming of the particles on the droplet surfaces prevents them from relaxation to a spherical geometry due to the high bending and Young's moduli of the droplet surfaces.[29,31] Non-spherical droplets can also result from the uneven dissipation of energy during homogenisation. Particles can also adsorb on the surfaces of such droplets making it impossible for them to relax to a spherical shape.[27] A plot of the average droplet diameter of the emulsions *versus* the [NaCl] is shown in Figure 3.22. The average droplet diameter of the Miglyol 812N emulsions stabilised by the cube-shaped $CaCO_3$ particles is not shown because of the non-spherical nature of the droplets. The average droplet diameter was obtained from at least 100 emulsion droplets (Figures 3.20 and 3.21). The droplet diameter of the tricaprylin-in-water emulsions (stabilised by rod-shaped $CaCO_3$) ranges from 14−126 μm (0−2 mM NaCl) and 30−153 μm (5−10 mM NaCl) with standard deviation of ≈ 12 μm. However, the droplet diameter of the Miglyol 812N-in-water emulsions (stabilised by rod-shaped $CaCO_3$) ranges from 20−311 μm (0−2 mM NaCl) and 23−179 μm (5−10 mM NaCl) with standard deviation of ≈ 30 μm. For the cube-shaped $CaCO_3$ particle-stabilised tricaprylin-in-water emulsions, the droplet diameter ranges from 9−183 μm (0−2 mM NaCl) and 12−315 μm (5−10 mM NaCl) with standard deviation of ≈ 30 μm. Generally, the average droplet diameter of the emulsions increases with an increase in [NaCl] such that for the Miglyol 812N emulsions stabilised by the cube-shaped particles, about 2.2 mm long emulsion droplet formed at the highest [NaCl] (*i.e.* 1000 mM, Figure 3.21(i)). Finally, the average droplet diameter of the cube-shaped $CaCO_3$ particle-stabilised tricapylin emulsions is smaller than the rod-shaped $CaCO_3$ particle-stabilised ones, but the reverse is true for the Miglyol 812N emulsions.

A plot of f_w (1 month after formation) and f_o (1 month after formation) *versus* [NaCl] of the emulsions is shown in Figures 3.23 and 3.24 respectively. Emulsions stabilised by the rod-shaped $CaCO_3$ particles are relatively stable to creaming, but the cube-shaped particle-stabilised ones creamed and the degree of creaming increases as [NaCl] increases as shown in Figure 3.23. Generally, the f_o released in the emulsions over time increases with increasing [NaCl] (Figure 3.24), consistent with previous findings for other particles.[19] In some emulsions, f_o reaches a maximum at [NaCl] = 100 mM, but decreases at concentrations above the same value and levels off at [NaCl] ≥ 500 mM. The general observation can be linked to the decrease in surface charge of the $CaCO_3$ particles with increasing [NaCl] as shown in Figure 3.1 (b). The decrease in surface charge allows emulsion droplets coated with the particles to approach each other closely and hence enhance van der Waals interaction, which drives coalescence. Finally, the rod-shaped $CaCO_3$ particle-stabilised emulsions released more oil than the cube-shaped $CaCO_3$ particle-stabilised emulsions. The cube-shaped $CaCO_3$ particle-stabilised emulsions released more water than the rod-shaped $CaCO_3$ particle-stabilised ones.

Figure 3.19. Photographs (1 month after preparation) of glass vials containing (a) tricaprylin-in-water and (b) Miglyol 812N-in-water emulsions (ϕ_o = 0.5) stabilised by rod-shaped $CaCO_3$ particles; (c) tricaprylin-in-water and (d) Miglyol 812N-in-water emulsions (ϕ_o = 0.5) stabilised by cube-shaped $CaCO_3$ particles. The emulsions were prepared by the powdered particle method using 4 wt. % of the particles at varying [NaCl] (given, mM). As can be seen, the cube-shaped $CaCO_3$ particle-stabilised emulsions are more sensitive to [NaCl] compared with the rod-shaped $CaCO_3$ particle-stabilised ones. The [NaCl] is with respect to the volume (7 cm^3) of the aqueous phase in the emulsions.

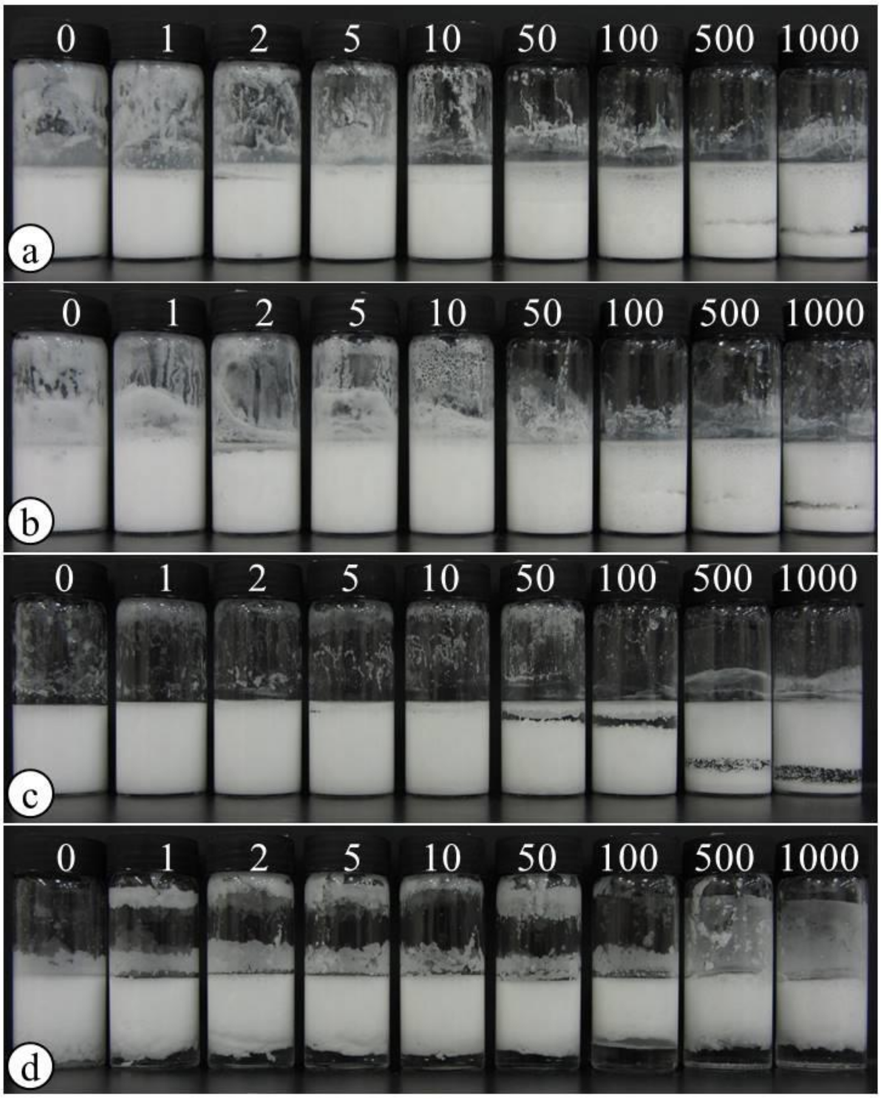

Figure 3.20. Optical micrographs (2 weeks after preparation) of tricaprylin-in-water (left) and Miglyol 812N-in-water (right) emulsions (Figure 3.19) stabilised by 4 wt. % of rod-shaped $CaCO_3$ particles in the presence of varying [NaCl]: (a) 0, (b) 1, (c) 2, (d) 5 and (e) 10 mM. Scale bar = 200 μm (except on (a) and (b) for tricaprylin emulsions). Droplets of emulsions containing [NaCl] > 10 mM are large enough to be seen by eye and their micrographs are not shown. All the emulsions (ϕ_o = 0.5) were prepared by the powdered particle method.

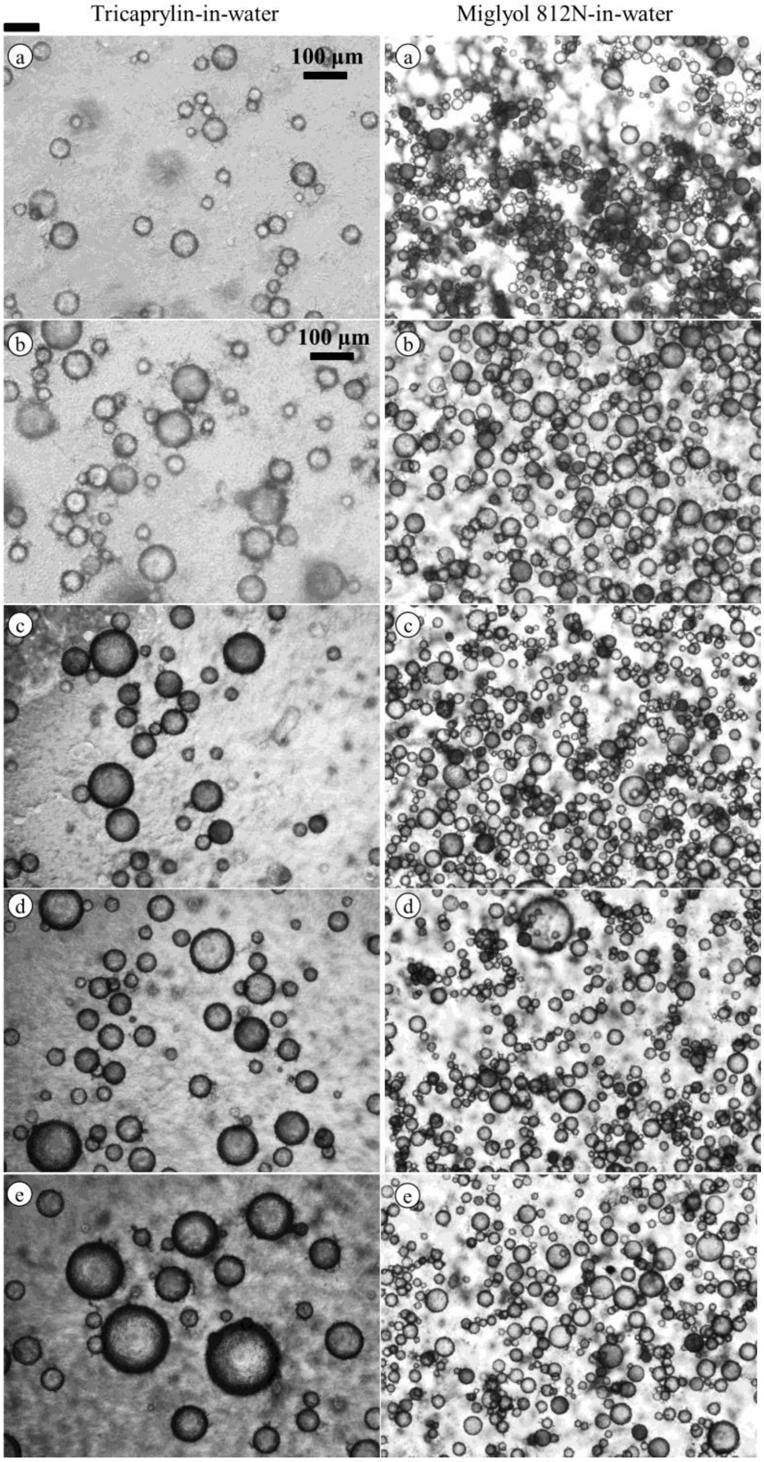

Figure 3.21. (2) Optical micrographs (2 weeks after preparation) of tricaprylin-in-water (above) and Miglyol 812N-in-water (below) emulsions (Figure 3.19) stabilised by 4 wt. % of cube-shaped $CaCO_3$ particles in the presence of varying [NaCl]: (a) 0, (b) 1, (c) 2, (d) 5, (e) 10, (f) 50, (g) 100, (h) 500 and (i) 1000 mM. Above 50 mM NaCl, the droplets of the cube-shaped $CaCO_3$ particle-stabilised tricaprylin-in-water emulsions are large enough to be seen by eye and hence their optical micrographs are not shown.

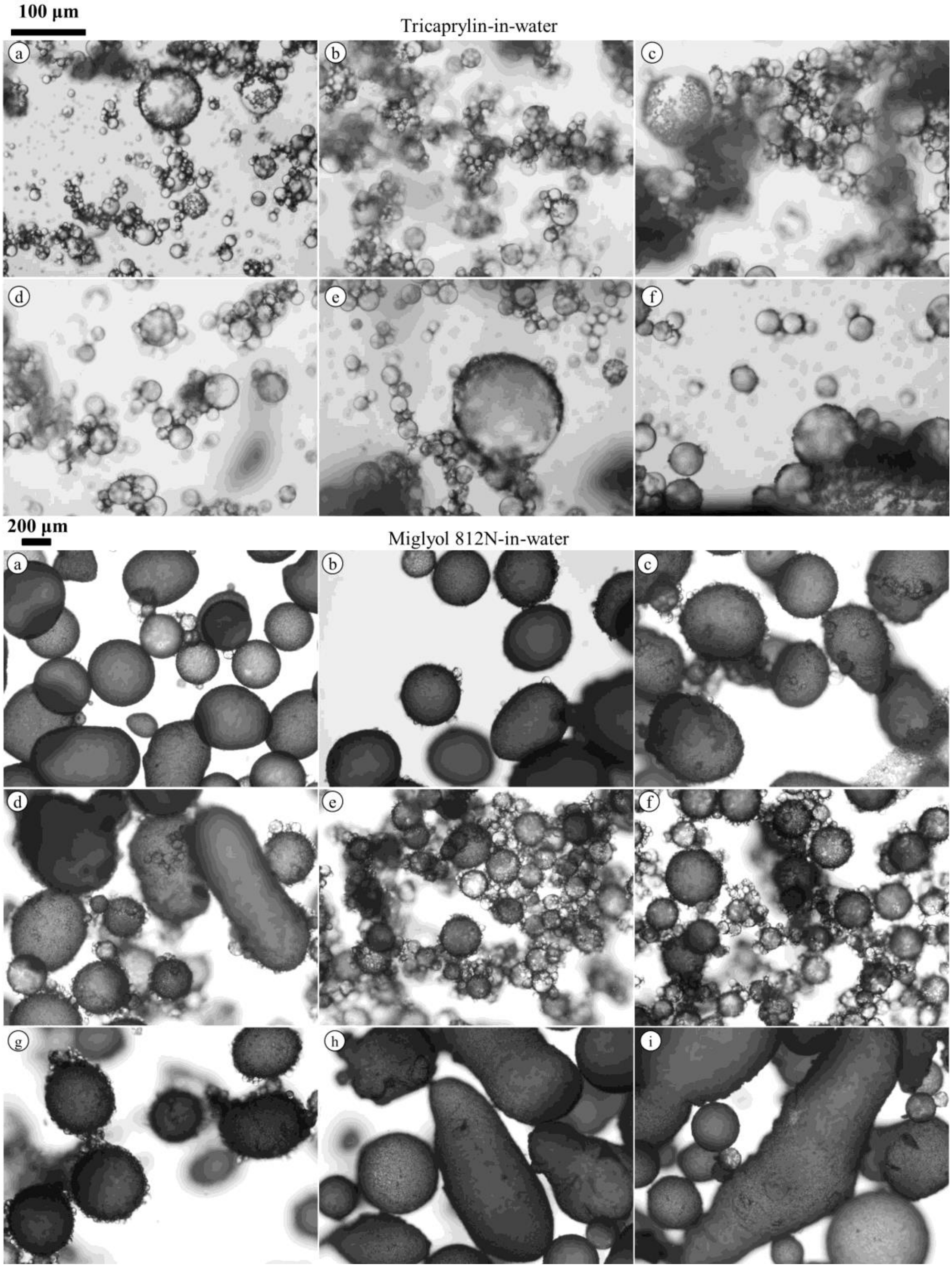

Figure 3.22. Plot of average droplet diameter of tricaprylin-in-water emulsions, stabilised by 4 wt.% of rod-shaped (▲) and cube-shaped (●) $CaCO_3$ particles and Miglyol 812N-in-water emulsions, stabilised by 4 wt. % of rod-shaped $CaCO_3$ particles (△), *versus* [NaCl]. The average droplet diameter of Miglyol 812N emulsions stabilised by the cube-shaped $CaCO_3$ particles is not shown due to the non-spherical nature of the droplets. The emulsions (ϕ_o = 0.5, Figure 3.19) were prepared by the powdered particle method. The [NaCl] is relative to the volume of the aqueous phase in the emulsions.

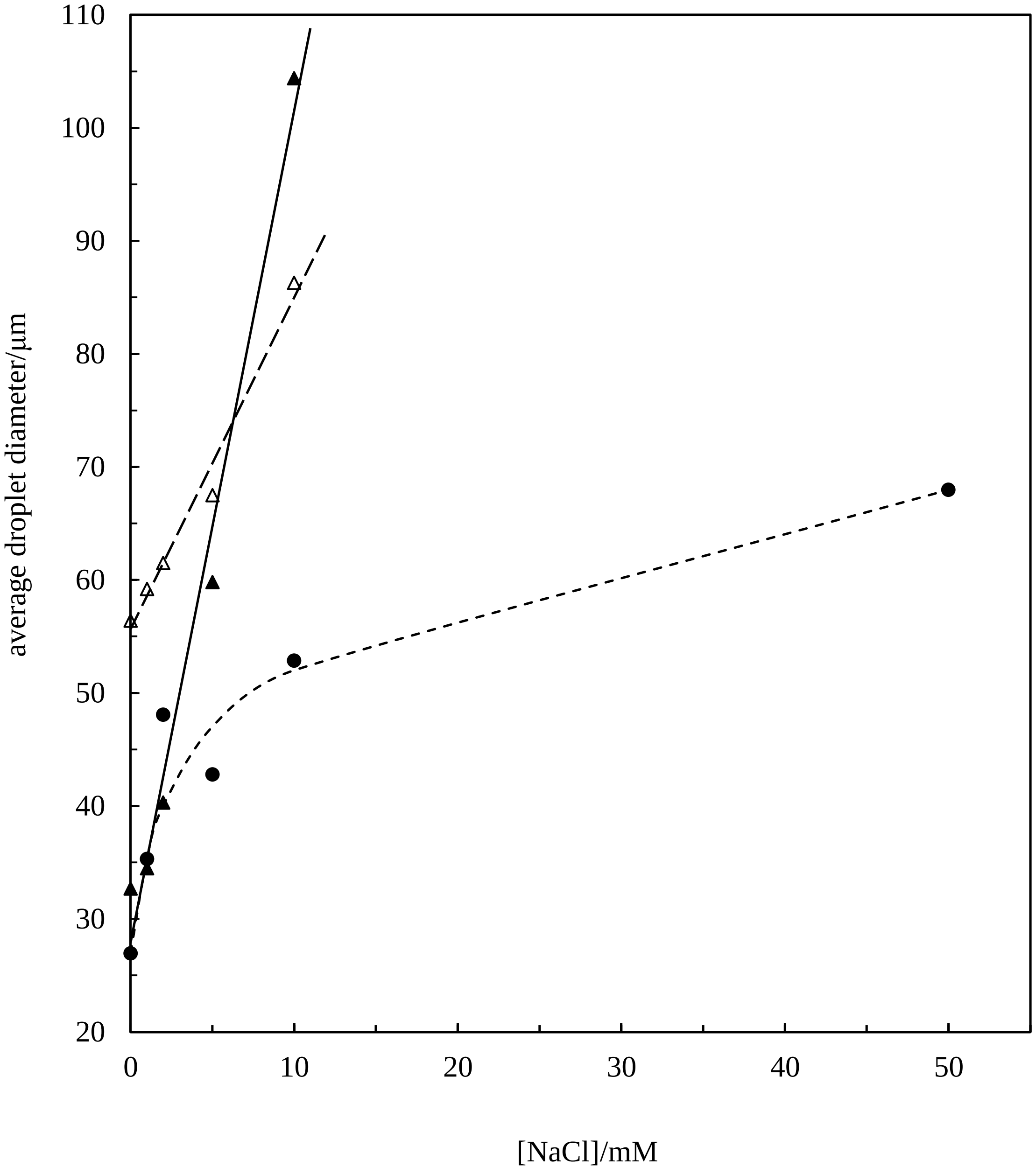

Figure 3.23. Fraction of water f_w (1 month after preparation) released in tricaprylin-in-water (●) and Miglyol 812N-in-water (○) emulsions (ϕ_o = 0.5) stabilised by 4 wt. % of cube-shaped $CaCO_3$ particles shown in Figure 3.19 *versus* [NaCl]. At 0 M NaCl, f_w is 0 (tricaprylin) and 0.064 (Miglyol 812N). Emulsions stabilised by the rod-shaped $CaCO_3$ particles are relatively stable to creaming and hence are not shown. The error bars are the propagation errors in the estimated values of f_w.

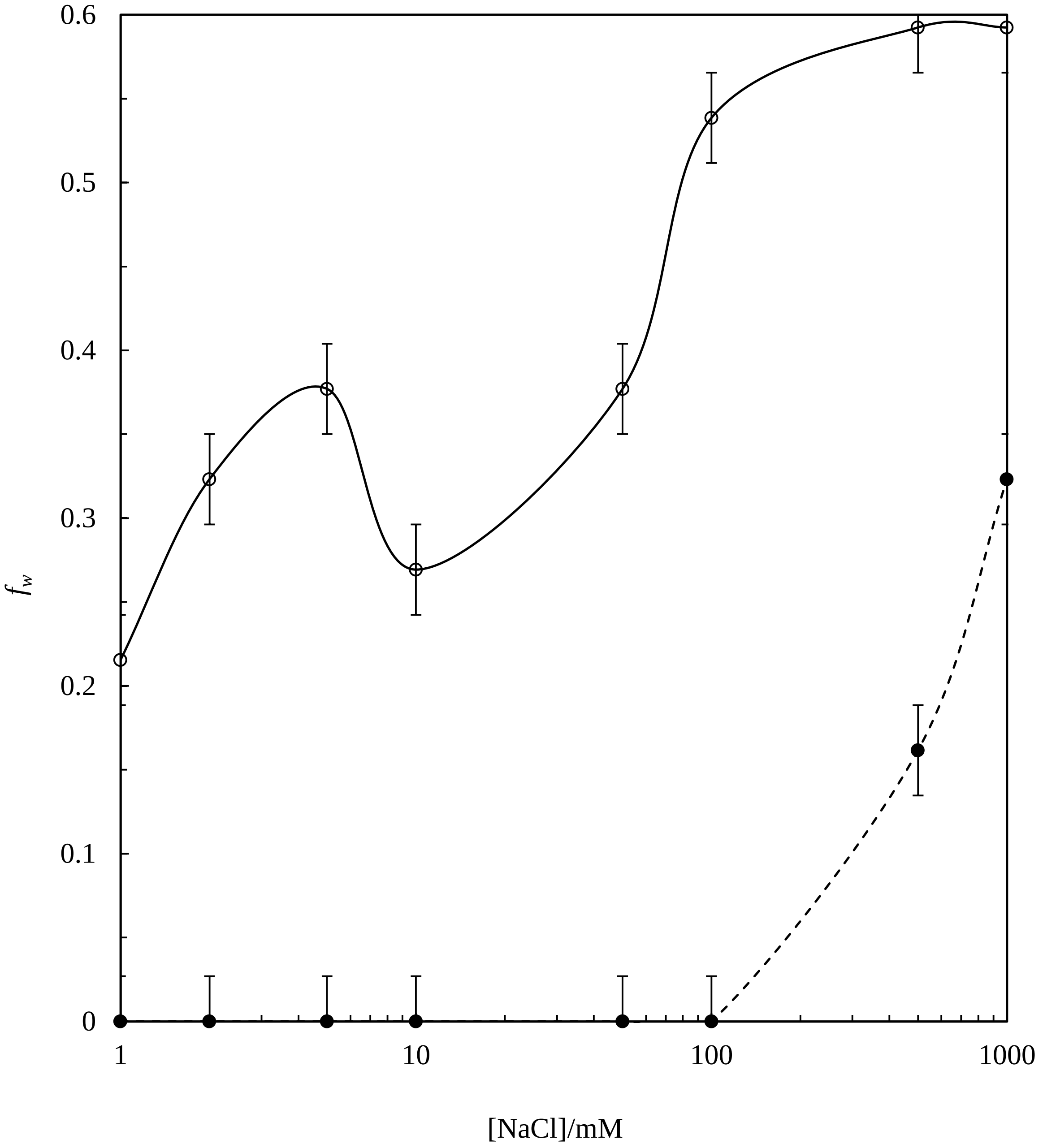

Figure 3.24. Fraction of oil f_o (1 month after preparation) released in the emulsions shown in Figure 3.19 *versus* [NaCl]. The data points are tricaprylin-in-water emulsions (●-stabilised by rod-shaped, ▲-stabilised by cube-shaped $CaCO_3$ particles) and Miglyol 812N-in-water emulsions (○-stabilised by rod-shaped, △-stabilised by cube-shaped $CaCO_3$ particles). At [NaCl] = 0 mM, f_o = 0.044 (rod-shaped $CaCO_3$) and 0.014 (cube-shaped $CaCO_3$) for the tricaprylin emulsions and 0.036 (rod-shaped $CaCO_3$) and 0.002 (cube-shaped $CaCO_3$), respectively, for the Miglyol 812N emulsions. The error bars are the propagation errors in the estimated values of f_o.

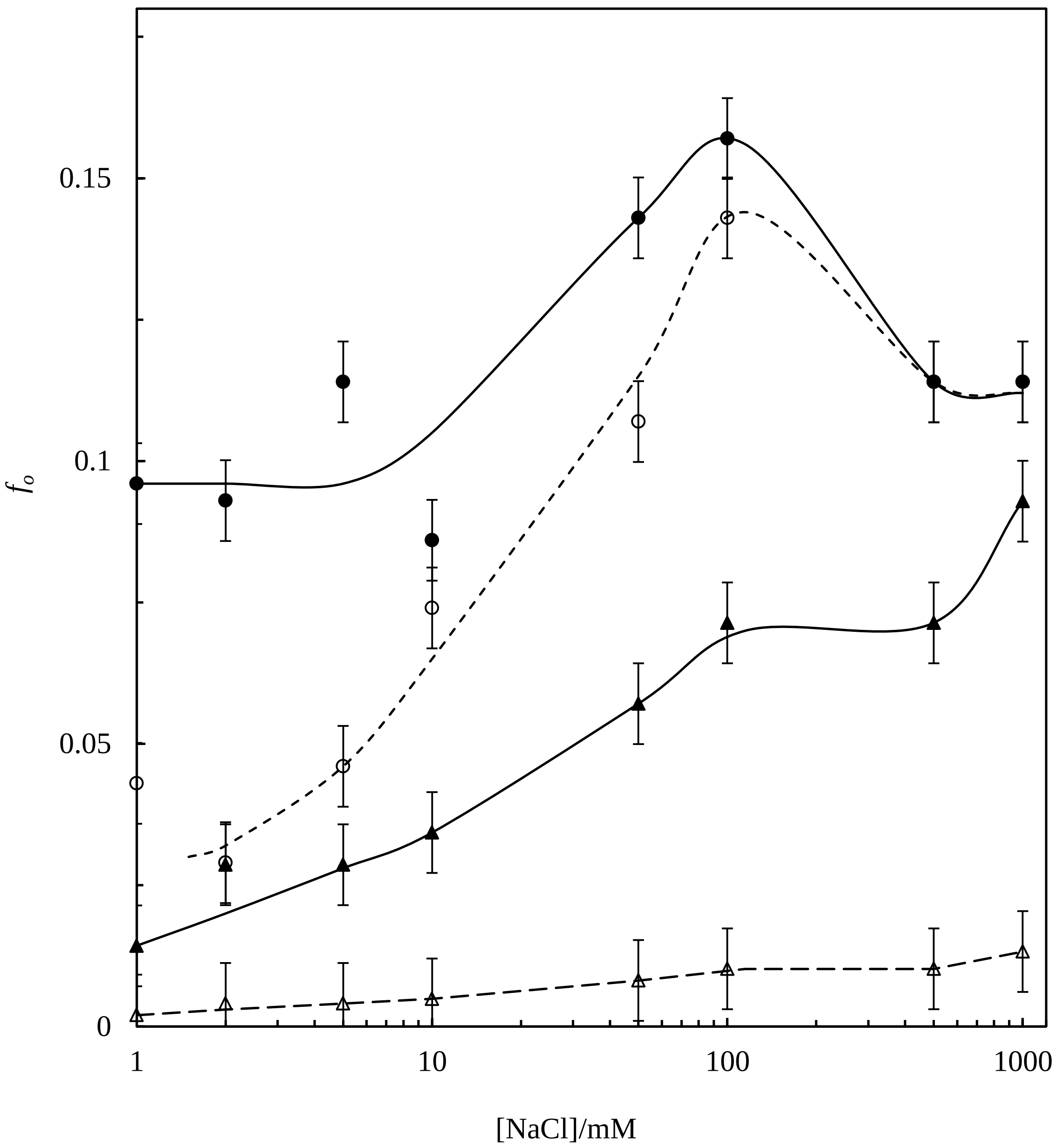

3.8 Effect of pH on the Stability of the Emulsions

The emulsions (ϕ_o = 0.5) were prepared with 4 wt. % of the $CaCO_3$ particles using the powdered particle method. Figure 3.25 shows photos of the emulsions and their optical micrographs are shown in Figure 3.26. The emulsions are also white, flocculated and polydisperse. Even though sizing was not possible in some cases, the average droplet diameter of the emulsions seems to decrease as pH increases as shown for Miglyol 812N-in-water emulsions stabilised by the cube-shaped $CaCO_3$ particles in Figure 3.27. A plot of f_w *versus* pH of the emulsions is given in Figure 3.28(a) and shows a general decrease in f_w as the pH increases. At pH 4 and 5, the emulsions are very unstable to both creaming and coalescence as the particles dissolve and desorb from the droplet surfaces into the aqueous phase after pH adjustment. As a result, a large volume of water and oil was resolved within 1 hour. Between the pH of 6 and 7, the emulsion droplets were large enough to be seen with the eyes, but no discernible phase separation was observed. A plot of f_o *versus* pH of the emulsions is given in Figure 3.28(b). At pH values higher than the natural (*i.e.* unadjusted) pH of the emulsions (≈ 8 or 9), the emulsions are stable to coalescence and very little oil is resolved after 1 month compared with other pH values. The f_o decreases with increasing pH reaching approximately zero at pH above 8, except in the cube-shaped $CaCO_3$ particle-stabilised emulsions where values of f_o are still around 0.07. The very stable rod-shaped $CaCO_3$ particle-stabilised emulsions (*i.e.* showing no sign of creaming, flocculation and even coalescence) are those at pH 12 and their average droplet diameter is 80 and 100 μm for tricaprylin and Miglyol 812N emulsions, respectively. No such stable emulsions were obtained with the cube-shaped $CaCO_3$ particles. This pH corresponds to that at which the particles are highly negatively charged (Figure 3.1(a)). The observation at pH 7 and below is consistent with the known behaviour of $CaCO_3$ particles. It has been reported that $CaCO_3$ particles dissolve in water at these pH values[32] losing their surface-active properties and hence the above observations.

Figure 3.25. Photographs of glass vials containing (a) tricaprylin-in-water and (b) Miglyol 812N-in-water emulsions $\phi_o = 0.5$ (1 month after formation) stabilised by 4 wt. % of (1) rod- and (2) cube-shaped $CaCO_3$ particles at varying pH (given). The emulsions were prepared by the powdered particle method. The natural emulsions (pH ≈ 8 and 9) are also shown. As can be seen, the cube-shaped $CaCO_3$ particle-stabilised emulsions are more sensitive to pH compared with the rod-shaped $CaCO_3$ particle-stabilised ones.

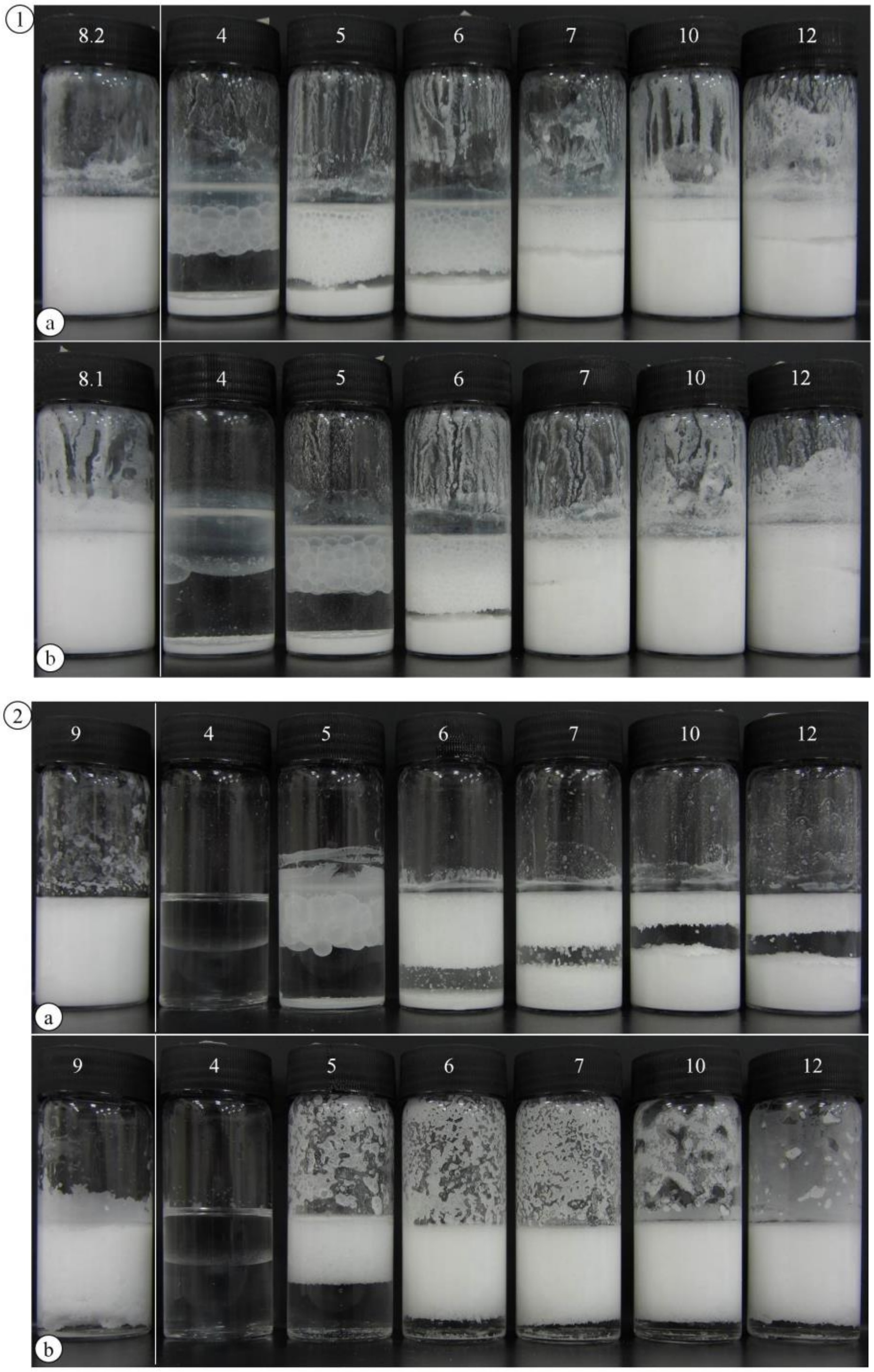

Figure 3.26. Optical micrographs (2 weeks after preparation) of (a) tricaprylin-in-water and (b) Miglyol 812N-in-water emulsions stabilised by 4 wt. % of (1) rod- and (2) cube-shaped $CaCO_3$ particles shown in Figure 3.25 at selected pH (given).

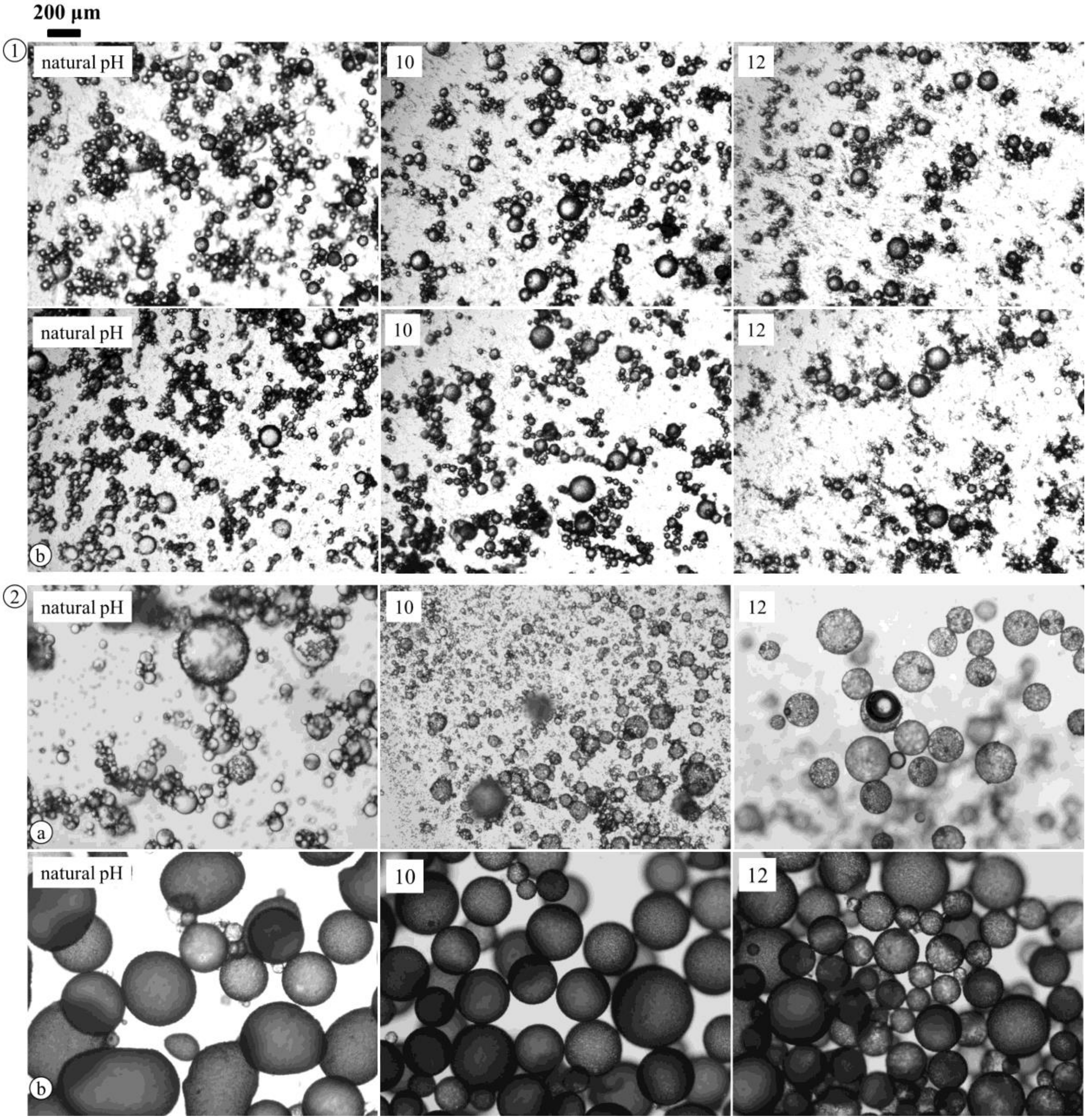

Figure 3.27. Plot of average droplet diameter of Miglyol 812N-in-water emulsions stabilised by 4 wt. % of cube-shaped $CaCO_3$ particles (shown in Figure 3.25) *versus* pH. The average droplet diameter was obtained from at least 100 emulsion droplets (Figure 3.26). The droplet diameter of the emulsions ranges from 82−1235 μm (pH 5−7) and 72−612 μm (pH 9−12) with standard deviation in the range of 80−244 μm and 80−129 μm respectively.

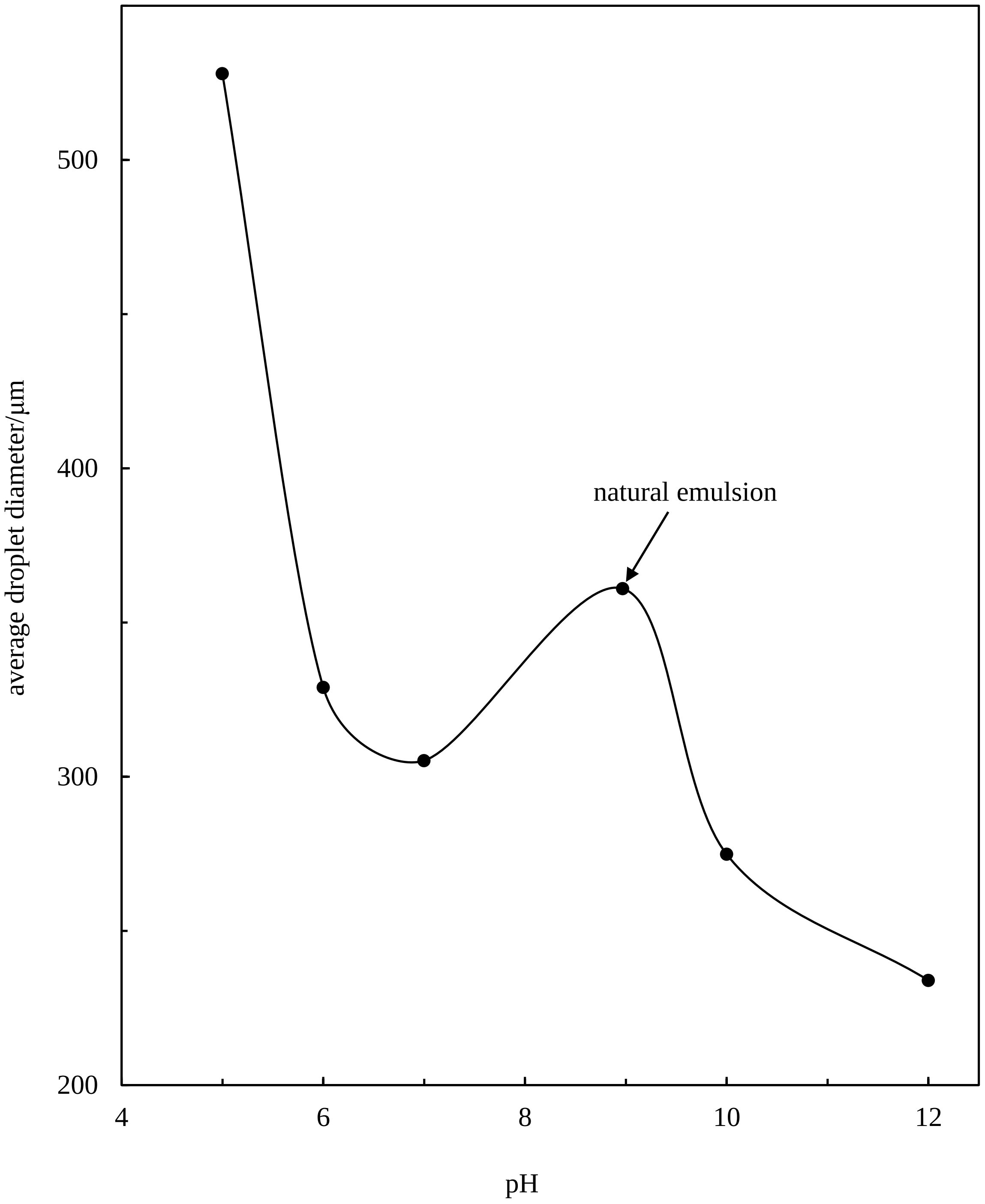

Figure 3.28. (a) Fraction of water f_w (1 month after preparation) *versus* pH of tricaprylin-in-water (●) and Miglyol 812N-in-water (○) emulsions (ϕ_o = 0.5) stabilised by 4 wt. % of cube-shaped $CaCO_3$ particles shown in Figure 3.25. Note that f_w of the rod-shaped $CaCO_3$ particle-stabilised emulsions is not shown due to the nature of the emulsions. (b) Fraction of oil f_o (1 month after preparation) *versus* pH of tricaprylin-in-water emulsions stabilised by 4 wt. % of rod-(▲) and cube-shaped (●) $CaCO_3$ particles and Miglyol 812N-in-water emulsions stabilised by the same concentration of the rod-(△) and cube-shaped (○) $CaCO_3$ particles shown in Figure 3.25. The error bars are the propagation errors in the estimated values of f_w and f_o.

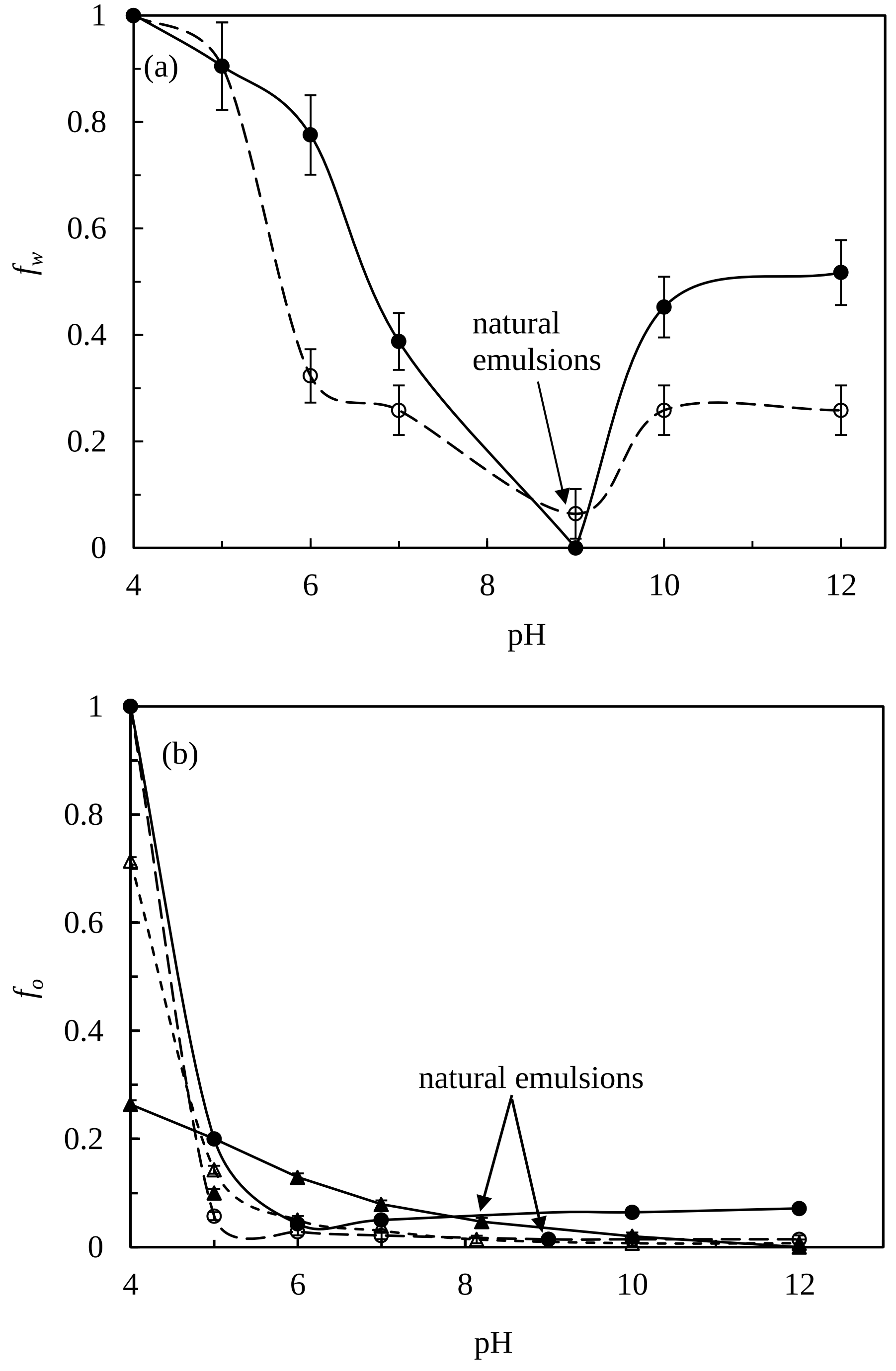

3.9 Conclusions

The following conclusions can be drawn about the rod- and cube-shaped $CaCO_3$ particle-stabilised edible o/w emulsions studied here. The emulsions are white, slightly basic (pH = 8−9) and flocculated. The creaming stability of the emulsions (ϕ_o = 0.5) increases with increasing particle concentration leading to relatively stable emulsions at relatively high particle concentrations (3−5 wt. %) as seen from the rod-shaped $CaCO_3$ particle-stabilised ones. Even though these emulsions were seen to release relatively small fraction of oil (< 0.1), they remained completely stable to creaming for over 3 years. The ϕ_o = 0.2 emulsions were unstable to both creaming and coalescence and those stabilised by 2−5 wt. % of the particles sedimented instead of creaming, as seen from the rod-shaped $CaCO_3$ particle-stabilised emulsions. Varying ϕ_o in the rod-shaped $CaCO_3$ particle-stabilised emulsions from 0.95 to 0.05, at constant (4 wt. %) particle concentration, led to the formation of 'oily liquids' when ϕ_o = 0.95−0.8, o/w emulsions which are completely stable to creaming (for over 3 years), but partially unstable to coalescence when ϕ_o = 0.7−0.5. Sedimented o/w emulsions where obtained when ϕ_o < 0.5. The relatively stable emulsions are sensitive to added electrolyte and pH change such that stability to creaming and coalescence is lost especially below their natural pH and relatively high electrolyte concentrations, irrespective of the $CaCO_3$ particle shape, as seen for the 4 wt. % particle-stabilised emulsions. However, relatively high pH (> 10) was seen to enhance the kinetic stability of the tricaprylin-in-water emulsions. Finally, in the absence of added electrolyte or pH change, the cube-shaped $CaCO_3$ particles form more stable emulsions than those stabilised by the rod-shaped $CaCO_3$ particles if the powdered particle method is used. However, if the particle dispersion method is used, the cube-shaped $CaCO_3$ particle-stabilised Miglyol 812N-in-water emulsion is more stable than the rod-shaped $CaCO_3$ particle-stabilised one, but the opposite is true for the tricaprylin-in-water emulsions. The reason for the difference in the stability of the rod- and cube-shaped $CaCO_3$ particle-stabilised emulsions is not clear, but might be due to the orientation of the particles (due to their shape) on the droplet surfaces or the size and nature of the particles themselves.

3.10 References

1. B.P. Binks and T.S. Horozov, eds., *Colloidal Particles at Liquid Interfaces*, Cambridge University Press, Cambridge, 2006.
2. L. Zhang, F. Zhang, Y.-S. Wang, Y.-L. Sun, W.-F. Dong, J.-F. Song, Q.-S. Huo and H.-B. Sun, *Soft Matter*, 2011, **7**, 7375−7381.
3. E. Tervoort, A.R. Studart, C. Denier and L. J. Gauckler, *RSC Adv.*, 2012, **2**, 8614−8618.
4. B.G. Mathapa and V.N. Paunov, *Phys. Chem. Chem. Phys.*, 2013, **15**, 17903−17914.
5. J.W.J. de Folter, E.M. Hutter, S.I.R. Castillo, K.E. Klop, A.P. Philipse and W.K. Kegel, *Langmuir*, 2014, **30**, 955−964.
6. B.P. Binks, W. Liu and J. A. Rodrigues, *Langmuir*, 2008, **24**, 4443−4446.
7. B.P. Binks and J.A. Rodrigues, *Langmuir*, 2007, **23**, 7436−7439.
8. B.P. Binks and S.O. Lumsdon, *Phys. Chem. Chem. Phys.*, 1999, **1**, 3007−3016.
9. W. Wu, R.F. Giese Jr and C.J. van Oss, *Colloids Surf. A*, 1994, **89**, 241−252.
10. B.P. Binks and C.P. Whitby, *Colloids Surf. A*, 2005, **253**, 105−115.
11. B.P. Binks and S.O. Lumsdon, *Langmuir*, 2000, **16**, 8622−8631.
12. Z. Xu and R.-H. Yoon, *J. Colloid Interface Sci.*, 1990, **134**, 427−434.
13. T.S. Horozov, B.P. Binks and T. Gottschalk-Gaudig, *Phys. Chem. Chem. Phys.*, 2007, **9**, 6398-6404.
14. G.L. Frear and J. Johnston, *J. Am. Chem. Soc.*, 1929, **51**, 2082−2093.
15. P. Somasundaran and G.E. Agar, *J. Colloid Interface Sci.*, 1967, **24**, 433−440.
16. Z.G. Cui, Y.Z. Cui, C.F. Cui, Z. Chen and B.P. Binks, *Langmuir*, 2010, **26**, 12567−12574.
17. Z.G. Cui, K.Z. Shi, Y.Z. Cui and B.P. Binks, *Colloids Surf. A*, 2008, **329**, 67−74.
18. S. Jailani, G.V. Franks and T.W. Healy, *J. Am. Ceram. Soc.*, 2008, **91**, 1141−1147.
19. B.P. Binks, R. Murakami, S.P. Armes and S. Fujii, *Langmuir*, 2006, **22**, 2050−2057.
20. Z.G. Cui, C.F. Cui, Y. Zhu and B.P. Binks, *Langmuir*, 2011, **28**, 314−320.
21. P. Finkle, H.D. Draper and J.H. Hildebrand, *J. Am. Chem. Soc.*, 1923, **45**, 2780−2788.
22. J.H. Schulman and J. Leja, *Trans. Farad. Soc.*, 1954, **50**, 598−605.
23. T.S. Horozov and B.P. Binks, *Angew. Chem. Int. Ed.*, 2006, **45**, 773−776.
24. F. Bresme and M. Oettel, *J. Phys. Condens. Matter*, 2007, **19**, 413101.
25. R. Aveyard, B.P. Binks and J.H. Clint, *Adv. Colloid Interface Sci.*, 2003, **100–102**, 503−546.
26. B.P. Binks, *Curr. Opin. Colloid Interface Sci.*, 2002, **7**, 21−41.
27. J.-W. Kim, D. Lee, H.C. Shum and D.A. Weitz, *Adv. Mater.*, 2008, **20**, 3239−3243.
28. S.A.F. Bon, S.D. Mookhoek, P.J. Colver, H.R. Fischer and S. van der Zwaag, *Eur. Polym. J.*, 2007, **43**, 4839−4842.
29. P.S. Clegg, E.M. Herzig, A.B. Schofield, T.S. Horozov, B.P. Binks, M.E. Cates and W. C.K. Poon, *J. Phys.: Condens. Matter*, 2005, **17**, S3433.
30. P.S. Clegg, E.M. Herzig, A.B. Schofield, S.U. Egelhaaf, T.S. Horozov, B.P. Binks, M.E. Cates and W.C.K. Poon, *Langmuir*, 2007, **23**, 5984−5994.
31. A.B. Subramaniam, M. Abkarian, L. Mahadevan and H.A. Stone, *Nature*, 2005, **438**, 930.
32. D.W. Thompson and P.G. Pownall, *J. Colloid Interface Sci.*, 1989, **131**, 74−82.

Chapter 4

Oil-Oil Pickering Emulsions

4.1 Introduction

Colloidal particles of suitable wettability, *i.e.* not completely wetted by the phases of a liquid-liquid interface, are surface-active and adsorb at the interface to stabilise emulsions when energy is applied.[1] Conceptually, simple emulsions are mixtures of two immiscible liquids phases (*e.g.* oil and water) in which one of the liquid phases is dispersed as microscopic droplets in the bulk of the other liquid phase in the presence of a stabiliser which could be a surfactant, polymer molecules or nanoparticles.[2,3] Particle-stabilised simple emulsions (Pickering emulsions) like o/w and w/o emulsions have attracted attention recently, largely due to their long term kinetic stability and have been studied extensively.[1,4-13] The excellent kinetic stability has been attributed to the large magnitude of particle adsorption free energy[1,14] and the high capillary pressure needed to coalesce two particle-coated droplets.[15] For spherical particles in oil-water systems (1:1), studies have shown that particle-stabilised o/w (w/o) are formed if the particles are preferentially wetted more by water than the oil phase (wetted more by oil than the water phase) leading to θ_{ow} of < 90° (> 90°).[16] As can be seen, the particles generally cause the more wetting liquid phase to form the continuous phase and the less wetting liquid phase to form the dispersed phase. A plausible explanation for this is that coalescence is better suppressed if the particles protrude far outside the droplets than if they protruded only slightly. Measurement of θ_{ow} non-spherical particles make with an oil-water interface is rather difficult, but the degree to which the oil and water phases wet them is also crucial to the type of emulsions they stabilise. For example, rod-shaped hydrophilic $CaCO_3$ particles have been shown to stabilise toluene/octane-in-water emulsions and water-in-toluene/octane emulsions when they were hydrophobised, *in-situ,* with moderate amount of sodium dodecyl sulphate.[17]

Another example of simple emulsions is o/o emulsions (*i.e.* non-aqueous emulsions), comprising of two immiscible oils *e.g.* certain vegetable oils and silicone oils[18] or certain non-aqueous solvents and vegetable oils,[19] in which microscopic droplets of one oil are dispersed in the bulk of the other oil in the presence of an emulsifier. Whilst aqueous emulsions have been well studied, only few studies on non-aqueous emulsions exist in the literature (see Table 4.1). These emulsions are important in many industries due to their unique and useful properties. For example, o/o emulsions can replace regular aqueous emulsions in applications where the presence of water is undesirable *e.g.* in the lubrication of metal parts, in cleaning systems that are sensitive to the formation of rust like engines and other mechanical systems or for performing sol-gel processes with hydrolysable metal alkoxides in organic media in a controlled way.[20-25] In the pharmaceutical industry and medicine, o/o emulsions can form the basis of transdermal formulations and can be used to encapsulate hydrolytically unstable drugs.[23-26] o/o emulsions can also be used in cosmetic formulations.[23-26] Polymerisable non-aqueous emulsions can act as nanoreactor systems for the polymerisation of water sensitive monomers or catalysts. Similar to aqueous emulsions, surfactants, polymers or colloidal particles have been used to stabilise non-aqueous emulsions for a range of applications as shown in Table 4.1. As can be seen, unlike in aqueous emulsions in which low molecular weight surfactants, relatively hydrophilic solid particles and certain polymers are required to obtain stable emulsions, hydrophobic colloidal particles, exotic surfactants and copolymers are needed to obtain stable non-aqueous emulsions. These stabilisers are expensive and difficult to come by and designing their substitute is a herculean task. Recently, stabilisation of non-aqueous emulsions using DCDMS-coated amorphous hydrophobic fumed silica particles or organo-modified laponite clay nanoparticles was described.[27] Crosslinked poly(*N*-isopropylacrylamide-*co*-2-acrylamido-2-methylpropane sulphonic acid) microgels[28] functionalised with a non-ionic polymerisable surfactant (polyoxyethylene-4-nonyl-2-propyl-phenyl maleate ester) have also been used in the stabilisation of non-aqueous emulsions. In the former, the outer and inner phases of the emulsions were non-aqueous solvents like glycerine, formamide, dimethyl sulfoxide, dimethyl formamide, clycohexane or vegetable oils like corn, olive, clove and castor oils.[27] However, in the latter, the emulsions were paraffin oil-in-formamide of excellent stability against creaming and coalescence for over 6 months if they contain above 5 wt. % of the microgel otherwise they creamed. Non-aqueous simple emulsions comprising of an alcohol and an alkane[29-31] or other non-aqueous solvents like nitromethane and ethylene glycol[32] have also been prepared. The emulsions were stabilised with partially hydrophobic silica particles. Based on the partial miscibility of ethylene carbonate (EC) and *p*-xylene, EC-in-xylene Pickering high internal phase emulsions (HIPE) have also been prepared using chemically modified fumed silica particles. The *p*-xylene was then evaporated off to obtain a semi-solid composite containing mainly the EC liquid phase and the silica particles.[33]

Table 4.1. Summary of some previous work on oil-in-oil emulsions.

Disperse phase	Continuous phase	Emulsifier	Application	Ref.
Silicone oil (polydimethylsiloxane PDMS, polymethylphenylsiloxane)	Mineral oil	Hydrophobic bentonite clay particles, di-C_1di-$C_{18}N^+$ (plates 0.002 × 0.08 × 0.8 μm)	Lubricants on natural and synthetic fibers	34
Silicone oil, > 300 cS (polydialkylsiloxane)	Mineral oil	Ethylene-vinyl acetate copolymer (low VA)	Foam inhibitor for lubricating oils	35
Silicone oil, 2500 cS (PDMS)	Chlorinated paraffin oil, 340 cS	None	Electro-rheological fluid	36
Chlorinated paraffin oil, 340 cS	Silicone oil, 2500 cS (PDMS)	None		
Silicone oil, 1000 cS (PDMS)	Thermotropic liquid crystal (mix of cyanobiphenyl and cyanoterphenyl)	Cyanobiphenyl-terminated PDMS oligomer	Electro-optical display devices	37
Thermotropic liquid crystal	Silicone oil, 1000 cS (PDMS)	Cyanobiphenyl-terminated PDMS polymer		
Mineral oil or soybean oil or olive oil or castor oil or palm kernel oil	Silicone oil, < 1000 cS (linear and cyclic-polysiloxanes)	Cross-linked elastomeric silicone polyether	Personal care and cosmetics	18
Silicone oil (PDMS)	Perfluoropolymethyl-isopropyl ether	Fluorinated silicone resin particles (spherical, diameter 4.5 μm)	Cosmetics	38
Silicone oil (PDMS)	Perfluoropolymethyl-isopropyl ether	Fluorinated calcium lauroyl taurate particles (plates 8 μm diameter)	Cosmetics	39

Table 4.1 (continued).

Disperse phase	Continuous phase	Emulsifier	Application	Ref.
Mineral oil or animal or vegetable oils or silicone oil	Silicone oil (PDMS)	Silicone block copolymer, *e.g.* *p*(butylacrylate)-PDMS-*p*(butylacrylate)	Personal care	40
Poly(tetrahydrofuran ester) or polyalkylene glycols	Poly(α-olefin) or mineral oil	None	Lubricants	41
Castor oil	Silicone oil, < 100 cS	Nonionic surfactants (octyl/nonylphenol polyoxyethylene ether)	Pharmaceutical formulations	23
Hydrocarbon	Fluorocarbon	Nonionic fluorocarbon surfactant	Vehicles for chemical reactions	42
Organic phosphate (di/trialkyl phosphate, tricresylphosphate) or silicone	Paraffin oil or white mineral oil or cyclic silicone	Hydrophobic fumed silica particles (spherical of diameter 20−40 nm) plus polymer co-stabiliser	Electro-optical modulating display devices, lubricating films for mechanical devices	43
Castor oil	Silicone oil, 20 cS (PDMS)	Silicone surfactant (PEG-PPG18-18) dimethicone)	Pharmaceutical formulations	44
Silicone oil, 20 cS (PDMS)	Castor oil	Silicone surfactant (silicone-EO-PO)		
Hydrogenated triglyceride oil (soybean, rapeseed, palm, castor)	Silicone oil, < 500 cS (PDMS)	Silicone surfactant	Lubricant on fibers	45
Organic phosphate	Hydrocarbon	Diblock or triblock copolymer	Liquid toning systems	46

Certain polymers are also immiscible with each other (*i.e.* the so called immiscible polymer blends), but become miscible/blends in the presence of certain hydrophilic or hydrophobic colloidal particles. For example, Poly(isobutylene)(30%)-in-poly(dimethylsiloxane) (70%) blends which are completely stable to coalescence have been prepared in the presence of hydrophobic fumed silica particles (1 wt. % based on volume of the total blend).[47,48] Stable polypropylene(70%)/polystyrene(30%) blends have also been prepared in the presence of hydrophilic or hydrophobic silica particles.[49] Hydrophilic pyrogenic and hydrophobic silica particles were also used to prepare stable polypropylene/poly(ethylene-*co*-vinyl acetate) blends.[50]

The aim of this work is explore the possibility of using a range of solid particles as sole stabilisers of o/o and o/o/o emulsions against creaming or sedimentation and coalescence. The oils will be vegetable and PDMS oils rather than non-aqueous solvents and oils reported by some authors. If the possibility is borne out, the conditions (*e.g.* the three-phase contact angle) favouring the formation of one emulsion type over the other would be investigated.

4.2 Oil-in-Oil Emulsions Containing Equal Volume Fraction of Oils Stabilised by Fumed Silica Particles

4.2.1 Emulsions from Vegetable Oil-PDMS Oil Systems Containing Particles Initially in the PDMS Oil Phase

The powdered particle method was used to prepare these emulsions. However, because the fumed silica particles were spontaneously wetted by the PDMS oils once on their surfaces, they are generally considered as being initially in the PDMS oil phase.

4.2.1.1 Oil-in-Oil Emulsions Stabilised by 75% SiOH Fluorinated Fumed Silica Particles

The emulsions contain equal volumes (5 cm^3) of the oils and were prepared by the powdered particle method as described in chapter 2. They were white, polydisperse, unflocculated and either vegetable oil or PDMS oil continuous. The homogenisation of a vegetable oil and PDMS 20 cS in the presence of the fumed silica particles gave PDMS 20 cS continuous emulsions, whilst that of a vegetable oil and PDMS 50 or 100 cS gave vegetable oil continuous emulsions as inferred from the drop test. The unstable PDMS oil continuous emulsions creamed, whilst the unstable vegetable oil continuous ones underwent sedimentation as expected. Photographs of these emulsions and some of their optical micrographs are shown in

Figures 4.1−4.3. The average droplet diameter of the vegetable oil continuous emulsions is plotted as a function of particle concentration in Figure 4.4. The stability of the emulsions to creaming or sedimentation and coalescence is described (in terms of f_{vo} or $f_{\mathrm{PDMS\ oil}}$) in Figures 4.5−4.7 in relation to the particle concentrations. The particle concentrations are with respect to the total volume (10 cm^3) of PDMS oil and vegetable oil in the emulsions. The vegetable oil-in-PDMS 20 cS emulsions are composed of relatively small droplets compared with the PDMS 50 cS- and 100 cS-in-vegetable oil emulsions which are composed of even millimetre-size droplets at relatively low (0.1–0.25 wt. %) particle concentrations. Just like in particle-stabilised aqueous emulsions,[51,52] the size of the PDMS 50 cS-and 100 cS-in-vegetable oil emulsion droplets decreases as the particle concentration increases and became constant at relatively high particle concentrations (Figure 4.4). The control vegetable oil-PDMS oil systems without particles were unstable to both creaming or sedimentation and coalescence and separated completely into their component phases within an hour after homogenisation. The stability of the emulsions to creaming or sedimentation and coalescence increased with increasing particle concentration (as expected) leading eventually to stable emulsions at relatively high particle concentrations (1.5−2 wt. %). At these particle concentrations, the emulsions remained completely stable to sedimentation and coalescence for over a month. However, stable vegetable oil-in-PDMS 20 cS emulsions were not obtained at all particle concentrations. Even at the highest particle concentration (2 wt. %), the emulsions were partially stable to creaming and coalescence. Clearly, large amount of particles is required for the stabilisation of these emulsions compared with oil-water emulsions where even 1 wt. % of particles can stabilise the emulsions against creaming or sedimentation and coalescence.[53]

Figure 4.1. (upper) Photographs of glass vials containing (a) sunflower oil-, (b) olive oil-, (c) rapeseed oil-in-PDMS 20 cS emulsions (1 month after preparation) stabilised by different concentrations (given, wt. %) of 75% SiOH fluorinated fumed silica particles. The emulsions contain equal volumes (5 cm^3) of vegetable oil and PDMS 20 cS. (lower) Corresponding optical micrographs (1 month after preparation) of the emulsions at selected particle concentrations (given, wt. %). Scale bar = 100 μm.

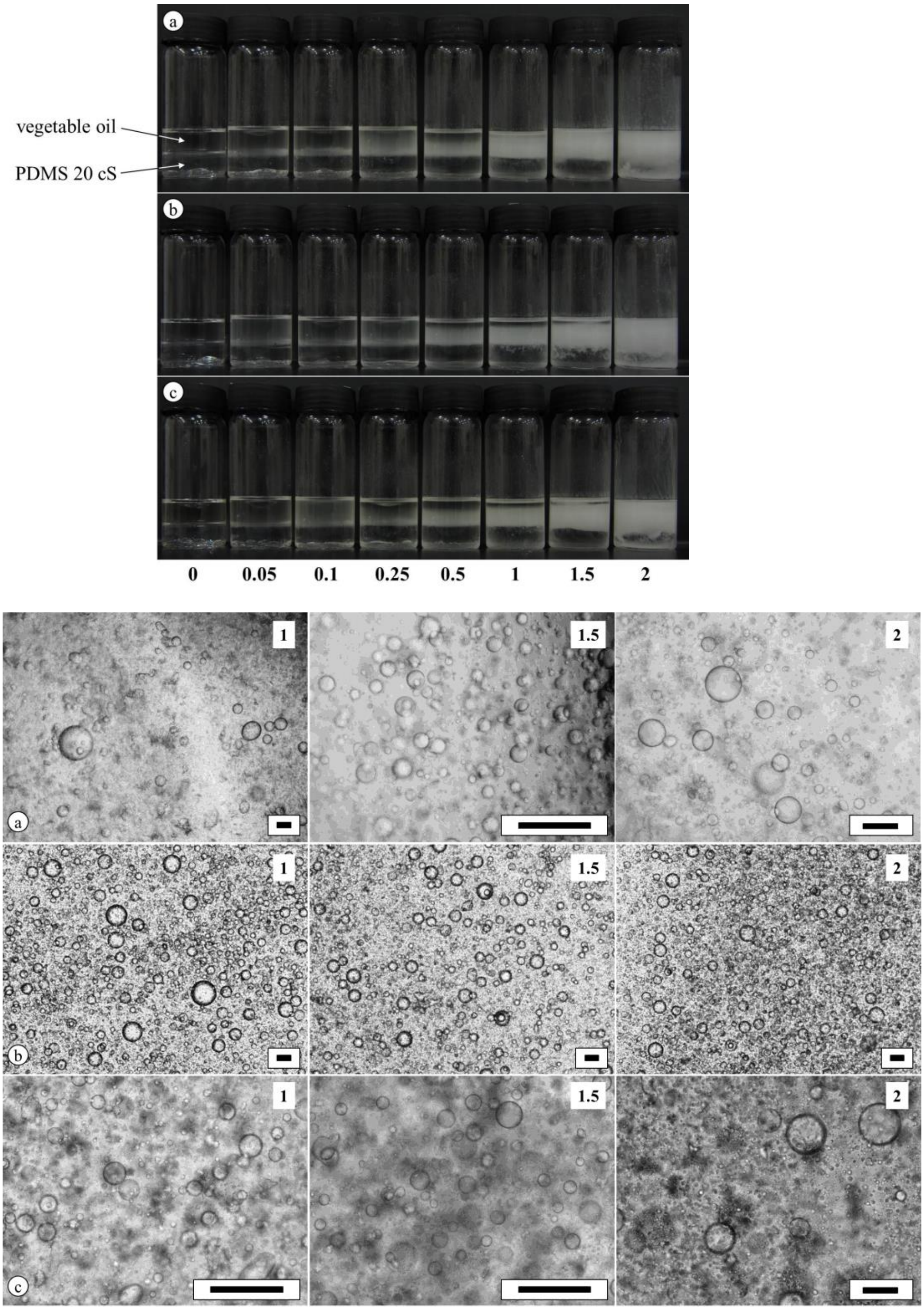

Figure 4.2. (upper) Photographs of glass vials containing PDMS 50 cS-in-(a) sunflower oil, (b) olive oil and (c) rapeseed oil emulsions (1 month after preparation) stabilised by different concentrations (given, wt. %) of 75% SiOH fluorinated fumed silica particles. The emulsions contain equal volumes (5 cm^3) of vegetable oil and PDMS 50 cS. (lower) Corresponding optical micrographs (1 month after preparation) of the emulsions at selected particle concentrations (given, wt. %). Scale bar = 100 μm.

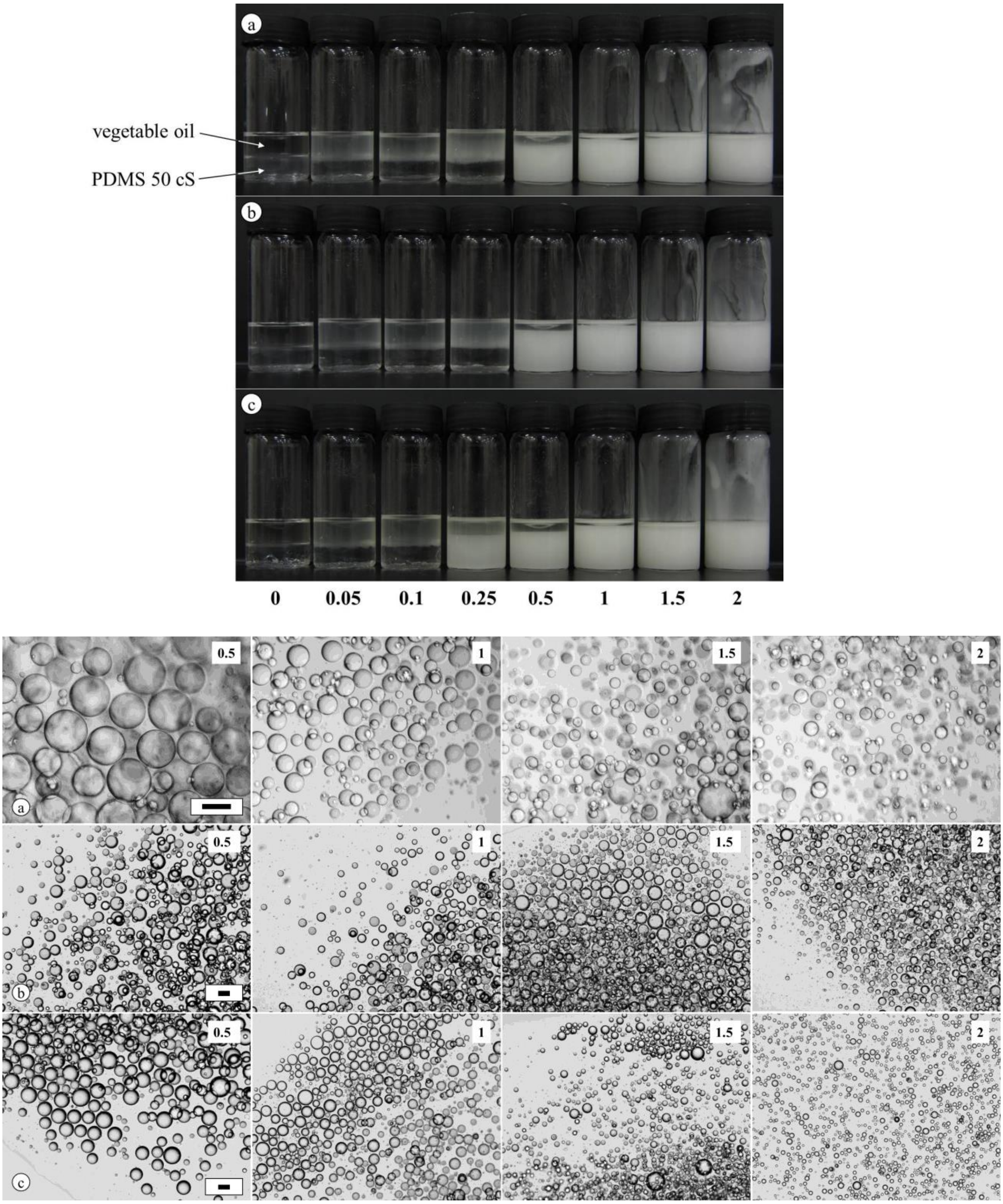

Figure 4.3. (upper) Photographs of glass vials containing PDMS 100 cS-in-(a) sunflower oil, (b) olive oil and (c) rapeseed oil emulsions (1 month after preparation) stabilised by different concentrations (given, wt. %) of 75% SiOH fluorinated fumed silica particles. The emulsions contain equal volumes (5 cm^3) of vegetable oil and PDMS 100 cS. (lower) Corresponding optical micrographs (1 month after preparation) of the emulsions at selected particle concentrations (given, wt. %). Scale bar = 100 μm.

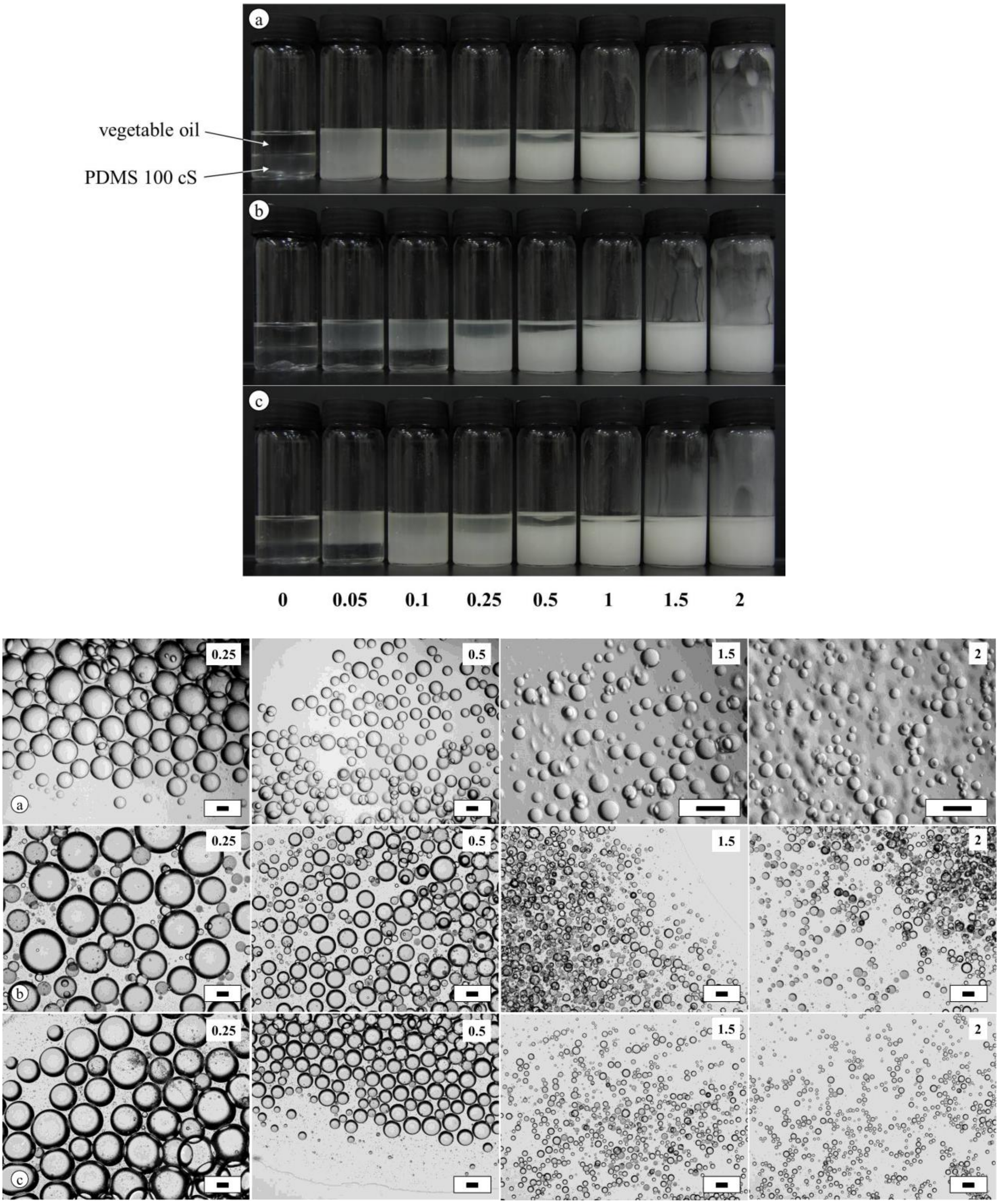

Figure 4.4. Average droplet diameter of 300 droplets of (a) PDMS 50 cS-in-sunflower oil (●), PDMS 50 cS-in-olive oil (▲) and PDMS 50 cS-in-rapeseed oil (◆) emulsions shown in Figure 4.2 and (b) PDMS 100 cS-in-sunflower oil (○), PDMS 100 cS-in-olive oil (△) and PDMS 100 cS-in-rapeseed oil (◇) emulsions shown in Figure 4.3 *versus* [75% SiOH fluorinated fumed silica]. The average droplet diameter of the emulsions was measured (1 month after preparation of the emulsions) from the optical micrographs (Figures 4.2 and 4.3) of the emulsions. The standard deviation of the measurements decreases from ≈ 40 μm (0.25 wt. % of particles) to ≈ 12 μm (2 wt. % of particles). The average droplet diameter of the vegetable oil-in-PDMS 20 cS emulsions is not shown because majority of the emulsions separated into their component phases before optical microscopy.

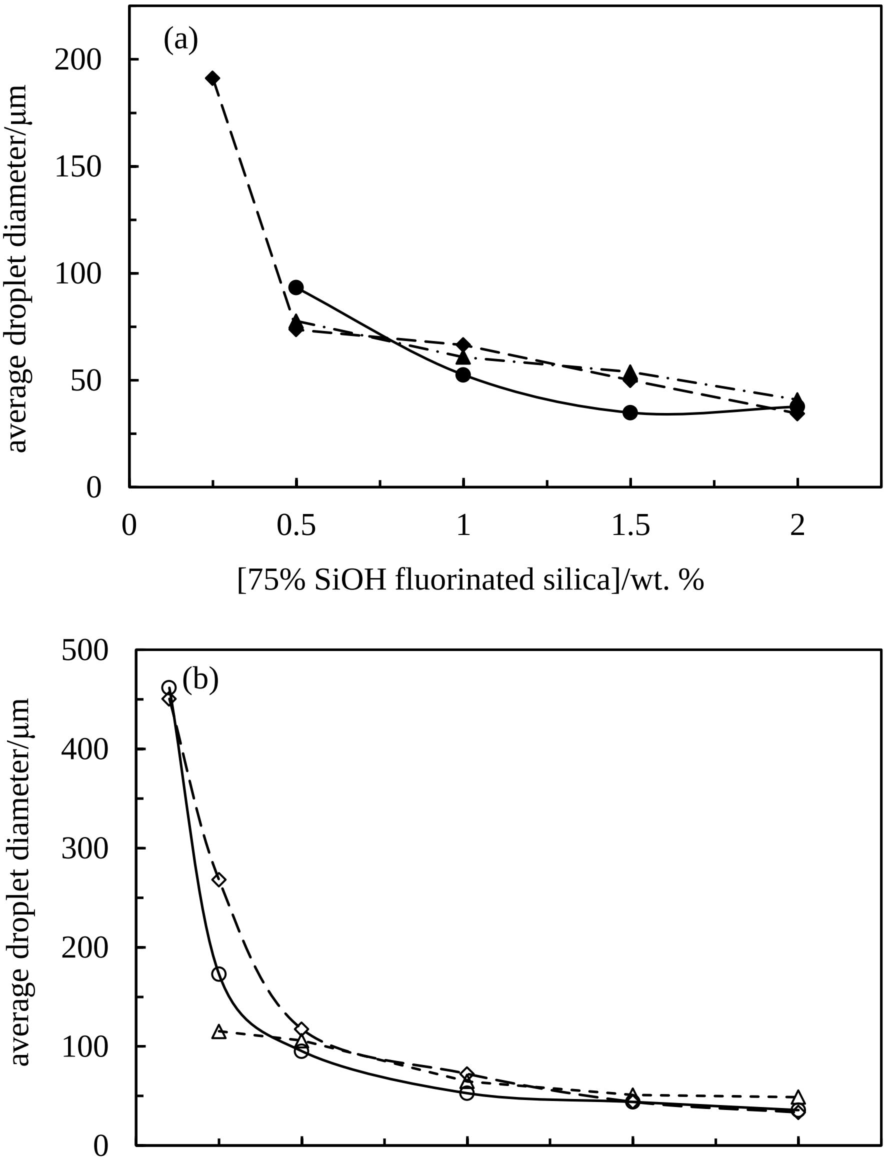

Figure 4.5. Plot of (a) fraction of PDMS 20 cS $f_{\text{PDMS 20 cS}}$ and (b) fraction of sunflower oil f_{suno}, fraction of olive oil f_{oo} and fraction of rapeseed oil f_{ro} released in the sunflower oil-in-PDMS 20 cS, olive oil-in-PDMS 20 cS and rapeseed oil-in-PDMS 20 cS emulsions, respectively, shown in Figure 4.1 *versus* [75% SiOH fluorinated silica]. The $f_{\text{PDMS 20 cS}}$, f_{suno}, f_{oo} and f_{ro} were measured 1 month after preparation of the emulsions. The stability of the emulsions to creaming is given by $f_{\text{PDMS 20 cS}}$ whilst that to coalescence is given by f_{suno}, f_{oo} and f_{ro}. The error bars represent the propagation error in the estimated values of $f_{\text{PDMS 20 cS}}$, f_{suno}, f_{oo} and f_{ro}.

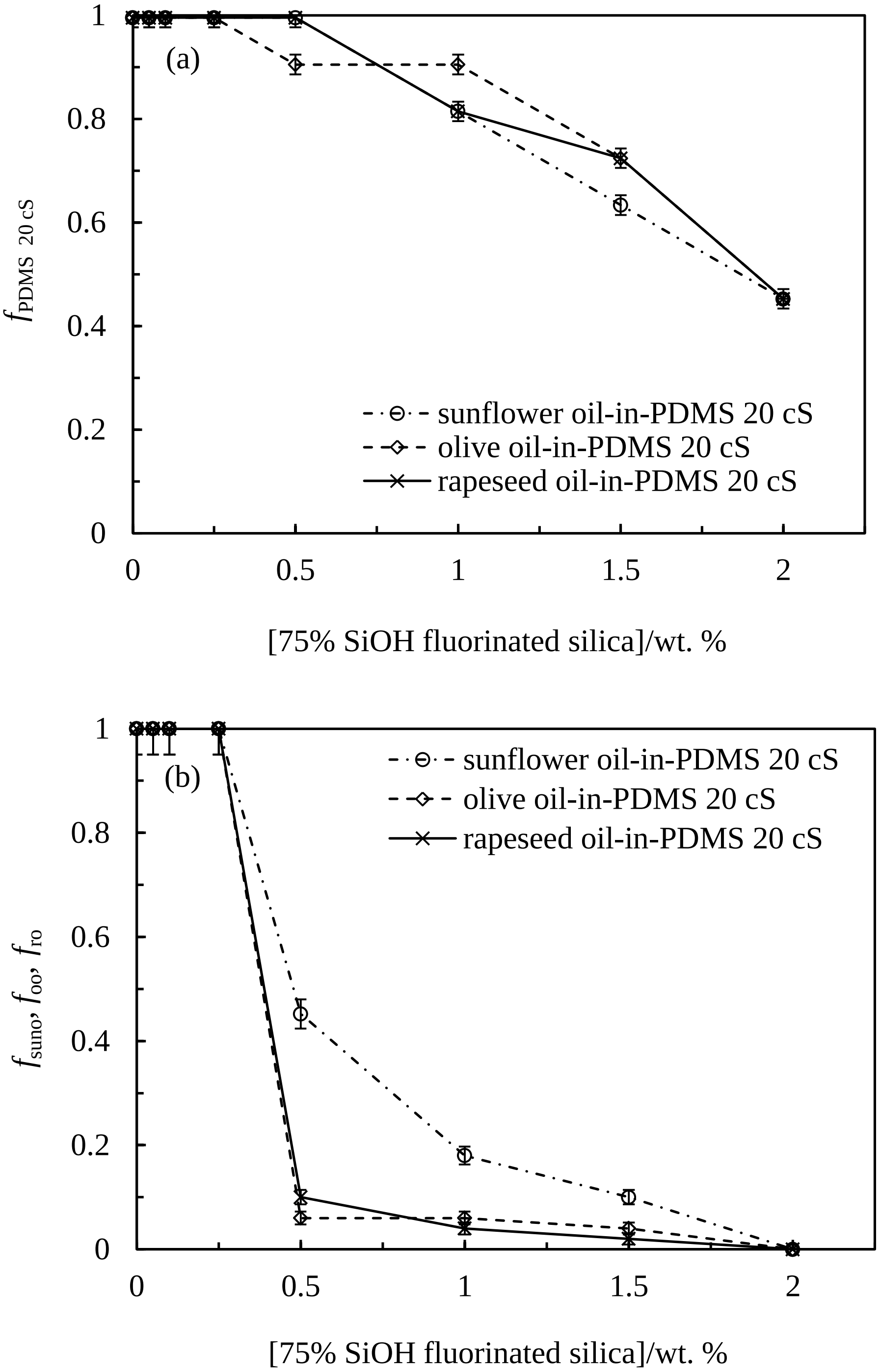

Figure 4.6. Plot of fraction of sunflower oil f_{suno} (○), fraction of olive oil f_{oo} (◇) and fraction of rapeseed oil f_{ro} (×) released in PDMS 50 cS-in-sunflower oil, PDMS 50 cS-in-olive oil and PDMS 50 cS-in-rapeseed oil emulsions, respectively, shown in Figure 4.2 *versus* [75% SiOH fluorinated silica]. The f_{suno}, f_{oo} and f_{ro} were measured 1 month after preparation of the emulsions as a measure of the stability of the emulsions to sedimentation. The error bars represent the propagation error in the estimated values of f_{suno}, f_{oo} and f_{ro}.

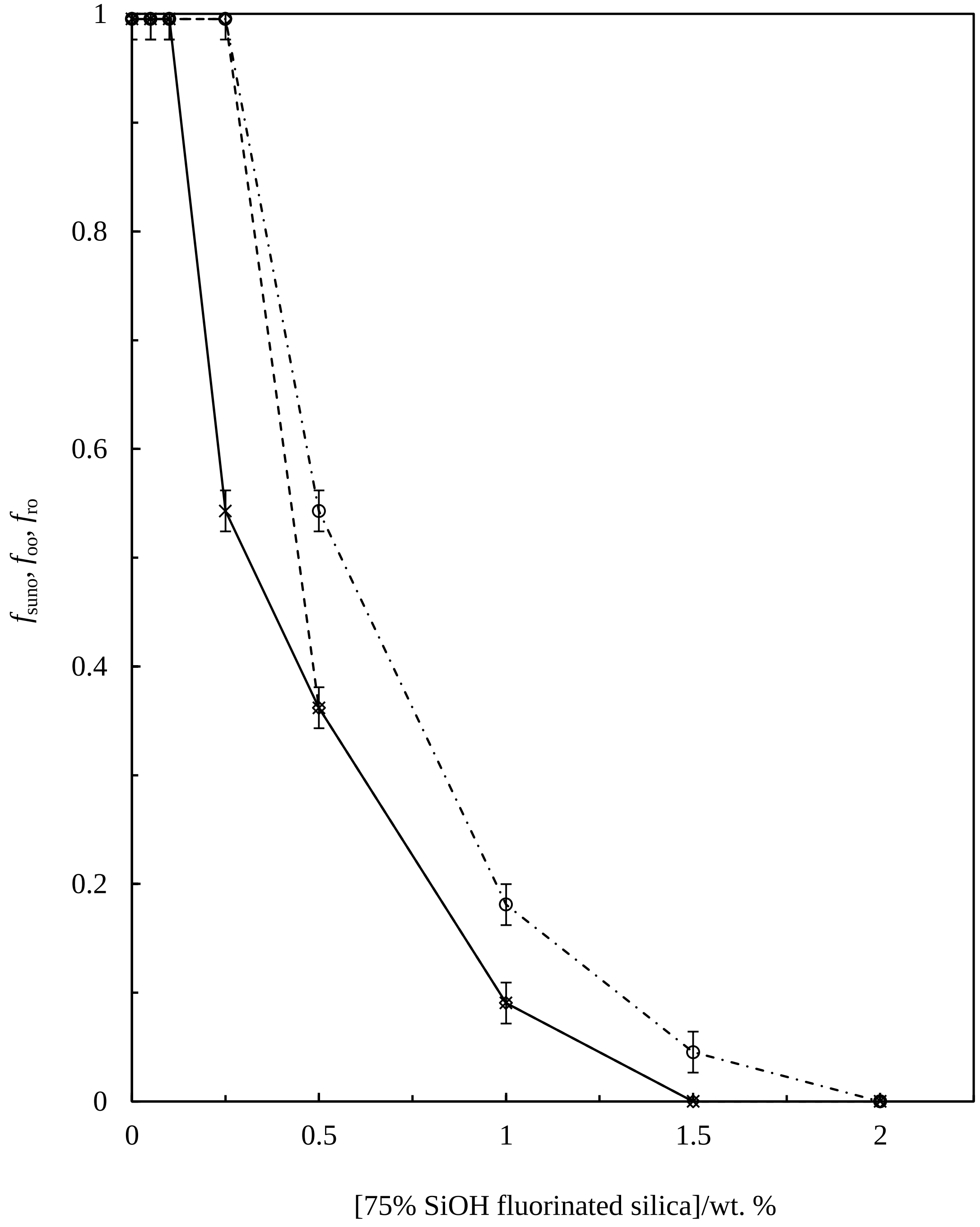

Figure 4.7. Plot of fraction of sunflower oil f_{suno} (○), fraction of olive oil f_{oo} (◇) and fraction of rapeseed oil f_{ro} (×) released in PDMS 100 cS-in-sunflower oil, PDMS 100 cS-in-olive oil and PDMS 100 cS-in-rapeseed oil emulsions, respectively, shown in Figure 4.3 *versus* [75% SiOH fluorinated silica]. The f_{suno}, f_{oo} and f_{ro} were measured 1 month after preparation of the emulsions as a measure of the stability of the emulsions to sedimentation. The error bars represent the propagation error in the estimated values of f_{suno}, f_{oo} and f_{ro}.

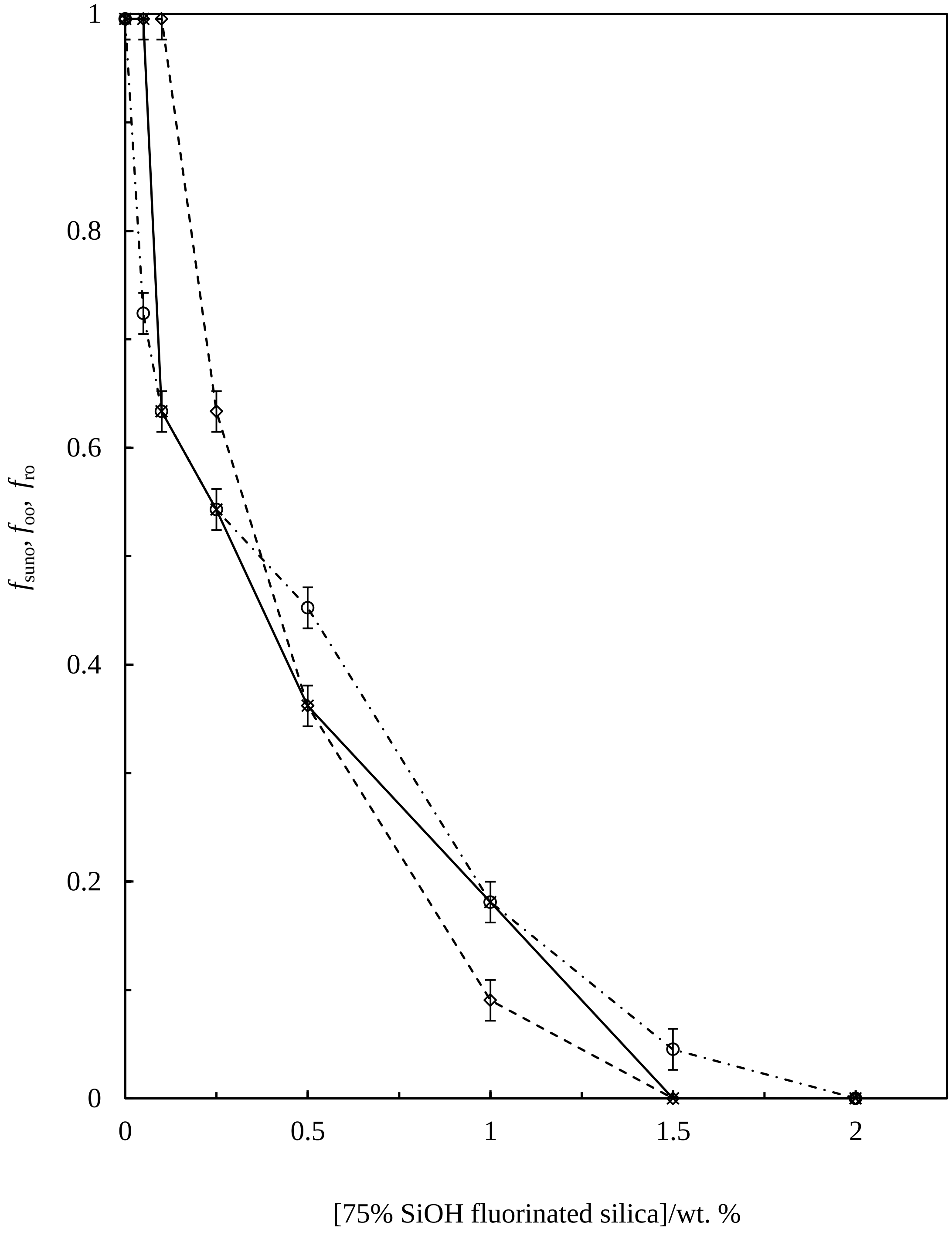

4.2.1.2 Oil-in-Oil Emulsions Stabilised by DCDMS-Coated and Fluorinated Fumed Silica Particles of Varying Percentage of Surface Residual SiOH Group

The emulsions contain equal volumes (5 cm^3) of vegetable oil and PDMS oil and were prepared by the powdered particle method. 1 wt. % of fumed silica particles (having 100−14% SiOH) was used. The particle concentration is relative to the total volume of PDMS oil and vegetable oil in the emulsions. The emulsions were also white, polydisperse and unflocculated. Depending on the vegetable oil/PDMS oil/silica particle combination and the % SiOH group on the particle surfaces, vegetable oil continuous, PDMS oil continuous or multiple emulsions were obtained (Appendix 4). Photographs and optical micrographs of these emulsions are shown in Figures 4.8−4.11. An optical micrograph of one of the multiple emulsions is shown also in Appendix 5. For the sunflower oil and olive oil/PDMS 20 cS/DCDMS-coated fumed silica particle combinations, very unstable PDMS 20 cS-in-sunflower oil and PDMS 20 cS-in-olive oil emulsions were obtained with particles having 100−25% surface SiOH group. These emulsions separated out almost completely into their component phases within 1 month after preparation as shown in Figures 4.12 and 4.13. Relatively stable PDMS 20 cS-in-sunflower oil and relatively unstable multiple PDMS 20 cS-olive oil emulsions were obtained with particles having 23% surface SiOH group. Thereafter, a transitional phase inversion occurred and relatively stable sunflower oil-in-PDMS 20 cS and olive oil-in-PDMS 20 cS emulsions were obtained with particles having 20−14% surface residual SiOH group. This type of transitional phase inversion has been reported in toluene-water system[7] and was said to be driven by change in particle wettability resulting from the silanisation of the particles with varying amounts of DCDMS. After inversion, the kinetic stability of the emulsions was seen to depend on the % SiOH group on the particle surfaces with the 14% SiOH silica (having the least % SiOH) giving relatively very stable emulsions. These emulsions were stable to creaming and coalescence and did not release oil for over a month. For the fluorinated fumed silica particles of surface residual SiOH group between 75 and 50%, only sunflower oil-in-PDMS 20 cS emulsions were obtained. The stability of these emulsions to creaming and coalescence was seen to depend on the % SiOH group on the particle surfaces as expected. As such, between 59 and 50% SiOH, the emulsions remained stable to both creaming and coalescence for over a month (Figures 4.12 and 4.13). Note that the olive oil-PDMS 20 cS system was not studied with the fluorinated silica particles.

As with the sunflower oil and olive oil/PDMS 20 cS/DCDMS-coated fumed silica particle combinations, transitional phase inversion was also observed in the sunflower oil and olive oil/PDMS 50 cS/DCDMS-coated fumed silica particle systems. A similar transitional phase inversion was also observed in the sunflower oil and olive oil/PDMS 100 cS/DCDMS-coated fumed silica particle systems. For the sunflower oil/PDMS 50 cS/silica particle combinations, relatively stable PDMS 50 cS-in-sunflower oil emulsions were obtained with the 100−23% SiOH fumed silica particles. These emulsions were completely stable to coalescence for over a month, but relatively unstable to sedimentation and released relatively small fraction of sunflower oil. Generally, the fraction of sunflower oil released decreased as the % SiOH group on the particle surfaces decreases (Figure 4.14(a)). Transitional phase inversion occurred when the % SiOH group on the particle surfaces was between 20−14% and relatively stable sunflower oil-in-PDMS 50 cS emulsions were obtained. These emulsions were stable to creaming and coalescence for over a month and did not release any oil. Similarly, PDMS 50 cS-in-olive oil emulsions were obtained for the olive oil-PDMS 50 cS systems with silica particles having % SiOH group between 100−23%. Phase inversion was observed in systems having 20 and 14% SiOH group giving rising to relatively stable olive oil-in-PDMS 50 cS emulsion and an unstable multiple emulsion respectively. The PDMS 50 cS-in-olive emulsions were completely stable to coalsescence (except for the 100% SiOH), but were relatively unstable to sedimentation releasing small fraction of olive oil. The fraction of olive oil released in the emulsions decreased as the % SiOH group on the particle surfaces decreases (Figure 4.14(b)). The olive oil-in-PDMS 50 cS emulsion, however, was stable to both creaming and coalescence for over a month and did not release oil. The formation of multiple emulsions in a single emulsification process in the presence of only one fumed silica particle type have been reported in aqueous systems.[54,55] Stable toluene-in-1-ethyl-3-methylimidazolium-in-toluene emulsion containing equal volumes of the liquids was obtained in a single emulsification process in the presence of 1 wt. % of 47% SiOH silica particles.[54] It was argued that contact angle hysteresis or that the distribution of individual particle is such that both emulsion types are formed and stabilised simultaneously during the emulsification. Using the powdered particle method, o/w emulsions (containing equal volumes of limonene and water) were inverted to o/w/o emulsions and then to w/o emulsions in a single emulsification process by increasing the concentration of 51−58% SiOH silica particles in the emulsions.[55] The concentration at which the multiple emulsions occurred was seen to increase with the hydrophilicity of the particles. It was argued that the particles behave more hydrophilic at relatively low particle concentrations where o/w emulsions occurred, due to insubstantial particle aggregation and agglomeration *via* hydrogen bonds from SiOH groups, than at relatively high particle concentrations where w/o emulsions occurred.[55] Particle aggregation and agglomeration was thought to increase with increase in particle concentration-being moderate at concentrations at which the multiple emulsions occurred and highest at those at which w/o occurred. It is not clear why multiple emulsions were obtained with silica particles of certain % SiOH in this study and more work needs to be done to account for their formation.

A similar trend was observed in the sunflower oil and olive oil/PDMS 100 cS/silica systems. Relatively stable PDMS 100 cS-in-sunflower (olive) oil emulsions were obtained with the 100−23% SiOH fumed silica particles. Thereafter, a transitional phase inversion occurred leading to the formation of sunflower (olive) oil-in-PDMS 100 cS emulsions with particles having 20−14% SiOH. The only exception is sunflower oil/PDMS 100 cS/14% SiOH silica system where an unstable multiple emulsion was formed. The PDMS 100 cS-in-sunflower (olive) oil emulsions were also completely stable to coalsescence, but were relatively unstable to sedimentation releasing a small fraction of sunflower (olive) oil. The fraction of sunflower (olive) oil released was seen to decrease with decreasing % SiOH group on the silica particle surfaces as shown in Figure 4.14. The sunflower (olive) oil-in-PDMS 100 cS emulsions were, however, stable to both creaming and coalescence for over a month and did not release oil. The relationship between the average droplet diameter of the PDMS 50 cS-in-sunflower (olive) oil and PDMS 100 cS-in-sunflower (olive) oil emulsions and the % SiOH group on the fumed silica particle surfaces is given in Figure 4.15. Though there are one or two exceptions, the average droplet diameter of the emulsions is seen to decrease as the % SiOH on the particle surfaces decreases.

The formation of relatively stable emulsions with the fumed silica particles having relatively high percentage of SiOH group (*e.g.* 100−51%) was not anticipated based on existing literature.[34,43] The formation of emulsions in the presence of these particles might be due to the tendency of the particles to behave ‘hydrophobically’ in the oils due to reduction in the effective SiOH content on the particles surfaces as a result of gel formation *via* SiOH−SiOH hydrogen bonding. In order to verify this, the manner in which the 100 and 14% SiOH fumed silica particles interact with one another once in the PDMS and vegetable oils was investigated. PDMS oil and vegetable oil dispersions of these particles were prepared at 2 wt. % and 5 wt. % of the particles in screw cap glass vials. Photographs of glass vials containing the oil-particle dispersions are shown in Figure 4.16. The PDMS oil dispersions containing 2 wt. % of 100% SiOH fumed silica was fluid, but those containing 5 wt. % of the particles gelled. The viscosity of the gels was seen (visually) to increase with the viscosity of the PDMS oils. On the contrary, the vegetable oil dispersions were fluid at both particle concentrations. However, those containing 5 wt. % of the particles were slightly viscous compared with those containing 2 wt. % of the particles. For the 14% SiOH fumed silica having relatively small percentage of surface SiOH groups, no gel was obtained with the PDMS oils at both 2 wt. % and 5 wt. % of the particles. However, those containing 5 wt. % of the particles were more viscous than those containing 2 wt. % of the particles. From the foregoing, it was inferred that the vegetable oil dispersions containing the 14% SiOH fumed silica would also not form gels. These findings indicate that the silica particles are interacting more (*via* hydrogen bonding) in the PDMS oils than in the vegetable oils.[56] Microscopic oil droplets can also be trapped in an oil-particle gel contributing to the overall stability of the emulsions. This is different in water where solvation of particle surfaces prevents the formation of SiOH−SiOH hydrogen bonding and particles behave hydrophilically.[56]

Figure 4.8. Photographs of glass vials containing sunflower oil-PDMS 20 cS emulsions stabilised by 1 wt. % of (a) DCDMS-coated and (b) fluorinated fumed silica particles and (c) olive oil-PDMS 20 cS emulsions stabilised by the DCDMS-coated fumed silica particles. The photographs were taken 1 month after preparation of the emulsions. The fumed silica particles have varying amount of surface residual % SiOH (given). The emulsions contain equal volumes (5 cm^3) of vegetable oil and PDMS 20 cS. As can be seen, the particles remain dispersed in sunflower oil and olive oil in systems where relatively unstable emulsions were obtained with relatively small number of PDMS 20 cS droplets (see Figure 4.9) in them.

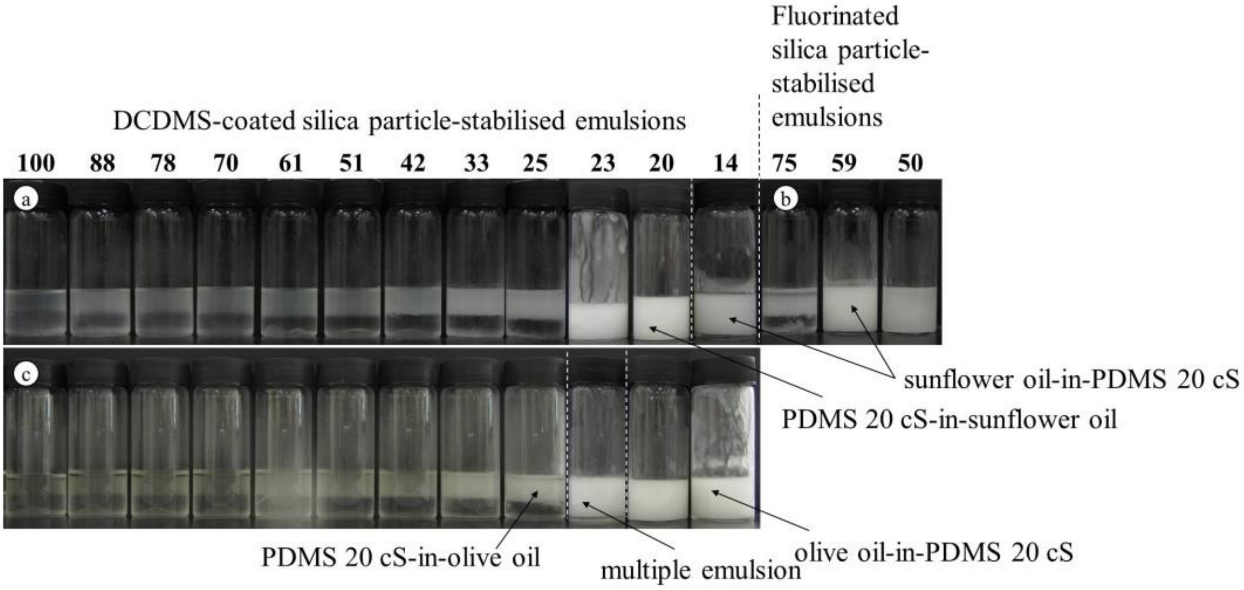

Figure 4.9. Corresponding optical micrographs (1 month after preparation) of the emulsions shown in Figure 4.8 at selected % of SiOH (given) on the silica surfaces.

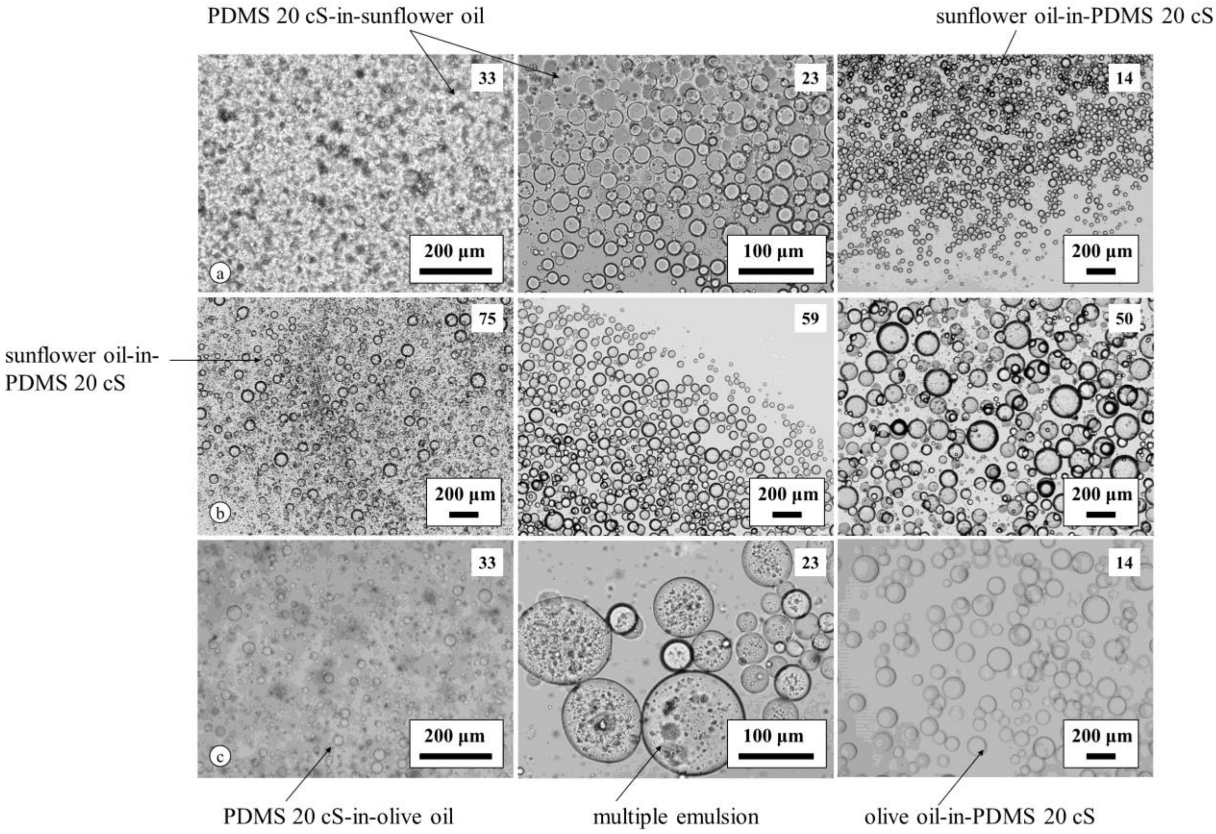

Figure 4.10. (upper) Photographs of glass vials containing (a) sunflower oil-PDMS 50 cS and (b) olive oil-PDMS 50 cS emulsions (1 month after preparation) stabilised by 1 wt. % of DCDMS-coated fumed silica particles having varying % of surface residual SiOH group (given). The emulsions contain equal volumes (5 cm^3) of vegetable oil and PDMS 50 cS. (lower) Corresponding optical micrographs (1 month after preparation) of the emulsions at selected % SiOH (given) on the silica surfaces. Scale bar = 200 μm.

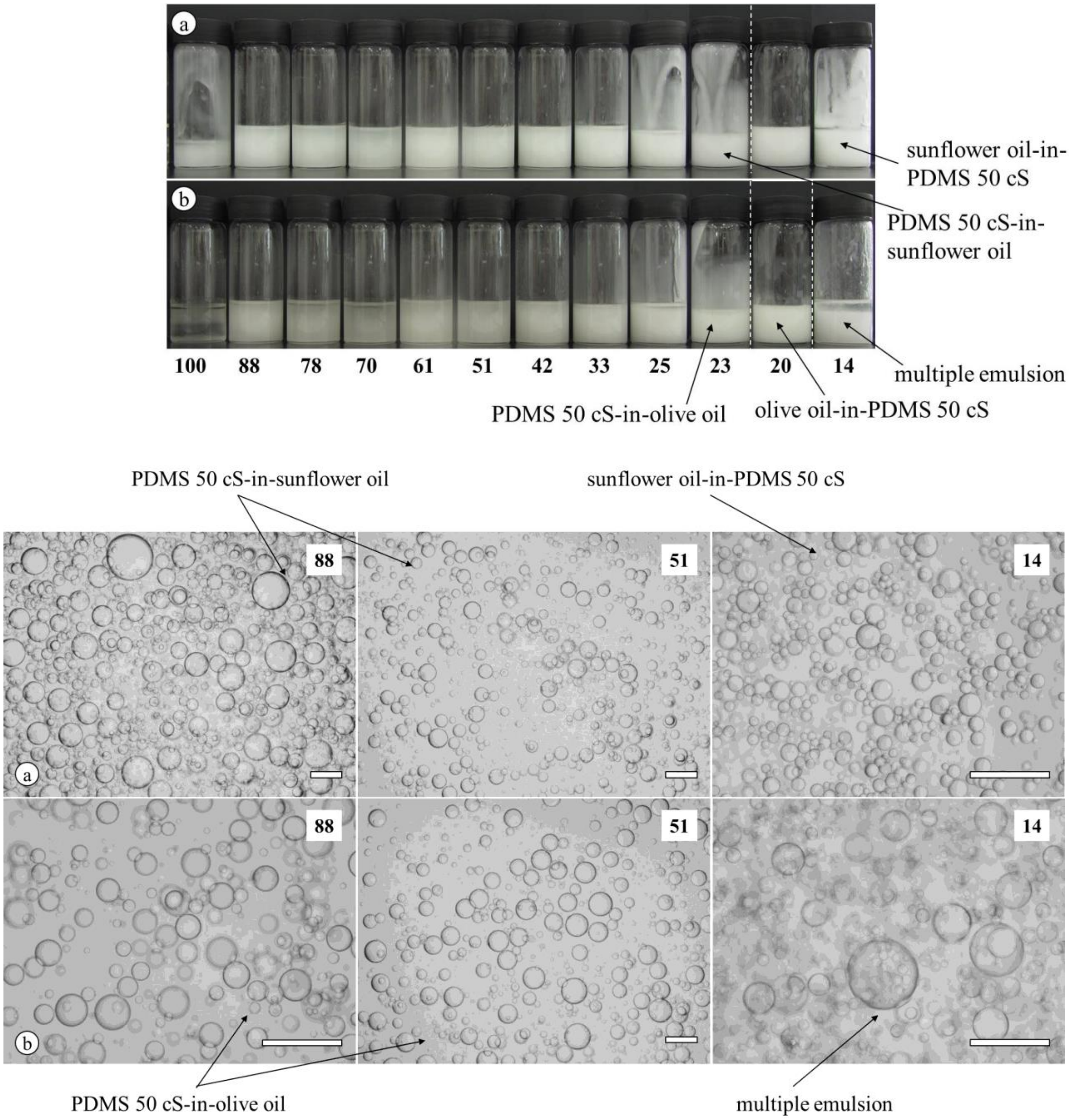

Figure 4.11. (upper) Photographs of glass vials containing (a) sunflower oil-PDMS 100 cS and (b) olive oil-PDMS 100 cS emulsions (1 month after preparation) stabilised by 1 wt. % of DCDMS-coated fumed silica particles having varying % of surface residual SiOH group (given). The emulsions contain equal volumes (5 cm^3) of vegetable oil and PDMS 100 cS. (lower) Corresponding optical micrographs (1 month after preparation) of the emulsions at selected % of SiOH (given) on the silica surfaces. Scale bar = 200 μm.

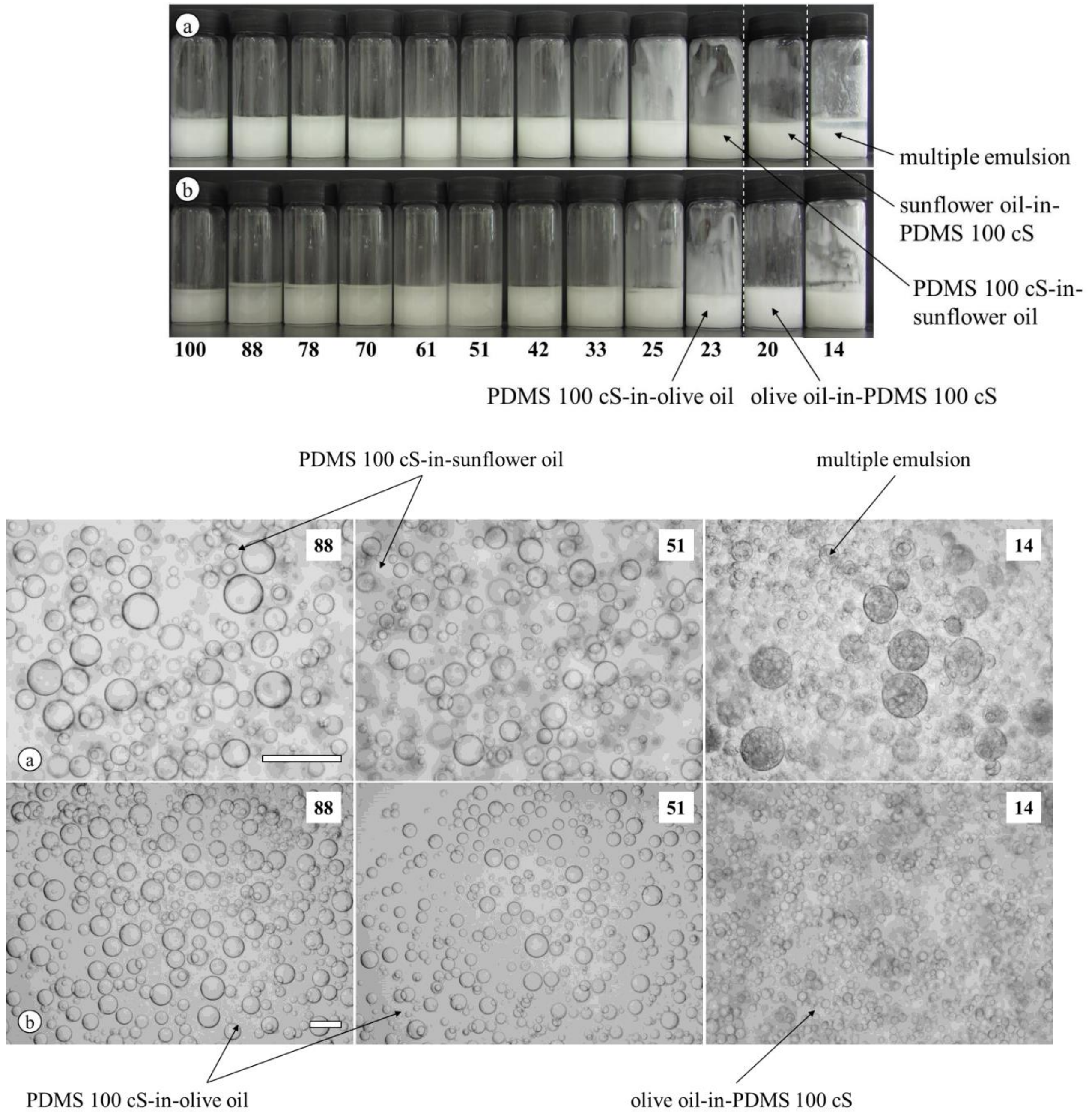

Figure 4.12. Fraction of PDMS 20 cS $f_{\text{PDMS 20 cS}}$ released in PDMS 20 cS-in-sunflower oil emulsions stabilised by 1 wt. % of DCDMS-coated fumed silica particles (●) or sunflower oil-in-PDMS 20 cS emulsions stabilised by 1 wt.% of fluorinated fumed silica particles (○) shown in Figure 4.8 *versus* % SiOH on the fumed silica particle surfaces. $f_{\text{PDMS 20 cS}}$ was measured 1 month after preparation of the emulsions as a measure of the stability of the emulsions to coalescence (●) or creaming (○). The $f_{\text{PDMS 20 cS}}$ released in the PDMS 20 cS-in-olive oil emulsions (1 month after preparation) is not plotted because the $f_{\text{PDMS 20 cS}}$ (sunflower oil emulsions) = $f_{\text{PDMS 20 cS}}$ from the PDMS 20 cS-in-olive oil emulsions. The only exception is the 23% SiOH silica-stabilised multiple olive oil-PDMS 20 cS emulsion where $f_{\text{PDMS 20 cS}} \approx 0.2$. The error bars are the propagation error in the estimated values of $f_{\text{PDMS 20 cS}}$.

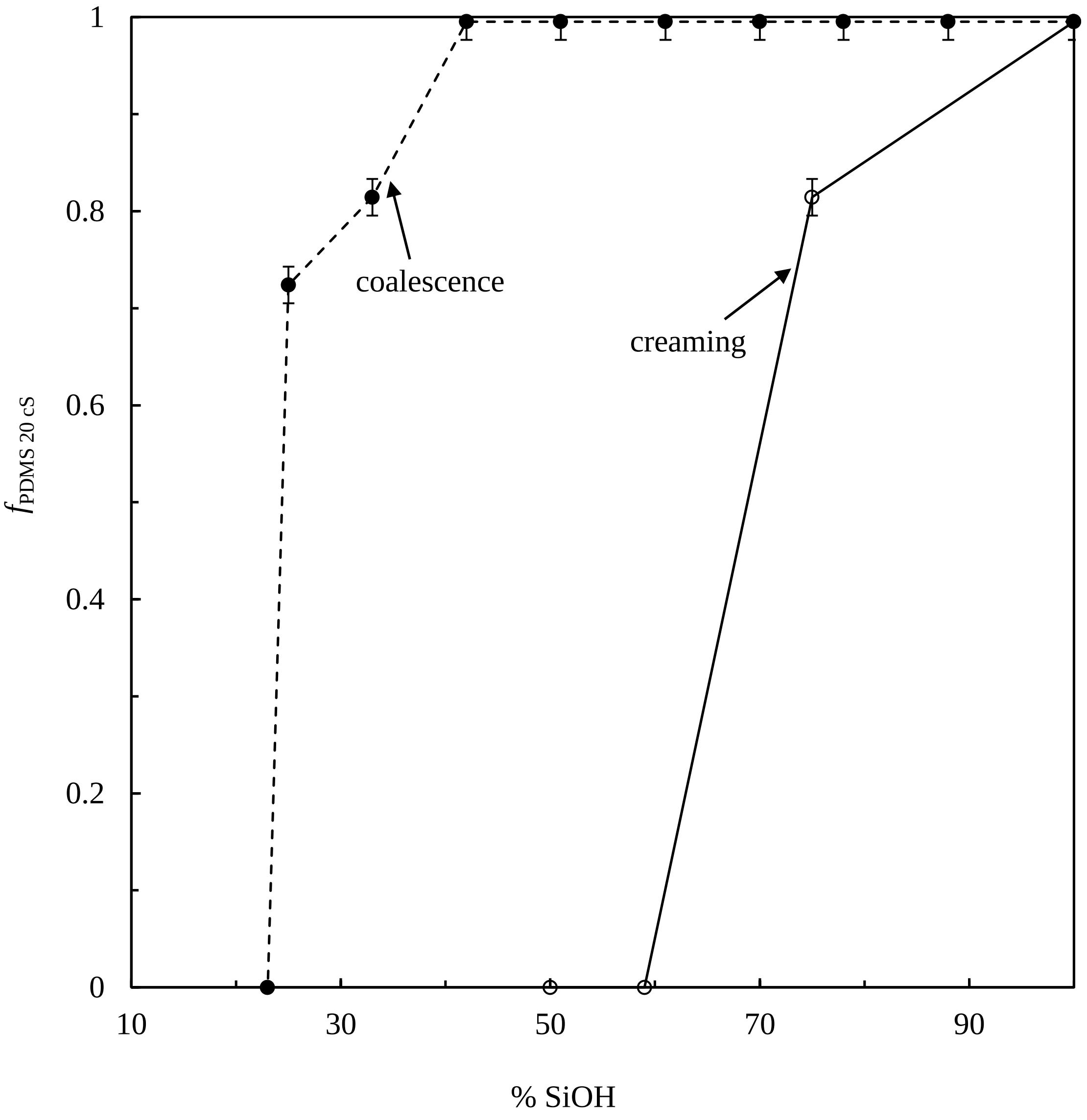

Figure 4.13. Fraction of sunflower oil f_{suno} released in PDMS 20 cS-in-sunflower oil emulsions stabilised by 1 wt. % of DCDMS-coated fumed silica particles (●) or sunflower oil-in-PDMS 20 cS emulsions stabilised by 1 wt.% of fluorinated fumed silica particles (○) shown in Figure 4.8 *versus* % SiOH on fumed silica particle surfaces. f_{suno} was measured 1 month after preparation of the emulsions as a measure of the stability of the emulsions to sedimentation (●) or coalescence (○). The fraction of olive oil f_{oo} released in the PDMS 20 cS-in-olive oil emulsions (1 month after preparation) is not plotted because $f_{suno} = f_{oo}$ from the PDMS 20 cS-in-olive oil emulsions. The error bars are the propagation error in the estimated values of f_{suno}.

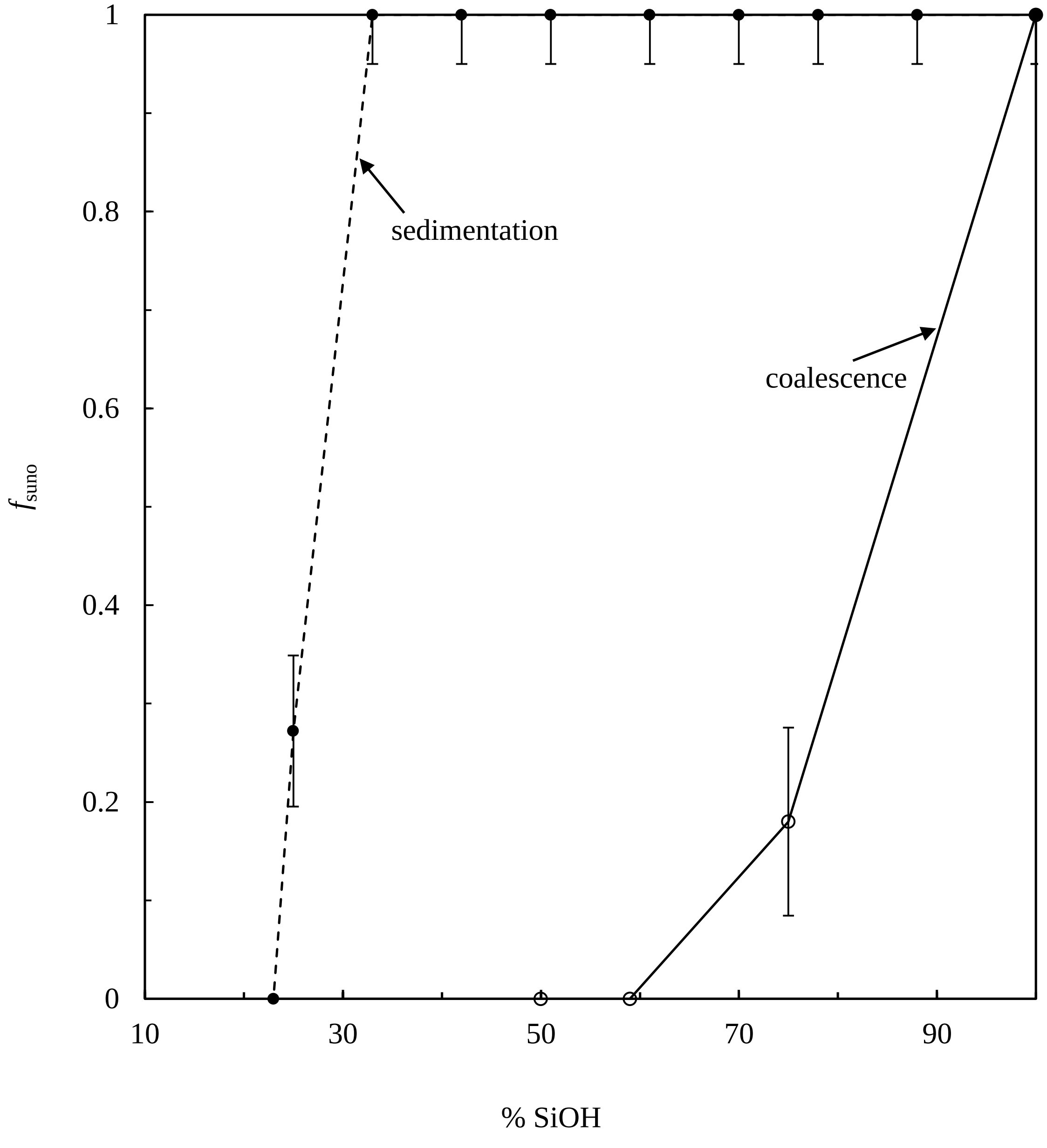

Figure 4.14. (a) Fraction of sunflower oil f_{suno} released from PDMS 50 cS-in-sunflower oil (●) and PDMS 100 cS-in-sunflower oil (○) emulsions (1 month after preparation) and (b) fraction of olive oil f_{oo} released from PDMS 50 cS-in-olive oil (◇) and PDMS 100 cS-in-olive oil (◆) emulsions (1 month after preparation) shown in Figures 4.10 and 4.11 *versus* % SiOH on DCDMS-coated fumed silica particle surfaces. The f_{suno} and f_{oo} serve as a measure of the stability of the emulsions to sedimentation. The error bars are the propagation error in the estimated values of f_{suno} and f_{oo}.

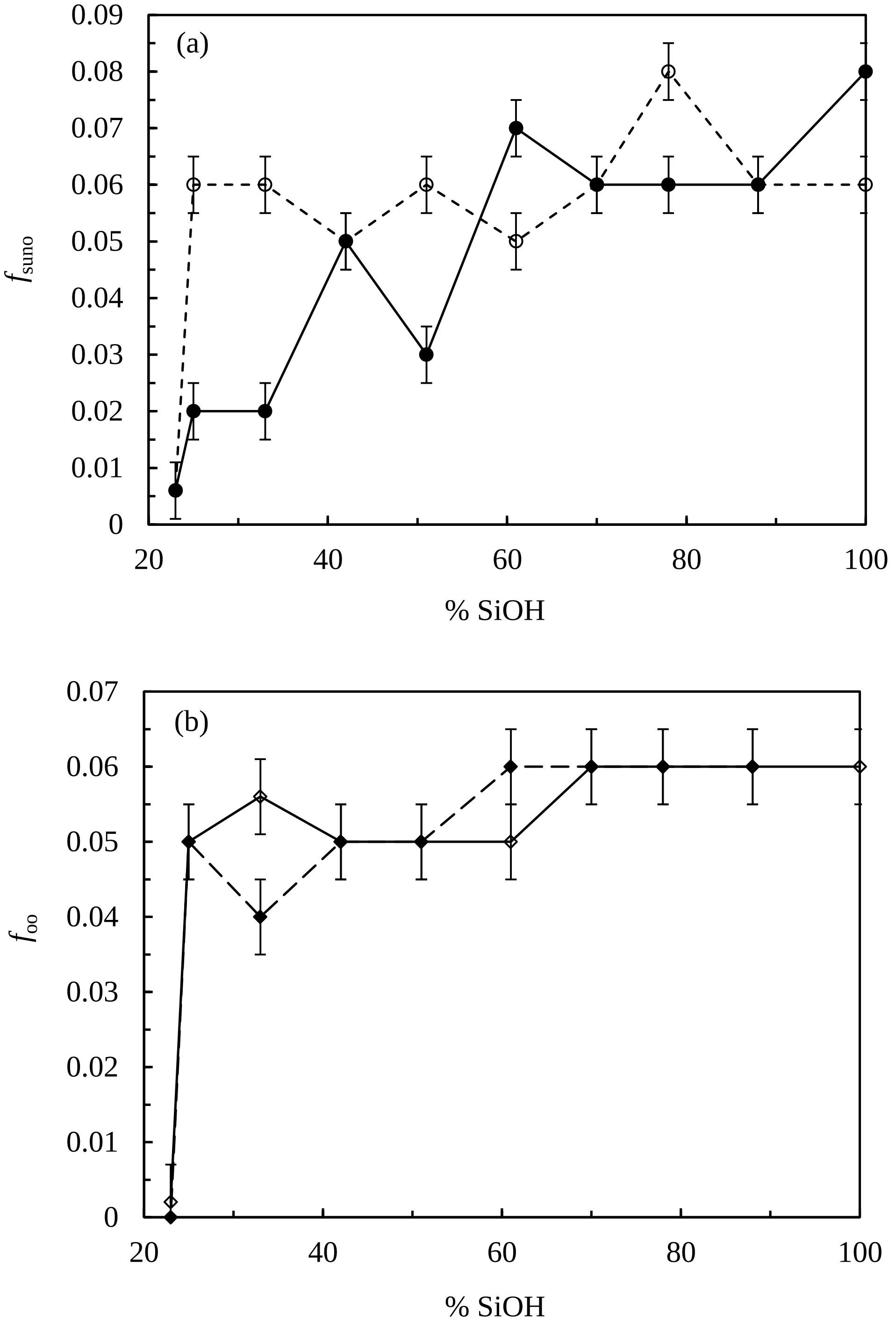

Figure 4.15. Plot of average droplet diameter of 300 droplets of PDMS 50 cS-in-sunflower oil (●), PDMS 100 cS-in-sunflower oil (○), PDMS 50 cS-in-olive oil (◆) and PDMS 100 cS-in-olive oil (◇) emulsions (1 month after preparation) obtained from their optical micrographs shown in Figures 4.10 and 4.11 *versus* % SiOH on DCDMS-coated fumed silica particle surfaces. The standard deviation of the measurements is generally in the range of 50 μm (at relatively high % SiOH) to 7 μm (at relatively low % SiOH).

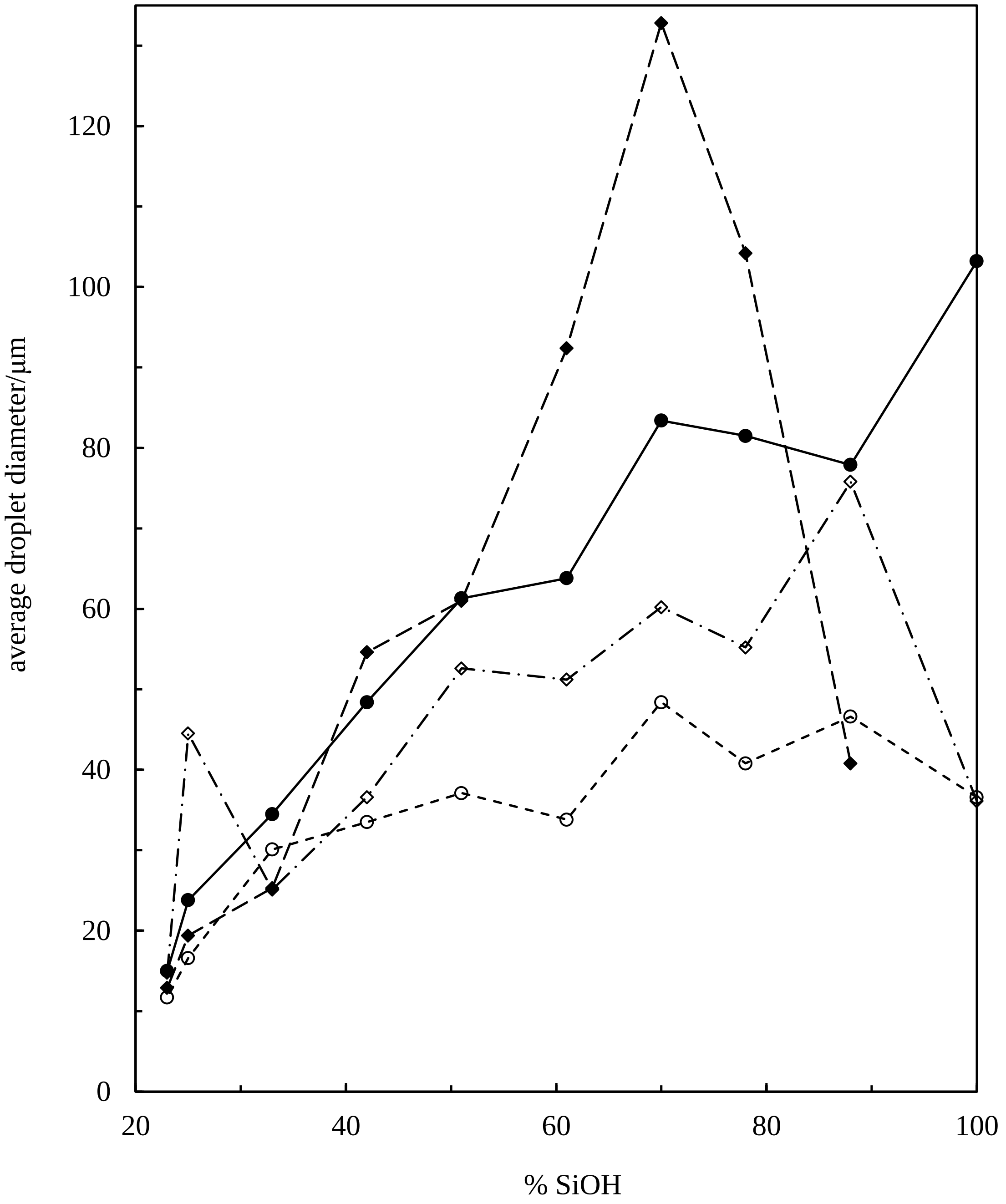

Figure 4.16. Photographs of inverted glass vials containing (i) PDMS (a) 20, (b) 50 and (c) 100 cS plus 2 wt. % (left) and 5 wt. % (right) of 100% SiOH fumed silica, (ii) (a) sunflower, (b) olive and (c) rapeseed oil plus 2 wt. % (left) and 5 wt. % (right) of 100% SiOH fumed silica and (iii) PDMS (a) 20, (b) 50 and (c) 100 cS plus 2 wt. % (left) and 5 wt. % (right) of 14% SiOH fumed silica particle dispersions (1 week after formation).

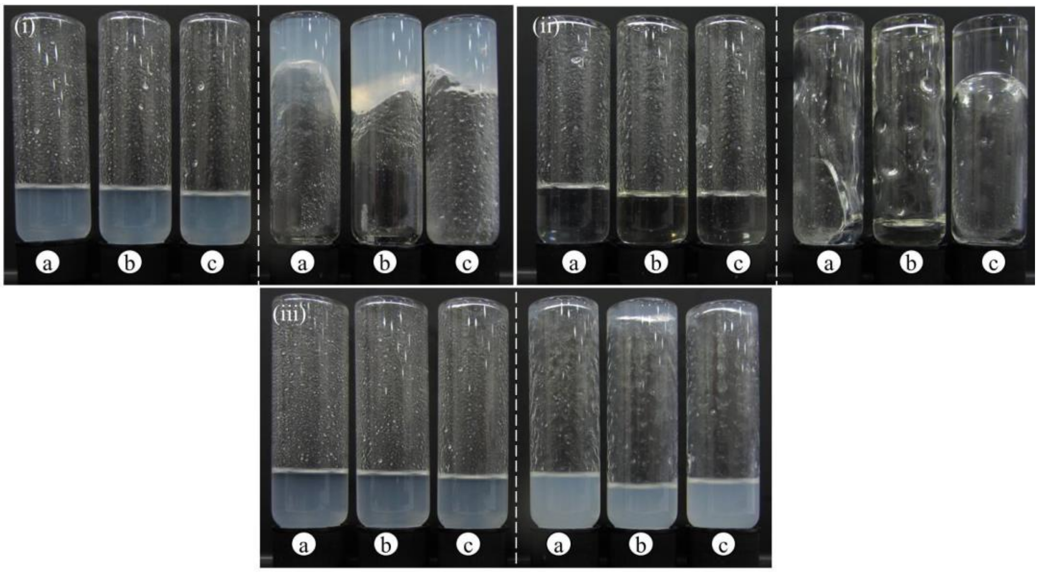

4.2.1.3 Oil-in-Oil-in-Oil Emulsions Containing Varying Volume Fraction of the Initial Oil-in-Oil Emulsions Stabilised by Fumed Silica Particles

Just like in the case of surfactant-stabilised aqueous emulsions where two different surfactants of opposite curvature are required for the stabilisation of multiple or double emulsions,[57] two different particles (*e.g*. hydrophilic and hydrophobic) are also required for the stabilisation of multiple Pickering emulsions. For aqueous multiple Pickering emulsions, kinetically stable o/w/o emulsions have been prepared using hydrophilic (inner oil droplets) and hydrophobic silica particles (outer water globules) in a double emulsification method.[58,59] In this study, by varying the percentage of surface residual SiOH group on the fumed silica particle surfaces in the sunflower oil-PDMS 50 cS and olive oil-PDMS 100 cS systems, it was observed that the 100−25% SiOH fumed silica particles prefer to stabilise vegetable oil continuous emulsions whilst the 14 and 20% SiOH ones prefer to stabilise PDMS oil continuous emulsions (sec. 4.2.1.2). Using a double emulsification method exploiting this variation of emulsion type with the particles, o/o/o emulsions were prepared using the 14 and 51% SiOH fumed silica. In the first emulsification, simple emulsions containing equal volumes (5 cm^3) of the oils were prepared by using high shear Ultra-Turrax homogeniser having an operating tool of inner diameter 1.3 cm operating at 12000 rpm for 2 min (see sec. 2.2.2.5.2.1). The emulsions were prepared by the powdered particle method using 1 wt. % of 14 or 51% SiOH fumed silica in screw cap glass vials (inner diameter 2.4 cm and height 7.2 cm). The particle concentration is with respect to the total volume of both oils in the emulsions. After preparation of the simple emulsions, attempts were made to prepare multiple emulsions using relatively high (6000 rpm using Ultra-Turrax homogeniser) and low shear (500 rpm using magnetic stirrer) for the second emulsification. Firstly, the simple sunflower oil-in-PDMS 50 cS and olive oil-in-PDMS 100 cS emulsions (stabilised by 1 wt. % of 14% SiOH silica) were re-emulsified, respectively, in sunflower oil and olive oil dispersions containing 2 wt. % of 51% SiOH silica using low shear or high shear. Secondly, the simple PDMS 50 cS-in-sunflower oil and PDMS 100 cS-in-olive oil emulsions (stabilised by 1 wt. % of 51% SiOH silica) were re-emulsified, respectively, in sunflower oil and olive oil dispersions containing 2 wt. % of 14% SiOH silica using low shear or high shear. A photo of glass vials containing the o/o/o emulsions prepared by using low shear and their corresponding optical micrographs are shown in Figures 4.17 and 4.18 respectively. The sunflower oil-in-PDMS 50 cS-in-sunflower oil and olive oil-in-PDMS 100 cS-in-olive oil emulsions contain varying $\phi_{o/o}$ (*ca*. 0.3−0.7) of stable sunflower oil-in-PDMS 50 cS and olive oil-in-PDMS 100 cS emulsions stabilised by 14% SiOH silica (shown in Figure 4.17) respectively. The stability of the multiple emulsions to sedimentation is described in Figure 4.19, where it can be seen that the multiple emulsions containing $\phi_{o/o} = 0.5$ are less stable to sedimentation compared with those containing $\phi_{o/o} \approx 0.3$ and 0.7. On the contrary, using PDMS 50 cS-in-sunflower oil or PDMS 100 cS-in-olive oil emulsion stabilised by 51% SiOH fumed silica (shown in Figure 4.17) as a precursor simple emulsion rather led to catastrophic phase inversion and unstable o/o emulsions were obtained. These emulsions were sunflower oil-in-PDMS 50 cS or olive oil-in-PDMS 100 cS with no clear phase separation (Figure 4.17). It was also impossible to prepare multiple emulsions using relatively high shear as it induces catastrophic phase inversion. This was investigated with $\phi_{o/o} \approx 0.7$. Starting with the relatively stable sunflower oil-in-PDMS 50 cS or olive oil-in-PDMS 100 cS emulsion stabilised by 14% SiOH fumed silica, relatively unstable PDMS 50 cS-in-sunflower oil and PDMS 100 cS-in-olive oil emulsions were obtained (Figure 4.20). Although these emulsions are completely stable to coalescence for over a month, the f_{suno} and f_{oo} released from them after a month was *ca*. 0.10 and 0.14 respectively.

Figure 4.17. (i) Photograph (after 1 month) of glass vials containing initial simple (a) PDMS 50 cS-in-sunflower oil and (b) PDMS 100 cS-in-olive oil (both stabilised by 51% SiOH silica), (c) sunflower oil-in-PDMS 50 cS and (d) olive oil-in-PDMS 100 cS (both stabilised by 14% SiOH silica); photographs of glass vials containing ≈ 4.5 cm^3 of (ii) sunflower oil-in-PDMS 50 cS-in-sunflower oil (left) and sunflower oil-in-PDMS 50 cS (right) and (iii) olive oil-in-PDMS 100 cS-in-olive oil (left) and olive oil-in-PDMS 100 cS (right) emulsions (1 month after preparation). The emulsions contain $\phi_{o/o}$ ≈ (a) 0.3, (b) 0.5 and (c) 0.7 of the initial simple emulsions in (i). The multiple emulsions in (ii) and (iii) are from the simple sunflower oil-in-PDMS 50 cS or olive oil-in-PDMS 100 cS emulsions in (i) and are stabilised by 14% SiOH silica (inner droplets) and 51% SiOH silica (outer droplets). The simple emulsions in (ii) and (iii) are from PDMS 50 cS-in-sunflower oil and PDMS 100 cS-in-olive oil emulsions, respectively, and are stabilised by of 51 and 14% SiOH silica.

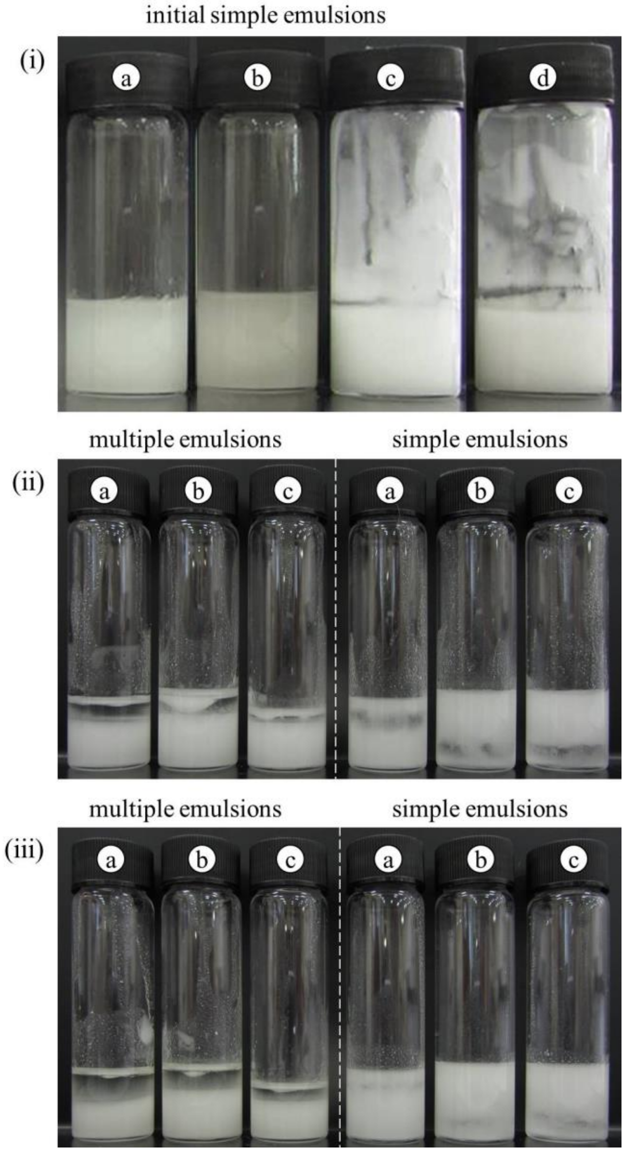

Figure 4.18. Corresponding optical micrographs (1 month after preparation) of (A) the multiple and simple emulsions shown in Figure 4.17(ii) and (B) the multiple and simple emulsions shown in Figure 4.17(iii).

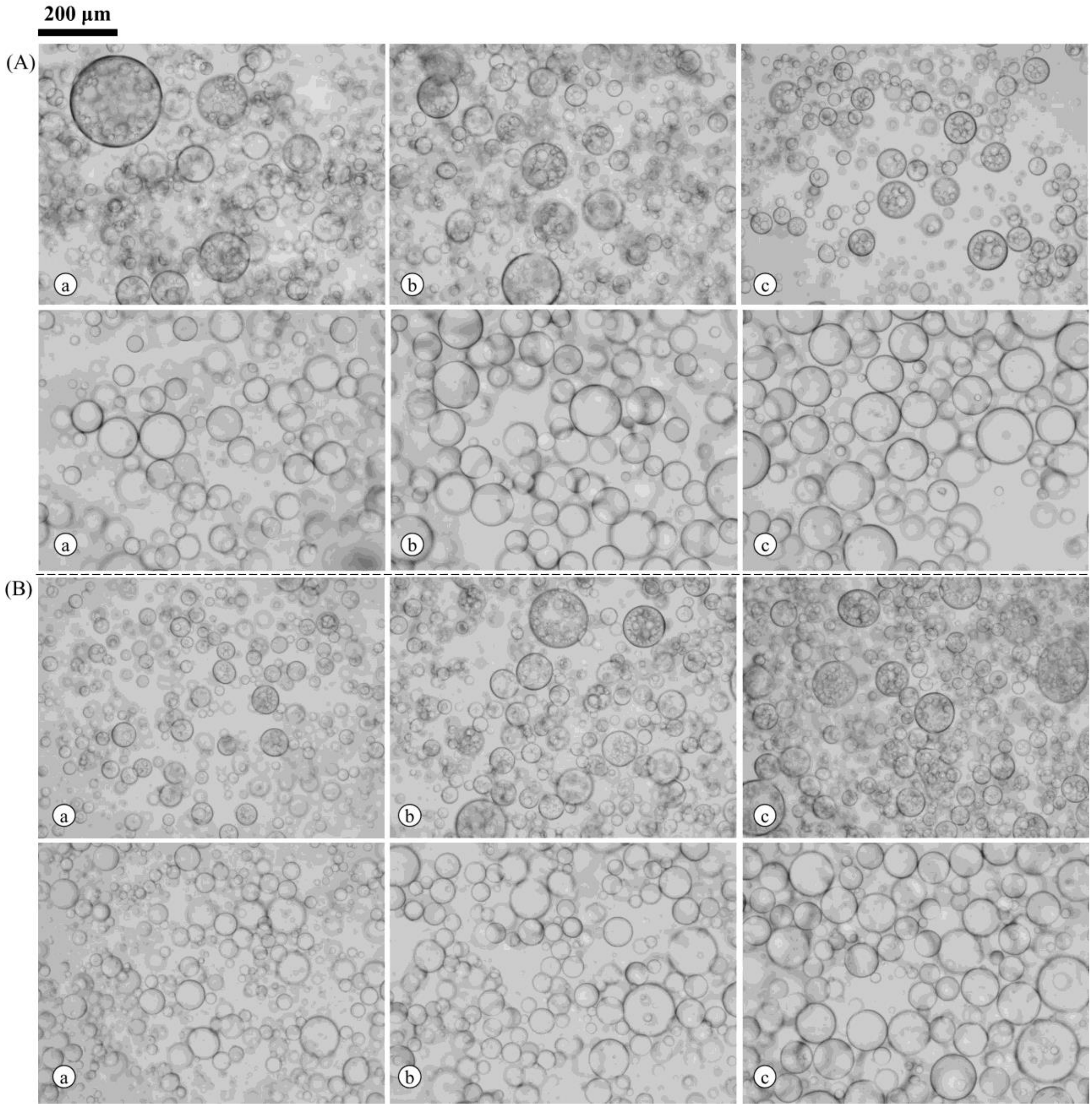

Figure 4.19. Fraction of sunflower oil f_{suno} (blue bars) and fraction of olive oil f_{oo} (red bars) released from sunflower oil-in-PDMS 50 cS-in-sunflower oil and olive oil-in-PDMS 100 cS-in-olive oil emulsions (shown in Figure 4.17) respectively *versus* the volume fraction of simple emulsions $\phi_{o/o}$ in them. f_{suno} and f_{oo} were measured 1 month after preparation of the emulsions as a measure of the stability of the emulsions to sedimentation. The error bars represent propagation error.

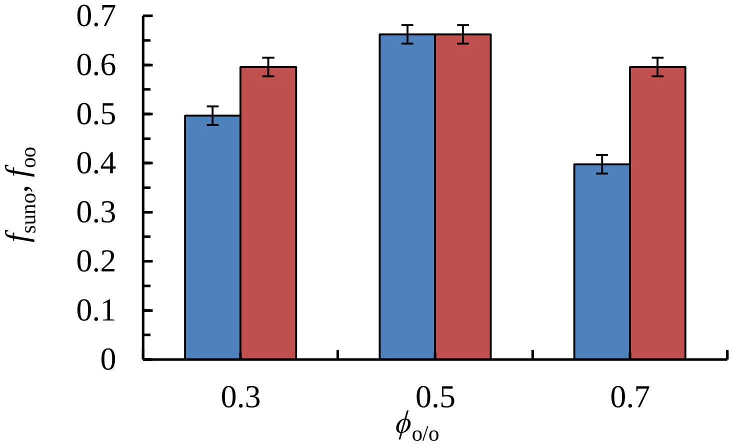

Figure 4.20. (i) Photograph of glass vials containing ≈ 15 cm^3 of (a) PDMS 50 cS-in-sunflower oil and (b) PDMS 100 cS-in-olive oil emulsions (1 month after preparation) stabilised by ≈ 1 wt. % of 51% SiOH and ≈ 1 wt. % of 14% SiOH fumed silica particles from an attempt to prepare o/o/o emulsions using relatively high shear. The particle concentrations are with respect to the volume of the final emulsions. The emulsions contain $\phi_{o/o} \approx 0.7$ of initial relatively stable sunflower oil-in-PDMS 50 cS or olive oil-in-PDMS 100 cS emulsions stabilised by 1 wt. % of 14% SiOH silica shown in Figure 4.17. (ii) Corresponding optical micrographs (1 month after preparation) of the emulsions in (i). Scale bar = 200 μm.

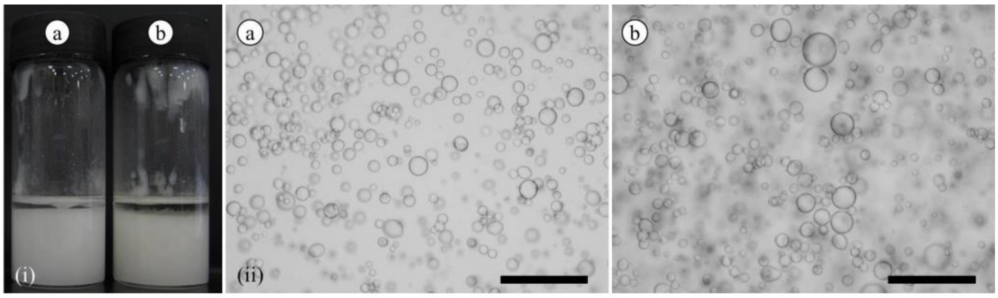

4.2.2 Effect of Initial Particle Location on Emulsion Type

For some particle-stabilised aqueous emulsions, the initial location of the particles in the oil or water phase dictates the type (*i.e.* o/w or w/o) of the final emulsion.[54] As such, the effect of the initial location of the fumed silica particles in the oil phases was also investigated for selected fumed silica particles. Photographs and the corresponding optical micrographs of the o/o emulsions (having equal volumes of the oils) prepared by the powdered particle method are shown in Figures 4.21−4.23. 75% SiOH fluorinated fumed silica, 51 and 14% SiOH DCDMS-coated fumed silica particles were used with the oils. Because the oils wet these particles spontaneously, the required amount (0.2 g) of particles was placed on the surface of vegetable oil or PDMS oil (5 cm^3). The particles were wetted completely by the oils and entered in them before the second oil phase was added. As such, the particles are considered as being initially in the vegetable oil or PDMS oil phase. For all the vegetable oil-PDMS oil combinations studied, the emulsion type is independent of the initial location of the particles (Table 4.2). The stability of the emulsions to creaming or sedimentation and coalescence is also summarised in Table 4.2 in terms of the necessary oil phase separated in a month along with their average droplet diameter. In some cases, the average droplet diameter of the emulsions is smaller if the particles are initially in the vegetable oil phase compared with when the particles are initially in the PDMS oil phase. Many of the emulsions are more kinetically stable if the particles are initially in the vegetable oil phase compared with when they are in the PDMS oil phase. These observations might be due to the interaction of the particles once in the vegetable oil or PDMS oil phase.

Figure 4.21. Photographs of glass vials containing emulsions of sunflower oil-PDMS (a) 20, (b) 50 and (c) 100 cS (left), olive oil-PDMS (a) 20, (b) 50 and (c) 100 cS (middle) and rapeseed oil-PDMS (a) 20, (b) 50 and (c) 100 cS (right) systems (1 month after preparation) stabilised by 1 wt. % of 75% SiOH fluorinated fumed silica particles. The emulsions contain equal volumes (5 cm^3) of the oils and were prepared by the powdered particle method. The particles (1 wt. %) were initially in the (i) PDMS oil or (ii) vegetable oil phase. The emulsions are (a) PDMS 20 cS continuous and vegetable oil continuous for (b) and (c), irrespective of the initial location of the particles.

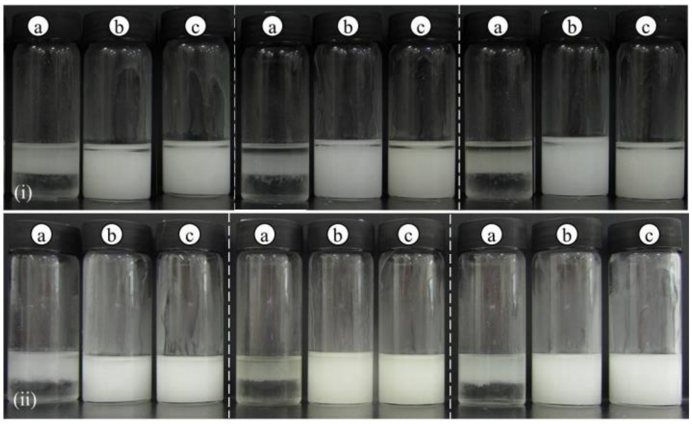

Figure 4.22. Corresponding optical micrographs (1 month after preparation) of the emulsions shown in Figure 4.21. Scale bar = 100 μm.

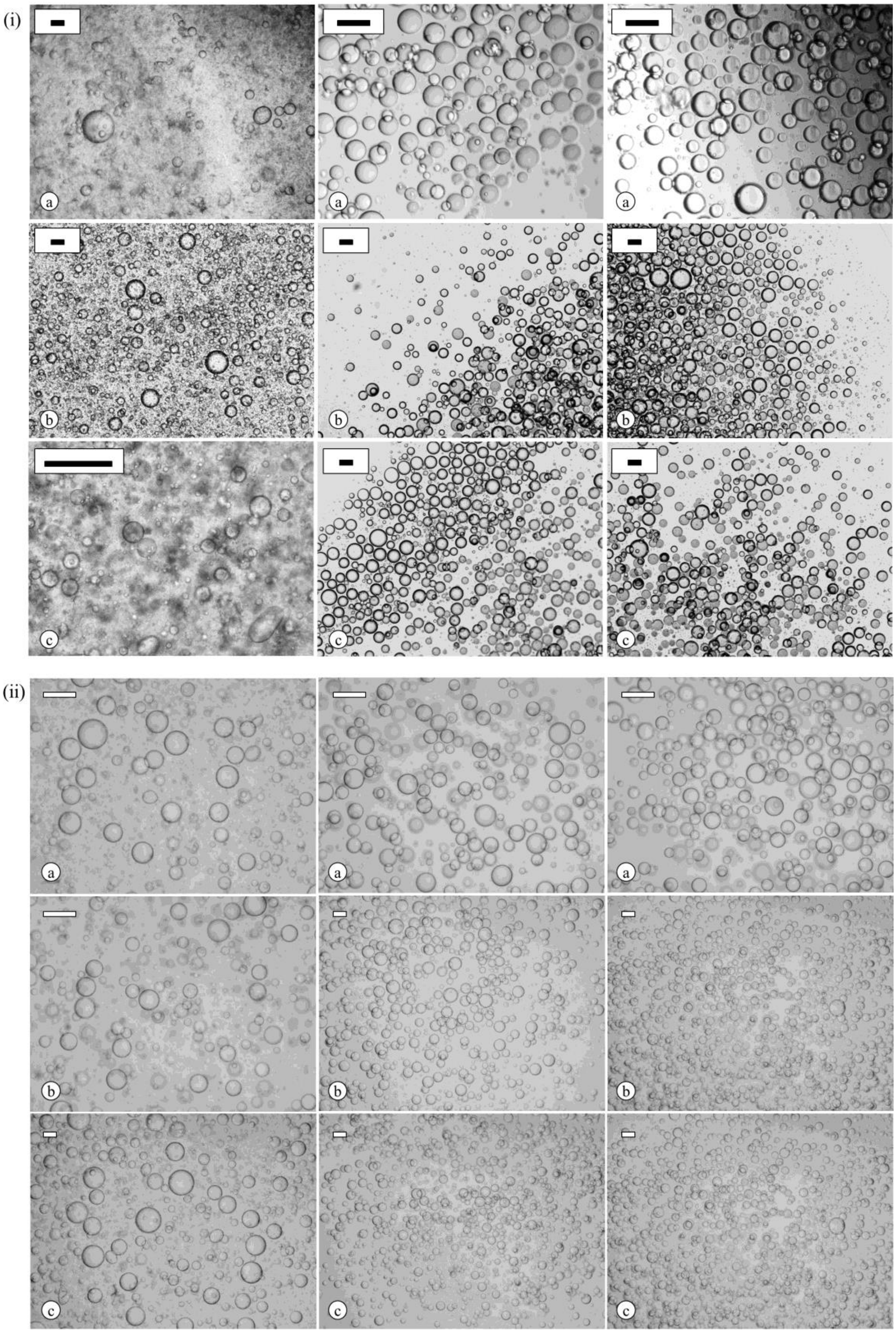

Figure 4.23. Photographs of glass vials containing emulsions (1 month after preparation) of (a) PDMS 50 cS-in-sunflower oil stabilised by 1 wt. % of 51 % SiOH fumed silica and (b) sunflower oil-in-PDMS 50 cS stabilised by 1 wt. % of 14% SiOH fumed silica (left); (a) PDMS 100 cS-in-olive oil stabilised by 1 wt. % of 51% SiOH fumed silica and (b) olive oil-in-PDMS 100 cS stabilised by 1 wt. % of 14% SiOH fumed silica (right). The emulsions contain equal volumes (5 cm^3) of the oils and were prepared by the powdered particle method. The particles (1 wt. %) were initially in the (i) PDMS oil or (ii) vegetable oil phase. (lower) Corresponding optical micrographs (1 month after preparation) of the emulsions. Scale bar = 200 μm.

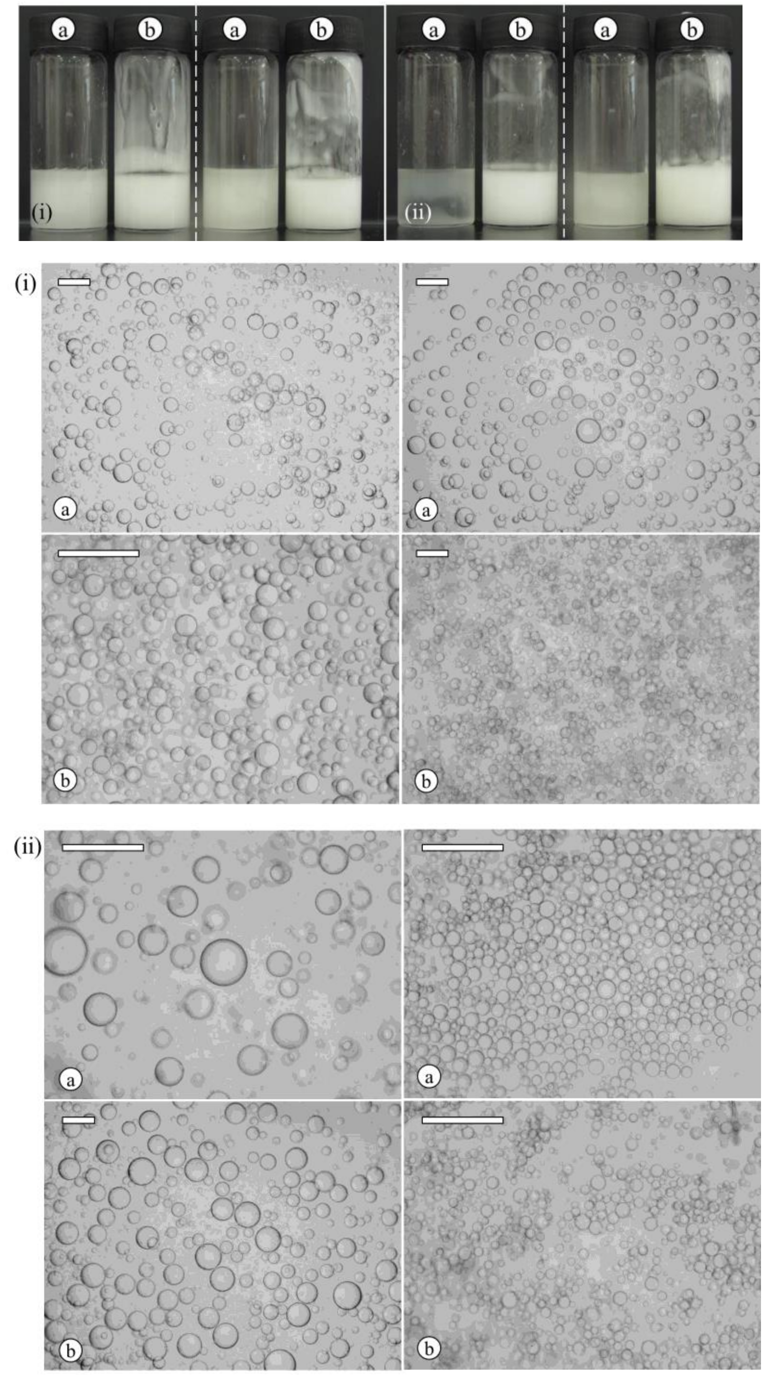

Table 4.2. Emulsion type, average droplet diameter (± standard deviation of 300 droplets), estimated fraction of vegetable oil f_{vo} and PDMS oil $f_{\mathrm{PDMS\ oil}}$ released from the emulsions (1 month after preparation) described in Figures 4.21−4.23. $f_{\mathrm{PDMS\ oil}}$ and f_{vo} provide a measure of the stability of the emulsions to creaming and coalescence, respectively, for PDMS oil continuous emulsions. For vegetable oil continuous emulsions, $f_{\mathrm{PDMS\ oil}}$ indicates stability to coalescence and f_{vo} indicates stability to sedimentation. The propagation error in values of $f_{\mathrm{PDMS\ oil}}$ and $f_{\mathrm{vo}} \approx 0.002$.

Emulsion	Average droplet diameter/μm	f_{vo}	$f_{\mathrm{PDMS\ oil}}$
Particles initially in the PDMS oil phase			
1 wt. % of 75% SiOH fluorinated fumed silica			
Sunflower oil-in-PDMS 20 cS	73 ± 40	≈ 1	≈ 1
PDMS 50 cS-in-sunflower oil	53 ± 17	0.2	0
PDMS 100 cS-in-sunflower oil	53 ± 15	0.2	0
Olive oil-in-PDMS 20 cS	58 ± 24	≈ 1	≈ 1
PDMS 50 cS-in-olive oil	61 ± 18	0.1	0
PDMS 100 cS-in-olive oil	65 ± 20	0.1	0
Rapeseed oil-in-PDMS 20 cS	22 ± 12	≈ 1	≈ 1
PDMS 50 cS-in-rapeseed oil	67 ± 22	0.1	0
PDMS 100 cS-in-rapeseed oil	72 ± 20	0.2	0
1 wt. % of 51% SiOH DCDMS-coated fumed silica			
PDMS 50 cS-in-sunflower oil	61 ± 20	0.03	0
PDMS 100 cS-in-olive oil	53 ± 22	0.05	0
1 wt. % of 14% SiOH DCDMS-coated fumed silica			
Sunflower oil-in-PDMS 50 cS	29 ± 12	0	0
Olive oil-in-PDMS 100 cS	45 ± 14	0	0
Particles initially in the vegetable oil phase			
1 wt. % of 75% SiOH fluorinated fumed silica			
Sunflower oil-in-PDMS 20 cS	37 ± 20	≈ 1	≈ 1
PDMS 50 cS-in-sunflower oil	39 ± 12	0	0
PDMS 100 cS-in-sunflower oil	35 ± 12	0.004	0
olive oil-in-PDMS 20 cS	39 ± 25	≈ 1	≈ 1
PDMS 50 cS-in-olive oil	64 ± 17	0.004	0
PDMS 100 cS-in-olive oil	50 ± 13	0.004	0
Rapeseed oil-in-PDMS 20 cS	81 ± 39	≈ 1	≈ 1
PDMS 50 cS-in-rapeseed oil	49 ± 15	0.004	0
PDMS 100 cS-in-rapeseed oil	42 ± 13	0.01	0
1 wt. % of 51% SiOH DCDMS-coated fumed silica			
PDMS 50 cS-in-sunflower oil	45 ± 29	≈ 1	≈ 1
PDMS 100 cS-in-olive oil	74 ± 33	0.01	0
1 wt. % of 14% SiOH DCDMS-coated fumed silica			
Sunflower oil-in-PDMS 50 cS	26 ± 8	0	0
Olive oil-in-PDMS 100 cS	21 ± 7	0	0

4.3 Oil-in-Oil Emulsions Containing Equal Volume Fraction of Oils Stabilised by Fluorinated Platelet Clay Particles

The PF-5 Eight Pearl 300S-Al fluorinated sericite particles were also used to prepare o/o emulsions comprising of equal volumes (5 cm^3) of vegetable and PDMS oils. The powdered particle method was used to make the emulsions. Unlike with the 75% SiOH fluorinated fumed silica particles where relatively stable o/o emulsions were obtained with many of the vegetable oil-PDMS oil combinations especially at relatively high particle concentrations, none of these combinations yielded a relatively stable o/o emulsion in the presence of the PF-5 Eight Pearl 300S-Al sericite particles even at high particle concentrations. Photographs of glass vials containing the emulsions are shown in Figures 4.24, 4.26 and 4.28 along with their optical micrographs. The emulsions obtained are also white, polydisperse and unflocculated. They are all vegetable oil-in-PDMS oil emulsions compared with the fluorinated fumed silica particle-stabilised ones where a transitional phase inversion resulted on going from PDMS 20 cS to PDMS 50 and 100 cS, yielding vegetable oil continuous emulsions. For sunflower and rapeseed oil-PDMS 100 cS combinations, the emulsions were kinetically very unstable within the particle concentration studied and separated out completely into the component phases within a month with the particles being largely in the PDMS oil phase (Figures 4.24 and 4.26). The rest of the vegetable oil-in-PDMS oil emulsions were also kinetically unstable, but did not separate out completely into their component phases especially at relatively high particle concentrations. Unlike the fumed silica-stabilised emulsions which are made up of relatively small (micrometer-size) oil droplets, these emulsions are composed of relatively large oil droplets of average droplet diameter of > 0.2 mm. In fact, at relatively low particle concentrations (≤ 0.5 wt. %), the emulsion droplets are large enough to be seen with the eye. The stability of the emulsions to creaming and coalescence is given in Figures 4.25, 4.27 and 4.29 in terms of $f_{\mathrm{PDMS\ oil}}$ and f_{vo}, respectively. Generally, the stability of the emulsions to creaming and coalescence was seen to increase as the particle concentration increases. By and large, at relatively high particle concentrations (≥ 1 wt. %), the emulsions are completely stable to coalescence for over a month but still susceptible to creaming.

As mentioned in chapter 2, the effect of particle fluorination on the stability of the emulsions was investigated in the sunflower oil-PDMS 20 cS system. The powdered particle method was used to make the emulsions in the presence of 1 wt. % of PF-0 Eight Pearl 300S-Al, PF-5, 8, 10 and 12 Eight Pearl 300S-Al fluorinated sericite. The emulsions contain equal volumes (5 cm^3) of sunflower oil and PDMS 20 cS. Particle concentration is with respect to the total volume of PDMS 20 cS and sunflower oil in the emulsions. These emulsions (Figure 4.30) are also white, polydisperse and unflocculated. Whilst a very unstable sunflower oil-in-PDMS 20 cS emulsion was obtained with the unmodified sericite particles, the fluorinated ones formed relatively stable sunflower oil-in-PDMS 20 cS emulsions of the same kinetic stability. Even though the degree of fluorination of the particles differs significantly from each other as indicated by the estimated apparent γ_{sa}, $f_{\text{PDMS 20 cS}}$ released in a month ≈ 0.5 (Figure 4.31). The emulsions were all stable to coalescence and no vegetable oil was released.

Figure 4.24. (upper) Photographs of glass vials containing sunflower oil-in-PDMS (a) 20, (b) 50 and (c) 100 cS emulsions (1 month after preparation), stabilised by different concentrations (given, wt. %) of PF-5 Eight Pearl 300S-Al particles. The emulsions contain equal volumes (5 cm^3) of the oils and were prepared by the powdered particle method. (lower) Corresponding optical micrographs (1 month after preparation) of the emulsions stabilised by the given concentrations (wt. %) of PF-5 Eight Pearl 300S-Al particles. Also shown on the optical micrographs is the average droplet diameter of the emulsions (1 month after preparation). The emulsion droplet diameter is in the range of 113−885 μm (at 1 wt. % of particles) and 92−510 μm (at > 1 wt. % of particles).

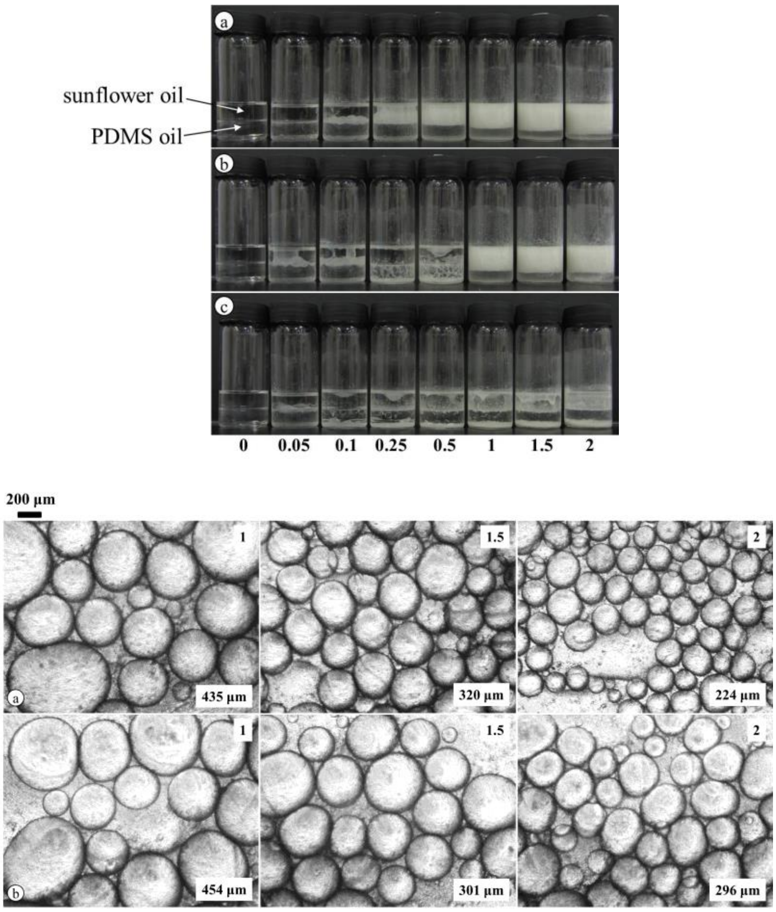

Figure 4.25. Fraction of sunflower oil f_{suno} (●) and fraction of PDMS oil $f_{\text{PDMS oil}}$ (○) released from sunflower oil-in-PDMS (a) 20 and (b) 50 cS emulsions (1 month after preparation) shown in Figure 4.24 *versus* [PF-5 Eight Pearl 300S-Al]. The $f_{\text{PDMS 20 cS}}$ ($f_{\text{PDMS 50 cS}}$) and f_{suno} represent the stability of the emulsions to creaming and coalescence respectively. The error bars represent propagation error.

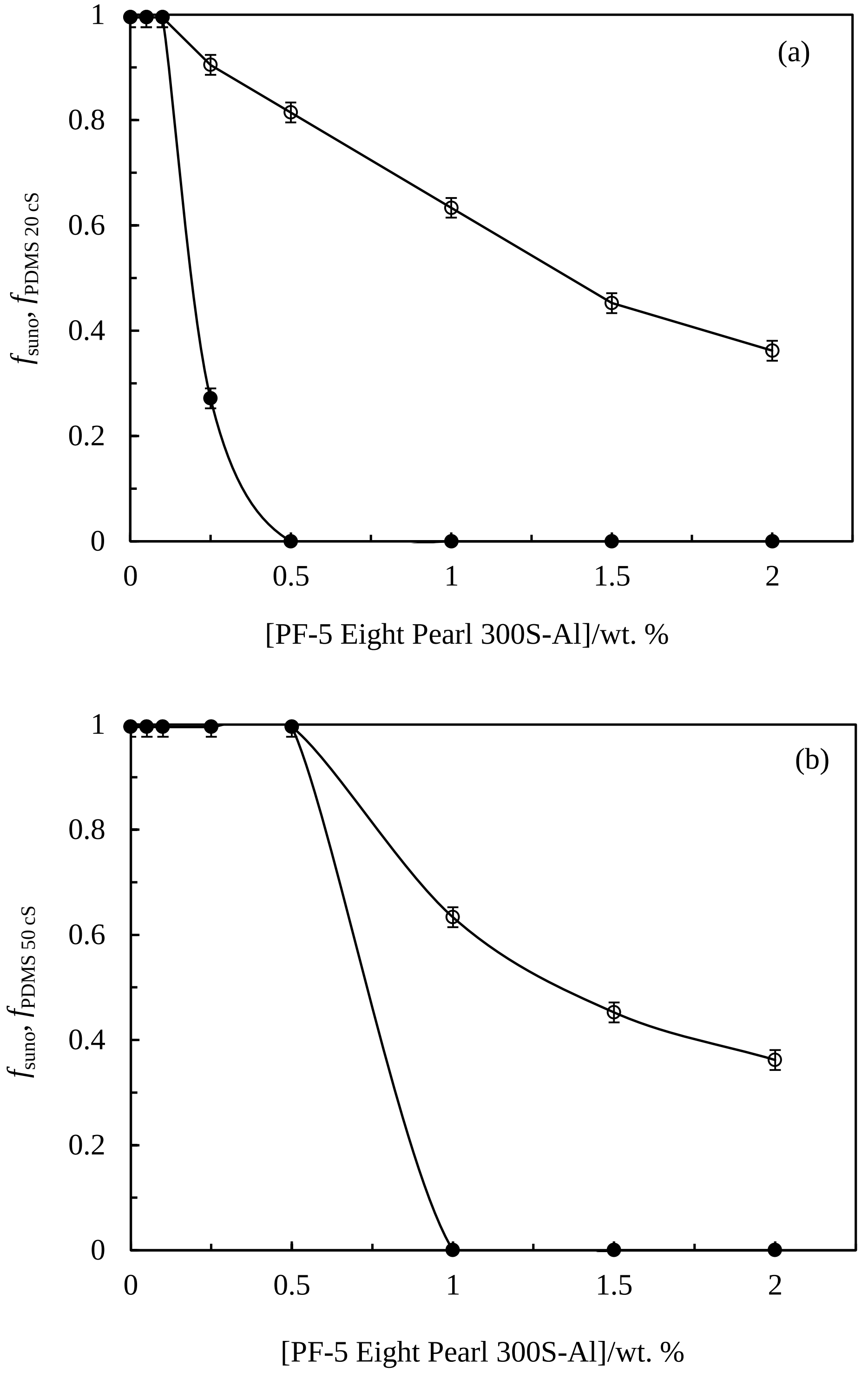

Figure 4.26. (upper) Photographs of glass vials containing rapeseed oil-in-PDMS (a) 20, (b) 50 and (c) 100 cS emulsions (1 month after preparation), stabilised by different concentrations (given, wt. %) of PF-5 Eight Pearl 300S-Al sericite particles. The emulsions contain equal volumes (5 cm^3) of the oils and were prepared by the powdered particle method. (lower) Corresponding optical micrographs (1 month after preparation) of the emulsions stabilised by the given concentrations (wt. %) of PF-5 Eight Pearl 300S-Al sericite particles. Also given on the optical micrographs is the average droplet diameter of the emulsions (1 month after preparation). The emulsion droplet diameter is in the range of 80−582 μm (at 1 wt. % of particles) and 46−407 μm (at > 1 wt. % of particles).

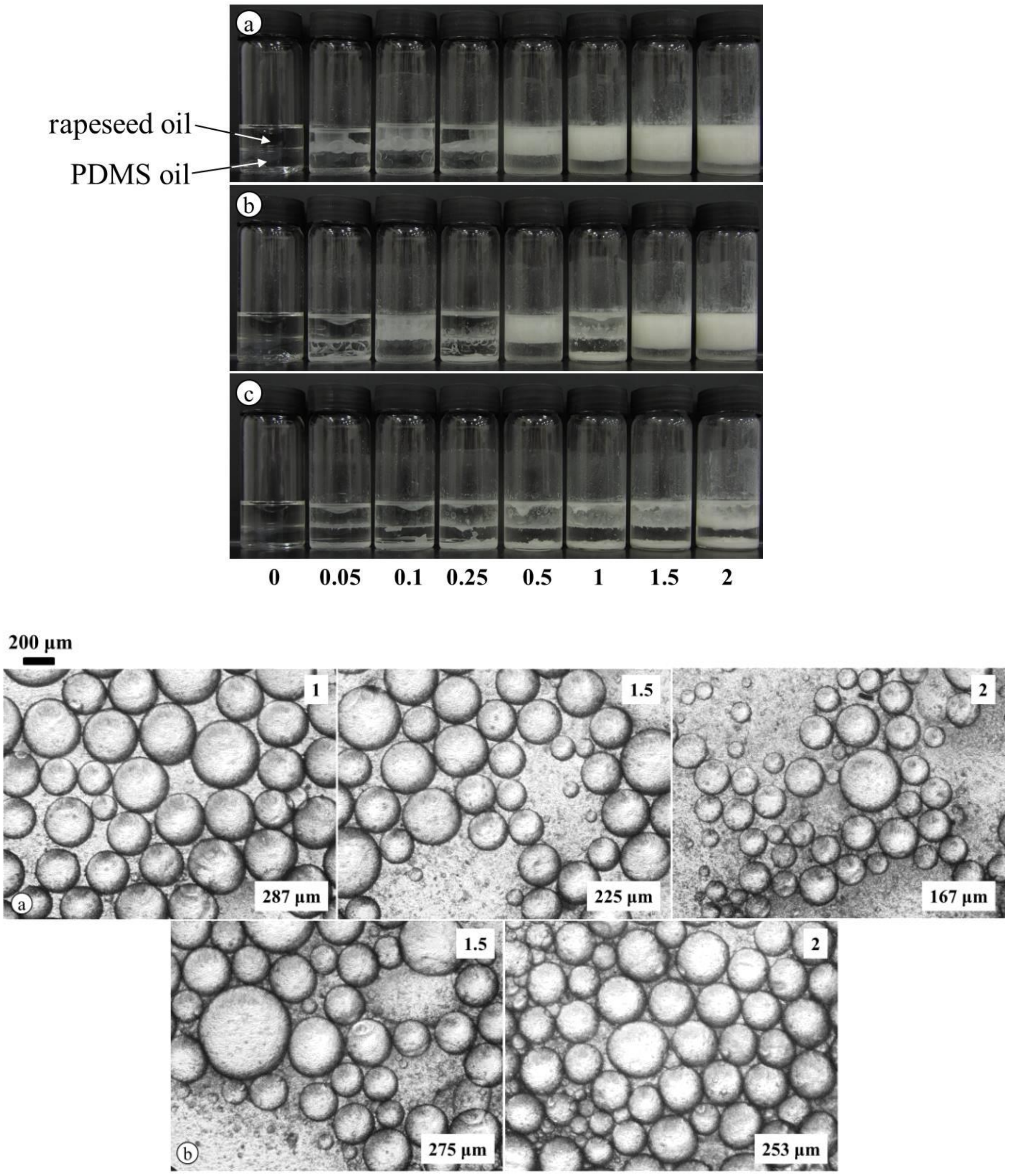

Figure 4.27. Fraction of rapeseed oil f_{ro} (●) and fraction of PDMS oil $f_{\mathrm{PDMS\ oil}}$ (○) released from rapeseed oil-in-PDMS (a) 20 and (b) 50 cS emulsions (1 month after preparation) shown in Figure 4.26 *versus* [PF-5 Eight Pearl 300S-Al]. The $f_{\mathrm{PDMS\ 20\ cS}}$ ($f_{\mathrm{PDMS\ 50\ cS}}$) and f_{ro} represent the stability of the emulsions to creaming and coalescence respectively. The error bars represent propagation error.

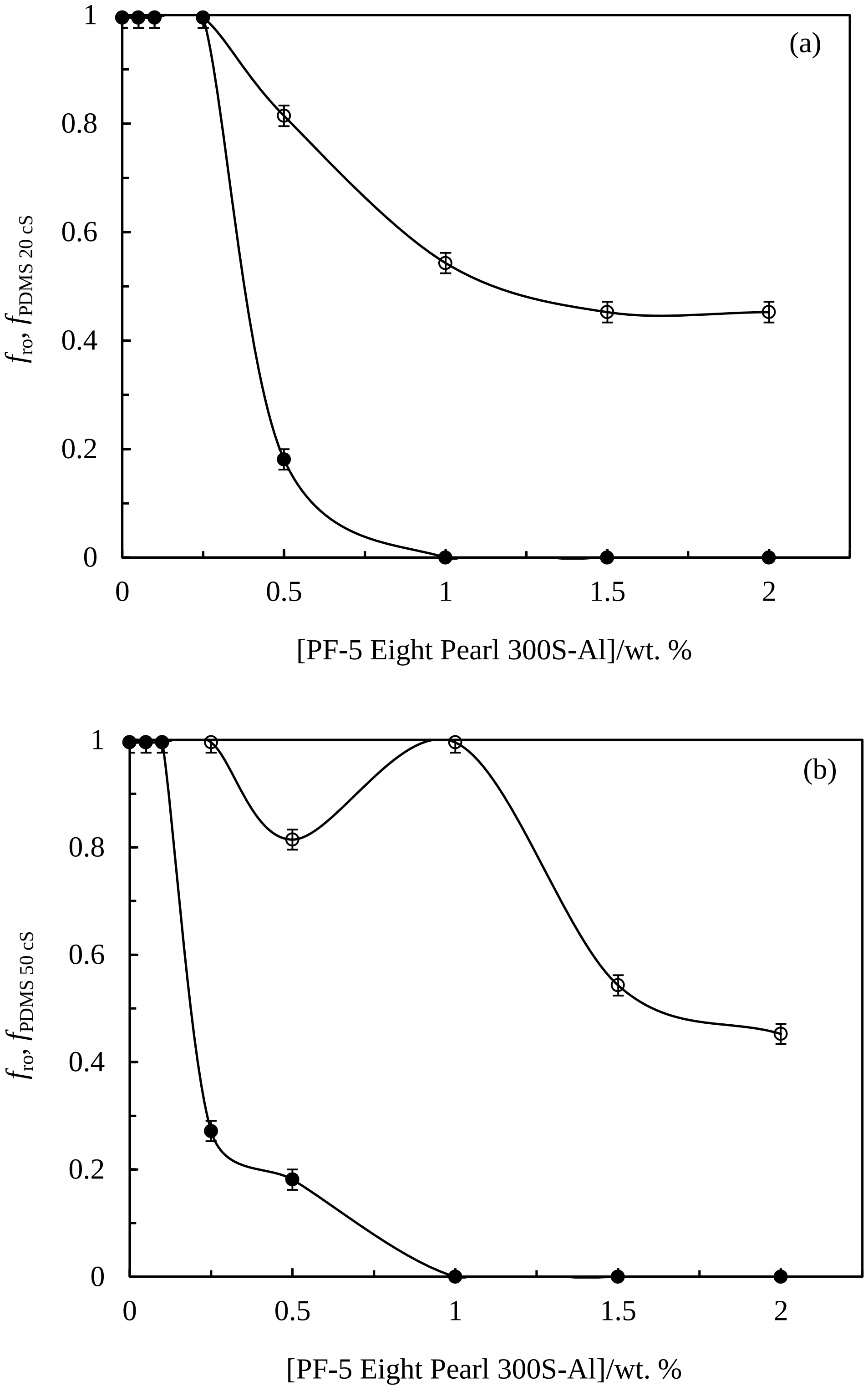

Figure 4.28. (upper) Photographs of glass vials containing olive oil-in-PDMS (a) 20, (b) 50 and (c) 100 cS emulsions (1 month after preparation), stabilised by different concentrations (given, wt. %) of PF-5 Eight Pearl 300S-Al sericite particles. The emulsions contain equal volumes (5 cm^3) of the oils and were prepared by the powdered particle method. (lower) Corresponding optical micrographs (1 month after preparation) of the emulsions stabilised by the given concentrations (wt. %) of PF-5 Eight Pearl 300S-Al particles. The average droplet diameter of the emulsions (1 month after preparation) is also given on the optical micrographs. The emulsion droplet diameter is in the range of 128−677 μm (at 1 wt. % of particles) and 73−411 μm (at > 1 wt. % of particles).

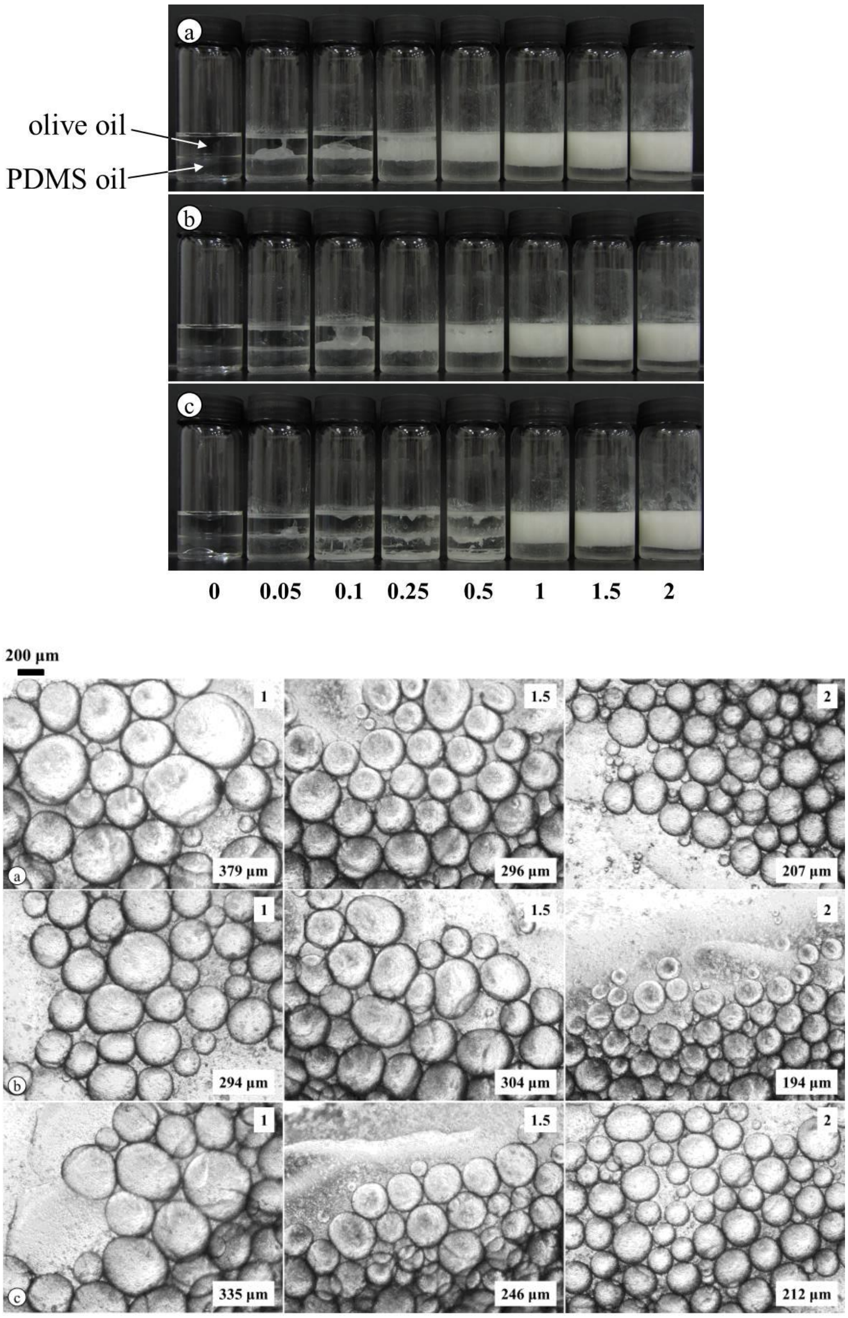

Figure 4.29. Fraction of olive oil f_{oo} (●) and fraction of PDMS oil $f_{\mathrm{PDMS\ oil}}$ (○) released from olive oil-in-PDMS (a) 20, (b) 50 and (c) 100 cS emulsions (1 month after preparation) shown in Figure 4.28 *versus* [PF-5 Eight Pearl 300S-Al]. The $f_{\mathrm{PDMS\ 20\ cS}}$, $f_{\mathrm{PDMS\ 50\ cS}}$ or $f_{\mathrm{PDMS\ 100\ cS}}$ and f_{oo} represent the stability of the emulsions to creaming and coalescence respectively. The error bars represent propagation error.

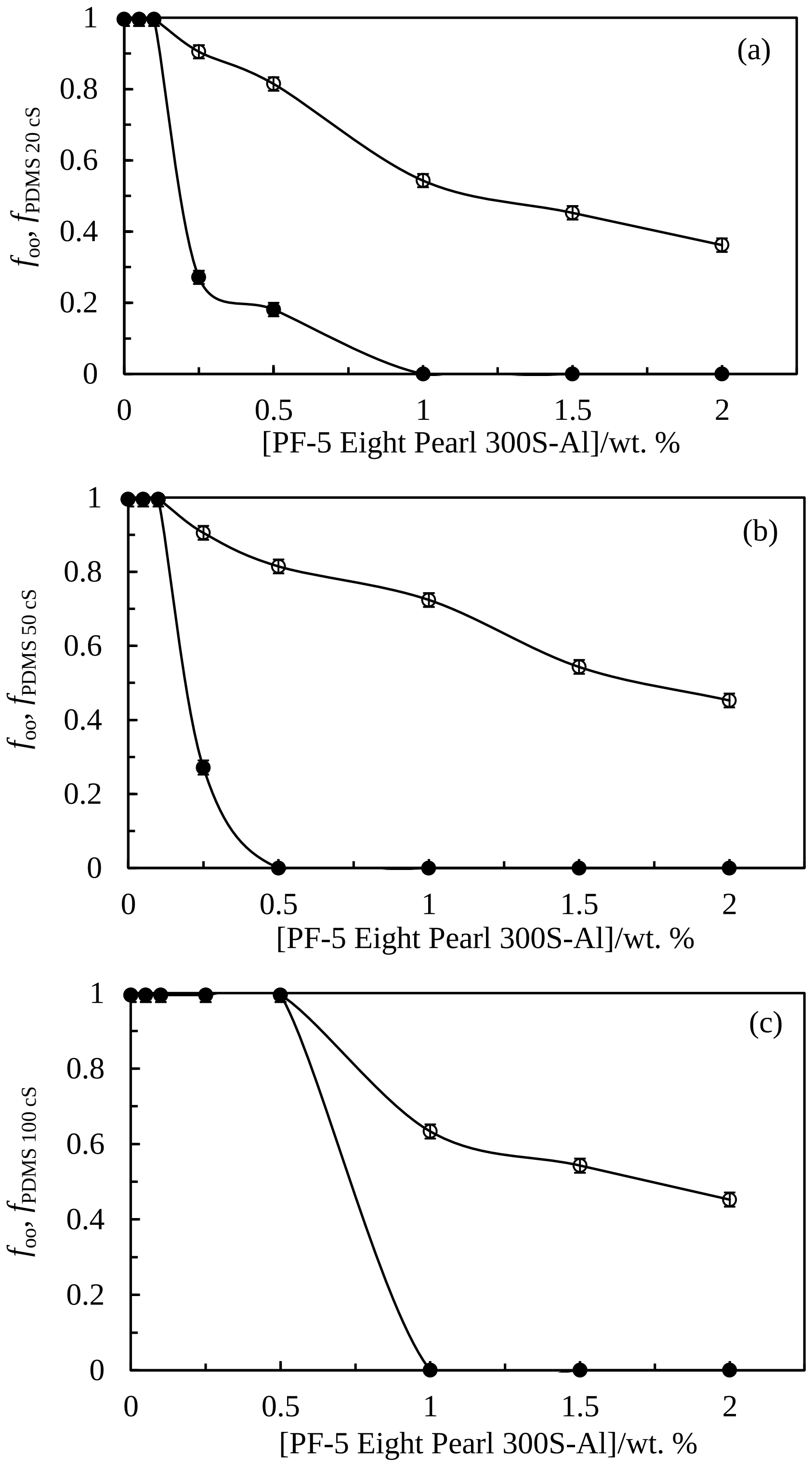

Figure 4.30. (upper) Photograph of glass vials containing sunflower oil-in-PDMS 20 cS emulsions (1 month after preparation) stabilised by 1 wt. % of (a) PF-0 Eight Pearl 300S-Al, PF-(b) 5, (c) 8, (d) 10 and (e) 12 Eight Pearl 300S-Al fluorinated sericite particles. Particle concentration is relative to the total volume of PDMS 20 cS and sunflower oil in the emulsions. The emulsions contain equal volumes (5 cm^3) of sunflower oil and PDMS 20 cS and were prepared by the powdered particle method. (lower) Corresponding optical micrographs (1 month after preparation) of the emulsions for PF-(a) 5, (b) 8, (c) 10 and (d) 12 Eight Pearl 300S-Al fluorinated sericite particle-stabilised emulsions. The average droplet diameter of 300 droplets (standard deviation ≈ 100 μm) of the emulsions is also shown on the optical micrographs.

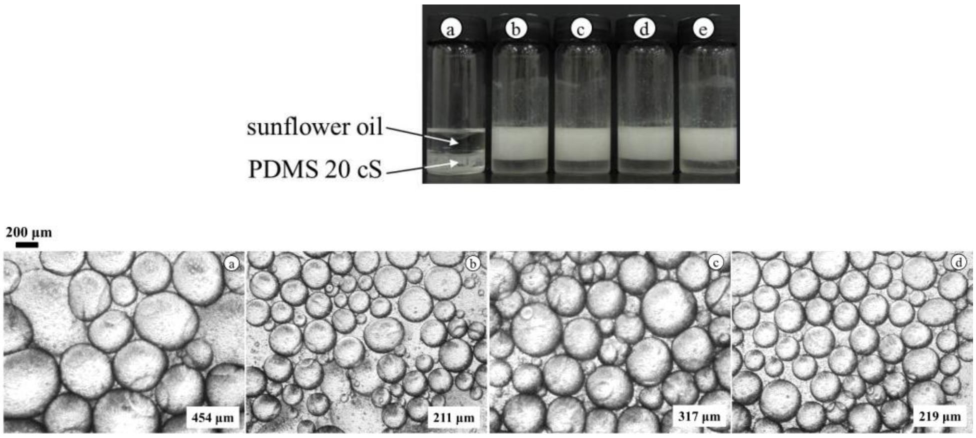

Figure 4.31. Fraction of PDMS 20 cS $f_{\mathrm{PDMS\ 20cS}}$ released from sunflower oil-in-PDMS 20 cS emulsions stabilised by 1 wt. % of PF-0 Eight Pearl 300S-Al and PF-5 to 12 Eight Pearl 300S-Al fluorinated sericite particles shown in Figure 4.30 *versus* apparent surface energy γ_{sa} of the particles. $f_{\mathrm{PDMS\ 20cS}}$ was measured 1 month after preparation of the emulsions as a measure of their stability to creaming. The emulsions were stable to coalescence for over a month and no sunflower oil was released. The error bars represent propagation error.

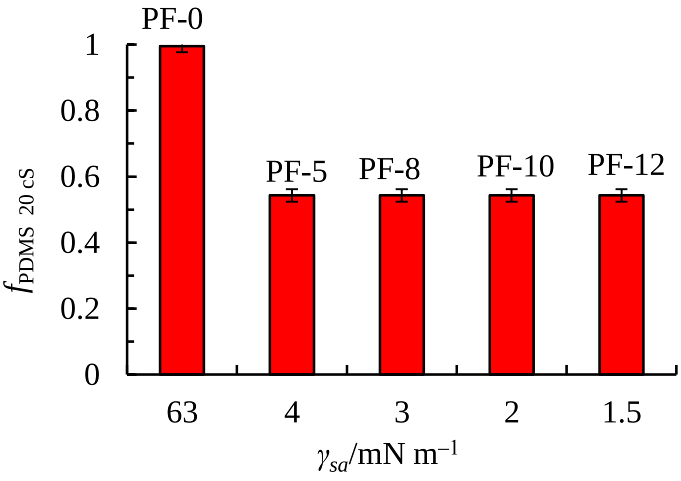

4.4 Sunflower oil-PDMS 20 cS Emulsions Stabilised by Fluorinated ZnO, Fluorinated Clay, Polytetrafluoroethylene, rod-shaped $CaCO_3$, Calofort SV and Bentone 34 Particles

Emulsions comprising of equal volumes (5 cm^3) of sunflower oil and PDMS 20 cS were also prepared in the presence of 1 wt. % of PFX-10 ZnO (TP), PFX-10 Kunipia F, PF-10 FSE-Al, PF-10 Eight Pearl 300S-Al^a, Bentone 34, PTFE, rod-shaped $CaCO_3$ or Calofort SV particles. The Particle concentration is with respect to the total volume of sunflower oil and PDMS 20 cS in the emulsions. PFX-10 Kunipia F and rod-shaped $CaCO_3$ particles are hydrophilic whilst the rest of the particles are hydrophobic. The aim of the study is to know whether these particles can also be used as sole stabilisers of o/o emulsions. The emulsions were prepared by the powdered particle method. The PFX-10 Kunipia F and rod-shaped $CaCO_3$ particles formed very unstable PDMS 20 cS-in-sunflower oil emulsions that separated out almost completely into their component phases within 4 days after preparation. The PF-10 Eight Pearl 300S-Al^a, PF-10 FSE-Al, PFX-10 ZnO (TP), PTFE, Calofort SV and Bentone 34 particles formed sunflower oil-in-PDMS 20 cS. These emulsions (Figure 4.32) are also white, polydisperse and unflocculated with average droplet diameter of > 0.2 mm except the Calofort SV particle-stabilised emulsion whose droplets are non-spherical. The possible reasons for formation of non-spherical emulsion droplets have been discussed in chapeter 3 (sec. 3.7). The Bentone 34 particle-stabilised emulsion was also very unstable and separated out almost completely into its component phases within 4 days after preparation. Apart from the PFX-10 ZnO (TP) particle-stabilised emulsion which released about 10 v/v. % of sunflower oil, the rest of the emulsions were completely stable to coalescence for over a month and did not release sunflower oil. However, these emulsions released > 50 v/v. % of PDMS 20 cS due to creaming as shown in Figure 4.33.

For the sunflower oil-PDMS 20 cS system studied, the hydrophilic particles prefer to stabilise PDMS 20 cS-in-sunflower oil emulsions whilst the hydrophobic ones prefer to stabilise sunflower oil-in-PDMS 20 cS emulsions. The former emulsions are very unstable compared with the latter ones. The origin of this difference is not clear as the particles are of different shape, size and chemical composition, but might be due to the wettability of the particles.

Figure 4.32. (upper) Photograph of glass vials containing (i) PDMS 20 cS-in-sunflower oil emulsions stabilised by 1 wt. % of (a) rod-shaped $CaCO_3$ and (b) PFX-10 Kunipia F particles and (ii) sunflower oil-in-PDMS 20 cS emulsions stabilised by 1 wt. % of (a) PFX-10 ZnO (TP), (b) PF-10 Eight Pearl 300S-Al^a, (c) PF-10 FSE-Al, (d) Bentone 34, (e) PTFE and (f) Calofort SV particles. The emulsions were prepared by the powdered particle method and they contain equal volumes (5 cm^3) of the oils. (lower) Corresponding optical micrographs of the sunflower oil-in-PDMS 20 cS emulsions stabilised by (a) PF-10 Eight Pearl 300S-Al^a, (b) PF-10 FSE-Al and (c) Calofort SV particles. The photograph and optical micrographs were obtained 1 month after preparation of the emulsions. Also shown on the optical micrographs of the PF-10 Eight Pearl 300S-Al^a and PF-10 FSE-Al particle-stabilised emulsions are the average droplet diamater of 300 droplets (standard deviation ≈ 100 μm) of the emulsions.

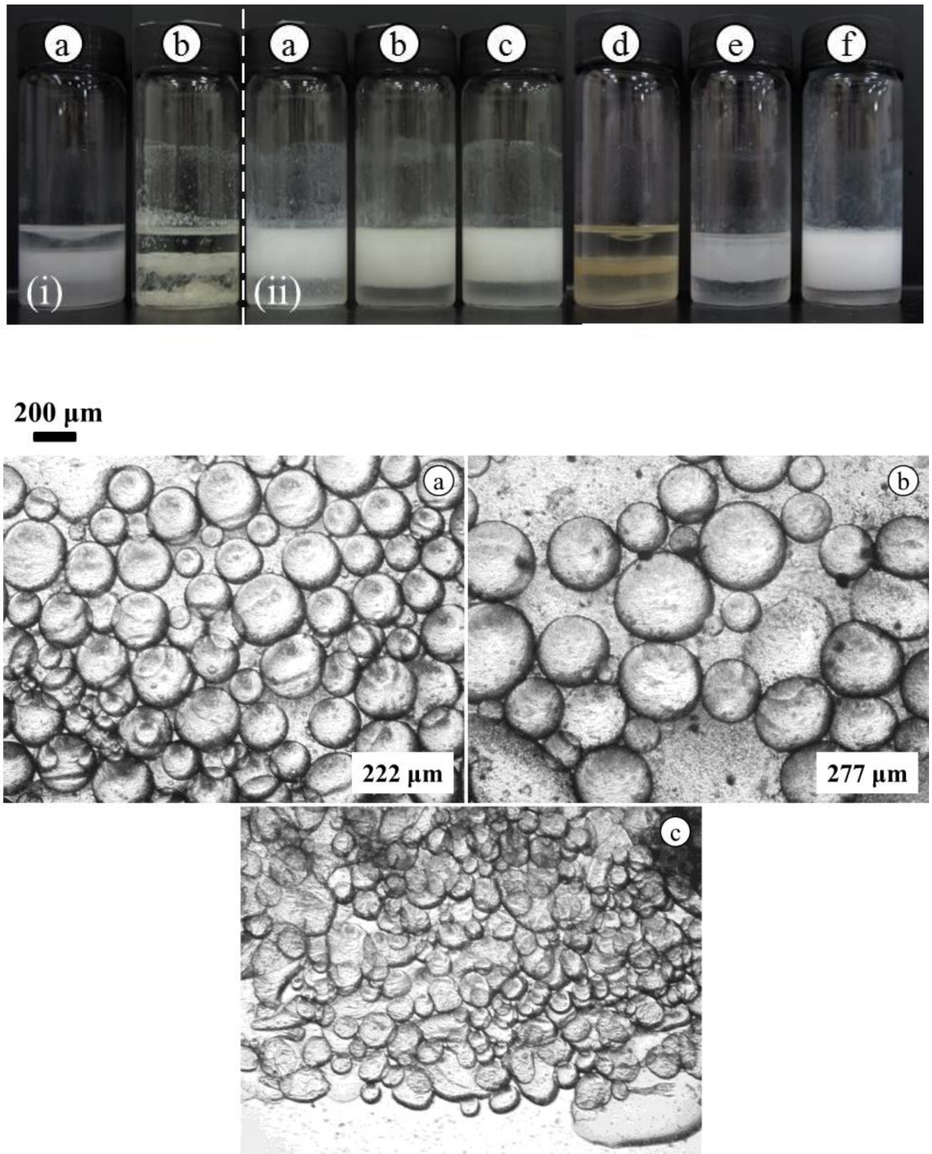

Figure 4.33. Fraction of PDMS 20 cS $f_{\mathrm{PDMS\ 20cS}}$ released from sunflower oil-PDMS 20 cS emulsions stabilised by 1 wt. % of solid particles (given) shown in Figure 4.32 *versus* (a) apparent surface energy of the particles and (b) other (particles) given. The emulsions are PDMS 20 cS-in-sunflower oil (for PFX-10 Kunipia F and rod-shaped $CaCO_3$) or sunflower oil-in-PDMS 20 cS (for all other particles). $f_{\mathrm{PDMS\ 20\ cS}}$ was measured 1 month after preparation of the emulsions as a measure of the stability of the emulsions to creaming or coalescence. The error bars represent propagation error.

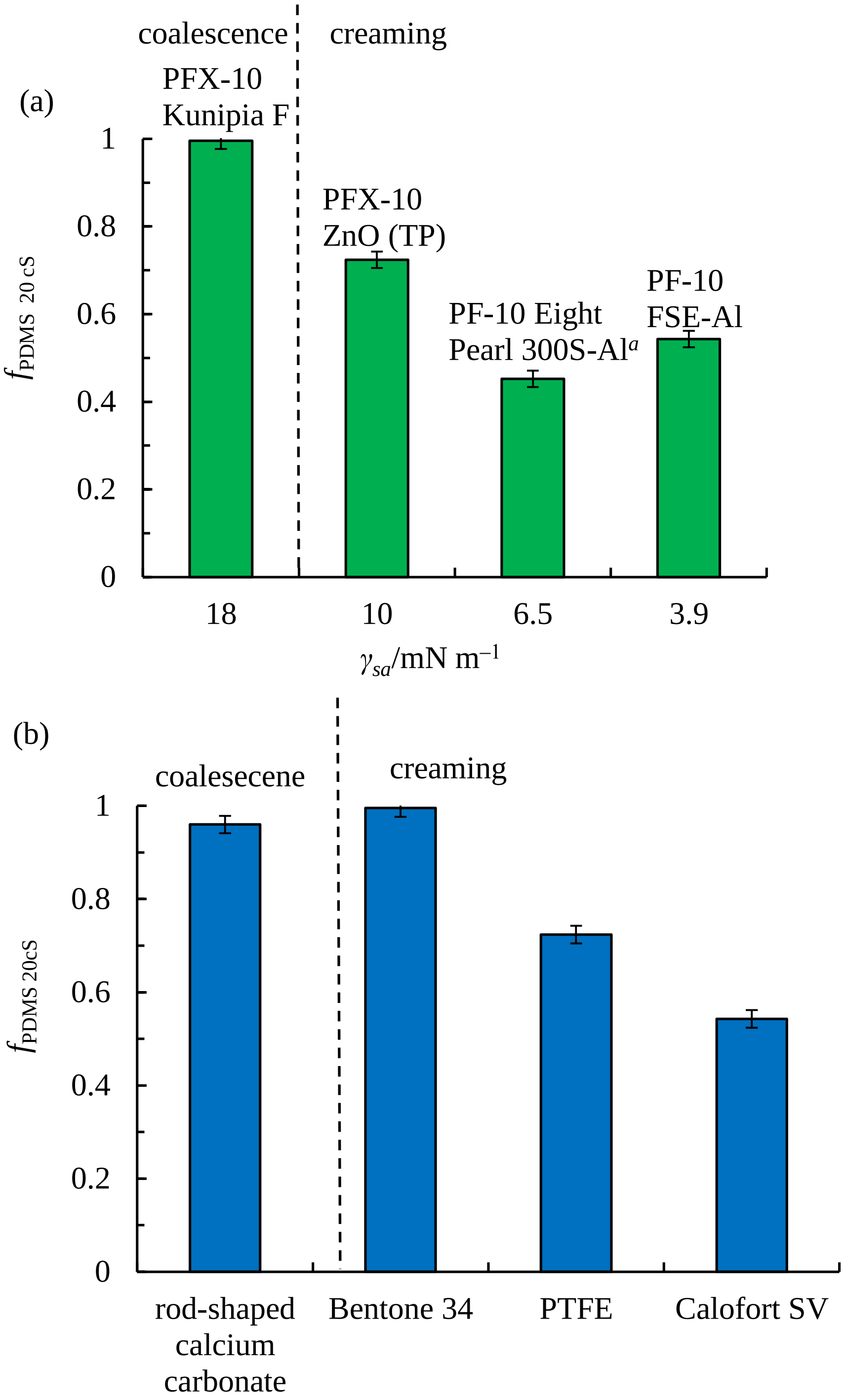

4.5 Oil-Oil Emulsions Containing Varying Volume Fraction of Sunflower Oil and PDMS 50 cS Stabilised by Fluorinated Silica and Fluorinated Sericite Particles

Using ternary phase diagrams, Nonomura *et al.*[38,39,60] have shown that ten different materials (inclusive of emulsions) can be obtained from shearing solid particle/liquid-1/liquid-2 mixtures depending on the fraction of the components of the mixture. Apart from emulsions which can exist in the presence of an excess phase of one of the liquids, these materials can be a 'powder' if the fraction of liquid-1 and 2 are relatively low compared with the solid particles and as such the powder contains liquid-1 and 2 in the inner spaces between the solid particles or a 'separated liquid' in which a transparent liquid is separated from the powdered mixture. Some of these materials were also observed in this work upon varying the volume fraction of sunflower oil ϕ_{suno} between 0.05 and 0.9 in sunflower oil-PDMS 50 cS system in the presence of 1 wt. % of 75% SiOH fluorinated fumed silica or PF-5 Eight Pearl 300S-Al fluorinated sericite particles. The particle concentration is with respect to the total volume (10 cm^3) of sunflower oil and PDMS 50 cS in the emulsions. Photographs of glass vials containing these systems are shown in Figure 4.34 and their optical microscope images at selected ϕ_{suno} are shown in Figure 4.35. Catastrophic phase inversion was induced upon increasing ϕ_{suno}. For the 75% SiOH fluorinated fumed silica/sunflower oil/PDMS 50 cS mixtures, catastrophic phase inversion was observed at ϕ_{suno} of between 0.4 and 0.5. Initially, a 'separated oil state,' a sunflower oil-in-PDMS 50 cS emulsion and a multiple emulsion were formed at $\phi_{\text{suno}} \leq 0.1$, (0.2 and 0.4) and 0.3 respectively. The multiple emulsion dispersed readily in PDMS 50 cS. PDMS 50 cS-in-sunflower oil emulsions were then observed at $\phi_{\text{suno}} > 0.4$ due to catastrophic phase inversion. These emulsions are white. The droplets of the multiple and the simple emulsions are polydisperse and looked somewhat flocculated in some cases. The sunflower oil-in-PDMS 50 cS emulsion at $\phi_{\text{suno}} = 0.2$ was unstable, but had no clear phase separation. At $\phi_{\text{suno}} = 0.4$, the sunflower oil-in-PDMS 50 cS emulsion was stable to coalescene for over a month but prone to creaming and released ≈ 75 v/v. % of PDMS 50 cS within a month. The multiple emulsion was stable to coalescence for over a month, but susceptible to creaming and as such released ≈ 52 v/v. % of PDMS 50 cS within a month. The PDMS 50 cS-in-sunflower oil emulsions were also stable to coalescence for over a month, but prone to sedimentation and the degree of sedimentation was observed to increase as ϕ_{suno} increases (Figure 4.36). Catastrophic phase inversion was seen at ϕ_{suno} of between 0.5 and 0.6 for the PF-5 Eight Pearl 300S-Al fluorinated sericite particles/sunflower oil/PDMS 50 cS mixtures. However, unlike with the 75% SiOH fluorinated silica, only sunflower oil-in-PDMS

50 cS and PDMS 50 cS-in-sunflower oil emulsions were obtained. At $\phi_{\mathrm{suno}} \leq 0.1$, the sunflower oil-in-PDMS 50 cS emulsions occurred in the presence of excess PDMS 50 cS. The emulsions at $\phi_{\mathrm{suno}} = 0.2–0.5$ were susceptible to creaming, but stable to coalescence for over a month. The degree of creaming in the emulsions was seen to decrease with increasing ϕ_{suno} (Figure 4.37). PDMS 50 cS-in-sunflower oil emulsions occurred at $\phi_{\mathrm{suno}} > 0.5$ due to catastrophic phase inversion. These emulsions were very unstable and separated out completely into their component phases within a week. The average droplet diameter of the fluorinated silica particle-stabilised PDMS 50 cS-in-sunflower oil emulsions and the PF-5 Eight Pearl 300S-Al particle-stabilised sunflower oil-in-PDMS 50 cS emulsions are plotted in Figure 4.38 as a function of ϕ_{suno} in the emulsions. The average droplet diameter of the latter emulsions was seen to decrease with increasing ϕ_{suno} whilst that of the former emulsions increased as ϕ_{suno} increases.

Figure 4.34. Photographs of glass vials containing (a) a 'separated oil state', sunflower oil-in-PDMS 50 cS, PDMS 50 cS-in-sunflower oil or multiple emulsions stabilised by 1 wt. % of 75% SiOH fluorinated silica particles and (b) sunflower oil-in-PDMS 50 cS or PDMS 50 cS-in-sunflower oil emulsions stabilised by 1 wt. % of PF-5 Eight Pearl 300S-Al fluorinated sericite particles containing varying volume fraction of sunflower oil ϕ_{suno} (given). The photographs were taken 1 month after preparation of the materials.

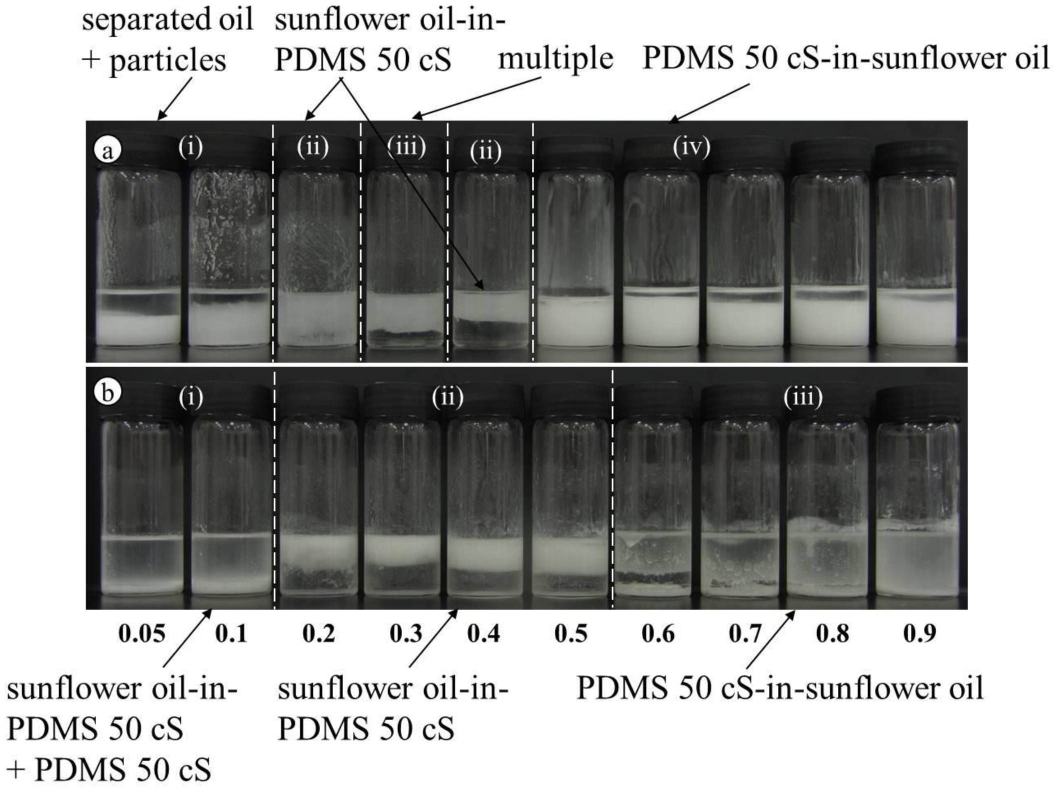

Figure 4.35. Corresponding optical micrographs (1 month after preparation) of the systems shown in Figure 4.34 at selected ϕ_{suno} (given). (a) 75% SiOH fluorinated silica-stabilised materials and (b) PF-5 Eight Pearl 300S-Al fluorinated particle-stabilised materials. Scale bar represents 100 μm.

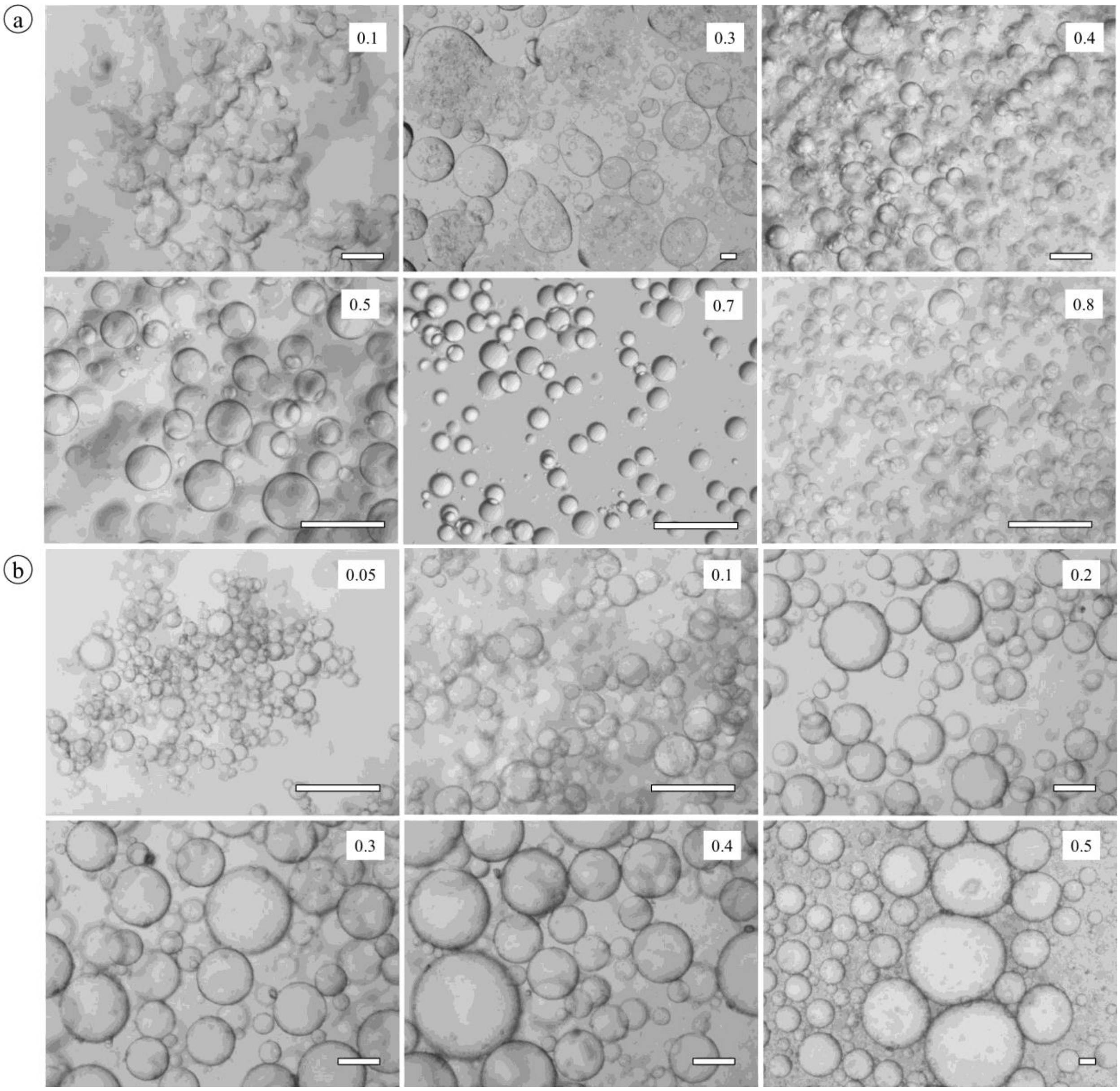

Figure 4.36. (a) Fraction of PDMS 50 cS $f_{\mathrm{PDMS\ 50cS}}$ (◇) and (b) fraction of sunflower oil f_{suno} (●) released from sunflower oil-PDMS 50 cS emulsions shown in Figure 4.34 (1 month after preparation) stabilised by 1 wt. % of 75% SiOH fluorinated silica particles *versus* volume fraction of sunflower oil ϕ_{suno} in the emulsions. The propagation error in the estimated values of $f_{\mathrm{PDMS\ 50cS}}$ and f_{suno} is ≈ ± 0.02. The emulsions (sunflower oil-in-PDMS 50 cS and PDMS 50 cS-in-sunflower oil) are separated by the dotted vertical line.

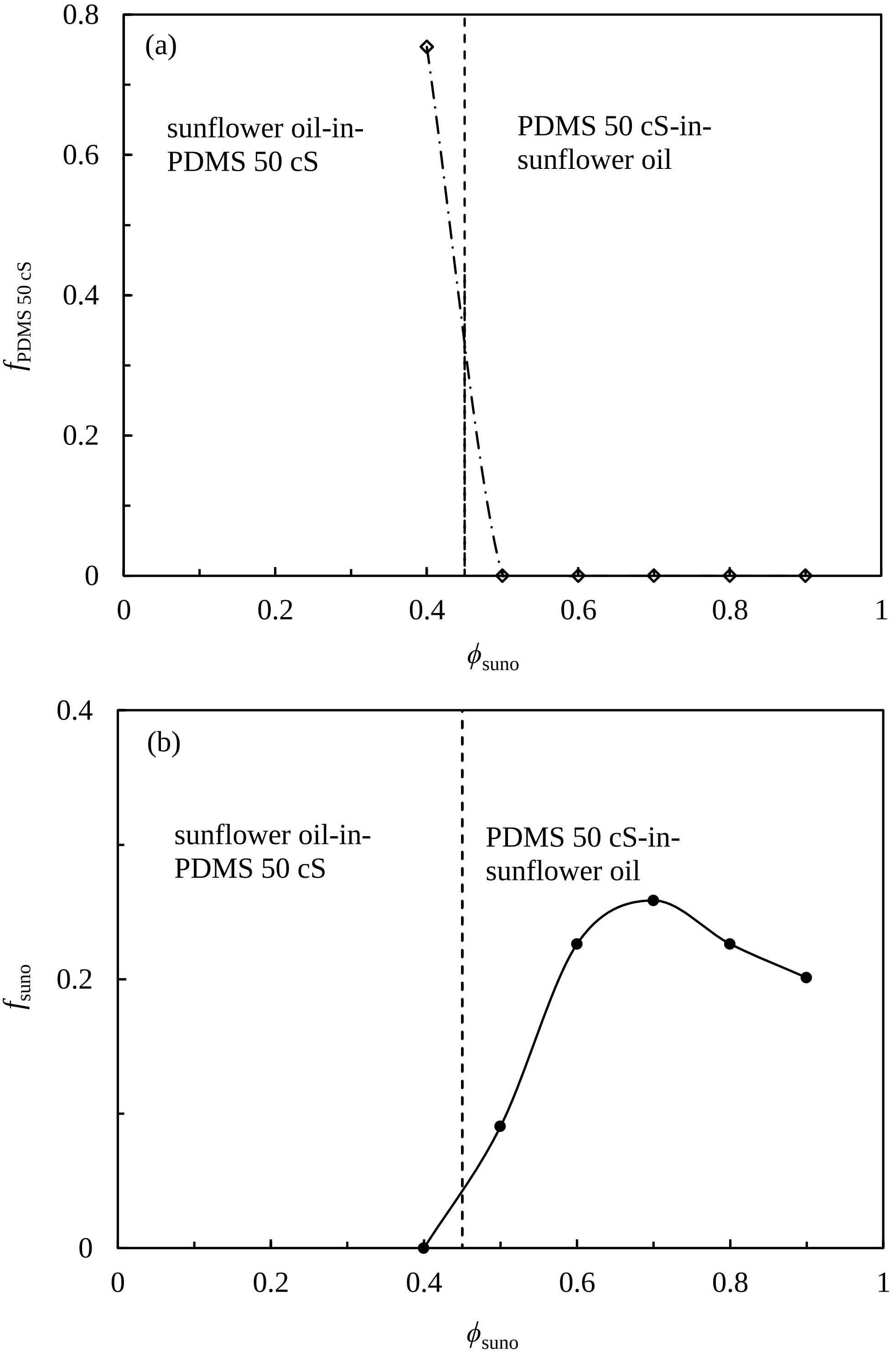

Figure 4.37. (a) Fraction of PDMS 50 cS $f_{\text{PDMS 50cS}}$ (○) and (b) fraction of sunflower oil f_{suno} (×) released from sunflower oil-PDMS 50 cS emulsions shown in Figure 4.34 (1 month after preparation) stabilised by 1 wt. % of PF-5 Eight Pearl 300S-Al fluorinated sericite particles *versus* volume fraction of sunflower oil ϕ_{suno} in the emulsions. The propagation error in the estimated values of $f_{\text{PDMS 50cS}}$ and f_{suno} is ≈ ± 0.02. The emulsions (sunflower oil-in-PDMS 50 cS and PDMS 50 cS-in-sunflower oil) are separated by the dotted vertical line.

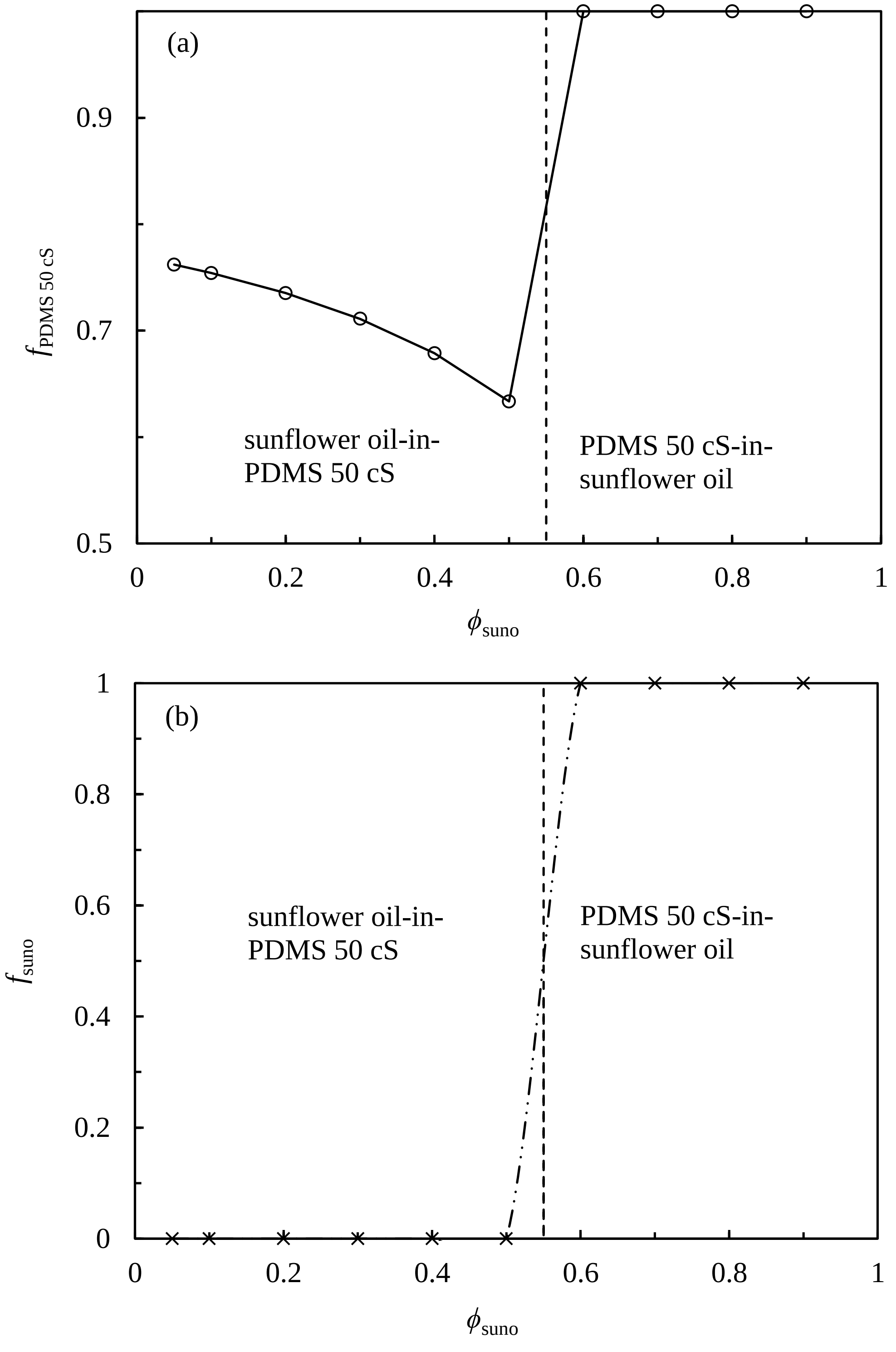

Figure 4.38. Average droplet diameter of 300 droplets of PDMS 50 cS-in-sunflower oil emulsions (1 month after preparation) stabilised by 1 wt. % of 75% SiOH fluorinated fumed silica (○) and sunflower oil-in-PDMS 50 cS emulsions (1 month after preparation) stabilised by 1 wt. % of PF-5 Eight Pearl 300S-Al fluorinated sericite (●) shown in Figure 4.34 *versus* volume fraction of sunflower oil ϕ_{suno} in the emulsions. The standard deviation of the measurements increases from 6 μm (ϕ_{suno} = 0.05) to 100 μm (ϕ_{suno} = 0.5) for the PDMS 50 cS-in-sunflower oil emulsions, but decreases from 17 μm (ϕ_{suno} = 0.5) to 2 μm (ϕ_{suno} = 0.9) for the sunflower oil-in-PDMS 50 cS emulsions.

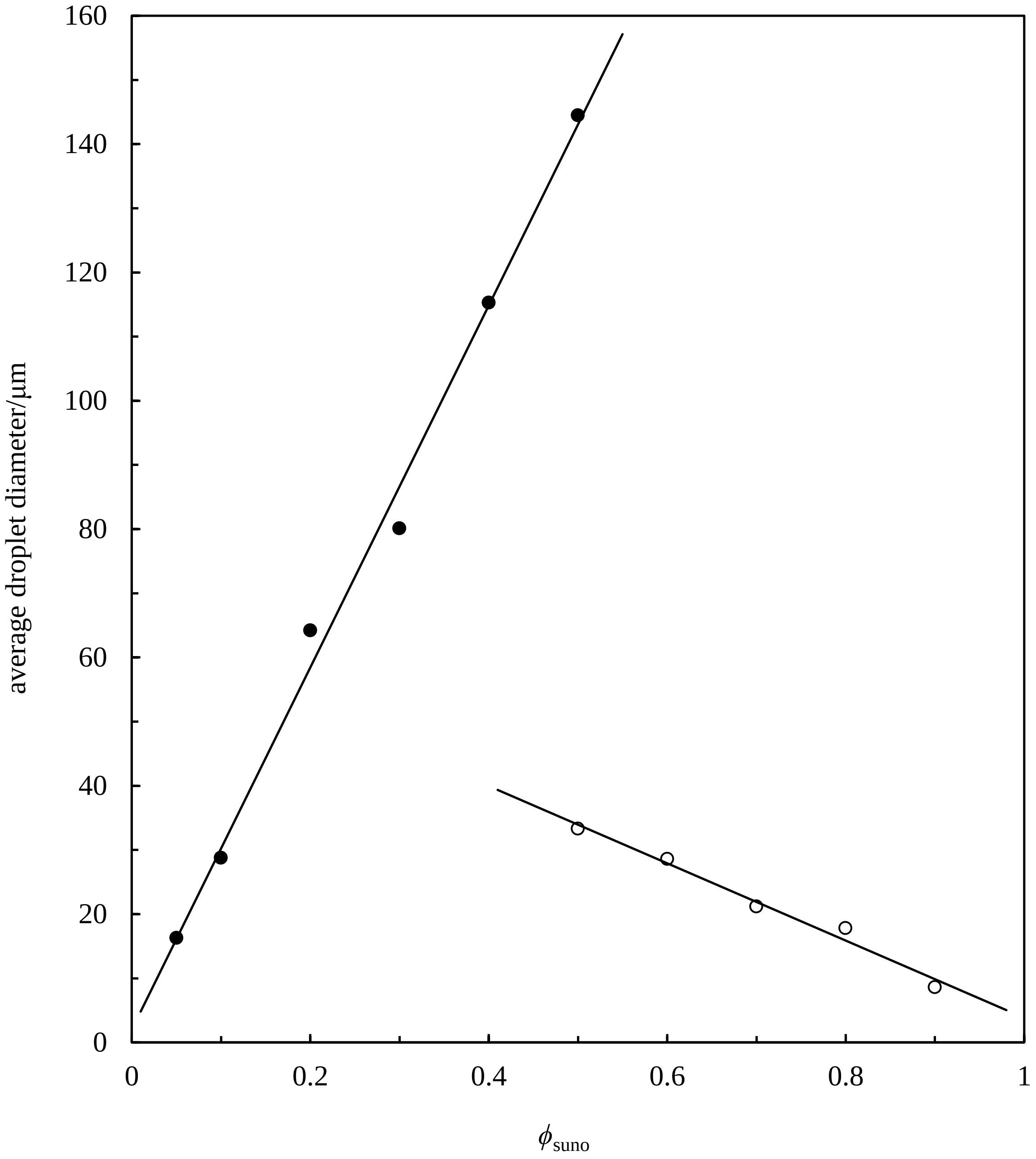

4.6 Solid Particle-Oil-Oil Three-Phase Contact Angles and Emulsion Type

The values of θ_{oo} (through PDMS oil) for the sunflower (olive) oil/PDMS oil/DCDMS-coated fumed silica particle systems calculated by using equation 2.15 are given in Appendix 4. The θ_{oo} increases as the % SiOH on the fumed silica particles increases (Figure 4.39). This is in contrast to oil/water/silica particle systems where the θ_{ow} decreases with increasing % SiOH on the silica particle surfaces.[61] Obviously, the calculated θ_{oo} values (as low as 0° and as high as 180°) for the above-named systems are unrealistic and do not correlate with the type of emulsions stabilised by some of the fumed silica particles. For example, they predict sunflower oil-in-PDMS oil at low % SiOH and PDMS oil-in-sunflower oil at high % SiOH but did not predict the position of inversion. In addition, they are sensitive to the γ_o^p and γ_o^d of the vegetable oils and PDMS oils tensions (which are not known precisely) as shown in Figure 4.40 for sunflower oil-PDMS 20 cS system and cannot be trusted. Figure 4.40 shows that calculated values of θ_{oo} increase with increasing γ_o^p of sunflower oil, but decrease with increasing γ_o^p of PDMS 20 cS. As a result, the position of inversion (θ_{oo} = 90°) varies. The θ_o of the individual oils in air and of θ_{oo} of the PDMS oils in sunflower/olive oil, measured on hydrophilic and DCDMS-coated glass slides (through the PDMS oil phase) and the type of emulsion obtained in any sunflower/olive oil-PDMS oil combinations are given in Table 4.3. As envisaged, for PDMS oil-sunflower/olive oil systems where $\theta_{oo} < 90°$ (> 90°), sunflower/olive oil-in-PDMS oil (PDMS oil-in-sunflower/olive oil) emulsions were obtained. The only exceptions are sunflower oil/PDMS 100 cS/14% SiOH silica and olive oil/PDMS 50 cS/14% SiOH silica where relatively unstable multiple emulsions were rather obtained. This finding is consistent with the principle developed by Finkle *et al.*[16] in aqueous systems which says that ‘in a mixture of two liquid phases and solid particles, the liquid phase wetting the particles less (more) becomes the dispersed (continuous) phase when the mixture is homogenised.’ This is the first time this principle has been verified in oil/oil/particle systems.

Figure 4.39. Plot of θ_{oo} (through PDMS oil) *versus* % SiOH on DCDMS-coated fumed silica particle surfaces for sunflower oil-PDMS 20 cS (diamonds), sunflower oil-PDMS 50 cS (circles) and sunflower oil-PDMS 100 cS (triangles) systems calculated by using equation 2.15 for measured (filled symbols) and calculated (open symbols) $\gamma_{o_1o_2}$. For the calculations, $\gamma_o{}^p$ = 0.4 mN m^{-1} and $\gamma_o{}^d$ = 32.9 mN m^{-1} for sunflower oil, $\gamma_o{}^p$ = 0.9 mN m^{-1} and $\gamma_o{}^d$ = 19.9 mN m^{-1} for PDMS 20 cS, $\gamma_o{}^p$ = 0.9 mN m^{-1} and $\gamma_o{}^d$ = 20.1 mN m^{-1} for PDMS 50 cS and $\gamma_o{}^p$ = 0.9 mN m^{-1} and $\gamma_o{}^d$ = 20.5 mN m^{-1} for PDMS 100 cS as given in Table 2.14. Inset: sketch of a silica particle at sunflower oil-PDMS oil interface.

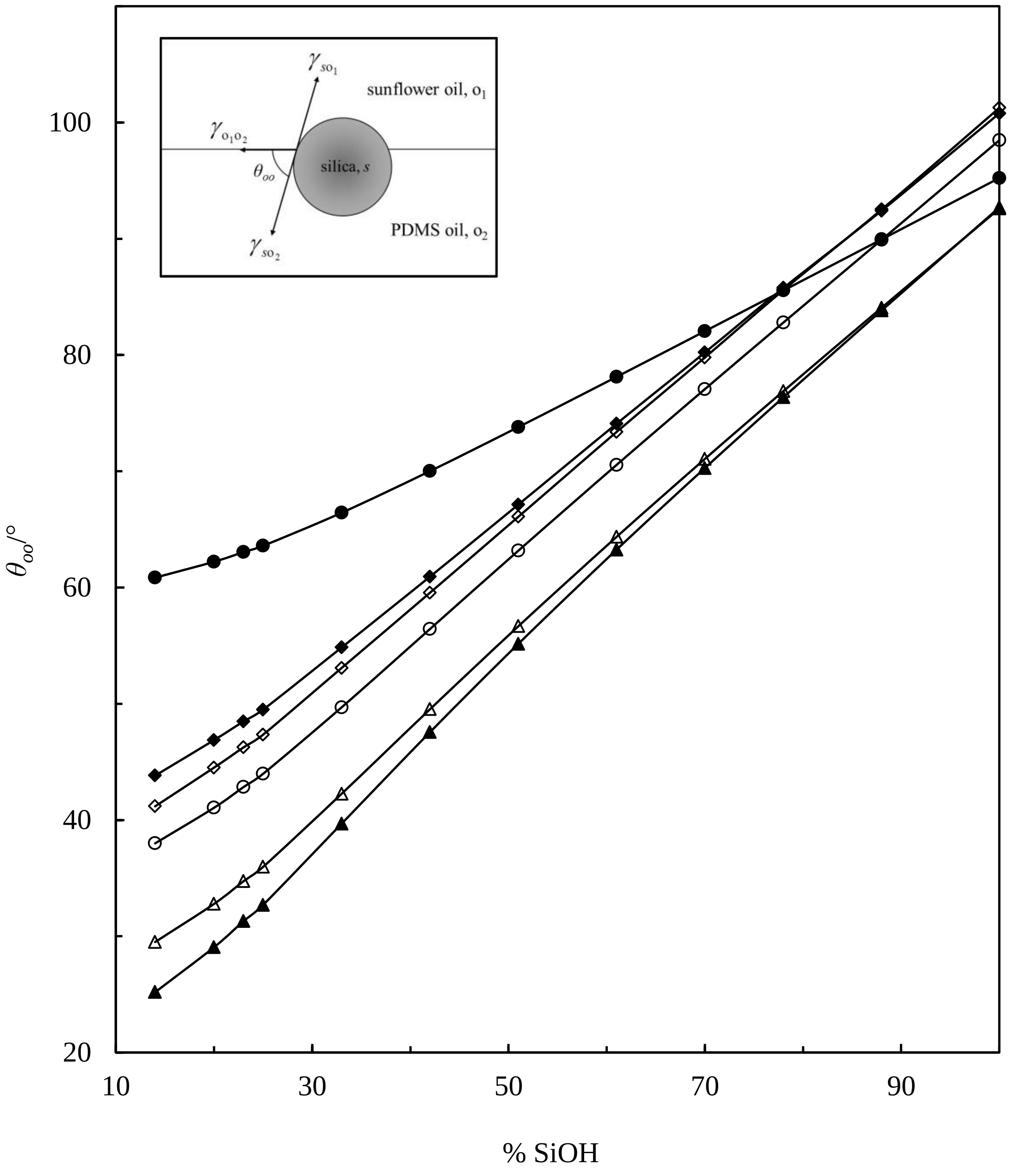

Figure 4.40. Plot of θ_{oo} *versus* % SiOH on DCDMS-coated fumed silica particle surfaces for sunflower oil-PDMS 20 cS at (a) γ_o^p; γ_o^d = 0; 33.3 (+), 0.2; 33.1 (◇), 0.4; 32.9 (○), 0.6; 32.7 (●), 1; 32.3 (×) and 1.4; 31.9 (△) mN m^{-1} for sunflower oil and γ_o^p; γ_o^d = 0.9; 19.9 mN m^{-1} for PDMS 20 cS and (b) γ_o^p; γ_o^d = 0; 20.8 (+), 0.2; 20.6 (◇), 0.4; 20.4 (○), 0.6; 20.0 (●), 1; 19.8 (×) and 1.4; 19.4 (△) mN m^{-1} for PDMS 20 cS and γ_o^p; γ_o^d = 0.4; 32.9 mN m^{-1} for sunflower oil.

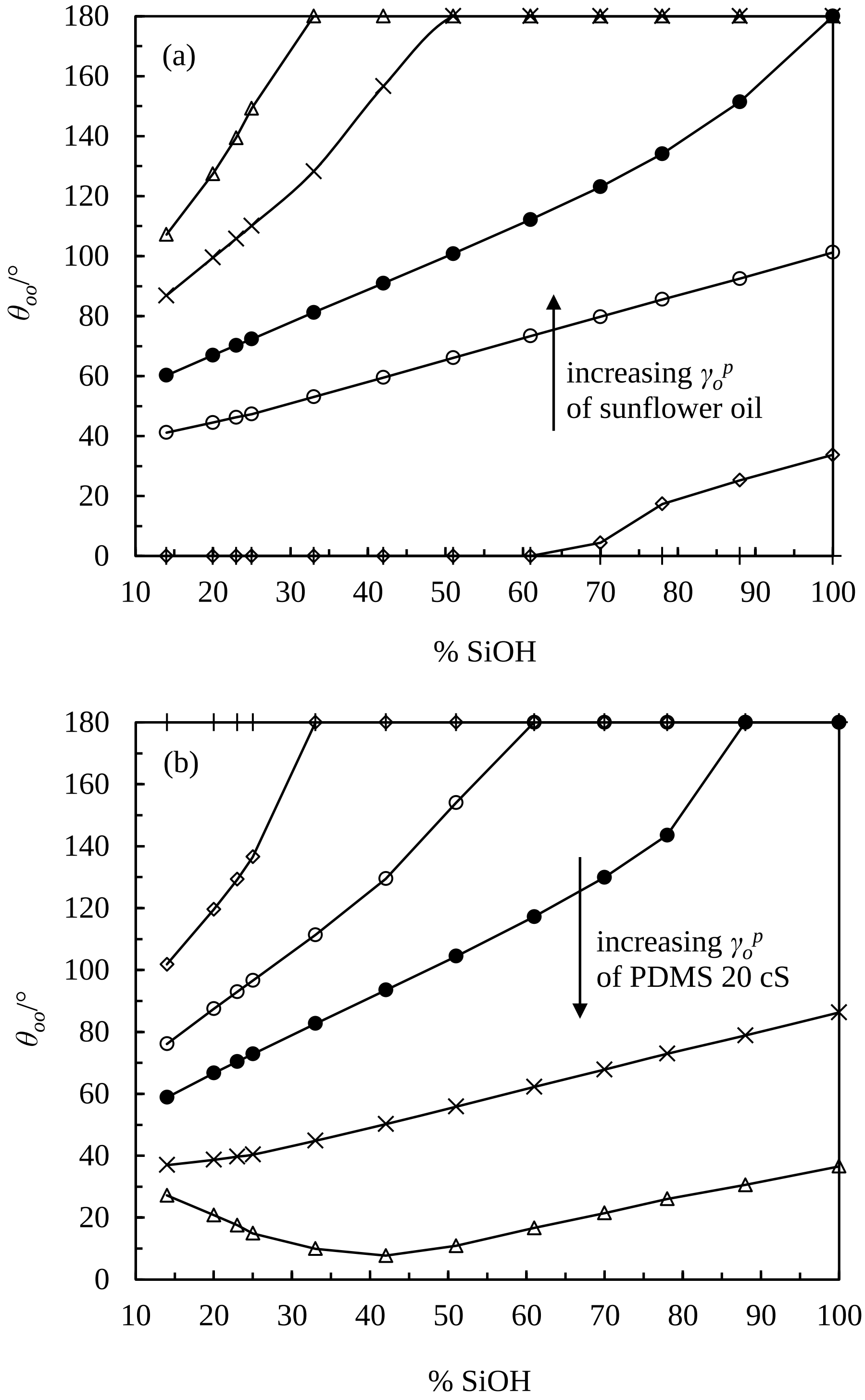

Table 4.3. Advancing (first entry) and receding (second entry) of θ_o (through oil) of the individual oils in air and advancing (first entry) and receding (second entry) of θ_{oo} (through PDMS oil) of the PDMS oils in the vegetable oils, measured on (a) hydrophilic and (b) DCDMS-coated glass slides and the type of emulsion formed in any vegetable oil-PDMS oil combination. Also shown is whether the emulsions stabilised by the 100 and 14% SiOH silica, considered to be equivalent to the hydrophilic and DCDMS-coated glass slides, respectively, are expected (✓) or not (×). The θ_o(θ_{oo}) is quoted to ± 1(2°) which is the standard deviation of four separate measurements. [a]Contact angle is θ_{wa} (through water). [b]Contact angle is θ_{ow} (through water). The values of the θ_{wa} on the hydrophilic and DCDMS-coated glass slides are consistent with the literature.[54]

Glass surface	System	θ_o/θ_{oo}	Emulsion type	Comment
(a)	Water	< 5, 0[a]		
	Sunflower oil	< 5, 0		
	Olive oil	< 5, 0		
	PDMS 20 cS	< 1, 0		
	PDMS 50 cS	< 1, 0		
	PDMS 100 cS	< 1, 0		
	Sunflower oil-water	52, 32[b]	Not studied	
	Olive oil-water	43, 19[b]	Not studied	
	Sunflower oil-PDMS 20 cS	150, 150	Unstable PDMS 20 cS-in-sunflower oil	✓
	Sunflower oil-PDMS 50 cS	148, 160	Stable PDMS 50 cS-in-sunflower oil	✓
	Sunflower oil-PDMS 100 cS	152, 158	Stable PDMS 100 cS-in-sunflower oil	✓
	Olive oil-PDMS 20 cS	148, 151	Unstable PDMS 20 cS-in-olive oil	✓
	Olive oil-PDMS 50 cS	148, 150	Unstable PDMS 50 cS-in-olive oil	✓
	Olive oil-PDMS 100 cS	152, 154	Stable PDMS 100 cS-in-olive oil	✓
(b)	Water	107, 110[a]		
	Sunflower oil	52, 35		
	Olive oil	58, 34		
	PDMS 20 cS	< 2, 0		
	PDMS 50 cS	< 2, 0		
	PDMS 100 cS	< 2, 0		
	Sunflower oil-water	168, 171[b]	Not studied	
	Olive oil-water	167, 169[b]	Not studied	
	Sunflower oil-PDMS 20 cS	67, 44	Stable sunflower oil-in-PDMS 20 cS	✓
	Sunflower oil-PDMS 50 cS	72, 34	Stable sunflower oil-in-PDMS 50 cS	✓
	Sunflower oil-PDMS 100 cS	81, 42	Unstable multiple emulsion	×
	Olive oil-PDMS 20 cS	70, 36	Stable olive oil-in-PDMS 20 cS	✓
	Olive oil-PDMS 50 cS	82, 32	Unstable multiple emulsion	×
	Olive oil-PDMS 100 cS	71, 45	Stable olive oil-in-PDMS 100 cS	✓

4.7 Conclusions

Oil-oil Pickering emulsions comprising of sunflower/olive/rapeseed oil and PDMS oils (20−50 cS) were prepared using DCDMS-coated and fluorinated fumed silica particles having % surface SiOH group of 100−14 and 75−50%, respectively, fluorinated ZnO, fluorinated sericite and bentonite clay particles as stabilisers. Other solid particles like rod-shaped $CaCO_3$, PTFE, Bentone 34 and Calofort SV were also used. The emulsions (average droplet diameter of mm to μm) were either vegetable oil or PDMS oil continuous depending on the particle type and the % of surface SiOH group for the DCDMS-coated fumed silica particles. The kinetic stability of the emulsions increased with increasing particle concentration, as expected. Some of the emulsions containing relatively high particle concentration ($\geq$ 1 wt. %) remained stable for over a month, but some did not. The stable emulsions where white and composed of polydisperse and unflocculated droplets. Transitional and catastrophic phase inversions were observed in the fumed silica particle-stabilised emulsions. The transitional phase inversion occurred if the viscosity of the PDMS oils in a vegetable oil is varied in the presence of 75% SiOH fluorinated fumed silica particles or the % surface SiOH on the DCDMS-coated fumed silica particles in a vegetable oil-PDMS oil combination is varied from 100−14% SiOH. For the DCDMS-coated fumed silica particles, multiple emulsions were observed near the point (23 and 20% SiOH) of inversion in some cases. The multiple emulsions occurred before or after inversion. The catastrophic phase inversion occurred at ϕ_{suno} of between 0.4 and 0.5 when the ϕ_{suno} in sunflower oil-PDMS 50 cS emulsions is varied between 0.05 and 0.9 in the presence of 75% SiOH fluorinated fumed silica. In the same systems, catastrophic phase inversion occurred at ϕ_{suno} of between 0.5 and 0.6 when PF-5 Eight Pearl 300S-Al sericite particles were used. Vegetable oil-PDMS oil-hydrophilic/DCDMS-coated glass three-phase contact angles were measured and they were seen to correlate with the type of emulsions stabilised by the 100% SiOH and 14% SiOH DCDMS-coated fumed silica particles. Generally, the relatively hydrophobic particles formed more stable emulsions compared with the hydrophilic ones.

4.8 References

1. B. P. Binks and T. S. Horozov, eds., *Colloidal Particles at Liquid Interfaces*, Cambridge University Press, Cambridge, 2006.
2. B. P. Binks, *Curr. Opin. Colloid Interface Sci.*, 2002, **7**, 21−41.
3. S. Tcholakova, N. D. Denkov and A. Lips, *Phys. Chem. Chem. Phys.*, 2008, **10**, 1608−1627.
4. B. P. Binks, A. N. Boa, M. A. Kibble, G. Mackenzie and A. Rocher, *Soft Matter*, 2011, **7**, 4017−4024.
5. R. Aveyard, B. P. Binks and J. H. Clint, *Adv. Colloid Interface Sci.*, 2003, **100–102**, 503−546.
6. B. P. Binks and S. O. Lumsdon, *Phys. Chem. Chem. Phys.*, 2000, **2**, 2959−2967.
7. B. P. Binks and S. O. Lumsdon, *Langmuir*, 2000, **16**, 8622−8631.
8. B. P. Binks and S. O. Lumsdon, *Langmuir*, 2000, **16**, 2539−2547.
9. B. P. Binks and S. O. Lumsdon, *Langmuir*, 2001, **17**, 4540−4547.
10. B. P. Binks and S. O. Lumsdon, *Phys. Chem. Chem. Phys.*, 1999, **1**, 3007−3016.
11. I. Akartuna, A. R. Studart, E. Tervoort, U. T. Gonzenbach and L. J. Gauckler, *Langmuir*, 2008, **24**, 7161−7168.
12. T. S. Horozov and B. P. Binks, *Angew. Chem. Int. Ed.*, 2006, **45**, 773−776.
13. T. S. Horozov, B. P. Binks and T. Gottschalk-Gaudig, *Phys. Chem. Chem. Phys.*, 2007, **9**, 6398−6404.
14. B. P. Binks and P. D. I. Fletcher, *Langmuir*, 2001, **17**, 4708−4710.
15. N. D. Denkov, I. B. Ivanov, P. A. Kralchevsky and D. T. Wasan, *J. Colloid Interface Sci.*, 1992, **150**, 589−593.
16. P. Finkle, H. D. Draper and J. H. Hildebrand, *J. Am. Chem. Soc.*, 1923, **45**, 2780−2788.
17. Z. G. Cui, K. Z. Shi, Y. Z. Cui and B. P. Binks, *Colloids Surf. A*, 2008, **329**, 67−74.
18. Z. Lin, W. J. Schulz and J. M. Smith, *Oil-in-oil and three-phase emulsions*, US Pat., 6 238 657 B1, 2001, Dow Corning Corporation.
19. R. V. Petersen and R. D. Hamill, *J. Soc. Cosmetic Chemists*, 1968, **19**, 627−640.
20. A. Imhof and D. J. Pine, *Nature*, 1997, **389**, 948−951.
21. A. Imhof and D. J. Pine, *Chem. Eng. Technol.*, 1998, **21**, 682−685.
22. A. Imhof and D. J. Pine, *J. Colloid Interface Sci.*, 1997, **192**, 368-374.
23. V. Jaitely, T. Sakthivel, G. Magee and A. T. Florence, *J. Drug Del. Sci. Tech.*, 2004, **14**, 113−117.
24. T. Sakthivel, V. Jaitely, N. V. Patel and A. T. Florence, *Int. J. Pharm.*, 2001, **214**, 43−48.
25. O. Suitthimeathegorn, V. Jaitely and A. T. Florence, *Int. J. Pharm.*, 2005, **298**, 367−371.
26. V. Jaitley, T. Sakthivel, G. Magee and A. T. Florence, *J. Drug Del. Sci. Tech*, 2004, **14**, 113−117.
27. A. K. F. Dyab and H. N. Al-Haque, *RSC Advances*, 2013, **3**, 13101−13105.
28. A. K. F. Dyab and A. M. Atta, *RSC Advances*, 2013, **3**, 25662−25665.
29. P. S. Clegg, E. M. Herzig, A. B. Schofield, T. S. Horozov, B. P. Binks, M. E. Cates and W. C. K. Poon, *J. Phys.: Condens. Matter*, 2005, **17**, S3433.
30. J. H. J. Thijssen and P. S. Clegg, *Soft Matter*, 2010, **6**, 1182−1190.
31. P. S. Clegg, E. M. Herzig, A. B. Schofield, S. U. Egelhaaf, T. S. Horozov, B. P. Binks, M. E. Cates and W. C. K. Poon, *Langmuir*, 2007, **23**, 5984−5994.
32. N. Hijnen and P. S. Clegg, *Mater. Horiz.*, 2014, **1**, 360−364.
33. D. Cai, J. H. T. Thijssen and P. S. Clegg, *Appl. Mater. Interfaces*, 2014, **6**, 9214−9219.
34. R. D. Vartanian, *Stable mineral oil-silicone oil compositions*, US Pat., 3 445 385, 1969, American Cyanamide Company.

35. A. Guillaume and F. Sagi, *Homogeneous dispersions of diorganopolysiloxane compositions in mineral oils*, US Pat., 4 115 343, 1978, Rhone-Poulenc Industries.
36. X.-D. Pan and G. H. McKinley, *J. Colloid Interface Sci.*, 1997, **195**, 101−113.
37. J. C. Loudet, H. Richard, G. Sigaud and P. Poulin, *Langmuir*, 2000, **16**, 6724−6730.
38. Y. Nonomura, T. Sugawara, A. Kashimoto, K. Fukuda, H. Hotta and K. Tsujii, *Langmuir*, 2002, **18**, 10163−10167.
39. Y. Nonomura, K. Fukuda, S. Komura and K. Tsujii, *Langmuir*, 2003, **19**, 10152-10156.
40. H. Lannibois-Drean, J.-M. Ricca, M. Destaract and P. Olier, *Oil-in-oil emulsions comprising a silicone, dispersions and use for said emulsions*, EP Pat., WO 03/000396 A1, 2003, Rhodia Chimie.
41. T.R. Forbus, *Oil-in-oil emulsion lubricants for enhance lubrication*, US Pat., 2004/0002429 A1, 2004, ExxonMobil Research & Engineering Company.
42. C. Holtze, R. E. Guerra, J. Agresti, D. A. Weitz, K. Ahn, J. B. Hutchison, A. Griffiths, A. El Harrak, O.J. Miller, J.-C. Baret, V. Taly, M. Ryckelynck and C. Merten, *Fluorocarbon emulsion stabilising surfactants*, EP Pat., WO 2008/021123 A1, 2008, Harvard College.
43. T. K. Jones and M. Nair, *Oil-in-oil dispersions stabilised by solid particles and methods of making the same*, US Pat., 8 323 392 B2, 2012, Eastman Kodak Company.
44. S. Verma and J. S. Dangi, *Ind. J. Novel Drug Del.*, 2012, **4**, 223.
45. G. H. Greene, J. C. Phillips and J. F. Stults, *Non-aqueous emulsion of silicone oil and stearine*, EP Pat., WO 1991010771 A1, 1991,
46. M. Nair, T. K. Jones and M. C. Brick, *Oil-in-oil emulsions*, US Pat., 2007/0189998 A1, 2007, Eastman Kodak Company.
47. P. Thareja and S. Velankar, *Rheol. Acta*, 2007, **46**, 405−412.
48. J. Vermant, G. Cioccolo, K. Golapan Nair and P. Moldenaers, *Rheol. Acta*, 2004, **43**, 529−538.
49. L. Elias, F. Fenouillot, J. C. Majeste and P. Cassagnau, *Polymer*, 2007, **48**, 6029−6040.
50. L. Elias, F. Fenouillot, J. C. Majesté, P. Alcouffe and P. Cassagnau, *Polymer*, 2008, **49**, 4378−4385.
51. S. Arditty, C. P. Whitby, B. P. Binks, V. Schmitt and F. Leal-Calderon, *Eur. Phys. J. E*, 2003, **11**, 273−281.
52. M. Destribats, B. Faure, M. Birot, O. Babot, V. Schmitt and R. Backov, *Adv. Funct. Mater.*, 2012, **22**, 2642−2654.
53. J. W. J. de Folter, M. W. M. van Ruijven and K. P. Velikov, *Soft Matter*, 2012, **8**, 6807−6815.
54. B. P. Binks, A. K. F. Dyab and P. D. I. Fletcher, *Phys. Chem. Chem. Phys.*, 2007, **9**, 6391−6397.
55. B. P. Binks, P. D. I. Fletcher, B. L. Holt, P. Beaussoubre and K. Wong, *Phys. Chem. Chem. Phys.*, 2010, **12**, 11954-11966.
56. B. P. Binks, J. Philip and J. A. Rodrigues, *Langmuir*, 2005, **21**, 3296−3302.
57. T. K. Law, T. L. Whateley and A. T. Florence, *J. Control. Release*, 1986, **3**, 279−290.
58. B. P. Binks, A. K. F. Dyab, P. D. I. Fletcher and H. Barthel, *Multiple emulsions of either o/w/o or w/o/w stabilised solely by fumed silica particles*, EP Pat., 2002, Wacker- Ž Chemie GmbH.
59. S. Zou, C. Wang, Q. Gao and Z. Tong, *J. Dispersion Sci. Technol.*, 2012, **34**, 173−181.
60. Y. Nonomura and N. Kobayashi, *J. Colloid Interface Sci.*, 2009, **330**, 463−466.
61. B. P. Binks and J. H. Clint, *Langmuir*, 2002, **18**, 1270−1273.

Chapter 5

Influence of the Degree of Fluorination on the Behaviour of Fumed Silica Particles at Oil-Air Surfaces

5.1 Introduction

It is now evident that colloidal particles of suitable wettability can self-adsorb at oil-water, water-air and oil-air interfaces and thus act as sole stabilisers of related materials like emulsions,[1,2] aqueous foams[3,4] or water liquid marbles[5] and oil foams[6,7] or oil liquid marbles[8] respectively. For fumed silica particles (primary particle diameter of 20−30 nm), varying the degree of surface coating (*i.e*. hydrophobicity) using DCDMS permits stabilisation of air-in-water foams[9] and o/w emulsions[10] when the particles are relatively hydrophilic and w/o emulsions[10] and water-in-air powders (or dry water)[11] when the particles become hydrophobic. The change in curvature of the water-air interface by increasing the hydrophobicity of the particles led to the inversion of foam into dry water powder[11] which is "a collection of large number of tiny water marbles." For oil-air interfaces, the particles need to be oleophobic or omniphobic[6,7] and possess γ_{sa} that is lower than that of typical hydrophobic particles (hydrocarbon-coated) before adsorption can occur as the γ_{la} of many oils is relatively low. Since the γ_{sa} of fluorocarbons is lower than that of hydrocarbons, fluorocarbon-coated particles have been shown to meet the prerequisite.[12] The surfaces of hydrophilic fumed silica nanoparticles were modified with 1H,1H,2H,2H-perfluorodecyltriethoxysilane to omniphobic fluorinated silica particles.[12] The static θ_{la} (through liquid) of the fluorinated particles with microdrops (5 μL) of oils of tensions between 29−31 mN m^{-1}, diiodomethane (γ_{la} = 50.8 mN m^{-1}) and water (γ_{la} = 72.8 mN m^{-1}) measured on glass slides spin coated with the particles is *ca*. 140−147, 159 and 168° respectively. Notice that the γ_{la} of liquids above and throughout this chapter are quoted at 20 °C. Other examples of fluorocarbon-coated particles/surfaces and fluorocarbon particles exhibiting oleophobic properties to certain oils include fluoroalkyl-polyhedral oligomeric silsesquioxane (POSS),[13,14] poly[2-(perfluorooctyl)ethylacrylate] (PFA-C_8),[15] fluoroalkylsilane-coated silica particles[16] and fluorooctyltrichlorosilane-coated photoresist surfaces.[17] In the first example,[12] the advancing θ_{la} of an *n*-hexadecane drop in air measured through the oil phase on an electrospun-coated substrate was as high as 150°. The particles were also used to stabilise marbles of toluene (γ_{la} = 28.4 mN m^{-1}), *n*-hexadecane (γ_{la} = 27.5 mN m^{-1}), octane (γ_{la} = 21.6 mN

m^{-1}) and ethanol (γ_{la} = 22.4 mN m^{-1}). In the second example,[15] the PFA-C_8 microparticles (γ_{sa} = 7.82 mN m^{-1}) were used to stabilise diiodomethane, toluene and methanol (γ_{la} = 22.5 mN m^{-1}) marbles. In ref. 16, sol-gel films of silica were prepared and their surface energy and roughness were controlled using varying amounts of colloidal silica particles (10−15 nm) and a fluoroalkylsilane. The optimised surfaces exhibited advancing θ_{la} of 120 and 150° for dodecane and water respectively. For the other example,[17] super-oleophobic textured surfaces were formed on silicon wafers using photolithography. Pillars of a photoresist of diameter 3 μm and height 7 μm were subsequently coated with a long chain fluorooctyltrichlorosilane. The highest advancing θ_{la} for *n*-hexadecane was 161° and it was demonstrated that the wavy nature (300 nm) of the pillar walls was responsible for the high levels of oleophobicity.

As was mentioned in chapter 1, stable oil liquid marbles and particle-stabilised oil foams have only been reported in a few cases[6-8] despite the importance of oil foams in the oil, food and other related industries. In one of the studies, oil mixtures were used to effect the adsorption of oligotetrafluoroethylene (OTFE) particles to oil-air surfaces to form stable oil foams.[8] In the rest of the studies, OTFE and polytetrafluoroethylene (PTFE) particles were used to stabilise oil foams and in addition, the role of γ_{la} of the oil in achieving particle adsorption and foam stability was shown. In this chapter, the behaviour of fluorinated fumed silica in contact with a range of oils and non-aqueous liquids in relation to their ability to stabilise oil liquid marbles and oil foams is reported. By varying the degree of fluorination of the particles, the influence of particle wettability on the stability of these materials was investigated. Comparisons are made with hydrophilic fumed silica (100% SiOH silica) and very hydrophobic silica (14% SiOH silica) of the same primary particle size which have been coated with DCDMS. The behaviour of the 14% SiOH silica particles at both water-air and oil-water interfaces have been studied previously.[9,18] Although these particles are not the ideal choice of particles, they are one of the few particle types for which progressive surface modification and their influence on interfacial behaviour have been studied in detail. In addition, such particles have widespread industrial importance but their mode of action is unknown in most cases.

5.2 Behaviour of Fumed Silica Particles on Liquid Surfaces

The behaviour of a known mass of particles placed on the surface of all the liquids at rest is summarised in Figure 5.1. Particles were either wetted and entered the liquid or were non-wetted and remained on the liquid surface. The 100% SiOH silica particles were wetted by all the liquids (of γ_{la} between *ca*. 12 and 73 mN m^{-1}) as expected due to their high surface energy.

By contrast, the 14% SiOH silica particles of lower surface energy (coated with DCDMS) were wetted by all oils except liquids of γ_{la} higher than *ca*. 47 mN m^{-1} like diiodomethane and H-bonding solvents like glycerol and water. The fluorinated silica particles of lowest fluorine content (75% SiOH) were wetted by most oils of γ_{la} < 38 mN m^{-1}, but was not wetted by liquids of higher tension. The fluorinated silica particles of medium fluorine content (59% SiOH) were only wetted by oils of γ_{la} below *ca*. 21 mN m^{-1} and that having the highest fluorine content (50% SiOH) was wetted by isopropyl myristate and liquids having γ_{la} below 27 mN m^{-1}. Clearly, the wettability of the particles changes upon hydrophobisation with DCDMS or fluorination and more markedly as the degree of fluorination increases.

Since the powdered fumed silica particles contain air (in addition to that trapped in the glass vials) which must be expelled before the fumed silica particles will be in contact with the liquid, the glass vials were hand shaken vigorously for 30 s and the resulting observations are given in Table 5.1. The 100% SiOH fumed silica particles gave either clear or cloudy dispersions with all the liquids. The 14% SiOH fumed silica particles gave clear dispersions with oils and climbing films with the non-aqueous solvents and water which did not wet them at rest. Climbing films have been observed previously in systems containing hydrophobic solid particles and water and have been linked to the coalescence of unstable particle-coated bubbles with the planar liquid-air surface.[19] This reduces the total interfacial area, increases the surface concentration of the adsorbed particles and hence increases the surface pressure of the planar interface causing the film to climb.[19] The 75% SiOH fluorinated fumed silica particles form clear dispersions with oils which wet them and either cloudy dispersions or climbing films with liquids which do not wet them at rest except in diiodomethane in which a small amount of foam was obtained. In the case of the 59% SiOH fluorinated fumed silica particles, particle dispersions were observed in oils of γ_{la} < 32 mN m^{-1} and foams (for both oils and polar solvent) for liquids of higher γ_{la}. Lastly, the 50% SiOH fluorinated fumed silica particles yielded either dispersions in oils which wet them, oil foams for many oils and climbing films in two non-aqueous solvents and water. It was confirmed that these materials do not form in the absence of particles implying that particle adsorption is implicated in their formation. It can be seen (Table 5.1) that upon increasing the degree of fluorination, a wider range of oils of lower γ_{la} can be foamed as particle adsorption is favoured due to the relatively lower γ_{sa} of the particles as shown previously.

Figure 5.1. Behaviour (at ambient conditions) of fumed silica particles (50 mg) on the surfaces of liquids (3 cm^3) of varying surface tension γ_{la}. On the abscissa: 1-particles were wetted by the liquid, 2-particles were partially wetted by the liquid (*i.e.* some particles entered the liquid) and 3-particles were not wetted by the liquid. The number in brackets after a liquid represents its γ_{la} (± 0.1 mN m^{-1}) at 20 °C.

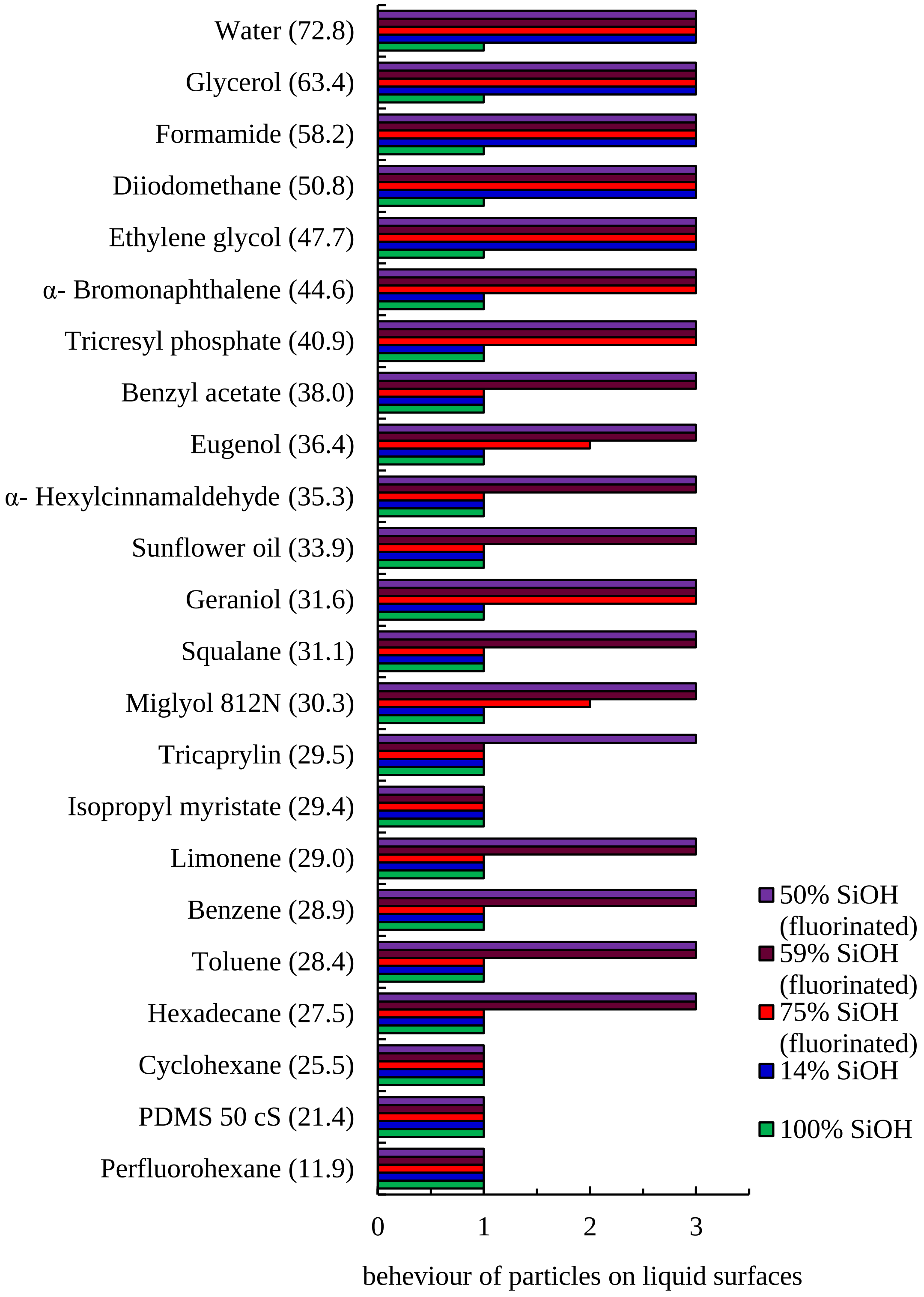

Table 5.1. Behaviour of fumed silica particles (50 mg) on the surfaces of the various liquids (3 cm^3) after agitation at ambient conditions.

Particle	Liquid	After agitation
100% SiOH silica	All liquids in Figure 5.1 except those below	Clear dispersion
	Perfluorohexane, α-bromonaphthalene, diiodomethane, glycerol	Cloudy dispersion
14% SiOH silica	All liquids in Figure 5.1 except those below	Clear dispersion
	Ethylene glycol, diiodomethane	Small bubbles + climbing films
	Formamide, glycerol, water	Climbing films
75% SiOH fluorinated silica	All liquids in Figure 5.1 except those below	Clear dispersion
	Geraniol, tricresyl phosphate, formamide, α-bromonapthalene, ethylene glycol	Cloudy dispersion
	Diiodomethane	Small bubbles
	Glycerol, water	Climbing films + fine foam
	Perfluorohexane, PDMS 50 cS, cyclohexane, toluene, isopropyl myristate	Clear dispersion
59% SiOH fluorinated silica	Hexadecane, benzene, limonene, tricaprylin, Miglyol 812N, squalane	Cloudy dispersion
	All other liquids in Figure 5.1 except water	Fine foam
50% SiOH fluorinated silica	Perfluorohexane, PDMS 50 cS, cyclohexane, isopropyl myristate	Clear dispersion
	Other liquids except those below	Fine foam
	Formamide, glycerol, water	Climbing films

5.3 Oil Foams Stabilised Solely by Fluorinated Fumed Silica Particles

Foams of a selection of oils and a non-aqueous polar solvent formed by the moderately fluorinated silica particles possessing 59% SiOH were investigated. The foams were prepared in four different ways. The first involves hand shaking the liquids with different concentrations of the powdered particles. The second involves dispersing the particles in the liquids using ultrasound before hand shaking. The third (and fourth methods) involve aerating the liquid-particle mixture with high shear Ultra-Turrax homogeniser for 1 min alone (followed by hand shaking), at a fixed particle concentration, as described in chapter 2. Photos of the foams formed by handing shaking the powdered particles with the liquids and the optical microscope image of that at 0.5 wt. % of the particles are shown in Figure 5.2. Unlike surfactant-stabilised aqueous foams, these non-aqueous foams are composed of relatively small bubbles (< 0.2 mm) possessing textured surfaces and are generally non-spherical in shape irrespective of particle concentration. The latter is due to the jamming of particles on bubbles surfaces which prevents relaxation to a spherical geometry.[20] The initial foam volume is seen to increase progressively as the particle concentration increases as expected (Figure 5.3) as it does with surfactant foaming agents below the critical micelle concentration.[21] For ethylene glycol (highest γ_{la}), climbing films were also observed on the walls of the glass vials. In sealed glass vials, these foams exhibited a small degree of liquid drainage alongside a small reduction in foam volume but after a day or so the foams remain ultra-stable for at least one year. On the other hand, if particles were first dispersed in the liquids using ultrasound and then shaken in the same manner (second method), no foam was obtained for any of the five liquids at 2 wt. % particles. It was observed that following this protocol in which particle agglomerates are broken down into smaller aggregates, viscous dispersions are formed which prevent the incorporation and breakup of air within by shaking. A three-dimensional network of particles is formed in the liquids by hydrogen bond formation between free SiOH groups on adjacent aggregates,[22] as opposed to the first method in which particle aggregates attach to air bubbles before entering the continuous phase. The visual and microscopic appearances of the foams produced from the third method are shown in Figure 5.4. The increase shear compared with hand shaking yields smaller bubbles of excellent stability to coalescence as shown in Figure 5.5. Photos and optical microscope images of the latter foams following additional hand shaking (fourth method) are shown in Figure 5.6 and their stability to coalescence is illustrated in Figure 5.7. After an initial small decrease in foam volume, foams of the oils remain stable to coalescence for at least 1 year except foams of α-hexylcinnamaldehyde which collapse slowly until no foam remains after 10 days. It was observed that the particles became progressively wetted by the oil and thus desorbed from the bubbles surfaces allowing coalescence to prevail. α-Hexylcinnamaldehyde exhibits the lowest γ_{la} of all the oils selected and obviously the system is very sensitive to the amount of shear imposed.

Figure 5.2. (upper) Photos of glass vials containing foams stabilised by different concentrations (given, wt. %) of 59% SiOH fluorinated fumed silica particles soon after preparation by hand shaking for (a) α-hexylcinnamaldehyde, (b) eugenol, (c) benzyl acetate, (d) α-bromonaphthalene and (e) ethylene glycol. (lower) Optical micrographs of the above-named foams at 0.5 wt. % of particles (1 day after preparation) for (a) α-hexylcinnamaldehyde, (b) eugenol, (c) benzyl acetate, (d) α-bromonaphthalene and (e) ethylene glycol.

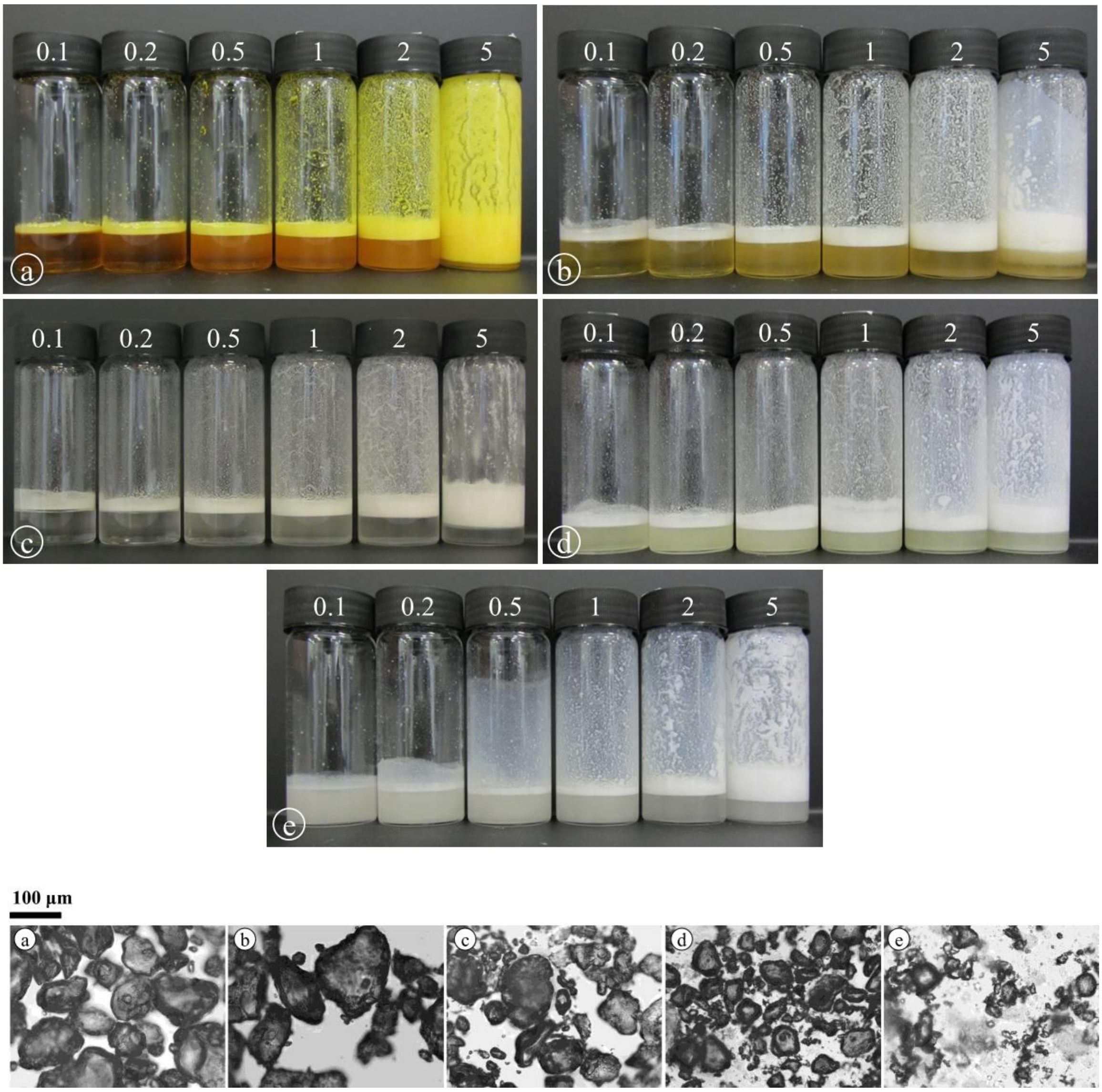

Figure 5.3. Initial foam volume *versus* particle concentration for the various foams described in Figure 5.2 (soon after preparation). The foam volume is quoted to ± 0.1 cm^3 which is the propagation error in the estimated foam volume.

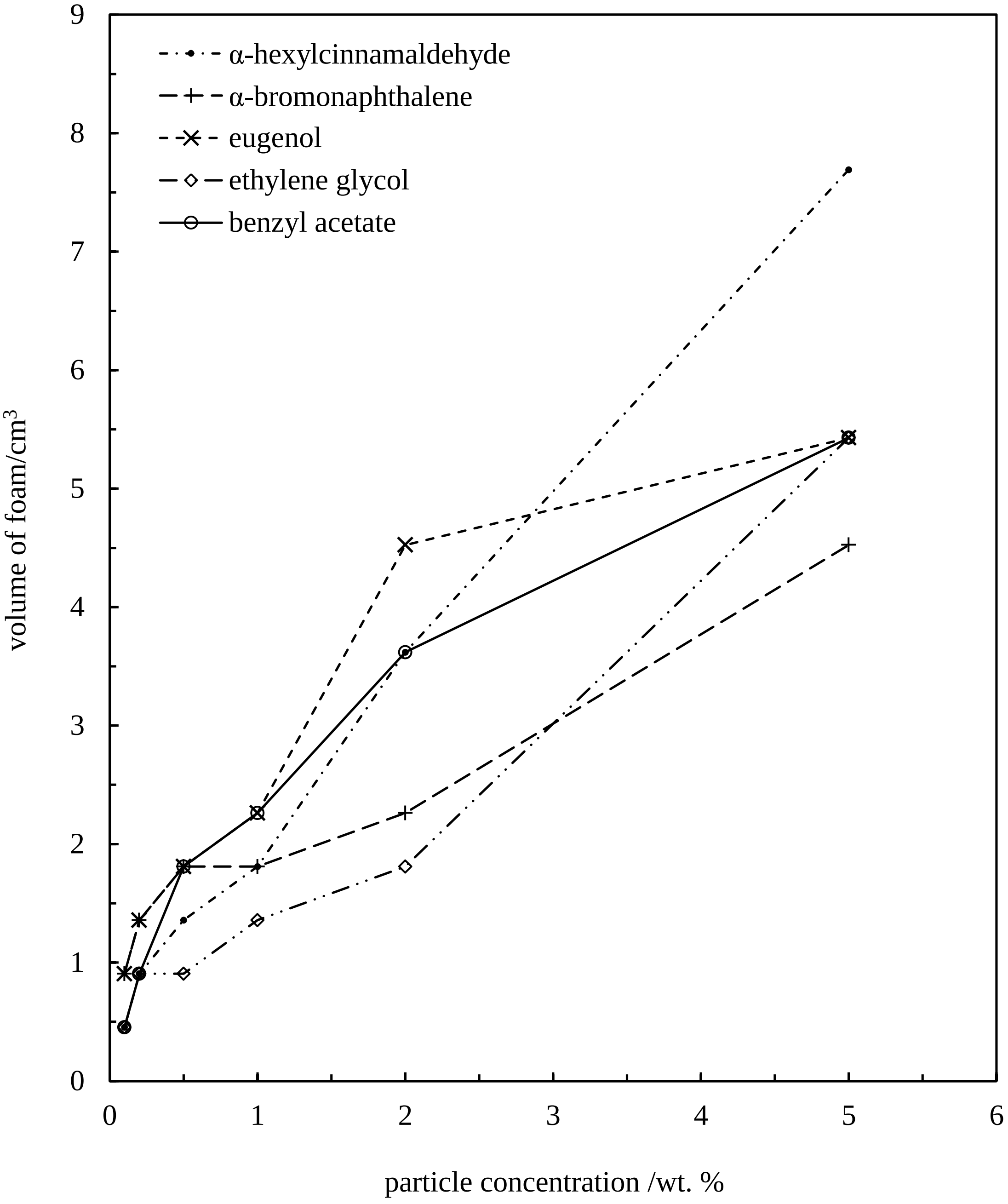

Figure 5.4. (upper) Visual appearance and (lower) optical micrographs of (a) *α*-hexylcinnamaldehyde, (b) *α*-bromonaphthalene, (c) benzyl acetate and (d) eugenol foams stabilised by 2 wt. % of 59% SiOH fluorinated fumed silica particles immediately after formation using Ultra-Turrax homogeniser.

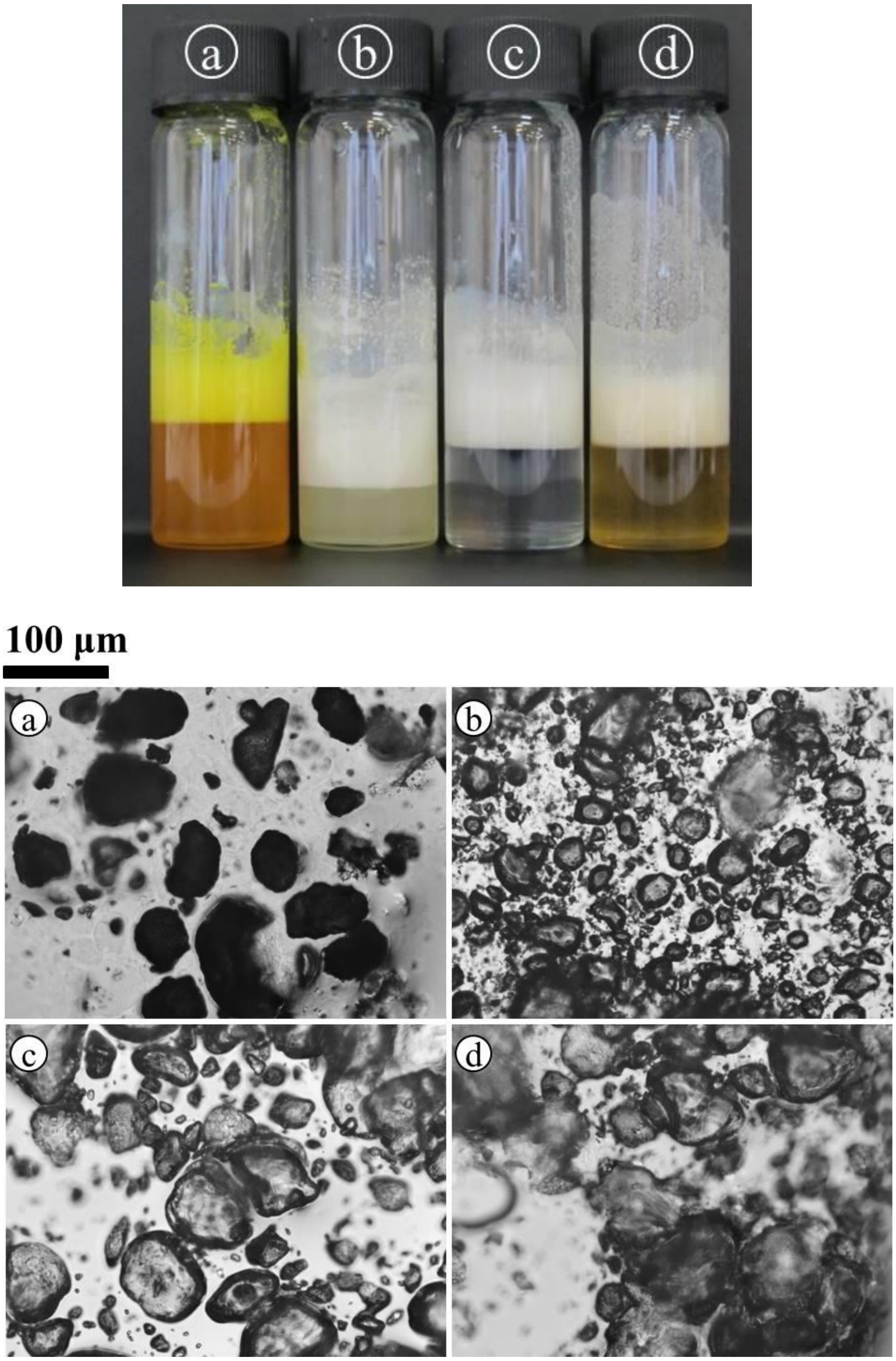

Figure 5.5. Volume of foams described in Figure 5.4 *versus* time. On the abscissa, the volume of foam at 0 day represents the initial foam volume (*i.e.* volume of foam soon after preparation). The foam volume is quoted to ± 0.1 cm^3 (propagation error in the estimated foam volume).

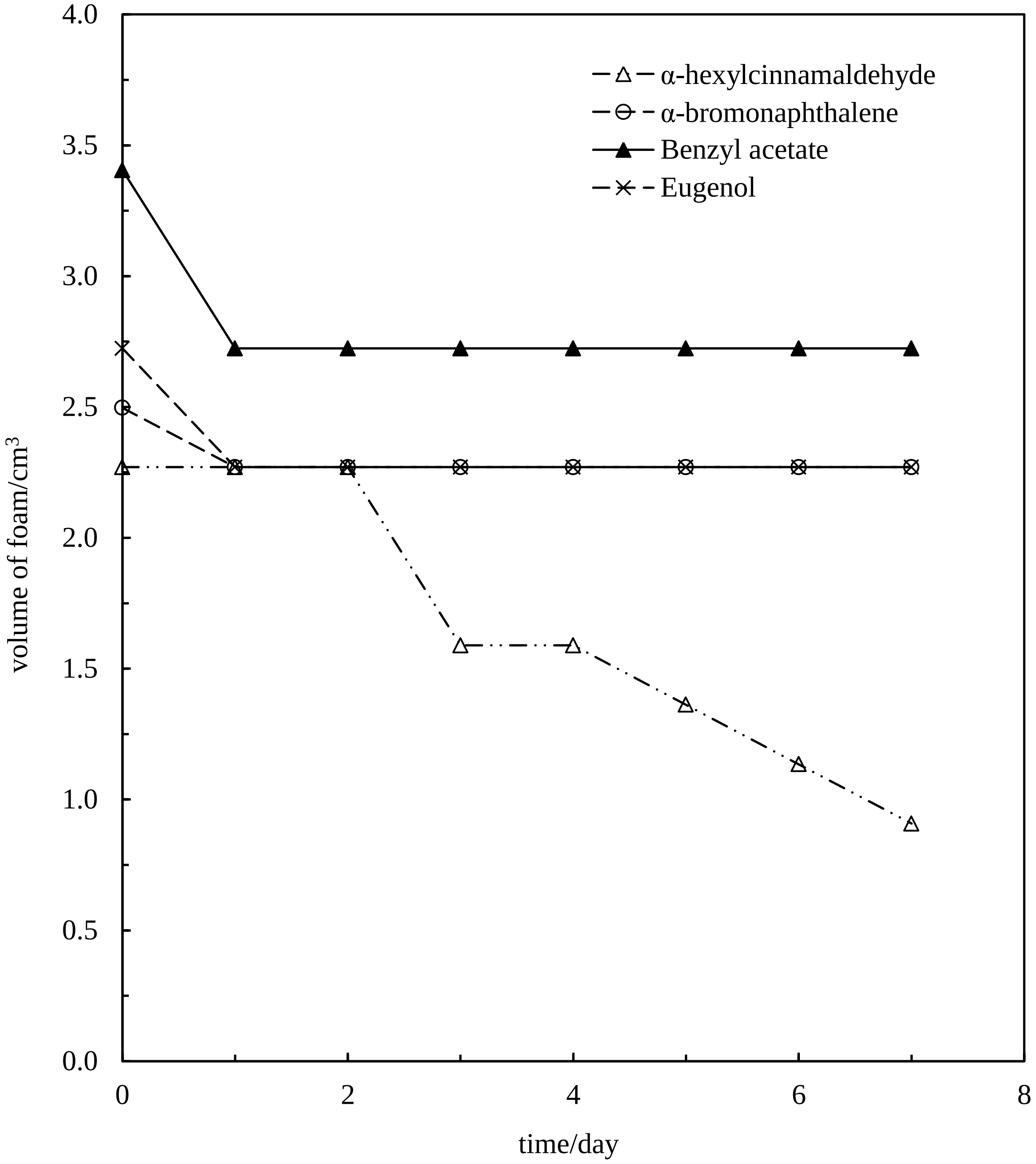

Figure 5.6. (upper) Photo and (lower) optical micrographs of (a) α-hexylcinnamaldehyde, (b) α-bromonaphthalene, (c) benzyl acetate and (d) eugenol foams stabilised by 2 wt. % of 59% SiOH fluorinated fumed silica particles immediately after formation using Ultra-Turrax homogeniser followed by hand shaking.

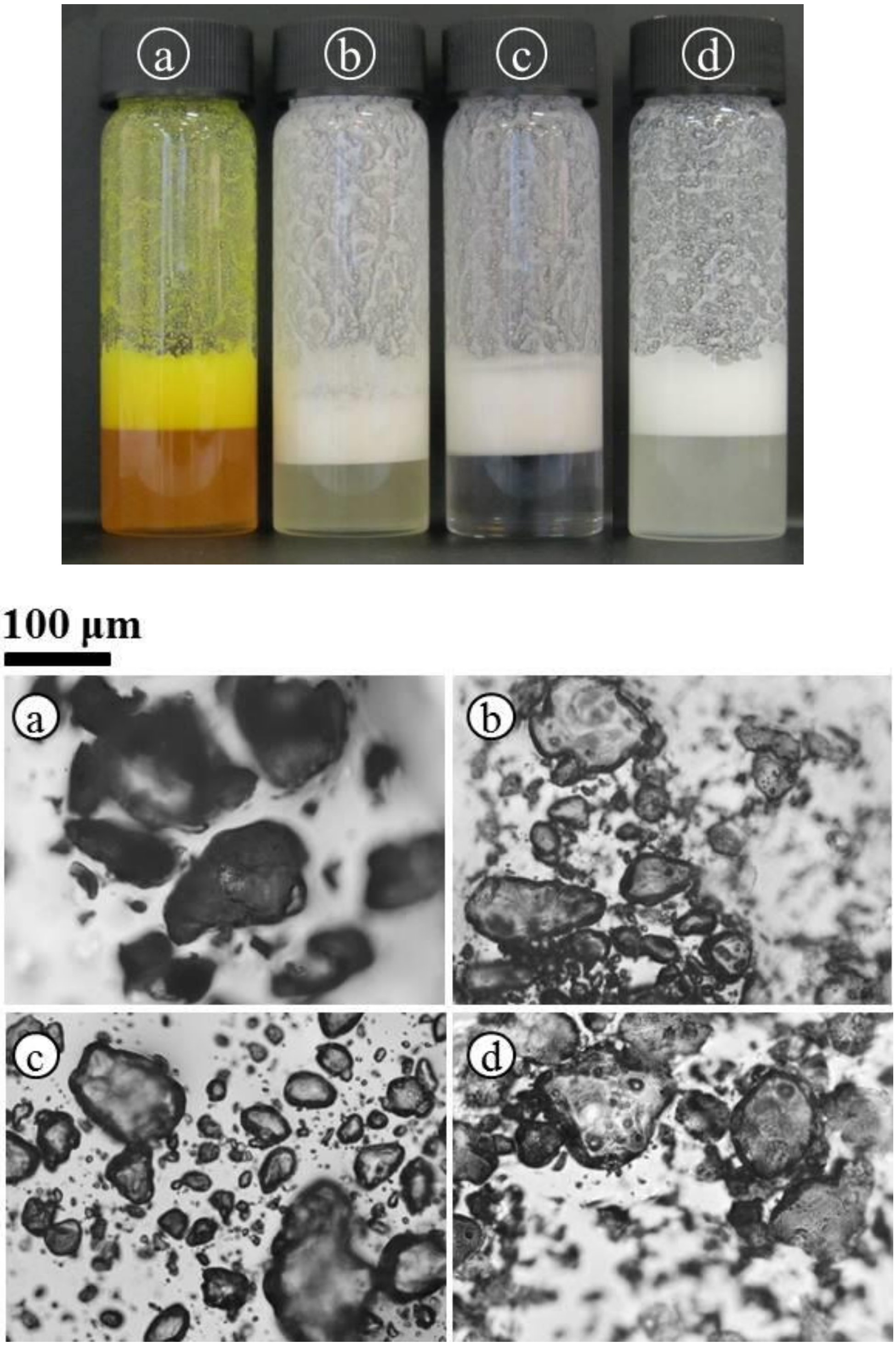

Figure 5.7. Volume of foams described in Figure 5.6 *versus* time. On the abscissa, the volume of foam at 0 day represents the initial foam volume (*i.e*. volume of foam soon after preparation). The foam volume is quoted to ± 0.1 cm^3 (propagation error in the estimated foam volume).

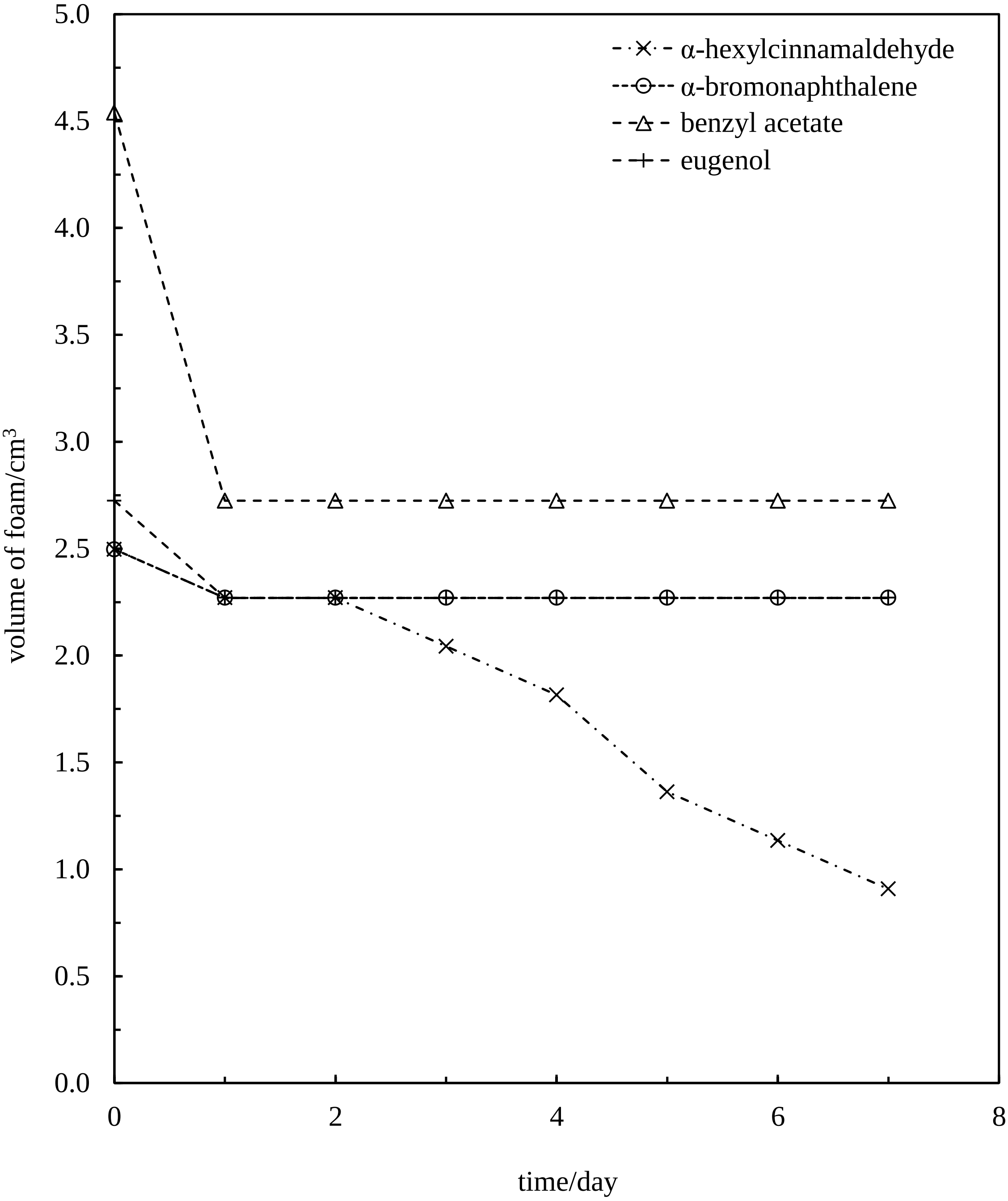

5.4 Oil Marbles Stabilised by Fluorinated Fumed Silica Particles

Attempts were made to prepare liquids marbles from all the liquids using all the particles. No marbles were stabilised by the 100% SiOH silica particles. However, the 14% SiOH silica particles were able to stabilise marbles of the relatively high tension (≥ 47.7 mN m^{-1}) liquids like ethylene glycol, formamide and water. The 75, 59 and 50% SiOH fluorinated silica particles of increasing fluorine content and degree of oleophobicity gave liquid marbles with liquids having $\gamma_{la} \geq 50.8$ mN m^{-1} (except formamide), $\gamma_{la} \geq 29.5$ mN m^{-1} and $\gamma_{la} \geq 27.5$ mN m^{-1} (except isopropyl myristate), respectively. Photos of some of the liquid marbles stabilised by 50% SiOH fluorinated fumed silica particles are shown in Figure 5.8. It can be seen that some of the marbles are white like the particles but some retain the colour of the encapsulated liquid, *e.g.* α-hexylcinnamaldehyde and diiodomethane. Also, many of the marbles are quasi-spherical, but a few of them have a puddle shape, *e.g.* diiodomethane liquid marble. Calculations (at 20 °C) show that for the quasi-spherical liquid marbles like water R' (1.34 mm) $< \kappa^{-1}$ (2.72 mm) and R' (1.34 mm) $> \kappa^{-1}$ (1.25 mm) for the puddle-shaped diiodomethane liquid marbles, as expected. For particles having the ability to stabilise liquid marbles, a liquid marble formed instantaneously when a drop of the liquid was placed on the powdered bed of particles. This type of behaviour has also been observed by McHale *et al.*[23] who suggested that this is as a result of the droplet attempting to minimise its surface area towards that of a sphere and the lack of any significant substrate resistance other than gravity as the solid particles are not bound to each other. The 59% SiOH fluorinated fumed silica particle-stabilised marbles (5 and 10 μL) were further investigated. Figure 5.9 shows that the contact length l (*i.e.* length of contact between marble and the substrate) of these marbles is inversely proportional to κ^{-1} of the liquids and directly proportional to the apparent contact angle θ_A of the marbles on the substrate. The θ_A was observed to be greater than θ'_A of the bare liquids on the PTFE substrate as shown in Figure 5.10. This is consistent with the observation of Matsukuma *et al.*[15] on 5 μL oil marbles. The 10 μL liquid marbles were allowed to evaporate on a Krüss DSA 10 instrument and their images were taken every 5 min for a period of 90 min. The volume V_{marble} of a quasi-spherical liquid marble at a given time was estimated from equation 5.1 where h and r_b represent the marble height and contact radius of the marble, respectively. Figure 5.11 shows a plot of V_{marble} *versus* time for the liquid marbles. Notice that the initial V_{marble} of the liquid marbles estimated using equation 5.1 is slightly greater than 10 μL because the particle layers on the marbles did not allow accurate determination of the parameters used in the equation.

$$V_{\text{marble}} = \frac{\pi h}{6}\left(3r_b^2 + h^2\right) \tag{5.1}$$

Figure 5.8. Photos (soon after formation) of 50% SiOH fluorinated fumed silica particle-stabilised liquid marbles (10 μL) resting on a hydrophilic glass slide in air.

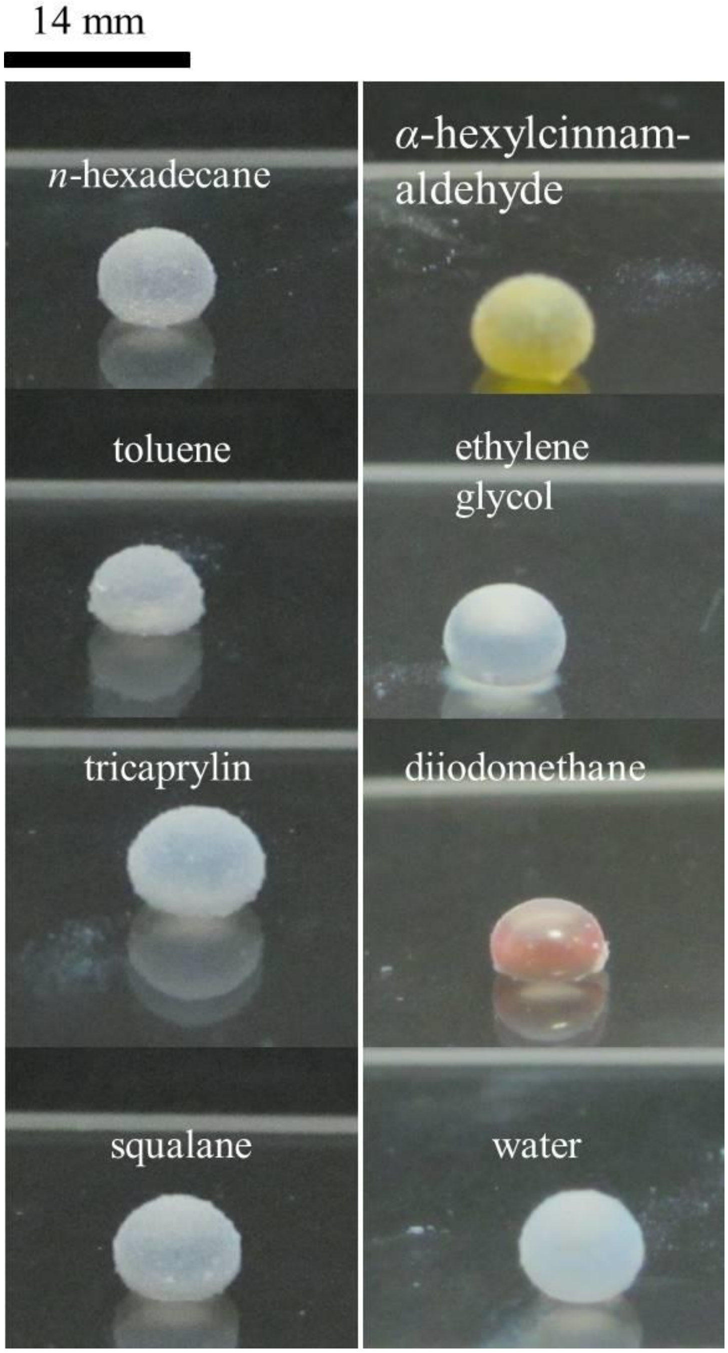

Figure 5.9. (A) contact length l and (B) apparent contact angle θ_A (± 2°; measured through the liquid) of either 5 (+) or 10 (▲) μL liquid marbles stabilised by 59% SiOH fluorinated fumed silica particles on a PTFE substrate *versus* the capillary length κ^{-1} of the liquid: (a) water, (b) formamide, (c) α-hexylcinnamaldehyde, (d) benzyl acetate, (e) α-bromonaphthalene, (f) ethylene glycol, (g) Miglyol 812N, (h) eugenol, (i) tricresyl phosphate, (j) diiodomethane and (k) tricaprylin.

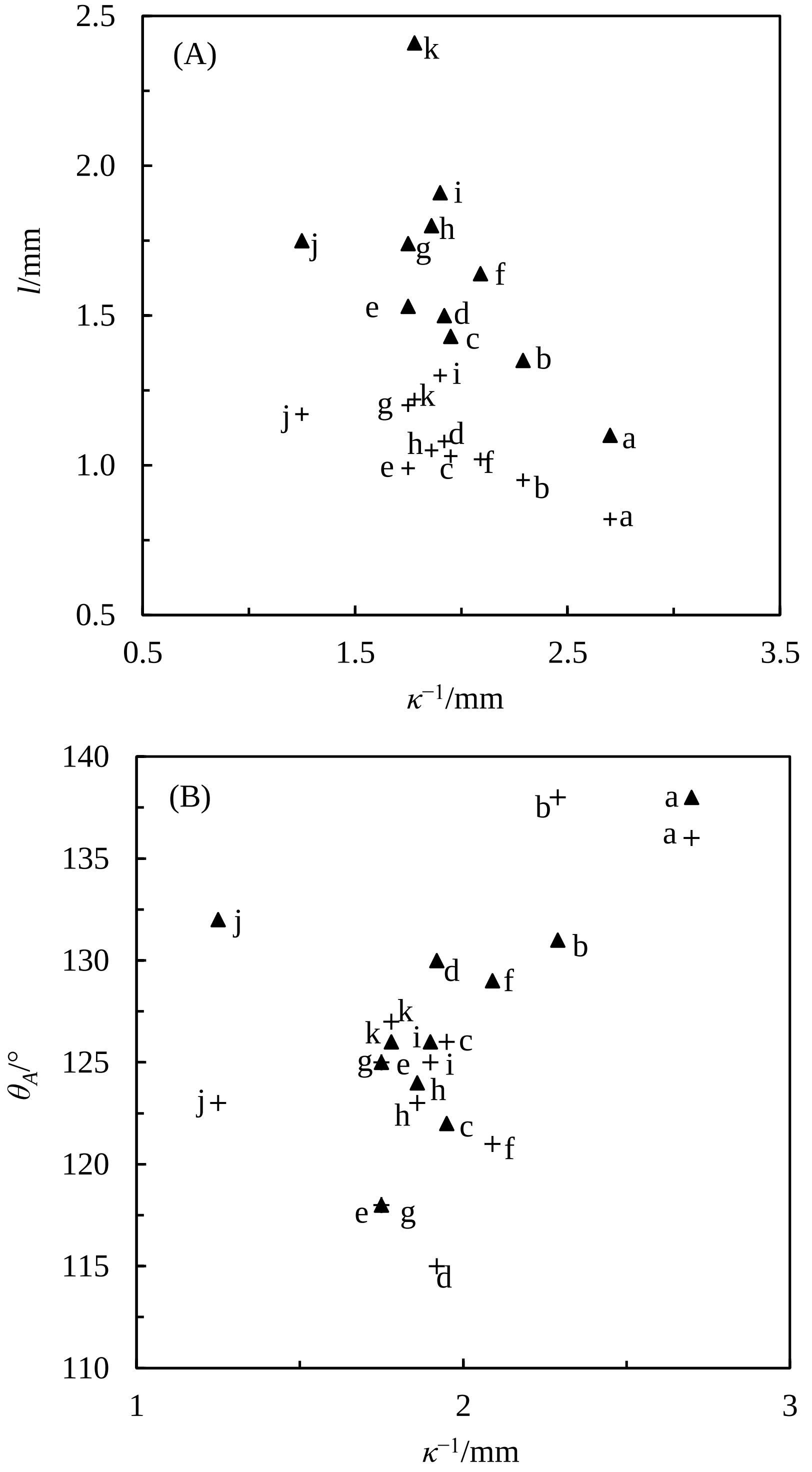

Figure 5.10. The apparent contact angle θ'_A (± 2°, through liquid) of bare liquids (10 μL) with PTFE substrate as a function of the capillary length κ^{-1}: (a) water, (b) formamide, (c) α-hexylcinnamaldehyde, (d) benzyl acetate, (e) α-bromonaphthalene, (f) ethylene glycol, (g) Miglyol 812N, (h) eugenol, (i) tricresyl phosphate, (j) diiodomethane and (k) tricaprylin.

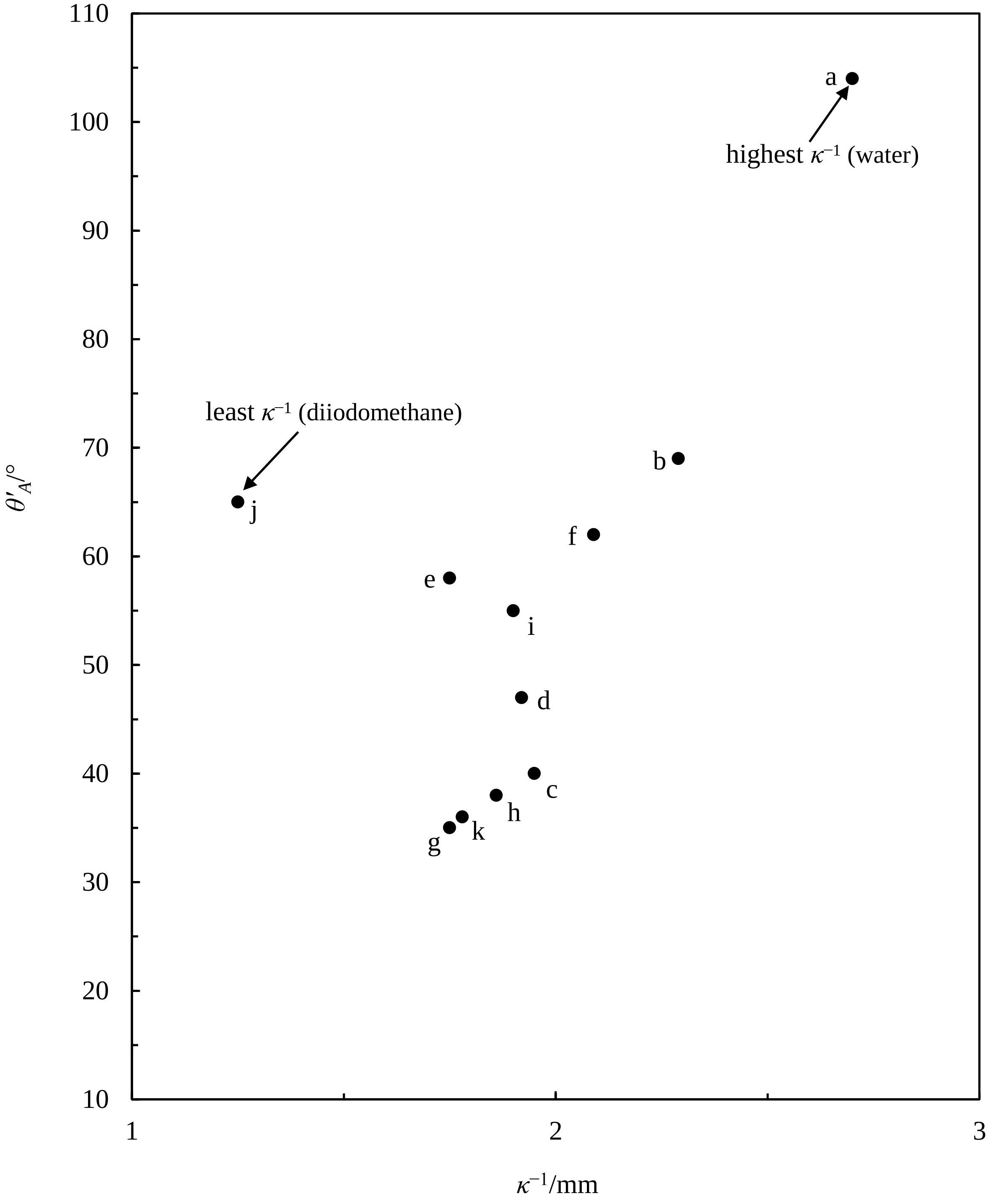

Figure 5.11. (upper) Volume V_{marble} of liquid marbles (10 μL) stabilised by 59% SiOH fluorinated fumed silica particles *versus* time as they rest on a PTFE substrate at ambient conditions. Also shown are data points for bare water and diiodomethane drops (10 μL). (lower) Images of the liquid marbles after 2 days for (a) benzyl acetate, (b) *α*-bromonaphthalene and (c) water.

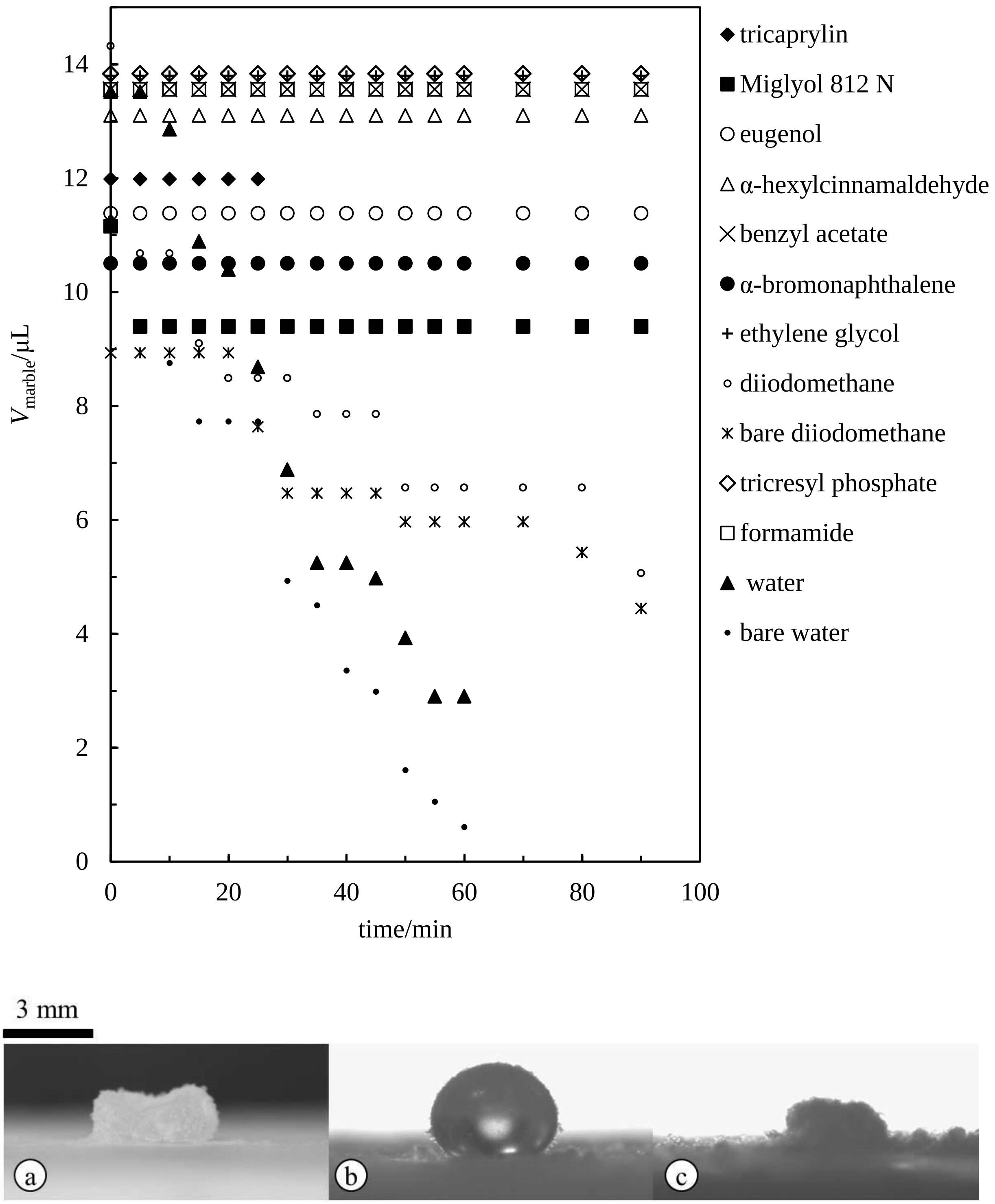

Some of the marbles did not evaporate *e.g.* those of Miglyol 812N, benzyl acetate, eugenol, *α*-bromonaphthalene, tricresyl phosphate, formamide and ethylene glycol and were stable to evaporation for over a day whilst others evaporated slowly. Diiodomethane liquid marbles evaporated slowly and vanished within a day. The water liquid marbles also evaporated slowly and buckled within 90 min. Bare diiodomethane and water evaporated faster than the marbles suggesting that the particle coating reduced the evaporation of the encapsulated liquid. The rate of evaporation of the liquid marbles and the bare liquids is related to the vapour pressure of the liquids (water = 3.17 kPa(24), diiodomethane = 0.16 kPa(25) and other liquids *e.g.* *α*-bromonaphthalene = 7.13×10^{-4} kPa(26)) at 25 °C. It can be seen that bare water (water liquid marble) of relatively higher vapour pressure evaporated faster than bare diiodomethane (diiodomethane liquid marble) of relatively lower vapour pressure and that the extremely low vapour pressure liquids like *α*-bromonaphthalene did not evaporate all. Tricaprylin liquid marble broke up after 24 min and *α*-hexylcinnamaldehyde liquid marble did not evaporate but crumpled within a day.

5.5 Relationship between Solid-Liquid-Air Three-Phase Contact Angle and the Type of Materials Formed

As explained in chapter 1, the θ_{la} a particle makes with the liquid-air interface determines which material is stabilised on mixing air, particles and liquids.[6] Unfortunately, measurement of such angles for nanoparticles is extremely challenging especially if the particles are not all spherical and polydisperse in size like fumed silica. As a result, the contact angle a drop of liquid in air makes with glass slides spin coated with the particles were measured to gain an idea of θ_{la}. It is anticipated that such angles will have contributions from both the inherent γ_{sa} of the particle films as well as their detailed roughness and many studies have investigated the effect of controlled surface roughness on the wettability of particle films by liquids in designing superhydrophobic or superhydrophilic surfaces.[27-35] Plots of cos θ_{la} (apparent advancing) *versus* the γ_{la} of all the liquids studied for different particle-coated glass slides are shown in Figure 5.12(i) and both the apparent advancing and receding θ_{la} are listed in Table 5.2 alongside the type of materials formed for any particle/liquid combinations. Such plots are often linear with a negative slope at least for relatively smooth substrate.[36,37] As described in chapter 2, glass slides composed of the 100 and 14% SiOH fumed silica and 75, 59 and 50% SiOH fluorinated fumed silica particles were spin coated from a 9 wt. % particle dispersion in a ethanol-water mixture (1:3), 5 wt. % particle dispersion in ethanol, 8 wt. % particle dispersion in ethanol, 5 wt. %

particle dispersion in acetone and 4 wt. % particle dispersion in cyclohexane respectively. A complete coating of the glass substrate is formed at these concentrations. Although the solvent is different for any particle type, the SEM micrographs (Figure 5.12(ii)) of the spin coated glass slides show that the particle layers are not more than 16 μm thick except the 50% SiOH fluorinated fumed silica particles whose surfaces have particle coating of ≈ 60 μm thick. In measuring θ_{la} on these surfaces, it is assumed that θ_{la} will be independent of the thickness of the particle layer except in cases where it is significantly small (*e.g.* < 0.2 μm) and independent of the nature of solvent, but would depend largely on particle oleophobicity and on roughness of the spin coated glass surfaces. Thus, θ_{la} measured on these surfaces should give an idea of the degree of oleophobicity of the particles which the glass slide is composed of. The surfaces of the 100% SiOH and 75% SiOH fluorinated silica particle-spin coated glass substrates are relatively smooth compared with the rest of the surfaces coated with the other particles. The apparent advancing θ_{la} of all the liquids (from perfluorohexane to water) measured through the liquid were all ≤ 16° for surfaces composed of 100% SiOH silica particles, indicating an omniphilic surface. In contrast, the 14% SiOH silica particle-coated surfaces exhibited a high apparent advancing θ_{la} for water (147°) with no hysteresis, but a low value for *n*-hexadecane (7°), with that for several other liquids being between these extremes. The apparent advancing θ_{la} for water and *n*-hexadecane on a smooth DCDMS-coated glass substrate plateau at 102° and 25° respectively at high concentrations of DCDMS.[38]

For substrates composed of films of the fluorinated fumed silica particles, a non-linear dependence of cos θ_{la} on γ_{la} was observed in which cos θ_{la} is more or less constant over a range of values of γ_{la} for liquids exhibiting high (> 140°) apparent advancing θ_{la}. Similar findings were reported recently[39] for fluorinated ZnO microparticle surfaces in which apparent advancing θ_{la} was *ca*. 150° for water-ethanol mixtures of γ_{la} between 35 and 73 mN m^{-1}. Using the 75% SiOH fluorinated fumed silica particles; all the liquids exhibited apparent advancing θ_{la} of < 20° except diiodomethane, glycerol and water for which apparent advancing θ_{la} > 20°. The transition from wetting towards non-wetting occurs abruptly at γ_{la} around 65 mN m^{-1}. Considering the similarity in behaviour of these particle surfaces to those of the 14% SiOH silica particles, it can be deduced that despite the presence of low energy fluoro groups, the high percentage of residual SiOH groups renders them of similar wettability to the 14% SiOH silica particles (Table 5.2). For the 59% SiOH fluorinated fumed silica particle-coated substrates, the abrupt transition from wetting towards non-wetting occurs at a lower γ_{la} around 33 mN m^{-1} and as such the surface is oleophobic (*i.e.* apparent advancing θ_{la} < 130°) to several oils like benzyl acetate and eugenol. The surfaces of the 50% SiOH fluorinated fumed silica particles (most fluorinated) were oleophobic to many oils and only oils of tension less than around 28 mN m^{-1} wetted them completely. For oils exhibiting very high apparent θ_{la} (up to *ca*. 150°), the hysteresis between advancing and receding angles is very small (≈ 5°, Table 5.2), an indication of the roughness of the substrate surfaces. SEM images of the fluorinated fumed silica particle-coated glass surfaces are given in Figure 5.12(ii). An increase in oleophobicity with increasing degree of fluorination (and thus decreased apparent γ_{sa}) is thus observed and the so-called omniphobic surfaces[39,40] can be prepared quite easily with these particles.

Figure 5.12. (i) Cosine of apparent advancing contact angle θ_{la} (measured through the liquid) of 0.1 cm^3 of various liquids in air on glass slides spin coated with 100% SiOH silica (×), 75 (□), 59 (○) and 50% SiOH (▲) fluorinated fumed silica particles *versus* surface tension γ_{la} of the liquids at 20 °C. (ii) SEM images of particle-coated glass slides for (a) 75, (b) 59 and (c) 50% SiOH fluorinated fumed silica particles.

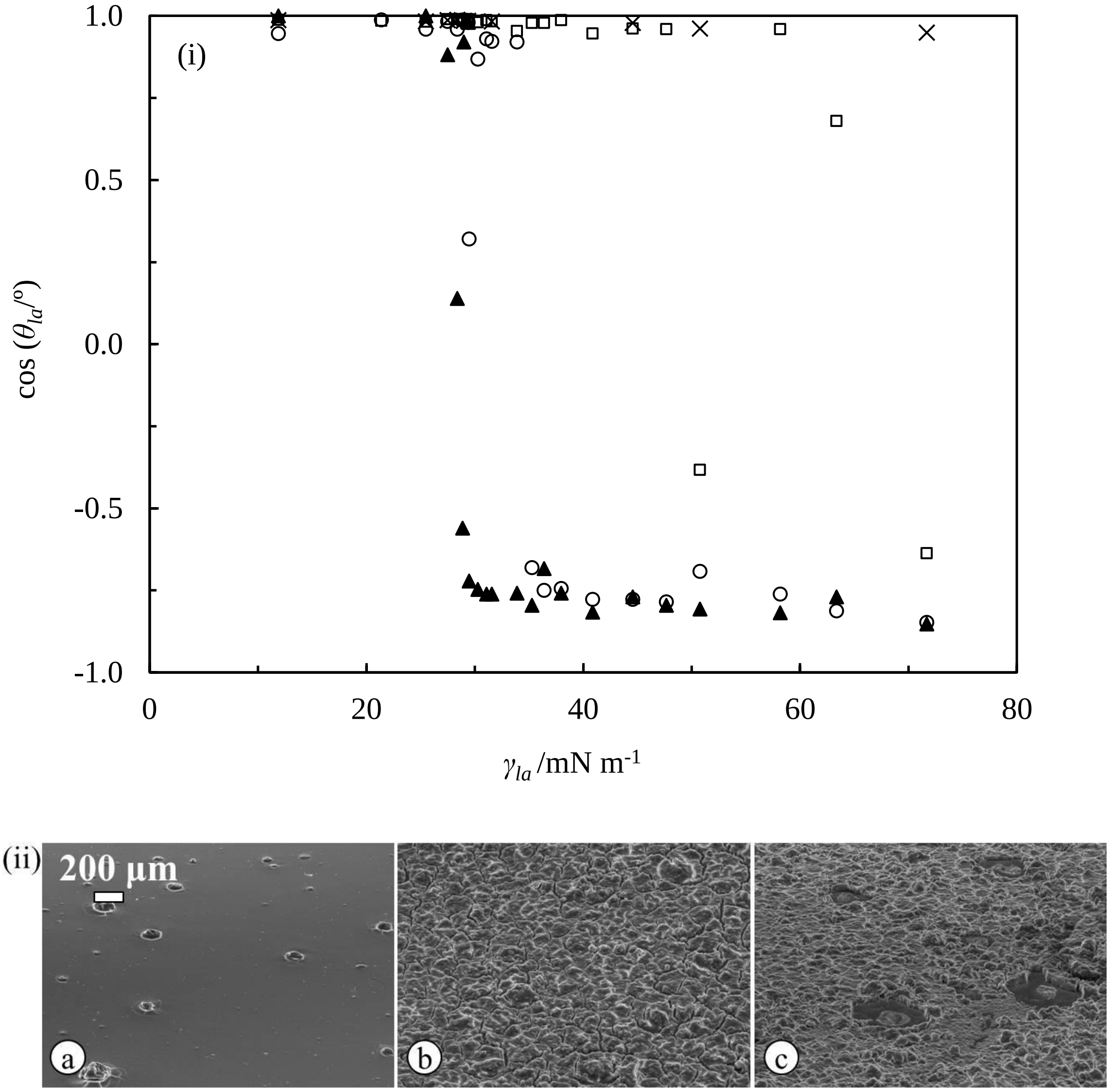

Table 5.2. Apparent advancing (first entry) and receding (second entry) θ_{la} in degrees (measured into the liquid) of 0.1 cm^3 (advancing) and 0.05 cm^3 (receding) drop of liquid in air on glass slides spin coated with the particles at room temperature (22.7 ± 1.1°C). All angles quoted are ± 2° (standard deviation of 4 separate measurements). The types of materials obtained after agitating the systems described in Figure 5.1 are also given: ○-liquid gave particle dispersion, ●-liquid gave substantial amount of foam, ◗-liquid gave insignificant amount of foam, ■-liquid gave foam + climbing films and †-liquid gave climbing films. For marbles: ×-liquid did not form marble, ✓-liquid formed marble.

			Fluorinated fumed silica particles		
Liquid	100% SiOH[a]	14% SiOH	75% SiOH	59% SiOH	50% SiOH
Perfluorohexane	9, 0	×, ○	10, 10: ×, ○	19, < 5: ×, ○	< 5, 5: ×, ○
PDMS 50 cS		×, ○	10, < 5: ×, ○	9, < 5: ×, ○	< 5, 5: ×, ○
Cyclohexane	11, 0	×, ○	11, < 5: ×, ○	17, < 5: ×, ○	< 5, 5: ×, ○
n-Hexadecane	8, 8	7, 7: ×, ○	9, 8: ×, ○	16, 8: ×, ○	28, 25: ✓, ●
Toluene	9, 0	×, ○	9, < 5: ×, ○	17, < 5: ×, ○	82, 22: ✓, ●
Benzene		×, ○	10, < 5: ×, ○	17, < 5: ×, ○	124, 133: ✓, ●
Limonene	10, 0	×, ○	9, < 5: ×, ○	13, < 5: ×, ○	23, 13: ✓, ◗
Isopropyl myristate	10, 0	×, ○	9, < 5: ×, ○	10, < 5: ×, ○	11, < 5: ×, ◗
Tricaprylin		×, ○	10, 10: ×, ○	71, 20: ✓, ○	136, 131: ✓, ●
Miglyol 812N		×, ○	11, 10: ×, ○	30, 16: ✓, ○	138, 132: ✓, ●
Squalane		×, ○	10, 10: ×, ○	22, 13: ✓[b], ○	140, 130: ✓, ●
Geraniol	11, 11	×, ○	11, 11: ×, ○	23, 14: ✓[b], ○	140, 130: ✓, ●
Sunflower oil		×, ○	18, 13: ×, ○	23, 11: ✓[b], ○	139, 131: ✓, ●
α-Hexylcinnamaldehyde		×, ○	12, 11: ×, ○	133, 107: ✓, ●	142, 139: ✓, ●
Eugenol		×, ○	12, 11: ×, ○	139, 108: ✓, ●	133, 132: ✓, ●
Benzyl acetate		×, ○	10, 10: ×, ○	138, 108: ✓, ●	139, 139: ✓, ●
Tricresyl phosphate		×, ○	19, 12: ×, ○	141, 130: ✓, ●	145, 139: ✓, ■
α-Bromonaphthalene	12, 12	×, ○	16, 10: ×, ○	141, 132: ✓, ●	140, 139: ✓, ■
Ethylene glycol		✓, †	17, 11: ×, ○	140, 106: ✓, ■	143, 140: ✓, ■
Diiodomethane	16, 16	✓, †	113, 87: ✓, ●	134, 122: ✓, ●	144, 127: ✓, ■
Formamide		✓, †	17, 11: ×, ○	140, 138: ✓, ■	145, 142: ✓, †
Glycerol		✓, †	47, 33: ✓, ●	144, 144: ✓, ■	140, 137: ✓, †
Water	15, 15	147, 146: ✓, †	130, 105: ✓, ■	148, 143: ✓, †	149, 145: ✓, †

[a] No liquid marbles could be formed for these particles with any liquid.

[b] Marble formed at rest but broke up whilst rolling.

It can be seen in Table 5.2 that liquids exhibiting apparent advancing $\theta_{la} \geq 28^o$ with the fluorinated fumed silica particles formed stable marbles and foams (provided the apparent advancing θ_{la} is between 82 and 145°) with them. The only exception is the case ($\theta_{la} = 28^o$) where *n*-hexadecane marble and foam are formed by the 50% SiOH fluorinated fumed silica particles. For *n*-hexadecane and squalane of relatively low tension in which molecules interact mainly through dispersion forces, foams and marbles are obtained only with the most fluorinated silica particles. This is in contrast to *α*-bromonaphthalene and diiodomethane of relatively high tension, and in which molecules also interact mainly by dispersion forces, where there is a clear transition from particle dispersions to foams and then foams + climbing films in addition to marbles as the degree of fluorination increases. Water of highest tension in which molecules interact through hydrogen bonds, polar and dispersion forces, however, formed mainly climbing films and marbles with both the fluorinated and hydrocarbon-coated silica particles. Marbles formed not just for liquids exhibiting high apparent advancing angles with the particles, but also those exhibiting low apparent advancing angles like *n*-hexadecane/50% SiOH fluorinated silica and glycerol/75% SiOH fluorinated silica. It is thought that these marbles are stabilised mainly by particle multilayers. Comparing these systems with aqueous ones, two important observations are apparent. Firstly, in aqueous systems, stable foams are obtained only with particles making apparent θ_{la} significantly more than 0° but less than 90° and stable marbles are obtained only with particles exhibiting apparent θ_{la} significantly > 90°. Secondly, stabilisation of both foams and marbles (*i.e.* inversion of curvature of liquid-air surfaces) without changing either the surface chemistry of the particles or properties of the liquids does not happen in aqueous systems as it occurs here in some cases. The formation of both foams and liquid marbles in the presence of these particles might be due to the difference in the methods used for preparation of these materials or contact angle hysteresis. The findings relating to fluorinated silica particle-oil-air systems are summarised in Figure 5.13. In the upper sketch, the θ_{la} of a particle at the oil-air interface measured through the oil is shown. This can be tuned from zero to intermediate to high values upon either increasing the γ_{la} of the oil (*i.e.* using different oil types) or decreasing the γ_{sa} of the particles (by fluorination). In the lower sketch, the type of bulk materials formed in the presence of many particles for the corresponding θ_{la} scenario is illustrated. By progressively increasing θ_{la}, the transition dispersion → foam → marble is achieved.

Figure 5.13. (upper) Position of a fluorinated silica particle (sphere) at the liquid (or oil)-air interface as a function of surface tension γ_{la} or surface energy γ_{sa}. The angle θ_{la} increases from zero to medium to high values from left to right. (lower) Corresponding bulk materials formed: (i) dispersion, *e.g*. diiodomethane plus 100% SiOH silica (apparent advancing θ_{la} = 16°), (ii) air-in-oil foam, *e.g*. diiodomethane plus 75% SiOH fluorinated silica (apparent advancing θ_{la} = 113°) and (iii) oil-in-air marble, *e.g*. diiodomethane plus 50% SiOH fluorinated silica (apparent advancing θ_{la} = 135°).

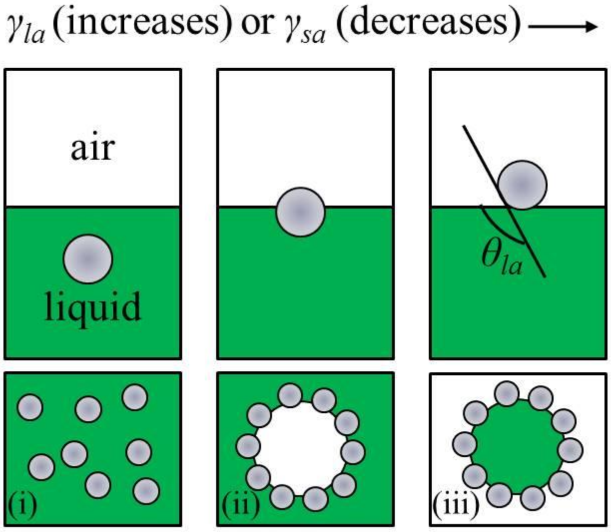

5.6 Conclusions

The behaviour of fluorinated fumed silica particles of increasing degree of fluorination in mixtures of air and liquid, for liquids ranging from non-polar hydrocarbons and polar oils to high cohesive energy density liquids like glycerol and water has been investigated. Comparisons are made with hydrophilic and very hydrophobic fumed silica particles. The materials which form after aeration depend on both the γ_{la} and the degree of fluorination of the particles which dictates the degree of wetting of the particles by the liquids. An oil dispersion of particles forms in liquids of relatively low γ_{la} with particles of low fluorine content where apparent advancing θ_{la} < 20°. Particle-stabilised a/o foams were obtained in oils of relatively high tension (> 32 mN m^{-1}) and particles of moderate fluorine content and with oils of lower tension (> 27 mN m^{-1}) and particles of high fluorine content where apparent advancing θ_{la} lies between 82 and 145°. In many cases, oil liquid marbles were also stabilised, with particles of highest fluorine content encapsulating oils of lower γ_{la}.

5.7 References

1. B. P. Binks, *Curr. Opin. Colloid Interface Sci.*, 2002, **7**, 21−41.
2. R. Aveyard, B. P. Binks and J. H. Clint, *Adv. Colloid Interface Sci.*, 2003, **100–102**, 503−546.
3. A. Stocco, F. Garcia-Moreno, I. Manke, J. Banhart and D. Langevin, *Soft Matter*, 2011, **7**, 631−637.
4. A. Stocco, E. Rio, B. P. Binks and D. Langevin, *Soft Matter*, 2011, **7**, 1260−1267.
5. P. Aussillous and D. Quéré, *Nature*, 2001, **411**, 924−927.
6. B. P. Binks and A. Rocher, *Phys. Chem. Chem. Phys.*, 2010, **12**, 9169−9171.
7. B. P. Binks, A. Rocher and M. Kirkland, *Soft Matter*, 2011, **7**, 1800−1808.
8. R. Murakami and A. Bismarck, *Adv. Funct. Mater.*, 2010, **20**, 732−737.
9. B. P. Binks and T. S. Horozov, *Angew. Chem. Int. Ed.*, 2005, **44**, 3722−3725.
10. B. P. Binks and S. O. Lumsdon, *Langmuir*, 2000, **16**, 8622−8631.
11. B. P. Binks and R. Murakami, *Nat. Mater.*, 2006, **5**, 865−869.
12. Y.-C. Sheen, Y.-C. Huang, C.-S. Liao, H.-Y. Chou and F.-C. Chang, *J. Polym. Sci. Part B: Polym. Phys.*, 2008, **46**, 1984−1990.
13. A. Tuteja, W. Choi, M. Ma, J. M. Mabry, S. A. Mazzella, G. C. Rutledge, G. H. McKinley and R. E. Cohen, *Science*, 2007, **318**, 1618−1622.
14. Y. Xue, H. Wang, Y. Zhao, L. Dai, L. Feng, X. Wang and T. Lin, *Adv. Mater.*, 2010, **22**, 4814-4818.
15. D. Matsukuma, H. Watanabe, H. Yamaguchi and A. Takahara, *Langmuir*, 2011, **27**, 1269−1274.
16. M. Hikita, K. Tanaka, T. Nakamura, T. Kajiyama and A. Takahara, *Langmuir*, 2005, **21**, 7299−7302.
17. H. Zhao, K.-Y. Law and V. Sambhy, *Langmuir*, 2011, **27**, 5927−5935.
18. R. G. Alargova, D. S. Warhadpande, V. N. Paunov and O. D. Velev, *Langmuir*, 2004, **20**, 10371−10374.
19. B. P. Binks, J. H. Clint, P. D. I. Fletcher, T. J. G. Lees and P. Taylor, *Chem. Commun.*, 2006, 3531−3533.
20. A. B. Subramaniam, M. Abkarian, L. Mahadevan and H. A. Stone, *Nature*, 2005, **438**, 930.
21. D. Exerowa and P. M. Krglyakov, *Foam and Foam Films*, Elsevier, Amsterdam, 1998.
22. A. B. Subramaniam, M. Abkarian, L. Mahadevan and H. A. Stone, *Langmuir*, 2006, **22**, 10204−10208.
23. G. McHale, N. J. Shirtcliffe, M. I. Newton, F. B. Pyatt and S. H. Doerr, *Appl. Phys. Lett*, 2007, **90**.
24. L. Haar, J. S. Gallagher and G. S. Kell, *NBS/NRC Steam Tables*, Hemisphere Publishing Corp., New York, 1984.
25. C. L. Yaws, *Chemical Properties Handbook*, McGraw-Hill, New York, 1999.
26. M. Urbani, R. Gigli and V. Piacente, *J. Chem. Eng. Data*, 1980, **25**, 97−100.
27. T. Onda, S. Shibuichi, N. Satoh and K. Tsujii, *Langmuir*, 1996, **12**, 2125−2127.
28. W. Barthlott and C. Neinhuis, *Planta*, 1997, **202**, 1−8.
29. J. H. Ensikat, P. Ditche-Kuru, C. Neinhuis and W. Barthlott, *Beilstein J. Nanotechnol*, 2011, **2**, 152−161.
30. C. Ishino, K. Okumura and D. Quéré, *Europhys. Lett.*, 2004, **68**, 419.
31. H. Tsutsui, M. Mikami and R. Akashi, *Adv. Mater.*, 2004, **16**, 1925−1929.
32. Y. Xiu, L. Zhu, D. W. Hess and C. P. Wong, *Nano Lett.*, 2007, **7**, 3388−3393.
33. Y. Kwon, N. Patankar, J. Choi and J. Lee, *Langmuir*, 2009, **25**, 6129−6136.

34. S. Jung, M. Dorrestijn, D. Raps, A. Das, C. M. Megaridis and D. Poulikakos, *Langmuir*, 2011, **27**, 3059−3066.
35. H. Kim, C. Lee, M. H. Kim and J. Kim, *Langmuir*, 2012, **28**, 11250−11257.
36. H. W. Fox and W. A. Zisman, *J. Colloid Sci.*, 1950, **5**, 514−531.
37. H. W. Fox and W. A. Zisman, *J. Colloid Sci.*, 1952, **7**, 428−442.
38. B. P. Binks and T. S. Horozov, unpublished work.
39. G. Perry, Y. Coffinier, V. Thomy and R. Boukherroub, *Langmuir*, 2011, **28**, 389−395.
40. A. Tuteja, W. Choi, J. M. Mabry, G. H. McKinley and R. E. Cohen, *PNAS*, 2008, **105**, 18200−18205.

Chapter 6

Dry Oil Powders and Oil Foams Stabilised by Fluorinated Clay and Fluorinated ZnO Particles

6.1 Introduction

Following the pioneering work of Ramsden[1] and Pickering,[2] ultra-stable oil-water emulsions[3] and aqueous[4,5] and non-aqueous (oil) foams[6,7] have been prepared using small solid particles alone. For spherical particles, the extent to which the fluid phases wet the particles, quantified by θ_{la} (measured through the more polar phase) they make with the fluid-fluid interface, dictates the type of end material as described in chapter 1. It is known that in oil (o)-water (w) systems (equal volumes), relatively hydrophilic particles ($\theta_{ow} < 90°$) partition more in the water phase and tend to stabilise o/w emulsions whilst relatively hydrophobic ones ($\theta_{ow} > 90°$) partition more in the oil phase and prefer to stabilise w/o emulsions.[8] In the case of air (a)-water (w) systems, partially hydrophobic (very hydrophobic) particles are necessary for stabilisation of air-in-water (a/w) foams[9] (water-in-air (w/a) materials, *e.g.* liquid marbles).[10,11] In non-aqueous systems like oil, preparation of stable air-in-oil (a/o) foams and oil-in-air (o/a) materials (*e.g.* oil liquid marbles) requires relatively oleophilic ($\theta_{la} < 90°$) and oleophobic ($\theta_{la} > 90°$) particles, respectively.[12] Omniphilic particles have fairly large affinity for both water and oil and would stabilise a/w and a/o systems, whilst omniphobic particles having very little affinity for both water and oil tend to stabilise w/a and o/a systems. Oleophobic and omniphobic surfaces are created from hydrophilic precursors by surface chemical modification using suitable fluorocarbons of low surface energy.[13-15] Other properties that also influence the type of final product formed in liquid-air systems include the γ_{sa}, γ_{la} and the speed of mixing.[16] In oil-air systems, it has been shown that with appropriate agitation, a combination of relatively low γ_{la} and relatively high γ_{sa} oleophilic particles yields a particle dispersion, but a combination of liquids of intermediate (high) γ_{la} and oleophobic particles of intermediate (low) γ_{sa} gives oil foams (oil liquid marbles).[7]

Liquid marbles, first described by Aussillous and Quéré,[10] are now widely studied[17-20] and can be considered an element of dry liquid powdered materials, *i.e.* dry water (if the liquid is water) and dry oil powders (if the liquid is an oil). Dry water[21] (dry oil)[22] is a free-flowing powder containing numerous water (oil) droplets coated with small solid particles which are poorly wetted by them. The encapsulated liquid may be released by evaporation or on application of mechanical stress. The particles confer stability on the liquid droplets and allow them to move with minimum adhesion to a substrate. This principle is also used by nature, both in the self-cleaning mechanism of various plant leaves[23] and in the excretion of honeydew globules from aphids.[24] Even though both dry water and dry oil powders have potential applications in the cosmetic, pharmaceutical and other related industries, studies on them are few and far between, especially for dry oils. This is partly due to the relatively low γ_{la} of many oils and partly due to the relatively high γ_{sa} of many colloidal particles. Reports on oil liquid marbles are also limited for the same reason. From thermodynamic considerations,[25] this prevents particle adsorption and hence stabilisation of the related materials.[7] Papers on dry water include those from Binks and co-workers[21,26,27] and Forny *et al.*[28] Some potential applications of dry water have been reported by Forny *et al.*[29] and Carter *et al.*[30,31] Catastrophic phase inversion of particle-stabilised water-air systems, from a/w foams to w/a powders (containing about 98 wt. % of water with respect to the total mass) was demonstrated in ref. 21, by either a progressive change in silica-particle hydrophobicity at constant air : water ratio or by changing the air : water ratio at fixed particle wettability. The change in particle wettability was linked to the first inversion, whilst change in the volume fraction of the phase(s) was crucial for inversion in the second case.[21] Transitional phase inversion of dry water to aqueous foam was reported in ref. 26. Addition of charged surfactant to mixtures of air, water and hydrophobic silica nanoparticles under high shear initially formed dry water powder at low surfactant concentrations and a/w foam at higher surfactant concentrations.[26] In another study,[27] charged partially hydrophobic silica particles were used to show how changes in pH and salt concentration affect phase inversion of water-air-particle systems. Dry water formation was favoured at low pH or high salt concentration as the colloidal particles were made hydrophobic, but a high pH or low salt concentration resulted in charged, partially hydrophilic particles which were able to stabilise aqueous foams.[27] The θ_{la} and particle attachment energy ΔG_m needed for dry water formation by spherical hydrophobic particles were investigated in ref. 28. For these particles (R = 8 nm), θ_{la} of 118° and ΔG_m of $\approx -1.1 \times 10^3$ kT favoured dry water formation.[28] About the applications of dry water, dry water containing 98−99 wt. % of water by mass was used to store water,[29] enhance the kinetics of heterogeneous catalytic hydrogenation[30] and to enhance gas uptake rates in gas hydrates.[31] On dry oil powders, Murakami and Bismarck[22] used agglomerated oligomeric tetrafluoroethylene (OTFE) particles to prepare dry oil powders (containing 10–15 wt. % of oil relative to the total mass). The dry oil powders were prepared by spraying oils from a spray gun on particles placed on a Tefal frying pan. Another preparation of dry oil powders employed protein[32] or particle-stabilised[33] o/w emulsions as precursors followed by slow or rapid drying. Following this protocol, an oil powder containing about 90 wt. % of oil relative to the total mass which showed no sign of oil leakage over several months was prepared. This process however requires high energy and the drying stage is time consuming. A similar procedure which does not require evaporation of the continuous phase has been used to prepare oil-in-water-in-air (o/w/a) materials termed either a powdered emulsion[34] or a dry water emulsion.[35] To obtain powdered emulsions,[34] particle-stabilised o/w emulsions stable to coalescence were aerated with very hydrophobic solid particles using a blender at high shear. The hydrophobic particles coat the newly created water globules in air which encase the oil droplets in water. Similarly, o/w emulsions stabilised by branched copolymer surfactant were diluted before aerating in the presence of hydrophobic silica nanoparticles to obtain the dry water emulsion.[35] To the best of my knowledge, a systematic study on the preparation of dry oil powders is yet to be reported. In this study, using fluorinated solid particles of varying γ_{sa} and polar oils and *n*-alkanes of varying γ_{la} and low shear, it is shown that dry oil powders containing up to 80 wt. % of oil (relative to the total mass) can be prepared by simply hand shaking a mixture of fluorinated solid particles and oil. The dry oil powders invert to ultra-stable oil foams at high oil : particle ratio. These materials can be used for cosmetic applications.

6.2 Behaviour of Particles on Oil Surfaces with Agitation

Figure 6.1 summarises the results of the particle immersion experiment for the PF-0 to PF-12 Eight Pearl 300S-Al sericite particles. The most oleophilic particles of PF-0 Eight Pearl 300S-Al were wetted by all the oils and water and entered them within 30 s at rest. On agitation, a cloudy dispersion forms in the liquids. The following behaviour was observed for the other fluorinated particles. For the relatively low tension oils (γ_{la} below 22 mN m^{-1}), the particles were either partially or completely wetted at rest or were not wetted at rest but entered the oil after agitation to give a cloudy dispersion. Oils of relatively high surface tension (γ_{la} above 22 mN m^{-1}) did not wet the particles at rest. On agitation (apart from PDMS 20 cS and PF-5 Eight Pearl 300S-Al mixture which gave a cloudy dispersion), all the oils possessing γ_{la} between 22–32 mN m^{-1} produced a foam or a foam with a climbing film. Oils with γ_{la} between 32–37 mN m^{-1} gave foam and climbing films on agitation except cetyl 2-ethylhexanoate, macadamia nuts oil and jojoba oil that gave only foam with the least fluorinated particles and 2-ethyhexyl-4-methoxycinnamate that gave mainly climbing films with the most fluorinated ones. Water, possessing the highest γ_{la}, gave only a climbing film with the fluorinated particles. Photos of some of the materials formed by the particles with the various oils are shown in Figure 6.2. The transition from oil dispersions to oil foams and ultimately to non-wetting states as the γ_{la} of the liquid increases is consistent with earlier predictions and findings.[12]

Figure 6.1. Behaviour of the Eight Pearl 300S-Al sericite particles (50 mg) on the surfaces of the various liquids (3 cm^3) at rest. Abscissa: 1-particles were wetted by the liquid, 2-particles were partially wetted by the liquid (*i.e.* some particles entered the liquid whilst some did not) and 3-particles were not wetted by the liquid. Ordinate: number in brackets is liquid γ_{la} (± 0.1 mN m^{-1}) at 25 °C.

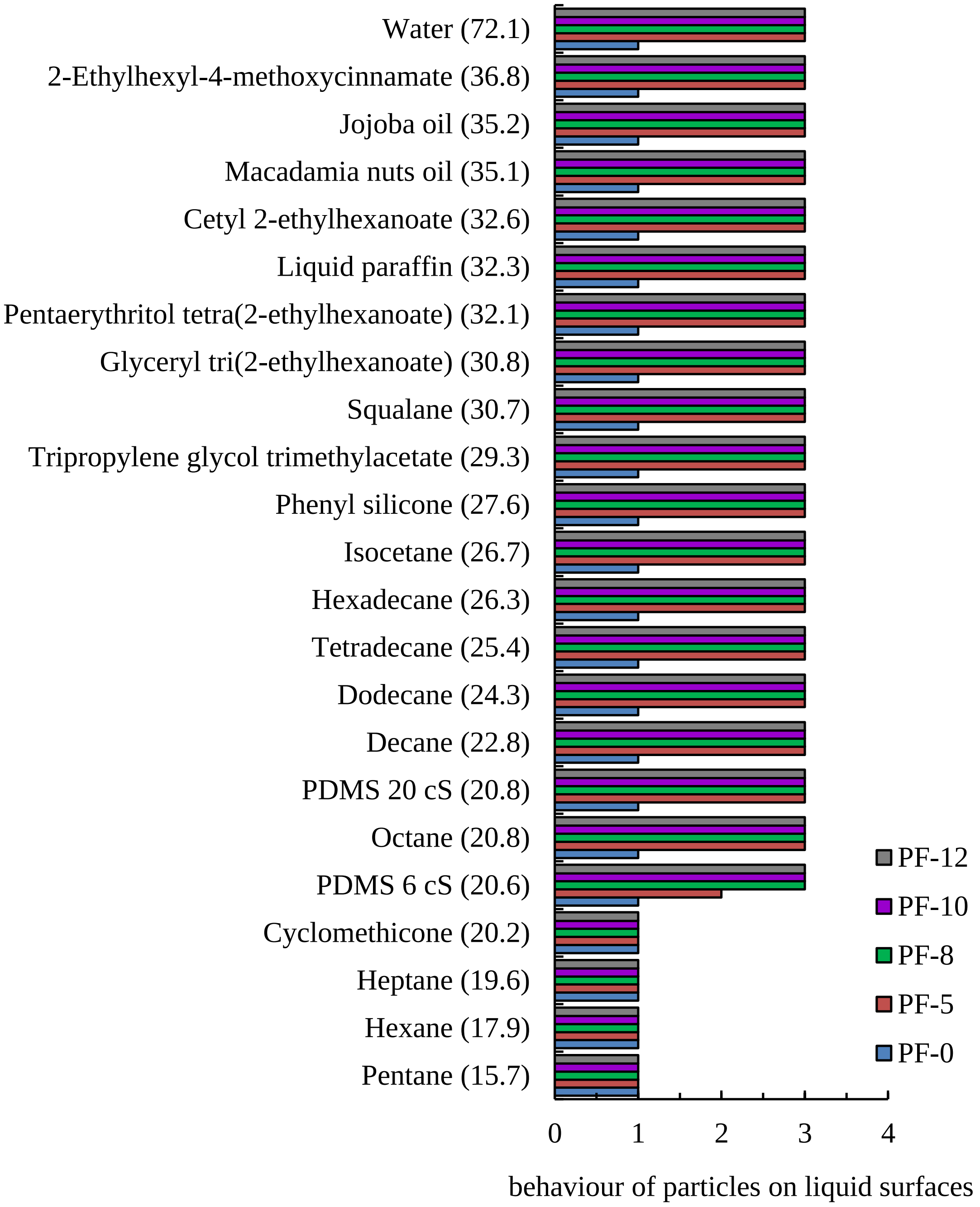

Figure 6.2. Photos of glass vials containing PF-(a) 0, (b) 5, (c) 8, (d) 10 and (e) 12 Eight Pearl 300S-Al sericite particles (50 mg) and liquids (3 cm^3) after agitation (30 s): (1) *n*-pentane-particle dispersions, (2) cyclomethicone-particle dispersions, (3) PDMS 20 cS-particle dispersion alone, dispersion + little foam or foam, (4) isocetane-particle dispersion or foam, (5) *n*-hexadecane-particle dispersion or foam, (6) squalane-particle dispersion alone, foam alone or foam + climbing films, (7) 2-ethylhexyl-4-methoxycinnamate-particle dispersion, foam + climbing films or climbing films and (8) water-particle dispersion or climbing films.

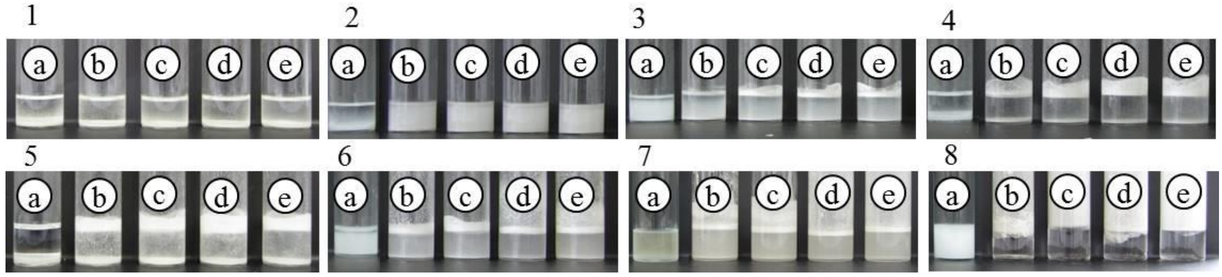

A summary of the particle immersion experiment for the PFX-10 Kunipia F, PFX-10 ZnO (TP), PF-10 Eight Pearl 300S-Al^a and PF-10 FSE-Al fluorinated particles is given in Appendix 6.1. It can be seen that PFX-10 Kunipia F was completely wetted by cyclomethicone, *n*-octane and water and entered them within 7 min at rest and was partially wetted by PDMS 6 and 20 cS, but was not wetted by the rest of the liquids. On agitation, a cloudy dispersion forms in all the liquids. The PFX-10 ZnO (TP) particles were completely or partially wetted by only liquids having γ_{la} below 21 mN m^{-1} like PDMS 6 and 20 cS. When agitated, a cloudy dispersion forms in these liquids and those of higher γ_{la} up to 25 mN m^{-1} which did not wet them previously, foams formed in liquids having $\gamma_{la} > 25$ mN m^{-1}, *e.g. n*-hexadecane, glyceryl tri(2-ethylhexanoate) and 2-ethylhexyl-4-methoxycinnamate and climbing films were formed in water. The PF-10 Eight Pearl 300S-Al^a and PF-10 FSE-Al particles were not wetted by all the liquids at rest. Upon agitation, cloudy dispersions were seen in liquids of γ_{la} below 26 mN m^{-1}, foams in liquids of higher tensions and climbing films in water of highest tension. Just like with the fluorinated sericite particles, a transition from oil dispersions to oil foams and ultimately to non-wetting state as the γ_{la} of the liquid increases for the PFX-10 ZnO (TP) to PF-10 FSE-Al was observed.

6.3 Oil Liquid Marbles and Dry Oil Powders Stabilised by Particles

As mentioned earlier, oil liquid marbles can be conceived as the smallest unit of dry oil powders, although the size of a marble is significantly larger and it can be seen by eye. Marble formation was possible with most oil and particle combinations that produced oil foams described above. As the degree of particle fluorination increases, the robustness of the marbles also increased. For water and many oils, it is generally accepted that relatively small (≤ 100 μL) liquid marbles, where the effect of γ_{la} dominates that of gravity, are quasi-spherical, whilst relatively large (> 100 μL) ones, where the effect of gravity dominates that of γ_{la}, are puddle-shaped.[17,36] Here, however, the oil marbles (10 μL) assume a 'sausage-like' shape if the oil droplet is rolled on the particle bed (to and fro) in only one direction. Otherwise, they are quasi-spherical (see later).

Based on the findings in chapter 5 and the foregoing, it was anticipated that the PFX-10 Kunipia F, PFX-10 ZnO (TP), PF-10 Eight Pearl 300S-Al[a] and PF-10 FSE-Al fluorinated particles exhibiting relatively low apparent γ_{sa} would stabilise marbles and dry oil powders of the oils under investigation. Even though the apparent γ_{sa} of the four particle types differs significantly from each other, marble formation was possible with all the oil/particle combinations except with four combinations, namely, cyclomethicone/PFX-10 Kunipia F, water/PFX-10 Kunipia F, cyclomethicone/PFX-10 ZnO (TP) and PDMS 6 cS/PFX-10 ZnO (TP). Apart from the PFX-10 ZnO (TP) particle-stabilised marbles which were all quasi-spherical as expected (considering their capillary length κ^{-1} and radius R'), many of the marbles stabilised by the rest of the particles had a 'sausage-like' shape especially if the oil droplet was rolled on the particle bed (to and fro) in only one direction just like in the case of the fluorinated sericite particles. This observation deviates from the general rule which says the effect of γ_{la} dominates that of gravity for relatively small liquid marbles having $R' << \kappa^{-1}$ and are quasi-spherical and *vice versa* for relatively large ones ($R' >> \kappa^{-1}$) which are puddle-shaped.[17,36] The reason for this deviation is not clear at the moment, but might be due to the shape of the particles considering the fact that the PFX-10 ZnO (TP) particles are spherical whilst the rest of the particle types are platelet.

Following successful preparation of liquid marbles with these oils and fluorinated particles, attempts were made to prepare dry oil powders from them too. This was done in five different ways as stated earlier, conscious of the critical oil : particle ratio COPR, with the best being the sequential approach whose results are discussed here. Dry oil powder formation was possible with the majority of the oil and particle combinations that formed oil marbles. Figure

6.3(a) shows that the COPR increases with an increase in the degree of fluorination for the PF-5 to PF-12 Eight Pearl 300S-Al sericite particles. The effect of the degree of fluorination and hence the apparent γ_{sa} on the COPR is shown in Figure 6.3(b) for isocetane, glyceryl tri(2-ethylhexanoate) and 2-ethylhexyl-4-methoxycinnamate for these particles. An inverse correlation exists between apparent γ_{sa} and the COPR. The amount of oil encapsulated within powders ranges from 44 (dry isocetane powder stabilised by PF-5 Eight Pearl 300S-Al particles) to 81 wt. % (2-ethylhexyl-4-methoxycinnamate powder stabilised by PF-12 Eight Pearl 300S-Al particles), the latter exceeding that reported earlier[22] by a factor of five. Similar to liquid marble formation, the most oleophilic PF-0 Eight Pearl 300S-Al and relatively high γ_{sa} particles did not adsorb at the liquid-air interfaces and thus did not enable dry oil formation. Dry oil formation for the rest of the particles and with oils possessing γ_{la} below 25 mN m^{-1} (*i.e.* cyclomethicone, PDMS 6 and 20 cS) was also not possible even though marbles could be prepared. Dry oil powders were successfully prepared from the rest of the oils and particle types *via* sequential addition of the required amount of oil to the particles, followed by low shear, up to the COPR. The dry oil powders invert to oil foams after COPR (see sec. 6.4). Formation of dry water was not possible because of the large difference between its γ_{la} and the apparent γ_{sa} of the particles. In addition, the high γ_{la} of water did not allow disruption of a big water drop into smaller droplets by gentle shaking unlike the case with the relatively low γ_{la} oils. Photos of some dry oil powders and their corresponding optical micrographs (alongside photos of some oil marbles) are shown in Figures 6.4 and 6.5, respectively. It can be seen that the oil droplets (> 100 μm) within the powders are non-spherical in shape. Such deviation from spherical shape has been reported previously for particle-coated fluid dispersed phases and is due to the jamming of particles at the interface preventing their relaxation to a spherical geometry.[37] A cryo-SEM image from an oil powder is included in Figure 6.5 where a fractured oil droplet coated with particles containing frozen oil within is clearly visible. Majority of the PFX-10 ZnO (TP), PF-10 Eight Pearl 300S-Al[a] and PF-10 FSE-Al particle/oil combinations that formed oil marbles previously also formed dry oil powders. However, the PFX-10 Kunipia F particles did not form any dry oil powders and this could be due to their relatively large particle size (> 400 μm) compared with the rest of the particles. For the PFX-10 ZnO (TP), PF-10 Eight Pearl 300S-Al[a] and PF-10 FSE-Al particles, the COPR increases as the γ_{la} of the liquids increases (Appendix 6.2) just like in the case of the PF-5 to PF-12 Eight Pearl 300S-Al sericite particles. The PFX-10 ZnO (TP) particle-stabilised dry oil powders appear (visually) to be composed of fine oil droplets and free-flowing compared with the rest of the dry oil powders. The amount of oil encapsulated within powders ranges from *ca.* 29 (dry cyclohexane powder stabilised by PFX-10 ZnO (TP) particles) to *ca.* 78 wt. %

(rapeseed oil powder stabilised by PF-10 Eight Pearl 300S-Al^{a} particles). Photographs of some dry oil powders stabilised by the PFX-10 ZnO (TP), PF-10 Eight Pearl 300S-Al^{a} and PF-10 FSE-Al particles and optical micrographs of some of them (along with photographs of some liquid marbles) are shown in Appendixes 6.3 and 6.4, respectively. A cryo-SEM image from an oil powder stabilised by the PFX-10 ZnO (TP) fluorinated particles is also included in Appendix 6.4 where frozen oil droplets coated with particles are clearly visible. It can be seen that the oil droplets (size 2−400 μm) within the powders are non-spherical in shape.

The absence of significant oil staining upon placing the dry oil powders on a filter paper and watch glass suggests that the oil droplets in the powder are stable against oil leakage. Apart from the *n*-alkanes powders that released some of the encapsulated alkane droplets after a week, the dry oil powders are stable to oil leakage and hence to phase separation for at least 2 years. However, they liquefy and cream releasing the encapsulated oil when sheared on the skin or a surface (Figure 6.6) except in cases where the oil content (relative to the total mass of powder) is less than 60 wt. % which form a paste. The dry oil powders invert to oil foams upon vigorous shaking as verified with squalane, liquid paraffin and jojoba oil stabilised by PF-8 Eight Pearl 300S-Al and PFX-10 ZnO (TP) fluorinated particles. This suggests that the dry oil powders are metastable with the stable state being oil foam.

Figure 6.3. The COPR *versus* (a) surface tension γ_{la} (25 °C) of the oils for PF-5 (◆), 8 (▲), 10 (●) and 12 (■) Eight Pearl 300S-Al particles and (b) apparent surface energy γ_{sa} (25 °C) of the particles for isocetane (▲), glyceryl tri(2-ethylhexanoate) (◆) and 2-ethylhexyl-4-methoxycinnamate (●). Inset: schematic of a/o foam above COPR and dry oil powder at or below COPR. For simplicity, the oil droplets and air bubbles are spherical. The error bars represent the minimum amount of oil required for phase inversion per gram of particles.

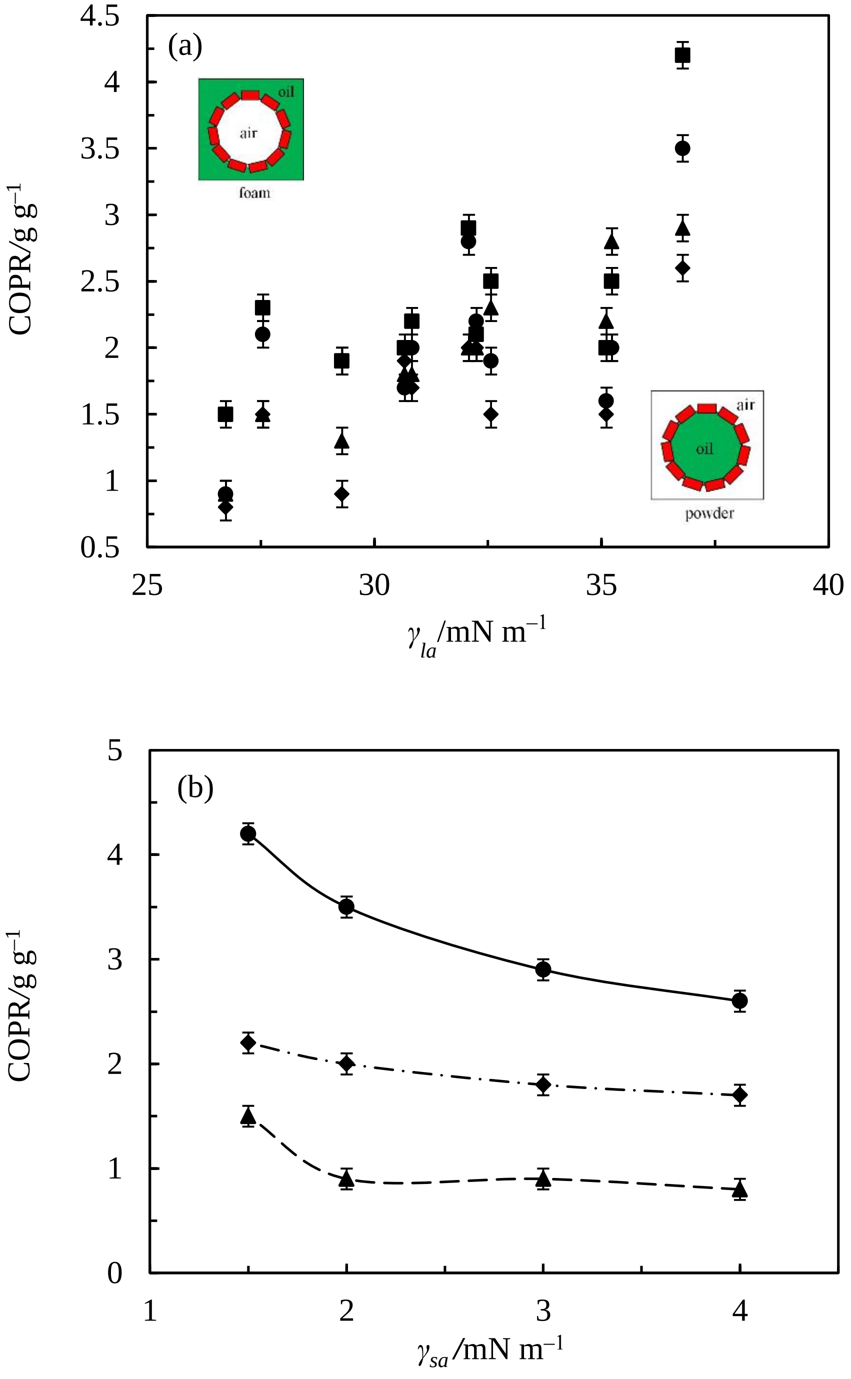

Figure 6.4. (upper) Photos of watch glasses containing dry oil powders 1 month after formation of (a) squalane, (b) liquid paraffin, (c) cetyl 2-ethylhexanoate and (d) macadamia nuts oil stabilised by PF-12 Eight Pearl 300S-Al sericite particles. (lower) Photo of corresponding dry liquid paraffin powder flowing through a glass funnel onto a Pyrex watch glass. Scale bar = 10 mm.

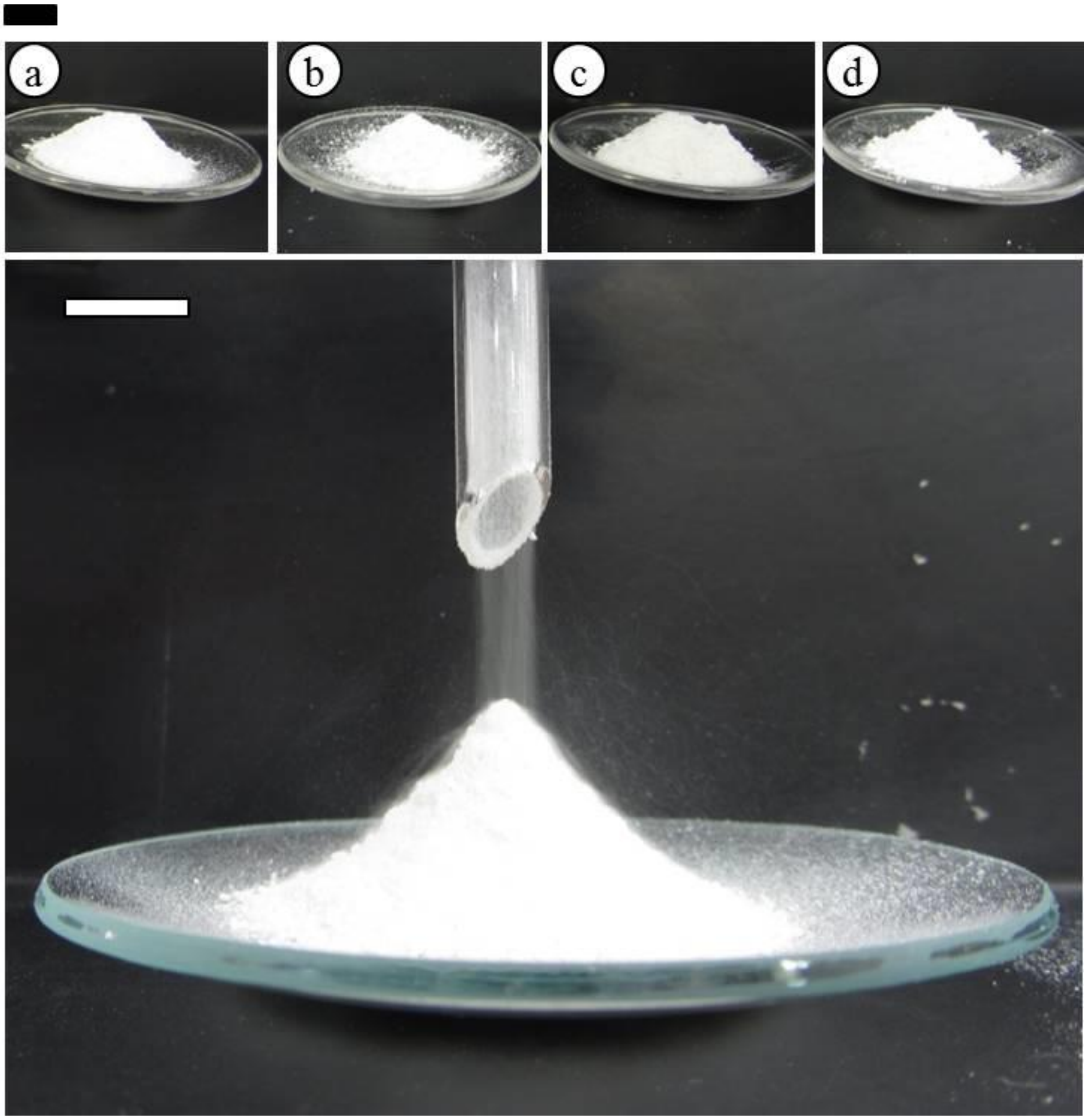

Figure 6.5. (upper) Optical micrographs soon after formation of dry (i) squalane powder stabilised by PF-5 Eight Pearl 300S-Al, (ii) liquid paraffin powder stabilised by PF-8 Eight Pearl 300S-Al, (iii) cetyl 2-ethylhexanoate powder stabilised by PF-10 Eight Pearl 300S-Al and (iv) cryo-SEM image (3 months after preparation) of 2-ethylhexyl-4-methoxycinnamate oil powder stabilised by PF-12 Eight Pearl 300S-Al particles. The oils (10 cm^3) were coloured with Sudan red dye (*ca*. 5 mg) to aid visualisation. (lower) Photos of liquid marbles (10 μL) resting on a hydrophilic glass slide in air stabilised by PF-12 Eight Pearl 300S-Al sericite particles soon after formation. The liquid is (a) phenyl silicone, (b) squalane, (c) pentaerythritol tetra(2-ethylhexanoate), (d) jojoba oil, (e) 2-ethylhexyl-4-methoxycinnamate and (f) water. The inset in (b) is a 10 μL squalane droplet, R' (1.34 mm) < κ^{-1} (1.98 mm), rolled in only one direction to and fro. Scale bar = 3 mm.

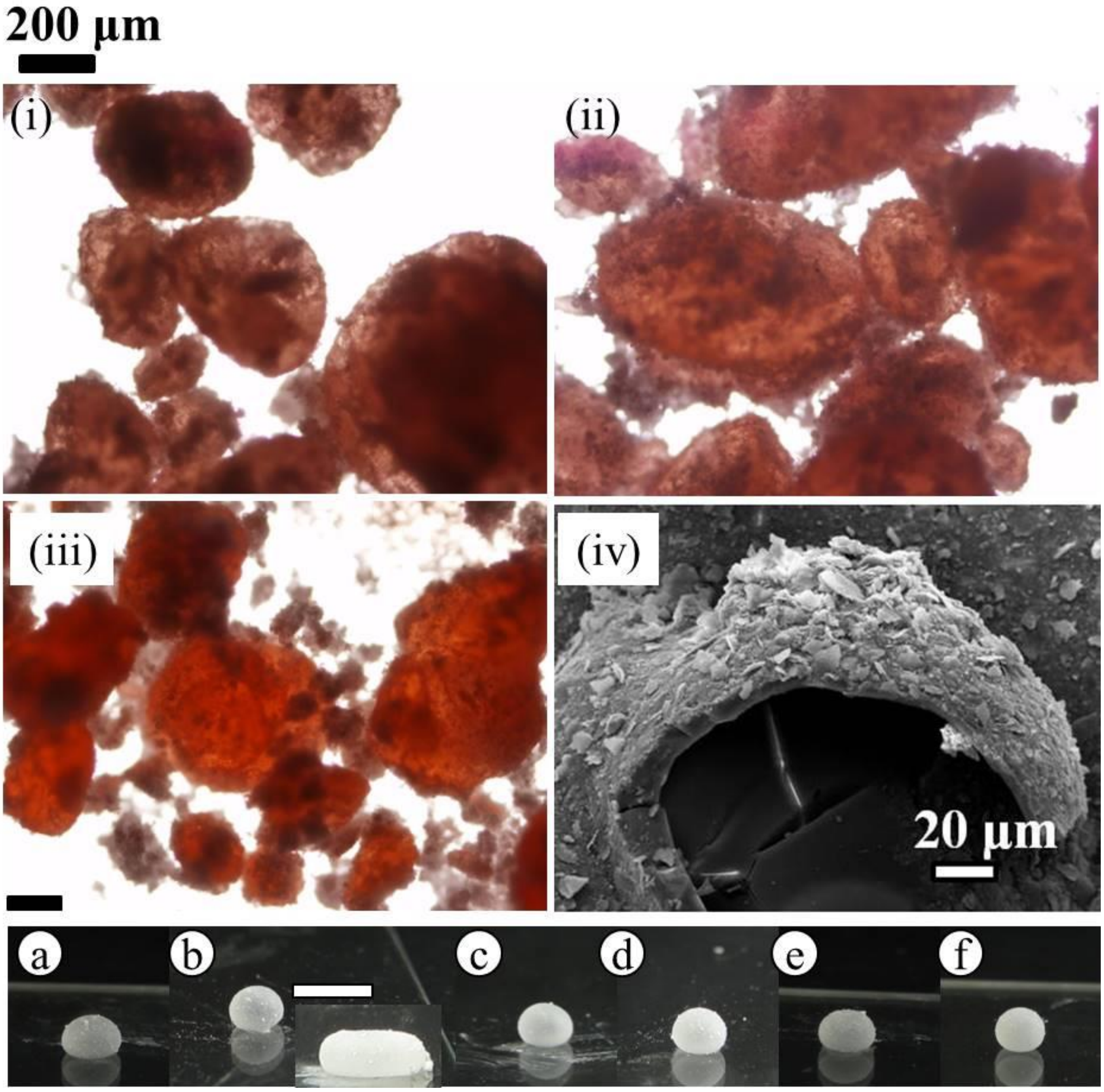

Figure 6.6. Photos of (a) 2-ethylhexyl-4-methoxycinnamate dry powder, (b) corresponding oil foam both stabilised by 0.5 g of PF-8 Eight Pearl 300S-Al sericite particles containing 1.45 and 1.50 g of oil, respectively, and (c) a cream obtained by shearing 8.5 mg of (a) on a dry glass slide.

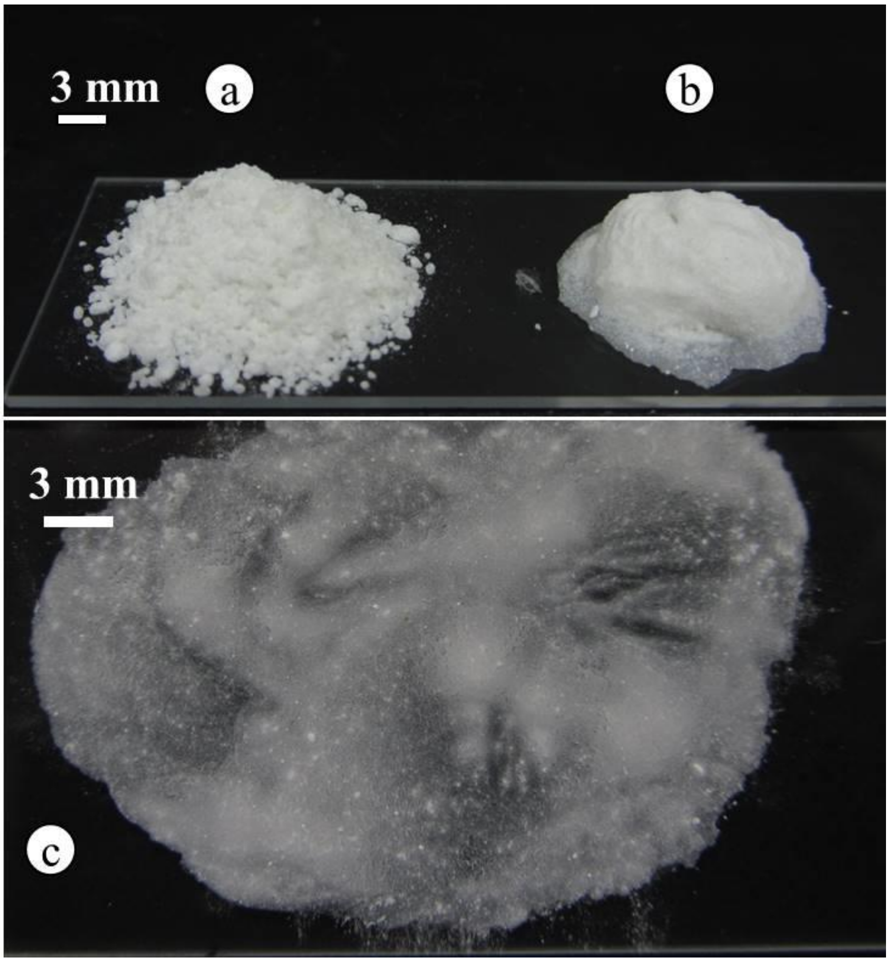

6.4 Catastrophic Phase Inversion of Dry Oil Powders to Oil Foams at High Oil : Particle Ratio

Above the COPR, catastrophic phase inversion from a dry oil powder to an ultra-stable oil foam was observed for all the oils and the stable air bubbles coated with particles are also non-spherical but smaller than the oil droplets in the dry oil powders. Particle-stabilised non-aqueous foams of excellent stability, in which the gas bubbles deviated from spherical geometry, were reported previously.[6,7,22] Phase inversion was confirmed by verification of the continuous phase of the materials through the dispersion test. The dry oil powders did not disperse in the neat oils whereas the foams readily did (Figure 6.7). This phase inversion is similar to that in emulsions (*i.e.* o/w to w/o and *vice versa*)[38] and is driven by the high oil : particle ratio.

Increasing the oil content at fixed mass of particles can potentially increase the size of the oil droplets or their number in the dry oil powder, but reduces the amount of non-adsorbed particles in the system. Evidence from Figure 6.8, for PF-8 Eight Pearl 300S-Al particles containing different amounts of liquid paraffin, suggests that the former is favoured over the latter. Above the COPR, there are little or no particles to sufficiently coat the oil droplets following oil addition. In other words, the total amount of oil surfaces the particles can coat and stabilise in the form of dry oil powder is greater than that of the air surfaces trapped in the glass vial. This makes the o/a powder metastable and hence it inverts to the stable a/o foam (Figure 6.9 and Appendix 6.5) upon gentle shaking. Such a catastrophic phase inversion has also been reported in aqueous systems in the context of dry water.[26] Most of the oil foams did not show any sign of drainage or coalescence for over two years, but some of them underwent limited drainage within the first week after formation to yield very stable foams subsequently. These were those of squalane or 2-ethylhexyl-4-methoxycinnamate stabilised by PF-8 Eight Pearl 300S-Al, cetyl 2-ethylhexanoate stabilised by PF-10 Eight Pearl 300S-Al and either glyceryl tri(2-ethylhexanoate), pentaerythritol tetra(2-ethylhexanoate) or jojoba oil stabilised by PF-12 Eight Pearl 300S-Al particles. A summary of the drainage and coalescence stability of the PFX-10 ZnO (TP), PF-10 Eight Pearl 300S-Al[a] and PF-10 FSE-Al particle-stabilised foams is given in Appendix 6.6. A relatively small fraction of oil was released in foams where drainage was observed. In foams where coalescence was observed, the particles entered the oils and the air bubbles were lost. In general, the foams are viscoelastic except those stabilised by the PFX-10 ZnO (TP) fluorinated particles which are ‘liquid-like’ (*cf.* Figure 6.9 and Appendix 6.5).

Figure 6.7. Photos of 400 mg of (a) 2-ethylhexyl-4-methoxycinnamate dry powder and (b) corresponding oil foam both stabilised by 0.5 g of PF-8 Eight Pearl 300S-Al sericite particles containing 1.45 and 1.50 g of oil, respectively, added to 20 cm^3 of 2-ethylhexyl-4-methoxycinnamate after vigorous stirring. The o/a powder (a) does not disperse whereas the a/o foam (b) does.

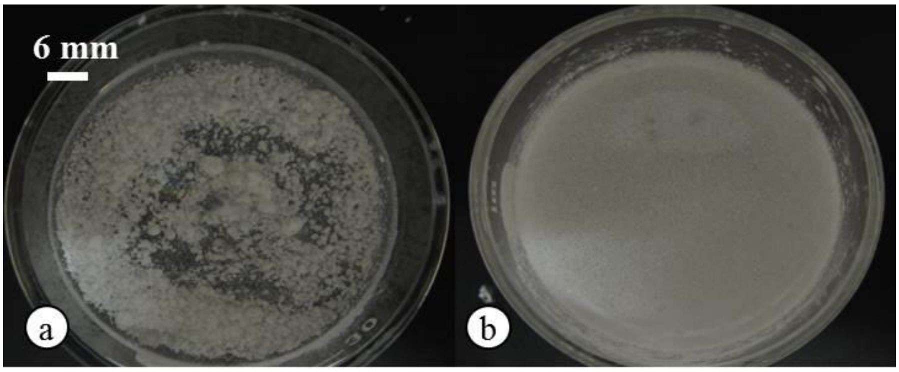

Figure 6.8. Optical micrographs of dry liquid paraffin powder stabilised by 0.5 g of PF-8 Eight Pearl 300S-Al sericite particles containing various amounts of liquid paraffin (given).

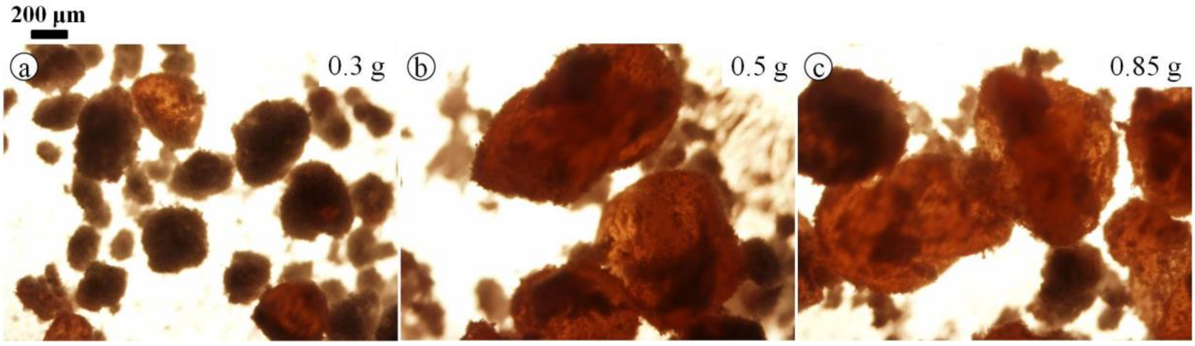

Figure 6.9. (a) Photo of liquid paraffin foam stabilised by PF-12 Eight Pearl 300S-Al particles, obtained from phase inversion of its corresponding powder, being forced out of a plastic syringe onto a black aluminium substrate, (b) corresponding optical micrograph of the liquid paraffin foam, (c) optical micrograph of squalane foam stabilised by PF-5 Eight Pearl 300S-Al particles and (d) cryo-SEM image of pentaerythritol tetra(2-ethylhexanoate) foam stabilised the PF-12 Eight Pearl 300S-Al particles obtained from phase inversion of their powders. The optical micrographs were obtained soon after foam formation whilst the cryo-SEM image was obtained 2 weeks after foam formation.

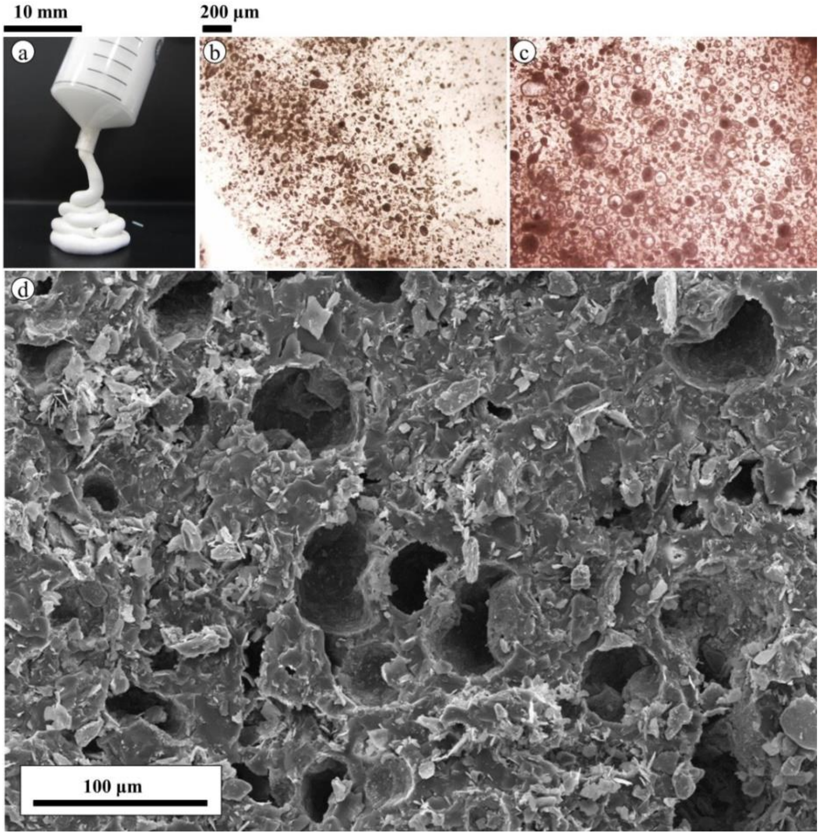

6.5 Relationship between Solid-Liquid-Air Three-Phase Contact Angle and the Type of Material Formed

Since the type of material a mixture of air, liquid and solid particles make depends on the contact angle which the particles make with the liquid, it is important to have an idea of this angle here. It is generally accepted that if a liquid completely wets the particles (θ_{la} = 0°) it gives a particle dispersion and for θ_{la} = 180° no adsorption occurs. For intermediate values of θ_{la}, particles are more wetted by the liquid (θ_{la} < 90°) or air (θ_{la} > 90°) phase and foams or liquid marbles/dry liquid powders are stabilised, respectively, at least in the case of water.[4,21] However, the θ_{la} reported here are not on the particles themselves but on disks composed of the particles with the danger being that certain surface groups are buried during particle compression. In addition, the particles are plate-like (except the PFX-10 ZnO (TP)) and the possibility exists that the fluoro-coating may be different on the edges compared with the faces. Also, a liquid may potentially wet the compressed disks less than it would wet the individual particles leading to an exaggeration of the magnitude of θ_{la}. The configuration of such asymmetric particles at the fluid interface within materials like oil foams and oil powders is unknown at present although Garrett discusses the likely configuration, albeit at a water-air surface, which depends on the particle geometry.[39] Based on the foregoing, values of θ_{la} are regarded as apparent angles. Consequently, unravelling a clear correlation between θ_{la} and material type is obviously a challenge. Table 6.1 and Appendix 6.7 show both the advancing and receding values of θ_{la} alongside the type of material that was obtained from the various oil and particle combinations in the case of vigorous mixing and gentle agitation. Notice that the liquids are arranged in order of increasing γ_{la}. With reference to Table 6.1, all the oils wet the oleophilic sericite (PF-0 Eight Pearl 300S-Al) particle disks (apparent advancing θ_{la} < 5° in many cases) as expected. For the other particle disks (*i.e.* PF-5 to PF-12 Eight Pearl 300S-Al) values of apparent advancing θ_{la} ranging from 0° (*n*-pentane) to 151° (water on PF-12 Eight Pearl 300S-Al disk) were obtained. In addition, relatively high (above 15°) hysteresis was observed which might be due to the relatively smooth nature of these surfaces[15] since contact angle hysteresis is usually low for rough surfaces.[40] Particle dispersions in liquid were obtained in liquids of relatively low γ_{la} where apparent advancing θ_{la} is between 0 and 73°. The only exception is the case of PDMS 20 cS and PF-10 Eight Pearl 300S-Al particles (θ_{la} = 73°) where foam is formed. In cases where γ_{la} was moderate (between 27–37 mN m^{-1}) and θ_{la} was between 73 and 130°, an oil foam or a foam + climbing films were observed. For water (highest γ_{la}) where apparent advancing $\theta_{la} \geq$ 140°, only climbing films were observed. In addition, oils marbles form not just for high θ_{la} systems like jojoba oil with PF-12 Eight Pearl 300S-Al, but also when the angle is as low as 30°, *e.g.* cyclomethicone with PF-5 Eight Pearl 300S-Al. This is very different to the case of water liquid marbles where very hydrophobic particles are required. It was further observed that the robustness of the marbles to transport increases as the degree of fluorination increases. In contrast to liquid marble formation, dry oil powder formation was only possible with particles exhibiting apparent advancing θ_{la} above *ca*. 65° and oils possessing tension above 27 mN m^{-1}. Based on Appendix 6.7, disks composed of the PFX-10 Kunipia F particles which were completely or partially wetted by few oils and water at rest gave values of apparent advancing θ_{la} ranging from 0°(water) to 104°(2-ethylhexyl-4-methoxycinnamate) with hysteresis of > 23° in many cases. Upon vigorous agitation, the liquid/particle combinations all form particle dispersions, but marbles were obtained with all the combinations except cyclomethicone and water where apparent advancing θ_{la} is 58° and 0° respectively. For the PFX-10 ZnO (TP), PF-10 Eight Pearl 300S-Al^{a} and PF-10 FSE-Al particle disks, values of apparent advancing θ_{la} were between 54° (cyclomethicone) and 127° (water), 61° (cyclomethicone) and 130° (water) and 49° (cyclomethicone) and 139° (water), respectively, with high (> 25°) hysteresis in many cases. Unlike the PFX-10 Kunipia F particle/liquid combinations, foams were obtained with the PFX-10 ZnO (TP), PF-10 Eight Pearl 300S-Al^{a} and PF-10 FSE-Al particle/liquid combinations upon vigorous agitation provided the γ_{la} of the liquid is above 26 mN m^{-1} otherwise a particle dispersion results. However, climbing films were obtained in water (highest tension). Also, the particles were able to stabilise marbles (and powders) of majority of the liquids under investigation. It can be seen (Table 6.1 and Appendix 6.7) that for all the fluorinated particles, there is a transition from dispersion to foam to liquid marbles as γ_{la} increases. Secondly, foams and marbles can be stabilised in one and the same system depending on the mixing conditions. Thirdly, omniphobic surfaces can be created with these fluorinated particles except with the PFX-10 Kunipia F particles which are wetted by water.

The cosine of both the apparent advancing and receding θ_{la} on the particle disks is plotted as a function of γ_{la} in Figure 6.10 and Appendix 6.8. The inset is an example of one of the disks on which θ_{la} was measured. The value of cos θ_{la} (apparent advancing) is more or less constant for all the liquids on PF-0 Eight Pearl 300S-Al surfaces, but decreases with increasing γ_{la} on the fluorinated particle surfaces as does the cosine of the apparent receding angles. For certain smooth substrates, such plots are often linear of negative gradient.[41] Also shown on the graphs are the regions where either dispersions, foams or climbing films occur upon vigorous agitation or dry oil powders forms upon gentle mixing. Since the apparent receding θ_{la} is always less than the apparent advancing one, the boundaries between the different regions depend on which angle is taken. It is not obvious which angle is operative during the mixing of particles with liquid. In the case of oil-water systems, the emulsion type was seen to depend on which liquid first makes contact with the particles and the observation was argued in terms of the difference between the apparent advancing and receding θ_{la}.[42] In general, Figure 6.10 and Appendix 6.8 show that for the particles under investigation (except PFX-10 Kunipia F), a particle dispersion forms when cos θ_{la} is approximately 1, foams are stabilised as it decreases and eventually only liquid marbles (and hence dry oil powders or climbing films) are obtained when it is close to –1. This is consistent with previous findings with PTFE[6] and fluorinated silica particles.[7]

Table 6.1. Apparent advancing (first entry) and receding (second entry) θ_{la} measured through the liquid of a drop (0.1 or 0.05 cm^3) of liquid in air on compressed disks of fluorinated sericite particles at room temperature. The apparent advancing θ_{la} on PF-0 Eight Pearl 300S-Al particle disks ranges from 0°(*n*-pentane) to *ca*. 27°(water), but the apparent receding angles were *ca*. 0° for all the liquids under investigation. The materials obtained after agitation of the liquid-particle mixtures (described in Figure 6.1) are also given: ○ -dispersion, ●-foam, ■-foam + climbing films, †-climbing films. For liquid marbles: ×-no marble and ✓-liquid formed marble.

	θ_{la}/± 2°			
Liquid	PF-5	PF-8	PF-10	PF-12
n-Pentane	0, 0: ○,×	0, 0: ○,×	0, 0: ○,×	0, 0: ○,×
n-Hexane	0, 0: ○,×	0, 0: ○,×	0, 0: ○,×	0, 0: ○,×
n-Heptane	43, 21: ○,×	56, 25: ○,×	50, 29: ○,×	46, 22: ○,×
Cyclomethicone	30, 12: ○,✓	37, 20: ○,✓	47, 27: ○,✓	39, 24: ○,✓
PDMS 6 cS	32, 18: ○,✓	36, 30: ○,✓	63, 39: ○,✓	62, 38: ○,✓
n-Octane	51, 27: ○,✓	66, 40: ○,✓	63, 36: ○,✓	63, 33: ○,✓
PDMS 20 cS	65, 42: ○,✓	71, 35: ○,✓	73, 43: ●,✓	73, 32: ○,✓
n-Decane	66, 36: ●,✓	88, 62: ●,✓	80, 47: ●,✓	84, 55: ●,✓
n-Dodecane	77, 63: ●,✓	92, 64: ●,✓	99, 65: ●,✓	95, 59: ●,✓
n-Tetradecane	82, 47: ●,✓	101, 69: ●,✓	106, 60: ●,✓	106, 73: ●,✓
Isocetane	63, 39: ●,✓	68, 44: ●,✓	79, 52: ●,✓	56, 34: ●,✓
n-Hexadecane	90, 65: ●,✓	98, 69: ●,✓	105, 73: ●,✓	118, 93: ●,✓
Phenyl silicone	95, 72: ●,✓	91, 65: ●,✓	89, 61: ●,✓	96, 65: ●,✓
Tripropyleneglycol trimethylacetate	78, 32: ●,✓	93, 44: ●,✓	76, 34: ●,✓	97, 56: ●,✓
Squalane	98, 76: ●,✓	111, 71: ●,✓	105, 70: ■,✓	107, 71: ■,✓
Glyceryl tri(2-ethylhexanoate)	106, 81: ●,✓	101, 60: ●,✓	93, 60: ●,✓	110, 80: ●,✓
Pentaerythritol tetra(2-ethylhexanoate)	110, 59: ●,✓	101, 57: ●,✓	97, 55: ■,✓	118, 64: ■,✓
Liquid paraffin	109, 83: ■,✓	121, 88: ■,✓	121, 87: ■,✓	126, 87: ■,✓
Cetyl 2-ethylhexanoate	112, 75: ●,✓	111, 73: ■,✓	94, 70: ■,✓	96, 71: ■,✓
Macadamia nuts oil	112, 76: ●,✓	101, 80: ■,✓	115, 83: ■,✓	128, 94: ■,✓
Jojoba oil	113, 78: ●,✓	121, 88: ■,✓	114, 82: ■,✓	123, 94: ■,✓
2-Ethylhexyl-4-methoxycinnamate	91, 64: ■,✓	117, 77: ■,✓	113, 81: ■,✓	118, 77: †,✓
Water	138, 111: †,✓	145, 119: †,✓	143, 123: †,✓	151, 127: †,✓

Figure 6.10. Cosine of apparent (a) advancing and (b) receding θ_{la} of a liquid droplet in air on compressed particle disks of PF-0 (○), PF-5 (●), PF-8 (△), PF-10 (×) and PF-12 (▲) Eight Pearl 300S-Al particles as a function of γ_{la} (at 25 °C). Inset: photograph of (a) side and (b) top view of a PF-10 Eight Pearl 300S-Al sericite disk made by compressing the powdered particles (scale bar = 6 mm). The type of material formed on vigorous agitation and with gentle mixing is also indicated.

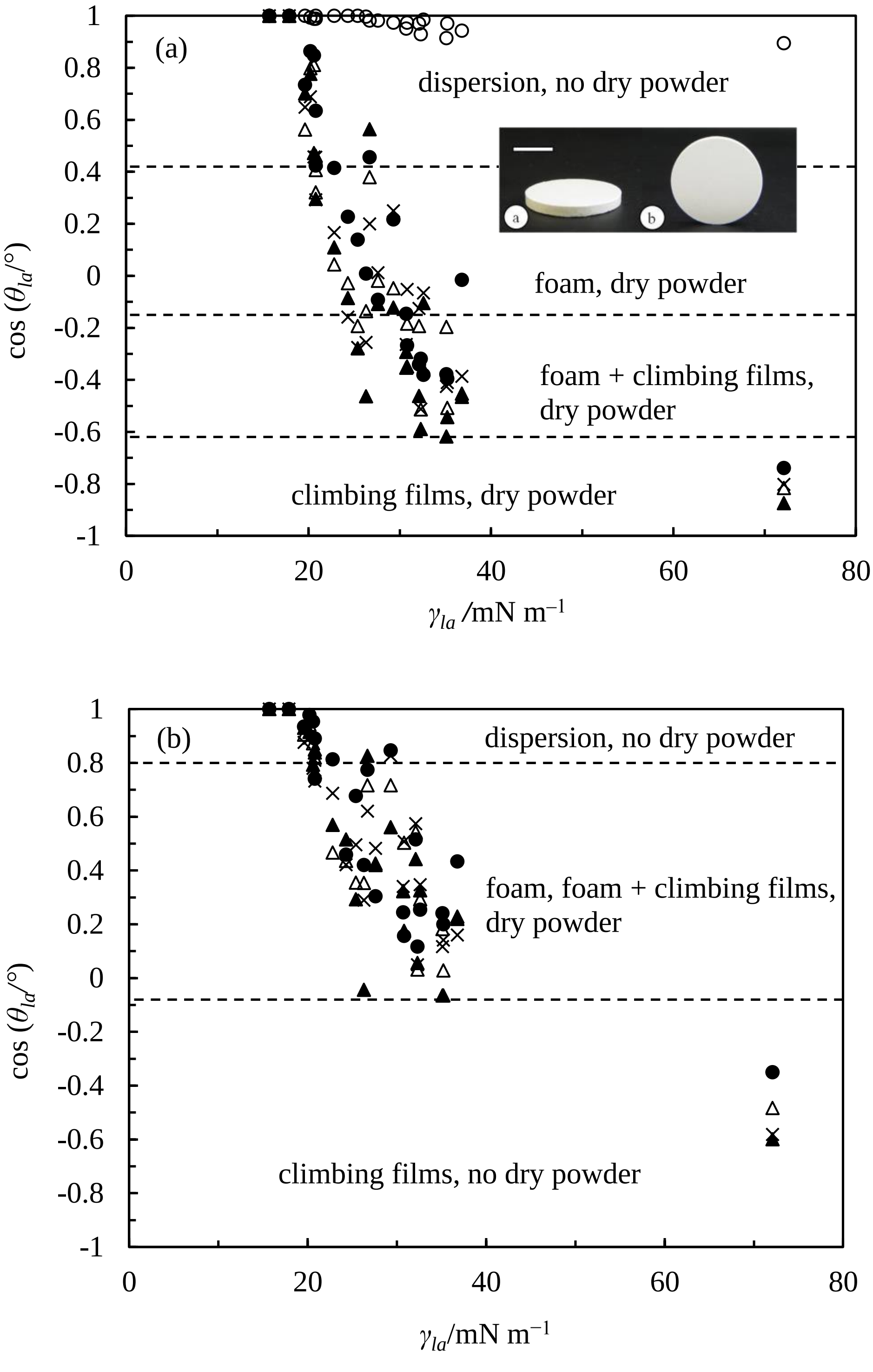

6.6 Conclusions

The behaviour of PF-5 to PF-12 Eight Pearl 300S-Al fluorinated sericite particles, PFX-10 Kunipia F, PFX-10 ZnO (TP), PF-10 Eight Pearl 300S-Al^a and PF-10 FSE-Al fluorinated particles in mixtures with air and oil has been studied. The material which forms after aeration depends on the γ_{la} of the oil, apparent γ_{sa} of the particles which controls their degree of wetting and energy input. Upon vigorous agitation (PF-5 to PF-12 Eight Pearl 300S-Al fluorinated sericite particles), oil dispersions are formed in liquids of relatively low tension (< 22 mN m^{-1}). Particle-stabilised air-in-oil a/o foams form in liquids of higher tension where apparent advancing θ_{la} lies between 73 and 130°. For oils of tension above 27 mN m^{-1} with particles for which apparent advancing θ_{la} > 65°, it was observed that dry oil powders in which oil droplets stabilised by particles forms by gentle mixing up to a COPR and do not leak oil for over 2 years. For many of the systems forming dry oil powders, stable oil liquid marbles were also prepared. For the PFX-10 Kunipia F, PFX-10 ZnO (TP), PF-10 Eight Pearl 300S-Al^a and PF-10 FSE-Al fluorinated particles, it was observed that vigorous agitation forms (a) oil dispersions in all the liquids containing PFX-10 Kunipia F particles and in liquids of relatively low γ_{la} (*i.e.* < 26 mN m^{-1}) like *n*-dodecane, PDMS 20 cS and cyclomethicone containing the other particles and (b) particle-stabilised a/o foam in liquids having γ_{la} > 26 mN m^{-1} where apparent advancing θ_{la} lies between 92 and 124°. On the contrary, oil-in-air marbles were obtained with all the oil/particle combinations, upon gentle agitation, except with water/PFX-10 Kunipia F, cyclomethicone/PFX-10 Kunipia F, cyclomethicone/PFX-10 ZnO (TP) and PDMS 6 cS/PFX-10 ZnO (TP) combinations for which apparent advancing θ_{la} is 0, 58, 54 and 56°, respectively. For oils of tension > 24 mN m^{-1}/PFX-10 ZnO (TP), PF-10 Eight Pearl 300S-Al^a and PF-10 FSE-Al particles where apparent advancing θ_{la} ≥ 87°, dry oil powders which do not leak oil for over 2 years were also stabilised by gentle agitation up to a COPR. The powders (stabilised by these particles and the previous particles) containing at least 60 wt. % of oil release the encapsulated oil when sheared on a substrate and become ‘creamy’. Above the COPR (oil powders stabilised by these particles and the previous particles), catastrophic phase inversion occurred and ultra-stable viscoelastic oil foams were obtained. Foams stabilised by the PFX-10 ZnO (TP) fluorinated particles were however ‘liquid-like.’ The oil foams disappear and leave an ‘oily’ surface when sheared on a substrate.

6.7 References

1. W. Ramsden, *Proc. Roy. Soc.*, 1903, **72**, 156−164.
2. S. U. Pickering, *J. Chem. Soc.*, 1907, **91**, 2001−2021.
3. R. Aveyard, B. P. Binks and J. H. Clint, *Adv. Colloid Interface Sci.*, 2003, **100–102**, 503−546.
4. B. P. Binks and T. S. Horozov, *Angew. Chem. Int. Ed.*, 2005, **44**, 3722−3725.
5. U. T. Gonzenbach, A. R. Studart, E. Tervoort and L. J. Gauckler, *Langmuir*, 2006, **22**, 10983−10988.
6. B. P. Binks, A. Rocher and M. Kirkland, *Soft Matter*, 2011, **7**, 1800−1808.
7. B. P. Binks and A. T. Tyowua, *Soft Matter*, 2013, **9**, 834−845.
8. J. H. Schulman and J. Leja, *Trans. Farad. Soc.*, 1954, **50**, 598−605.
9. A. Stocco, E. Rio, B. P. Binks and D. Langevin, *Soft Matter*, 2011, **7**, 1260−1267.
10. P. Aussillous and D. Quéré, *Nature*, 2001, **411**, 924−927.
11. P. McEleney, G. M. Walker, I. A. Larmour and S. E. J. Bell, *Chem. Eng. J.*, 2009, **147**, 373−382.
12. B. P. Binks and A. Rocher, *Phys. Chem. Chem. Phys.*, 2010, **12**, 9169−9171.
13. Y.-C. Sheen, Y.-C. Huang, C.-S. Liao, H.-Y. Chou and F.-C. Chang, *J. Polym. Sci. Part B: Polym. Phys.*, 2008, **46**, 1984−1990.
14. R. Campos, A. J. Guenthner, T. S. Haddad and J. M. Mabry, *Langmuir*, 2011, **27**, 10206−10215.
15. A. Tuteja, W. Choi, J. M. Mabry, G. H. McKinley and R. E. Cohen, *PNAS*, 2008, **105**, 18200−18205.
16. N. Eshtiaghi and K. P. Hapgood, *Powder Technol.*, 2012, **223**, 65−76.
17. P. Aussillous and D. Quéré, *Proc. R. Soc. Chem. Lond. A*, 2006, **462**, 973−999.
18. E. Bormashenko, *Curr. Opin. Colloid Interface Sci.*, 2011, **16**, 266−271.
19. E. Bormashenko and A. Musin, *Appl. Surf. Sci.*, 2009, **255**, 6429−6431.
20. J. Tian, T. Arbatan, X. Li and W. Shen, *Chem. Commun.*, 2010, **46**, 4734−4736.
21. B. P. Binks and R. Murakami, *Nat. Mater.*, 2006, **5**, 865−869.
22. R. Murakami and A. Bismarck, *Adv. Funct. Mater.*, 2010, **20**, 732−737.
23. W. Barthlott and C. Neinhuis, *Planta*, 1997, **202**, 1−8.
24. N. Pike, D. Richard, R. Foster and L. Mahadevan, *Proc. R. Soc. Lond. B*, 2002, **269**, 1211−1215.
25. P. A. Kralchevsky and K. Nagayama, *Adv. Colloid Interface Sci.*, 2000, **85**, 145−192.
26. B. P. Binks, A. J. Johnson and J. A. Rodrigues, *Soft Matter*, 2010, **6**, 126−135.
27. B. P. Binks, B. Duncumb and R. Murakami, *Langmuir*, 2007, **23**, 9143−9146.
28. L. Forny, K. Saleh, R. Denoyel and I. Pezron, *Langmuir*, 2009, **26**, 2333−2338.
29. L. Forny, I. Pezron, K. Saleh, P. Guigon and L. Komunjer, *Powder Technol.*, 2007, **171**, 15−24.
30. B. O. Carter, D. J. Adams and A. I. Cooper, *Green Chem.*, 2010, **12**, 783−785.
31. B. O. Carter, W. Wang, D. J. Adams and A. I. Cooper, *Langmuir*, 2009, **26**, 3186−3193.
32. R. Mezzenga and S. Ulrich, *Langmuir*, 2010, **26**, 16658−16661.
33. H. Adelmann, B. P. Binks and R. Mezzenga, *Langmuir*, 2012, **28**, 1694−1697.
34. R. Murakami, H. Moriyama, M. Yamamoto, B. P. Binks and A. Rocher, *Adv. Mater.*, 2012, **24**, 767−771.
35. B. O. Carter, J. V. M. Weaver, W. Wang, D. G. Spiller, D. J. Adams and A. I. Cooper, *Chem. Commun.*, 2011, **47**, 8253−8255.
36. E. Bormashenko, R. Progreb, G. Whyman and A. Musin, *Colloids Surf. A*, 2009, **351**, 78−82.

37. A. B. Subramaniam, M. Abkarian, L. Mahadevan and H. A. Stone, *Langmuir*, 2006, **22**, 10204−10208.
38. B. P. Binks, L. Isa and A. T. Tyowua, *Langmuir*, 2013, **29**, 4923−4927.
39. P. R. Garrett, in *Surfactant Science Series*, ed. P. R. Garrett, Marcel Dekker, New York, 1993, vol. 45, p. 1.
40. D. Quéré, *Annu. Rev. Mater. Res.*, 2008, **38**, 71−99.
41. H. W. Fox and W. A. Zisman, *J. Colloid Sci.*, 1952, **7**, 428−442.
42. B. P. Binks and J. A. Rodrigues, *Langmuir*, 2003, **19**, 4905−4912.

Chapter 7

A Summary of Conclusions and Future Work

7.1 Conclusions

The behaviour of different particle types at fluid interfaces (oil-water, oil-oil and oil-air) in terms of the type of materials they stabilise has been studied. For the oil-water interfaces, edible o/w emulsions were stabilised by the rod- and cube-shaped $CaCO_3$ particles. For the oil-oil interfaces, o/o and o/o/o emulsions were prepared using fluorinated and DCDMS-coated fumed silica, fluorinated ZnO, fluorinated sericite and bentonite clay, PTFE, Bentone 34, rod-shaped $CaCO_3$ and Calofort SV particles as stabilisers. Finally, for the oil-air interfaces, oil liquid marbles, dry oil powders and oil foams were also prepared using the fluorinated fumed silica, fluorinated ZnO, fluorinated sericite and bentonite clay particles. The following conclusions can be drawn from the study:

- Kinetically stable o/w Pickering emulsions containing tricaprylin and Miglyol 812N as oils and water, where the volume fraction of oil in the emulsion ranges from 0.5 to 0.7, can be stabilised using 4 wt. % of rod and cube-shaped hydrophilic $CaCO_3$ particles. The emulsions are white, basic (pH > 8), polydisperse, flocculated and kinetically stable for over 3 years, but released relatively small fraction of the oils. Depending on the oil and method of emulsion preparation, the cube-shaped $CaCO_3$ particle-stabilised emulsions released relatively small fraction of the oils compared with the rod-shaped $CaCO_3$ particle-stabilised ones.
- Kinetically stable oil-oil Pickering emulsions containing equal volumes of vegetable oils (sunflower, olive and rapeseed oils) and PDMS (20−100 cS) oils can be prepared using 1 wt. % of hydrophilic, hydrophobic (hydrocarbon-coated) and omniphobic (fluorocarbon-coated) silica particles. Omniphobic (fluorocarbon-coated) sericite and Calofort SV particles can also be used, but a relatively high particle concentration will be required. Vegetable oil-in-PDMS oil and PDMS oil-in-vegetable oil emulsions can be prepared depending on the particle type. For the silica particles, measured values of the three-phase contact angles correlated reasonably well with the emulsion type. The emulsions are white, polydisperse, largely unflocculated and kinetically stable for over a month, but released relatively small fraction of the the oils.

- Foams and liquid marbles of liquids (mainly oils) having surface tension (20 °C) in the range of 27−64 mN m^{-1} and water liquid marbles can be prepared using fluorinated silica particles of low apparent surface energy. Many of the foams are stable to coalescence for at least a year. Marbles of liquids of low vapour pressure are stable to evaporation for over 3 days. Liquid marbles, powders and foams of oils having surface tension (25 °C) in the range of 24−37 mN m^{-1} and water liquid marbles can be prepared using fluorinated platelet sericite and fluorinated ZnO particles of low apparent surface energy. Marbles of oils of low vapour pressure are stable to evaporation for over 3 days. The oil powders did not release the encapsulated oils for over 2 years. Many of the oil foams are also kinetically stable for over 2 years. The formation of these materials depends on the surface tension of the liquids (and/or oils), the degree of fluorination (and hence the apparent surface energy) of the particles and energy input. The apparent surface energy of the particles controls their wettability which is quantified in terms of the solid particle-liquid-air contact angle. Depending on the energy input, marbles, dry oil powders and foams can be prepared using the same particle.

7.2 Future Work

- The rod- and cube-shaped $CaCO_3$ particles used here to study the effect of particle anisotropy on the stability of Pickering emulsions are polydisperse and of irregular shape. Anisotropic particles which are less polydisperse and have approximately the same shape should be used to study the effect of particle anisotropy on the stability of Pickering emulsions. The results of such a study should be compared with that of an isotropic particle of the same material. Due to lack of time, the correlation between θ_{ow} and the type of emulsion these particles have stabilised was not established. The θ_{ow} should be measured and correlated with the o/w emulsions stabilised.
- Although the θ_{oo} values were inferred from planar microscope glass slides and correlated with the type of emulsions stabilised by the 100% SiOH and 14% SiOH DCDMS-coated fumed silica particles, the θ_{oo} the particles themselves make with oil-oil interfaces should be measured to make the correlation of θ_{oo} with the emulsion type more meaningful. Using a single emulsification route and a single particle type, multiple emulsions were obtained in some cases. Although the formation of these emulsions was argued in terms of contact angle hysteresis, further work should be done to verify this. For some industrial applications, the formation of an emulsion (be it aqueous or non-aqueous) is

undesirable. How to destabilise these oil-oil Pickering emulsions should be investigated for such applications.

- The reasons for the deviation of some of the relatively small (10 μL) oil liquid marbles from a quasi-spherical shape should be investigated. The behaviour of other fluorinated solid particles at oil-air interfaces should be investigated with the aim of stabilising oil liquid marbles, dry oil powders and oil foams of oils of relatively low tension (*e.g.* 12 mN m^{-1}). Attempts should be made to prepare more novel materials, *e.g.* dry o/o and o/o/o emulsion powders using the knowledge gained from this study, for potential applications in the cosmetic and pharmaceutical industries.

Appendixes

Appendix 1

Droplet diameter of (a) tricaprylin-in-water and (b) Miglyol 812N-in-water emulsions ($\phi_o = 0.5$) 3 days after preparation, stabilised by 2 wt. % of rod-shaped $CaCO_3$ particles, measured in the presence of 0 (●), 2 × 10^{-3} (○), 3 × 10^{-3} (◆) and 4 × 10^{-3} wt. % of rod-shaped $CaCO_3$ particles in water as the diluting phase at ambient conditions. The control measurement for only the $CaCO_3$ particle-dispersion (4 × 10^{-3} wt. %) is also shown (▲).

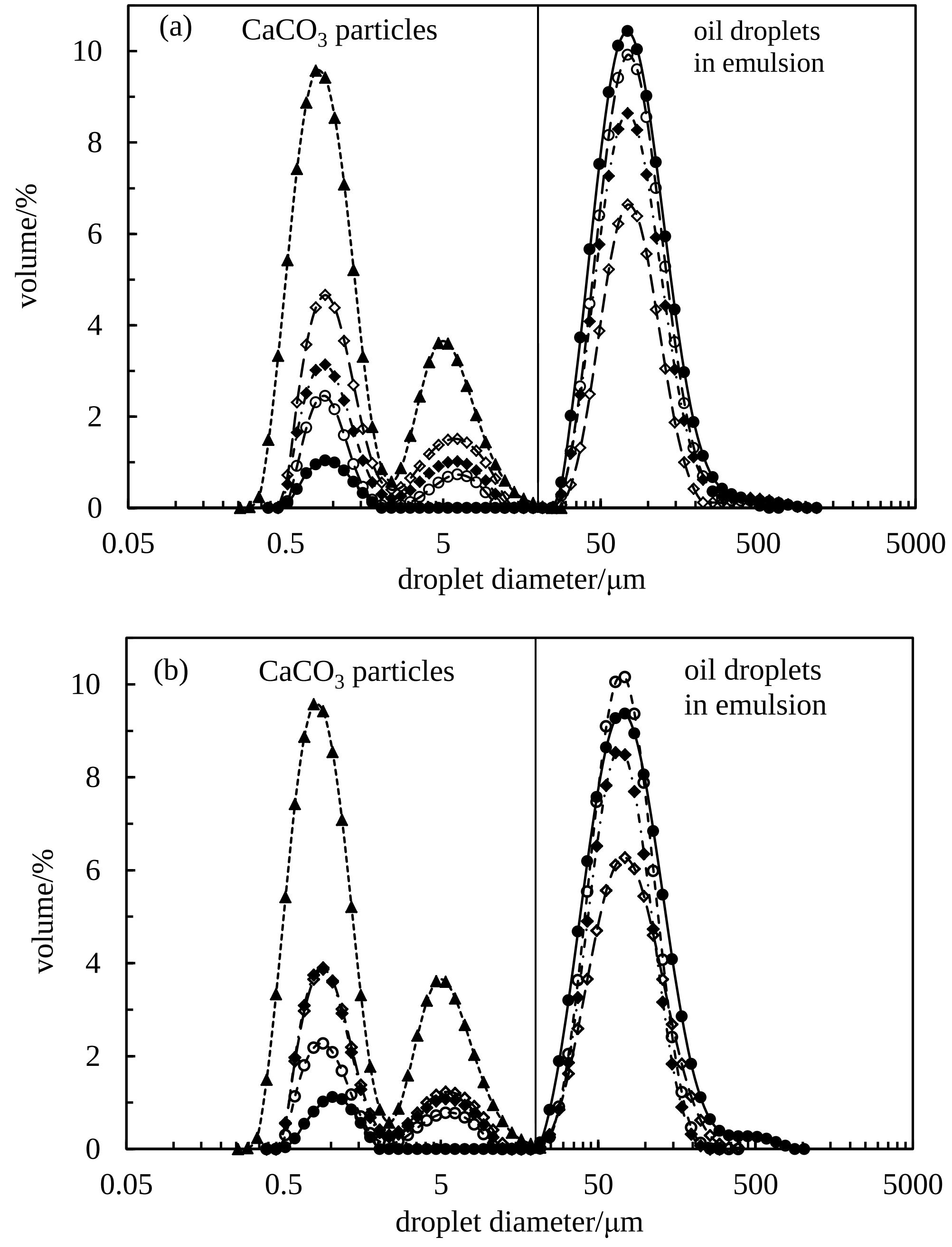

Appendix 2

EDX map of PF-8 Eight Pearl 300S-Al fluorinated sericite particles.

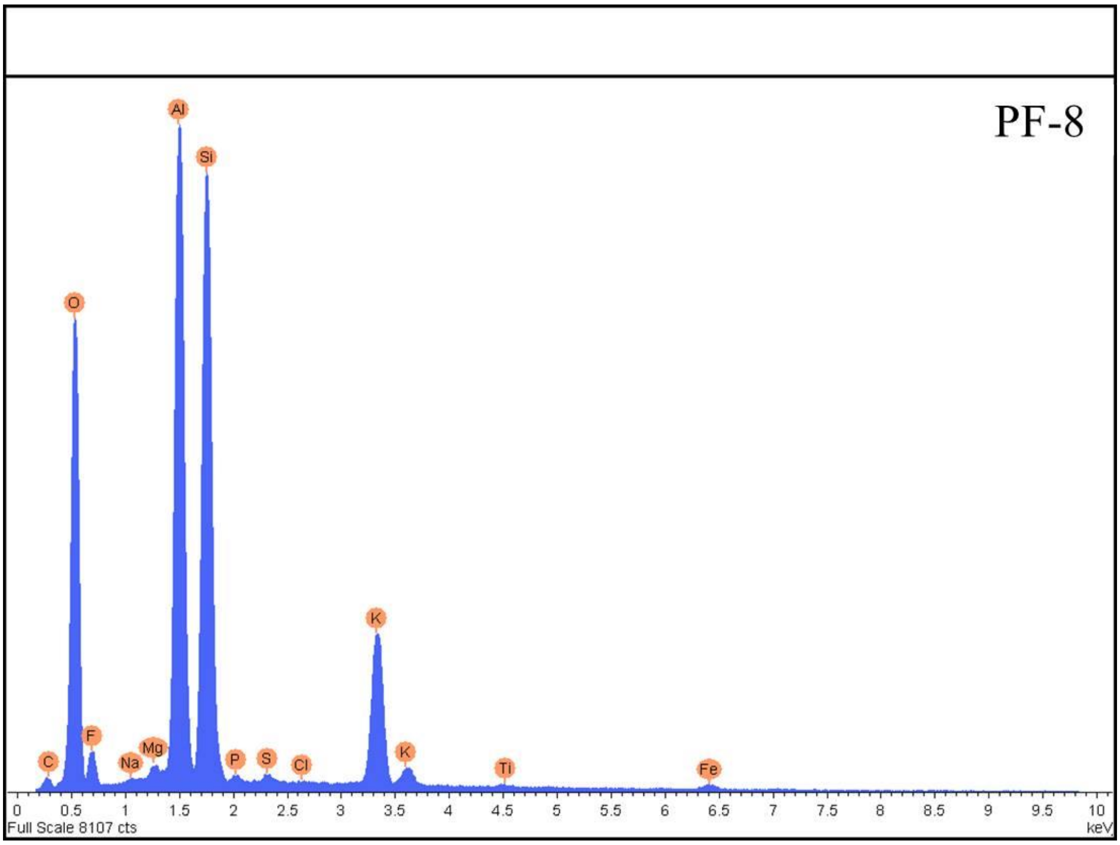

Appendix 3

For the spinning drop tensiometer, the vegetable oil-PDMS oil interfacial tension $\gamma_{o_1o_2}$ can be written as (B. Vonnegut, *Rev. Sci. Instr.*, **1941**, 13, 6–9):

$$\gamma_{o_1o_2} = \frac{\Delta\rho\omega^2 R_c^3}{4}\left(1 + \frac{2R_c}{3L_c}\right) \tag{1}$$

where ω = angular velocity (radians per second), R_c = radius of cylindrical vegetable oil drop, $\Delta\rho$ = density difference between the vegetable oil and PDMS oil and L_c = length of vegetable oil drop (excluding the hemispherical ends). This equation is valid only if the ratio of L_c to D_c is ≥ 4. In order to determine $\gamma_{o_1o_2}$, the following quantities were measured (in the stated units): N = rotation speed in revolutions per minute, $\Delta\rho$ (g cm^{-3}), D_c = apparent vegetable oil drop diameter in units of the microscope graticule, apparent vegetable oil drop length (L_c) in units of microscope graticule, n_{o_2} = refractive index of PDMS oils (25 °C) and n_T = refractive index of the thermostatting oil. Equation 1 must be modified to allow for the conversion of measured values of N into ω and of D_c into R_c. This is done as follows:

$$\omega\,(\text{radians per second}) = \left(\frac{2\pi}{60}\right)N = (0.10472)N \tag{2}$$

$$R_c = xD_c\left(\frac{n_T}{n_{o_2}}\right) \tag{3}$$

The factor x in equation 3 is used to convert measured D_c (in graticule units) to R_c (in metres) and it includes both the magnification of the microscope and the factor 2 (for conversion of R_c to D_c). In addition to the magnification of the microscope, there is additional magnification caused by the lens effect of the curved capillary which depends on the ratio of the n_T to n_{o_2} (L.M. Coucoulas, R.A. Dawe and E.G. Mahers, *J. Colloid Interface Sci.*, **1983**, 93, 281−284). Substituting equations 2 and 3 into equation 1 gives equation 4 which was used for calculating $\gamma_{o_1o_2}$.

$$\gamma_{o_1o_2} = N^2D_c^3A\Delta\rho\left(\frac{n_T}{n_{o_2}}\right)^3\left[1+\left(\frac{n_TD_c}{n_{o_2}}\right)\Big/3L_c\right] \tag{4}$$

The constant A (given by equation 5) contains all sample invariant conversion factors. The factor of 10^6 arises from the conversion of density unit from g cm^{-3} to kg m^{-3} and tension units from N m^{-1} to mN m^{-1}. For the lens magnification (× 2.5) and instrument (RED (site 04)) used here, x is 1.79×10^{-3} and thus $A = 1.572 \times 10^{-8}$.

$$A = 0.25 \times 0.10472^2 \times x^3 \times 10^6 \tag{5}$$

Appendix 4

Estimated θ_{oo} for sunflower/olive oil-PDMS oils and the corresponding emulsion type. Also shown is whether the emulsion obtained is expected (✓) or not (✗).

Appendix 4.1. Estimated θ_{oo} for sunflower oil-PDMS 20 cS and the corresponding emulsion type.

	Sunflower oil-PDMS 20 cS θ_{oo} (through PDMS 20 cS)/°			
Silica particles	Using cal'd $\gamma_{o_1o_2}$	Using meas'd $\gamma_{o_1o_2}$	Emulsion type	Comment
100% SiOH	101	101	Unstable PDMS 20 cS-in-sunflower oil	✓
88% SiOH	93	92	Unstable PDMS 20 cS-in-sunflower oil	✓
78% SiOH	86	86	Unstable PDMS 20 cS-in-sunflower oil	✗
70% SiOH	80	80	Unstable PDMS 20 cS-in-sunflower oil	✗
61% SiOH	73	74	Unstable PDMS 20 cS-in-sunflower oil	✗
51% SiOH	66	67	Unstable PDMS 20 cS-in-sunflower oil	✗
42% SiOH	60	61	Unstable PDMS 20 cS-in-sunflower oil	✗
33% SiOH	53	55	Unstable PDMS 20 cS-in-sunflower oil	✗
25% SiOH	47	50	Unstable PDMS 20 cS-in-sunflower oil	✗
23% SiOH	46	49	Stable PDMS 20 cS-in-sunflower oil	✗
20% SiOH	45	47	Stable PDMS 20 cS-in-sunflower oil	✗
14% SiOH	41	44	Stable sunflower oil-in-PDMS 20 cS	✓

Appendix 4.2. Estimated θ_{oo} for sunflower oil-PDMS 50 cS and the corresponding emulsion type.

	Sunflower oil-PDMS 50 cS θ_{oo} (through PDMS 50 cS)/°			
Silica particles	Using cal'd $\gamma_{o_1o_2}$	Using meas'd $\gamma_{o_1o_2}$	Emulsion type	Comment
100% SiOH	99	95	Stable PDMS 50 cS-in-sunflower oil	✓
88% SiOH	90	90	Stable PDMS 50 cS-in-sunflower oil	✓
78% SiOH	83	86	Stable PDMS 50 cS-in-sunflower oil	✗
70% SiOH	77	82	Stable PDMS 50 cS-in-sunflower oil	✗
61% SiOH	71	78	Stable PDMS 50 cS-in-sunflower oil	✗
51% SiOH	63	74	Stable PDMS 50 cS-in-sunflower oil	✗
42% SiOH	56	70	Stable PDMS 50 cS-in-sunflower oil	✗
33% SiOH	50	66	Stable PDMS 50 cS-in-sunflower oil	✗
25% SiOH	44	64	Stable PDMS 50 cS-in-sunflower oil	✗
23% SiOH	43	63	Stable PDMS 50 cS-in-sunflower oil	✗
20% SiOH	41	62	Stable sunflower oil-in-PDMS 50 cS	✓
14% SiOH	38	61	stable sunflower oil-in-PDMS 50 cS	✓

Appendix 4.3. Estimated θ_{oo} for sunflower oil-PDMS 100 cS and the corresponding emulsion type.

	Sunflower oil-PDMS100 cS θ_{oo} (through PDMS 100 cS)/°			
Silica particles	Using cal’d $\gamma_{o_1o_2}$	Using meas’d $\gamma_{o_1o_2}$	Emulsion type	Comment
100% SiOH	93	93	Stable PDMS 100 cS-in-sunflower oil	✓
88% SiOH	84	84	Stable PDMS 100 cS-in-sunflower oil	✗
78% SiOH	77	76	Stable PDMS 100 cS-in-sunflower oil	✗
70% SiOH	71	70	Stable PDMS 100 cS-in-sunflower oil	✗
61% SiOH	64	63	Stable PDMS 100 cS-in-sunflower oil	✗
51% SiOH	57	55	Stable PDMS 100 cS-in-sunflower oil	✗
42% SiOH	50	48	Stable PDMS 100 cS-in-sunflower oil	✗
33% SiOH	42	40	Stable PDMS 100 cS-in-sunflower oil	✗
25% SiOH	36	33	Stable PDMS 100 cS-in-sunflower oil	✗
23% SiOH	35	31	Stable PDMS 100 cS-in-sunflower oil	✗
20% SiOH	33	29	Stable sunflower oil-in-silicone 100 cS	✓
14% SiOH	30	25	multiple emulsion (disperses easily in sunflower oil)	✗

Appendix 4.4. Estimated θ_{oo} for olive oil-PDMS 20 cS and the corresponding emulsion type.

	Olive oil-PDMS 20 cS θ_{oo} (through PDMS 20 cS)/°			
Silica particles	Using cal’d $\gamma_{o_1o_2}$	Using meas’d $\gamma_{o_1o_2}$	Emulsion type	Comment
100% SiOH	0	0	Unstable PDMS 20 cS-in-olive oil	✗
88% SiOH	0	0	Unstable PDMS 20 cS-in-olive oil	✗
78% SiOH	0	0	Unstable PDMS 20 cS-in-olive oil	✗
70% SiOH	0	0	Unstable PDMS 20 cS-in-olive oil	✗
61% SiOH	0	0	Unstable PDMS 20 cS-in-olive oil	✗
51% SiOH	0	0	Unstable PDMS 20 cS-in-olive oil	✗
42% SiOH	0	0	Unstable PDMS 20 cS-in-olive oil	✗
33% SiOH	0	0	Unstable PDMS 20 cS-in-olive oil	✗
25% SiOH	0	0	Unstable PDMS 20 cS-in-olive oil	✗
23% SiOH	0	0	Unstable multiple emulsion (disperses easily in olive oil)	✗
20% SiOH	0	0	Stable olive oil-in-PDMS 20 cS	✗
14% SiOH	0	0	Stable olive oil-in-PDMS 20 cS	✗

Appendix 4.5. Estimated θ_{oo} for olive oil-PDMS 50 cS and the corresponding emulsion type.

	Olive oil-PDMS 50 cS θ_{oo} (through PDMS 50 cS)/°			
Silica particles	Using cal'd $\gamma_{o_1o_2}$	Using meas'd $\gamma_{o_1o_2}$	Emulsion type	Comment
100% SiOH	0	0	Unstable PDMS 50 cS-in-olive oil	✗
88% SiOH	0	0	Stable PDMS 50 cS-in-olive oil	✗
78% SiOH	0	0	Stable PDMS 50 cS-in-olive oil	✗
70% SiOH	0	0	Stable PDMS 50 cS-in-olive oil	✗
61% SiOH	0	0	Stable PDMS 50 cS-in-olive oil	✗
51% SiOH	0	0	Stable PDMS 50 cS-in-olive oil	✗
42% SiOH	0	0	Stable PDMS 50 cS-in-olive oil	✗
33% SiOH	0	0	Stable PDMS 50 cS-in-olive oil	✗
25% SiOH	0	0	Stable PDMS 50 cS-in-olive oil	✗
23% SiOH	0	0	Stable PDMS 50 cS-in-olive oil	✗
20% SiOH	0	0	Stable olive oil-in-PDMS 50 cS	✗
14% SiOH	0	0	Unstable multiple emulsion (disperses easily in olive oil)	✗

Appendix 4.6. Estimated θ_{oo} for olive oil-PDMS 100 cS and the corresponding emulsion type.

	Olive oil-PDMS 100 cS θ_{oo} (through PDMS 100 cS)/°			
Silica particles	Using cal'd $\gamma_{o_1o_2}$	Using meas'd $\gamma_{o_1o_2}$	Emulsion type	Comment
100% SiOH	0	0	Stable PDMS 100 cS-in-olive oil	✗
88% SiOH	0	0	Stable PDMS 100 cS-in-olive oil	✗
78% SiOH	0	0	Stable PDMS 100 cS-in-olive oil	✗
70% SiOH	0	0	Stable PDMS 100 cS-in-olive oil	✗
61% SiOH	0	0	Stable PDMS 100 cS-in-olive oil	✗
51% SiOH	0	0	Stable PDMS 100 cS-in-olive oil	✗
42% SiOH	0	0	Stable PDMS 100 cS-in-olive oil	✗
33% SiOH	0	0	Stable PDMS 100 cS-in-olive oil	✗
25% SiOH	0	0	Stable PDMS 100 cS-in-olive oil	✗
23% SiOH	0	0	Stable PDMS 100 cS-in-olive oil	✗
20% SiOH	0	11	Stable olive oil-in-PDMS 100 cS	✓
14% SiOH	0	25	Stable olive oil-in-PDMS 100 cS	✓

Appendix 5

Optical micrograph (1 month after preparation) of olive oil-PDMS 20 cS multiple emulsion stabilised by 1 wt. % of 23% SiOH DCDMS-coated fumed silica particles shown in Figure 4.8.

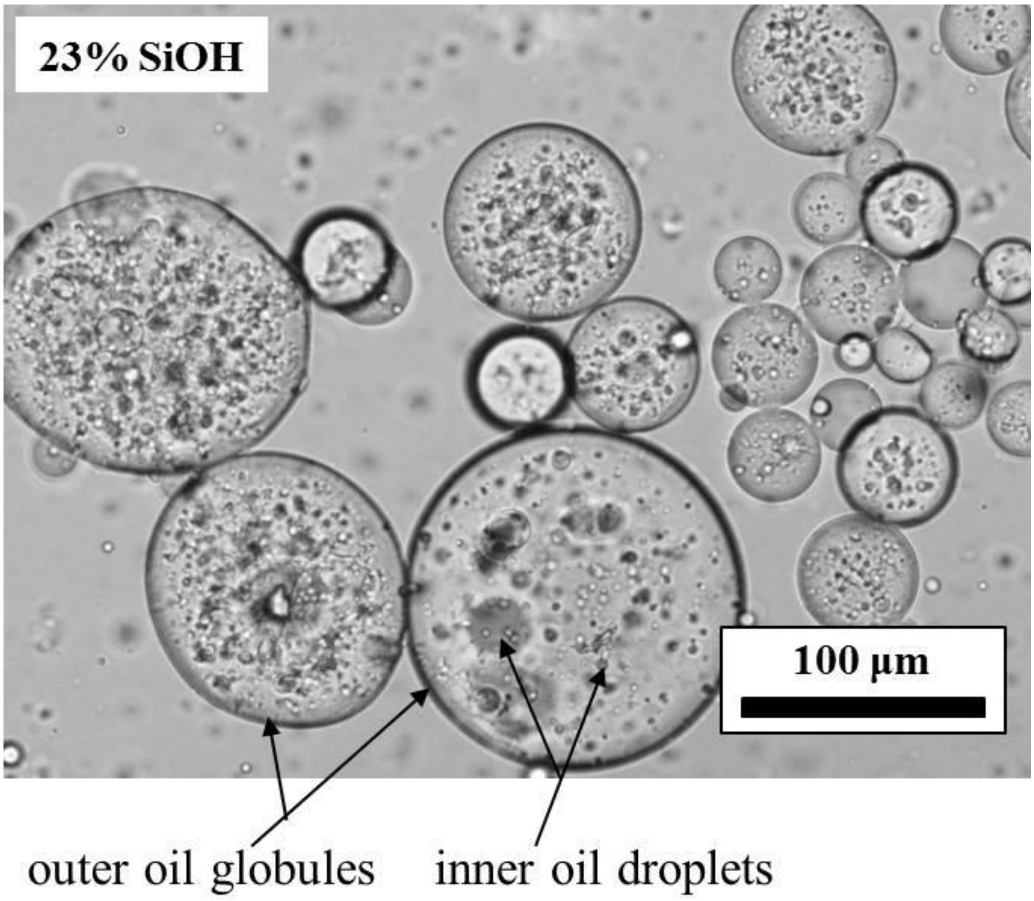

Appendix 6

Appendix 6.1. Behaviour of fluorinated platelet clay and fluorinated ZnO particles (50 mg) on liquid surfaces (3 cm^3) at rest. Abscissa: 1-particles were wetted by the liquid, 2-particles were partially wetted by the liquid and 3-particles were not wetted by the liquid. Ordinate: number in brackets is liquid surface tension (± 0.1 mN m^{-1}) at 25 °C.

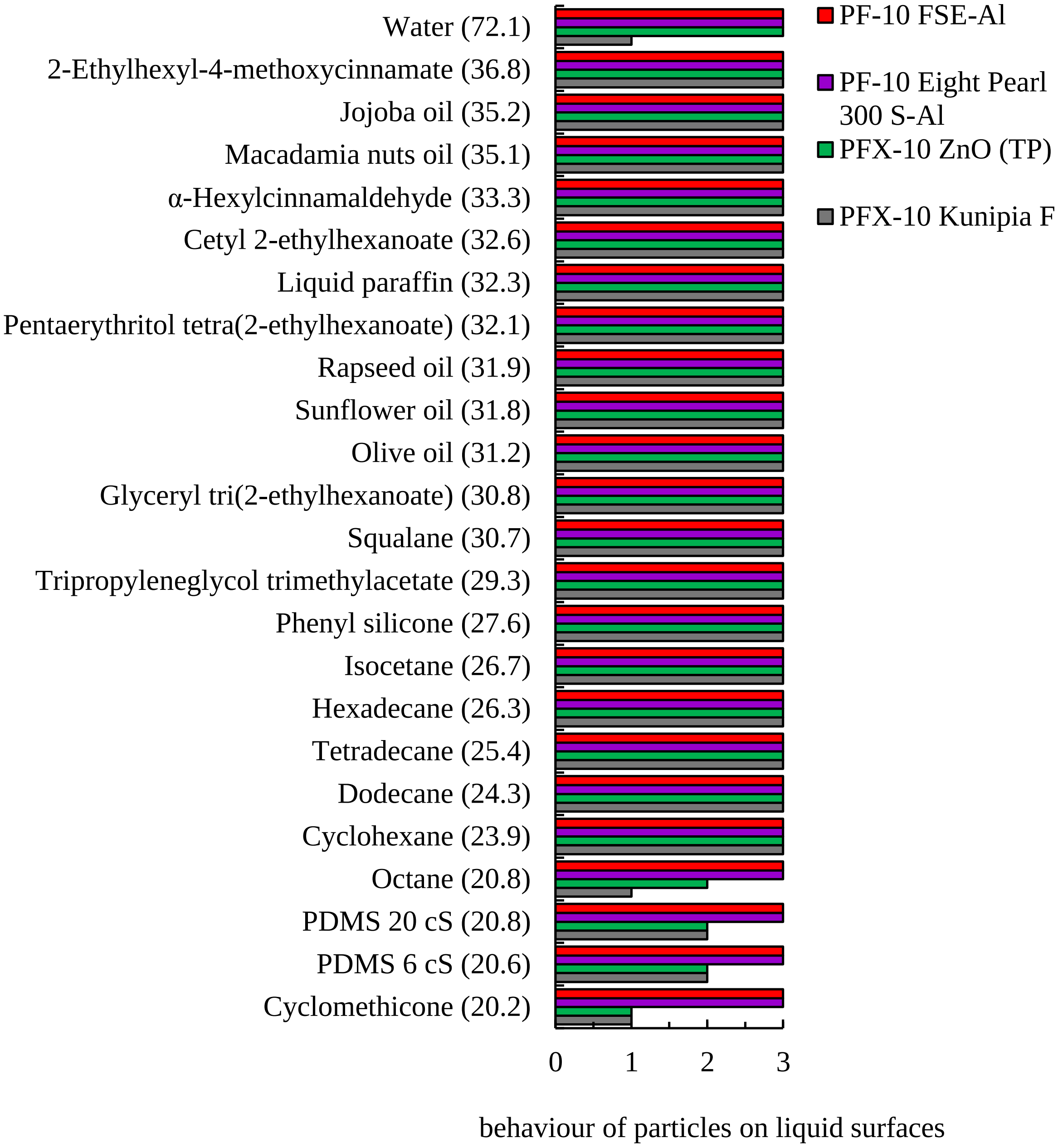

Appendix 6.2. The critical oil : particle ratio COPR *versus* surface tension γ_{la} (25 °C) of the oils for PFX-10 ZnO (TP) (●), PF-10 Eight Pearl 300S-Al^a (▲) and PF-10 FSE-Al (◆). Inset: schematic illustration of a/o foam above COPR and dry oil powder at or below COPR. For simplicity, the particles, oil droplets and air bubbles are spherical. The error bars represent the minimum amount of oil required for phase inversion per gram of particles.

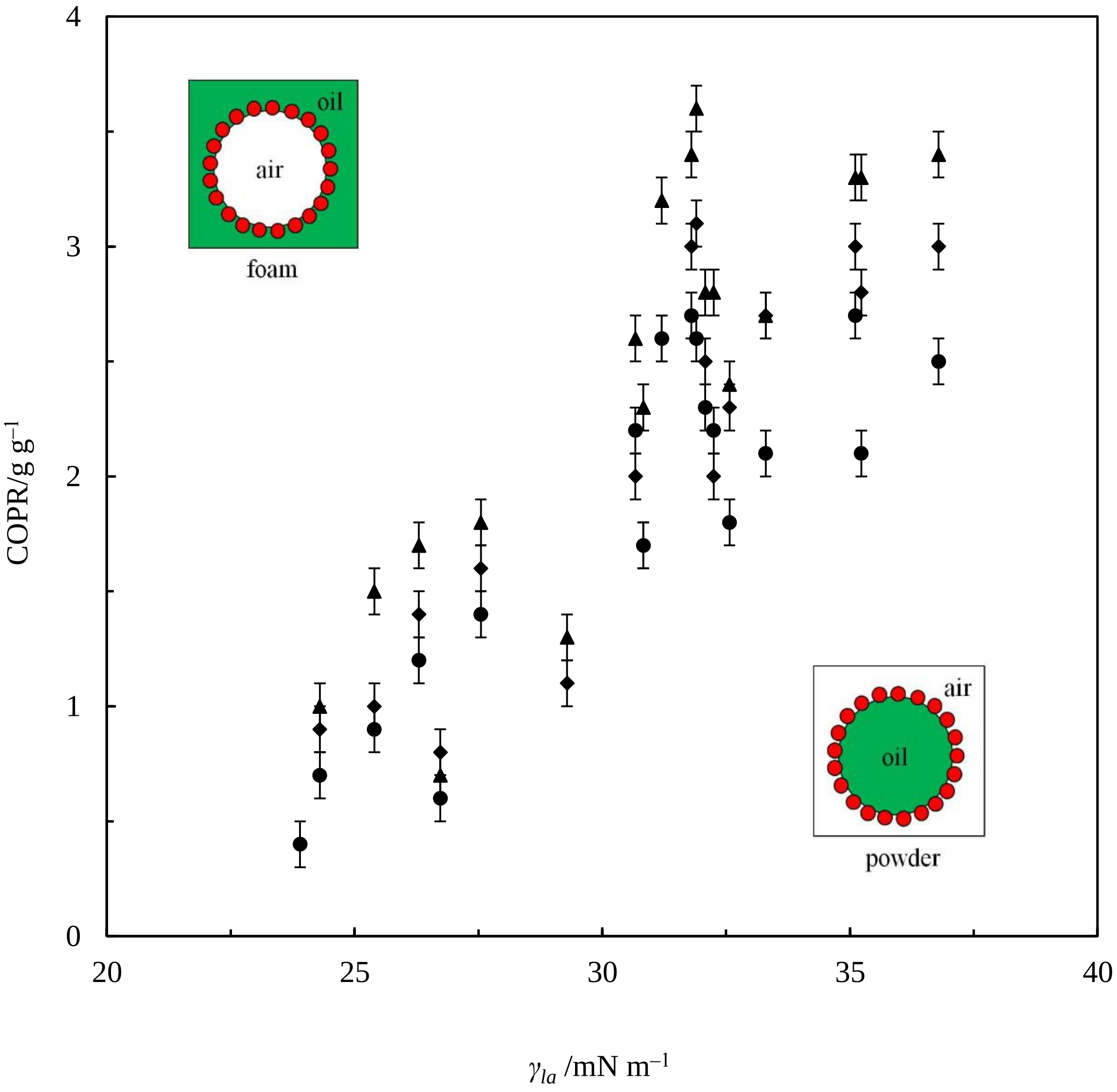

Appendix 6.3. (upper) Photographs of watch glasses containing dry oil powders (1 year after formation) of dry (a) squalane powder stabilised by PFX-10 ZnO (TP) particles, (b) olive oil stabilised by the PF-10 FSE-Al particles and (c) macadamia nuts oil stabilised by PF-10 Eight Pearl 300S-Al[a] particles. (lower) Photograph of corresponding dry squalane powder flowing freely through a glass funnel onto a Pyrex watch glass. Scale bar = 10 mm.

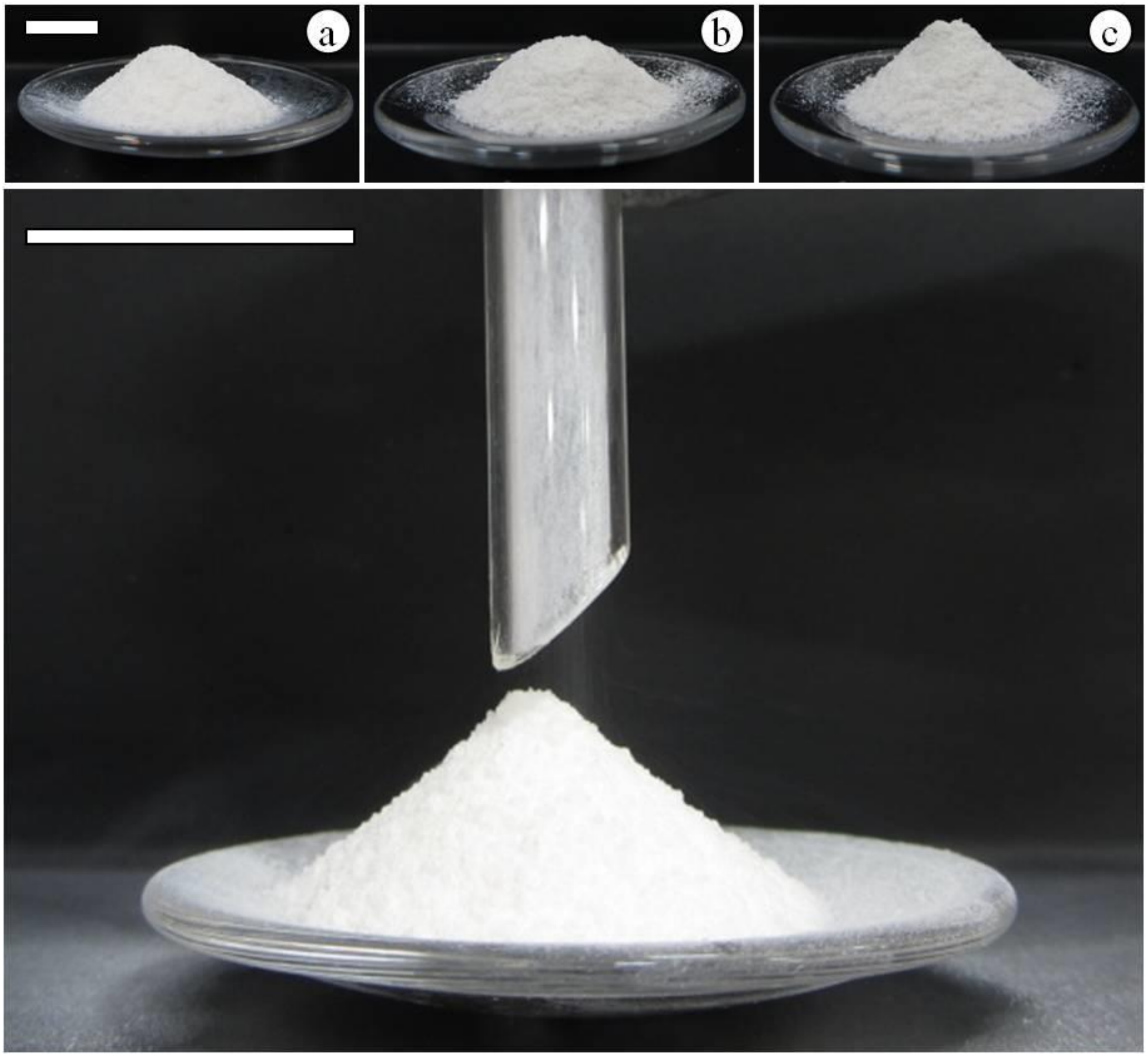

Appendix 6.4. Optical micrographs (soon after preparation) of dry oil powders of (i) squalane and (ii) sunflower oil stabilised by PFX-10 ZnO (TP) particles prepared from 5 cm^3 of the oils containing 4 mg of Sudan Red dye and (iii) cryo-SEM image (3 months after preparation) of dry squalane powder stabilised by PFX-10 ZnO (TP) particles. (lower) Photos of liquid marbles (10 μL) resting on a hydrophilic glass slide soon after preparation. The marbles are (a) olive oil liquid marble stabilised by PFX-10 Kunipia F, (b) olive oil liquid marble stabilised by PFX-10 ZnO (TP), (c) sunflower oil liquid marble stabilised by PFX-10 ZnO (TP), (d) macadamia nuts oil liquid marble stabilised by PF-10 Eight Pearl 300S-Al[a], (e) rapeseed oil liquid marble stabilised by PF-10 FSE-Al and (f) water liquid marble stabilised by PF-10 FSE-Al.

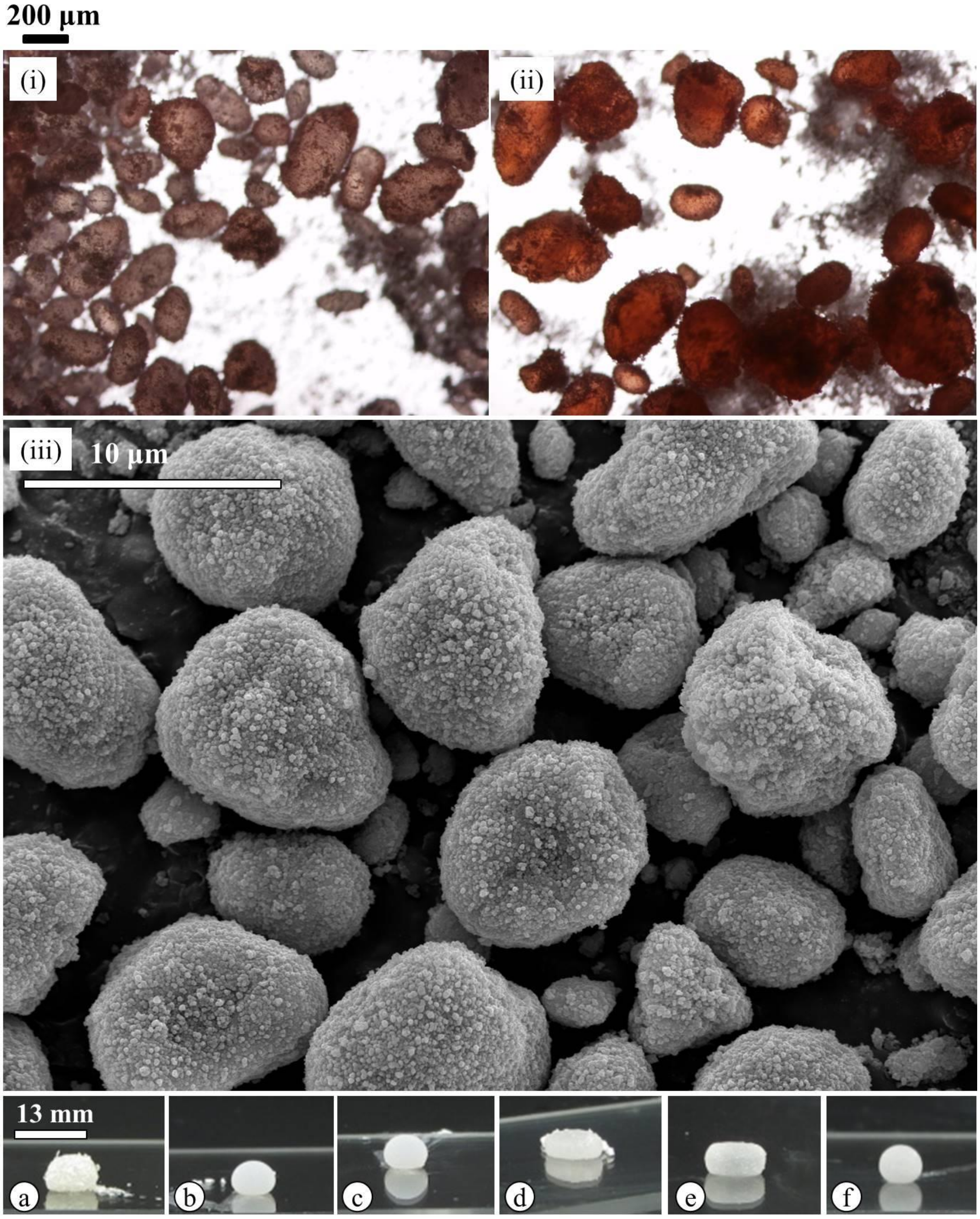

Appendix 6.5. Photo (soon after preparation) of (a) squalane foam stabilised by PFX-10 ZnO (TP) particles (containing 1.15 g of squalane) being poured onto a Pyrex watch glass, (b) corresponding optical micrograph of squalane foam in (a), (c) photo (soon after preparation) of squalane foam stabilised by PF-10 Eight Pearl 300S-Al[a] particles (containing 1.35 g of squalane) being forced from a plastic syringe onto a black aluminium substrate and (d) corresponding optical micrograph of squalane foam in (c). The foams were obtained by inverting the corresponding dry oil powders (Appendix 6.4) and were viewed soon after formation.

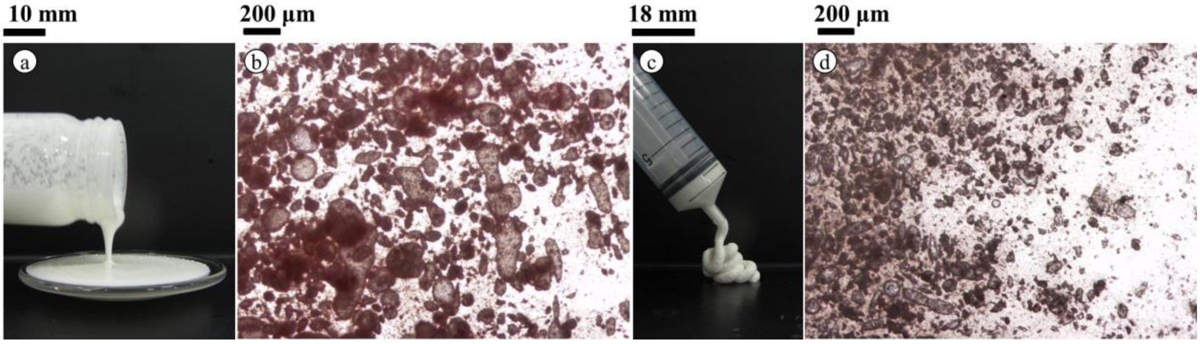

Appendix 6.6. List of oil foams that underwent drainage or coalescence and those ultra-stable to these processes.

Particle	Drainage	Coalescence	Ultra-stable foam
PFX-10 ZnO (TP)	Foams in Appendix 6.7 except those listed under the other headings	Olive oil, sunflower oil, α-hexylcinnamaldehyde and gylceryl tri(2-ethylhexanoate) foams	*n*-Dodecane and phenyl silicone foams
PF-10 Eight Pearl 300S-Al[a]	Foams in Appendix 6.7 except those listed under the other headings	Olive oil, rapeseed oil and α-hexylcinnamaldehyde foams	*n*-Dodecane, *n*-tetradecane isocetane, phenyl silicone and tripropyleneglycol trimethylacetate foams
PF-10 FSE-Al	Foams in Appendix 6.7 except those listed under the other headings	Tripropyleneglycol trimethylacetate, sunflower oil, rapeseed oil and α-hexylcinnamaldehyde foams	*n*-Dodecane, *n*-tetradecane, PDMS 20 cS, isocetane and phenyl silicone foams

Appendix 6.7. Apparent advancing (first entry) and receding (second entry) θ_{la} in degrees (measured into the liquid) of 0.1 cm^3 (advancing) and 0.05 cm^3 (receding) of selected liquids in air on compressed particle disks at ambient conditions. All angles quoted are ± 1° (standard deviation of 4 separate measurements). The type of material obtained after agitating the systems described in Appendix 6.1 is also shown as: ○-liquid gave dispersion, ●-liquid gave substantial amount of foam, ◗-liquid gave little foam and †-liquid gave climbing films. For marbles: ×-liquid did not form marble and ✓-liquid formed marble.

	Particle			
Liquid	[‡]PFX-10 Kunipia F	PFX-10 ZnO (TP)	PF-10 Eight Pearl 300S-Al[a]	PF-10 FSE-Al
Cyclomethicone	58,35: ×	54,39: ×,○	61,49: ✓,○	49,35: ✓,○
PDMS 6 cS	76,57: ✓	56,35: ×,○	69,48: ✓,○	69,44: ✓,○
PDMS 20 cS	72,41: ✓	60,33: ✓,○	72,47: ✓,○	73,47: ✓,○
n-Octane	72,45: ✓	71,32: ✓,○	75,39: ✓,○	68,38: ✓,○
Cyclohexane	71,46: ✓	87,44: ✓,○	92,59: ✓,○	79,36: ✓,○
n-Dodecane	✓	✓,○	✓,○	✓,○
n-Tetradecane	✓	✓,○	✓,◗	✓,●
n-Hexadecane	67,45: ✓	77,47: ✓,○	93,67: ✓,●	95,54: ✓,●
Isocetane	✓	✓,●	✓,●	✓,●
Phenyl silicone	88,53: ✓	92,63: ✓,●	105,75: ✓,●	109,75: ✓,●
Tripropylene glycol trimethylacetate	✓	✓,●	✓,●	✓,●
Squalane	100,68: ✓	123,90: ✓,●	114,83: ✓,●	106,82: ✓,●
Glyceryl tri(2-ethylhexanoate)	✓	✓,●	✓,●	✓,●
Olive oil	✓	✓,●	✓,●	✓,●
Sunflower oil	101,67: ✓	120,82: ✓,●	124,89: ✓,●	121,82: ✓,●
Rapseed oil	✓	✓,●	✓,●	✓,●
Pentaerythritol tetra(2-ethylhexanoate)	101,66: ✓	105,76: ✓,●	122,93: ✓,●	115,79: ✓,●
Liquid paraffin	✓	✓,●	✓,●	✓,●
Cetyl 2-ethylhexanoate	✓	✓,●	✓,●	✓,●
α-Hexylcinnamaldehyde	96,68: ✓	117,81: ✓,●	111,75: ✓,●	117,80: ✓,●
Macadamia nuts oil	98,77: ✓	111,81: ✓,●	122,89: ✓,●	115,83: ✓,●
Jojoba oil	✓	✓,●	✓,●	✓,●
2-Ethylhexyl-4-methoxycinnamate	104,76: ✓	117,89: ✓,●	122,90: ✓,●	111,79: ✓,●
Water	0,0: ×	127,88: ✓,†	130,101: ✓,†	139,94: ✓,†

[‡]Cloudy dispersion was obtained with all the liquid/particle mixtures.

Appendix 6.8. Cosine of apparent (a) advancing and (b) receding θ_{la} (through liquid) of a liquid droplet in air on compressed particle disks of PFX-10 Kunipia F (○), PFX-10 ZnO (TP) (●), PF-10 Eight Pearl 300S-Al^{a} (△) and PF-10 FSE-Al (+) particles *versus* γ_{la} (at 25 °C). Inset: photograph of (a) side and (b) top view of an PF-10 Eight Pearl 300S-Al^{a} disk made by compressing 500 mg of the powdered particles (scale bar = 6 mm). The type of material formed on vigorous agitation and gentle mixing is also shown.